NASA Conference Publication 3193

Joint University Program for Air Transportation Research 1991–1992

Compiled by
Frederick R. Morrell
NASA Langley Research Center
Hampton, Virginia

Proceedings of a conference sponsored by the Federal Aviation Administration, Washington, D.C., and the National Aeronautics and Space Administration, Washington, D.C., and held in Athens, Ohio June 18–19, 1992

National Aeronautics and Space Administration
Office of Management
Scientific and Technical Information Program
1993

PREFACE

The Joint University Program for Air Transportation Research is a coordinated set of three grants sponsored by NASA Langley Research Center and the Federal Aviation Administration, one each with the Massachusetts Institute of Technology (NGL-22-009-640), Ohio University (NGR-36-009-017), and Princeton University (NGL-31-001-252). These research grants, which were instituted in 1971, build on the strengths of each institution. The goals of this program are consistent with the aeronautical interests of both NASA and the FAA in furthering the safety and efficiency of the National Airspace System. The continued development of the National Airspace System, however, requires advanced technology from a variety of disciplines, especially in the areas of computer science, guidance and control theory and practice, aircraft performance, flight dynamics, and applied experimental psychology. The Joint University Program was created to provide new methods for interdisciplinary education to develop research workers to solve these large scale problems. Each university submits a separate proposal yearly and is dealt with individually by NASA and FAA. At the completion of each research task, a comprehensive and detailed report is issued for distribution to the program participants. Typically, this is a thesis that fulfills the requirements for an advanced degree or a report describing an undergraduate research project. Also, papers are submitted to technical conferences and archival journals. These papers serve the Joint University Program as visibility to national and international audiences.

To promote technical interchange among the students, periodic reviews are held at the schools and at a NASA or FAA facility. The 1991-1992 year-end review was held at Ohio University, Athens, Ohio, June 18-19, 1992. At these reviews the program participants, both graduate and undergraduate, have an opportunity to present their research activities to their peers, to professors, and to invited guests from government and industry.

This conference publication represents the twelfth in a series of yearly summaries of the program. (The 1990-1991 summary appears in NASA CP-3131). Most of the material is the effort of students supported by the research grants. Four types of contributions are included in this publication: a summary of ongoing research relevant to the Joint University Program is presented by each principal investigator, completed works are represented by full technical papers, research previously in the open literature (e.g., theses or journal articles) is presented in an annotated bibliography, and status reports of ongoing research are represented by copies of presentations with accompanying text.

Use of trade names of manufacturers in this report does not constitute an official endorsement of such products or manufacturers, either expressed or implied, by the National Aeronautics and Space Administration or the Federal Aviation Administration.

Frederick R. Morrell
NASA Langley Research Center

CONTENTS

PREFACE iii

MASSACHUSETTS INSTITUTE OF TECHNOLOGY

AN INVESTIGATION OF AIR TRANSPORTATION TECHNOLOGY AT THE MASSACHUSETTS INSTITUTE OF TECHNOLOGY, 1991–92 3
Robert W. Simpson

THE ASLOTS CONCEPT 9
Robert W. Simpson

HAZARD EVALUATION AND OPERATIONAL COCKPIT DISPLAY OF GROUND MEASURED WINDSHEAR DATA 21
Craig Wanke and R. John Hansman Jr.

HEAT TRANSFER ON ACCRETING ICE SURFACES 29
Keiko Yamaguchi and R. John Hansman Jr.

HAZARD ALERTING AND SITUATIONAL AWARENESS IN ADVANCED AIR TRANSPORTATION COCKPITS 35
R. John Hansman Jr., Craig Wanke, James Kuchar, Mark Mykityshyn, Edward Hahn, and Alan Midkiff

OHIO UNIVERSITY

INVESTIGATION OF AIR TRANSPORTATION TECHNOLOGY AT OHIO UNIVERSITY, 1991–92 49
Robert W. Lilley

A HYBRID VOICE/DATA MODULATION FOR THE VHF AERONAUTICAL CHANNELS 53
Dennis M. Akos

FAULT DETECTION AND ISOLATION 67
Greg Bernath

GPS MULTIPATH ERRORS IN THE PRECISION LANDING ENVIRONMENT 77
James D. Waid

PRINCETON UNIVERSITY

INVESTIGATION OF AIR TRANSPORTATION TECHNOLOGY AT PRINCETON UNIVERSITY, 1991–92 91
Robert F. Stengel

ADVANCED AIR TRAFFIC MANAGEMENT 101
J.P. Wangermann

COMPUTER AIDED CONTROL SYSTEM DESIGN (CACSD) 107
Frank T. Stoner

SYNTHESIS OF ROBUST CONTROLLERS 115
Chris Marrison

OPTIMAL RECOVERY FROM MICROBURST WIND SHEAR 129
Sandeep S. Mulgund

DYNAMIC RESPONSE AND CONTROL OF A JET-TRANSPORT AIRCRAFT ENCOUNTERING A SINGLE-AXIS VORTEX 141
Darin R. Spilman

INTELLIGENT FLIGHT CONTROL SYSTEMS 151
Robert F. Stengel

MASSACHUSETTS INSTITUTE OF TECHNOLOGY

AN INVESTIGATION OF AIR TRANSPORTATION TECHNOLOGY AT THE MASSACHUSETTS INSTITUTE OF TECHNOLOGY

1991 - 1992

Robert W. Simpson
Flight Transportation Laboratory
M.I.T., Cambridge, MA 02139

SUMMARY OF RESEARCH ACTIVITIES

1. INTRODUCTION

There are two completed projects and five new or continuing research activities under the sponsorship of the FAA/NASA Joint University Program as the 1991-92 period ends. There were a number of publications during the year which have been provided in this report. A brief summary of some of the continuing research projects is provided.

The completed projects were:

1. Hahn, E. and Hansman, R.J., "An Experimental Study of the Effect of Automation on Pilot Situational Awareness in the Datalink ATC Environment", MIT Aeronautical Systems Report, ASL-92-1, June 1992.

2. Midkiff, A., and Hansman, R.J., "Analysis of the Importance of Party Line Information in ATC Operations", MIT Aeronautical Systems Report, ASL-92-2, August 1992.

The active research projects are:

1. Extensions for the FASA (Final Approach Spacing Advisory) System (Chiang, M.C., Simpson, R.W.)

2. Radar Tracking around a Turn (Liu, Manly, and Simpson, R.W.)

3. Impact of Advanced Technologies on Single Pilot IFR Operations (Dershowitz, A., and Hansman, R. John)

4. System and Human Limitations in Millimeter Wave and Infrared Synthetic Vision Systems (Clarke, J.P., and Hansman, R. John)

5. Differences in Party Line Information Usage by Operational User Groups (Pritchett, Amy, and Hansman, R. John)

A publication from prior years, "Heat Transfer on Accreting Ice Surfaces" by K. Yamaguchi and R.J. Hansman, is included in this year's report. An annotated set of materials used to give a briefing at MIT Lincoln Laboratory on the continuing research on extending the FASA (Final Approach Spacing Advisory) system is also included.

The student thesis by Zhihang Chi (Reference 3.1) won the RTCA's William E. Jackson Award for 1991. Mr. Chi was a guest at the Annual RTCA Meeting on November 30, 1991 to receive the award and its $1500 prize.

2. REVIEW OF CONTINUING RESEARCH ACTIVITIES

2.1 Extending FASA (Final Approach Spacing Advisory) System

Prior research under JUP (Reference 3.1) created an initial version of an interactive decision support system to assist the controllers responsible for establishing the final approach spacings for aircraft at a busy airport. Current research is extending this work in a variety of ways in order to achieve capabilities described by a concept called ASLOTS (Adaptive Slots). The initial version only handled landing aircraft approaching a single runway. The current work is aimed at incorporating takeoff aircraft and multiple runways. It also will improve the dynamics of aircraft motion in the simulation and the representation of errors from radar surveillance and tracking. The original simulation was quickly constructed to provide a graphic means of demonstrating the real time operation of the logic and to investigate the problems of producing a robust code which implemented some of the desired capabilities of the ASLOTS concept. The logic and its code will be transferred to another, high fidelity airspace simulation called ATCSIM (which also simulates the motion of aircraft on the surface of the airport between runways and gates).

The FASA was implemented on an Apollo 3500 workstation in UNIX and the C language. It used X-Windows to provide a graphical display of aircraft and the landing slots. It is portable to other workstations and has been demonstrated by an IBM RS-6000. The logic will be incorporated into ATCSIM which runs on a network of SUN SPARCstations.

An annotated description of the ASLOTS concept is provided in this report.

2.2 Radar Tracking of Turning Aircraft

Under the assumption that a straight track at constant groundspeed is being flown, today's radar tracking processes provide a best estimate of current position, groundspeed, and track direction. These estimates are critical to the successful operation of various automated ATC processes such as Hazard Alert, Automated Final Approach Spacing, or Conformance Monitoring.

The best estimates are obtained from the recurrent position measurements on each scan of the radar which occur at 4.8 or 12 second intervals. There are three sources of noise in the measurements: 1)radar measurement errors in range and azimuth; 2) short term fluctuations in wind; and 3) aircraft maneuvering around the straight line path. The radar measurements are "filtered" or "time averaged" over the last several measurements to estimate speed and direction, and it requires several scans (30-60 seconds) to get an accurate and reliable estimate after tracking is initiated on a straight line path.

But if a simple turn is initiated at constant airspeed, current radar tracking processes will continue to assume a straight line path is being flown and severe transient errors can occur (e.g., $\pm$ 60° or 60 knots). It is possible to inhibit or modify the straight line tracking process, but it is difficult to create a successful method of turn detection using only successive, same direction, deviations from a straight line path. Some method of providing a turning signal to the tracker that the aircraft has changed to a turning mode of flight is needed. With the advent of Mode S radar, it is possible for the aircraft to send a "Turning Signal" indicating a left or right turn on any scan (e.g., if bank angle has exceeded 10° for 2.5 seconds, create a Turning Signal).

Given a Turning Signal, there are two options:

1. Turn off the Straight Line Tracker during the turn, and use the measured turn positions to estimate the initial values of groundspeed and track direction to re-initiate the tracker on the next straight line segment.

2. Switch to a Turning Tracker, using the measured turn positions to estimate values for groundspeed, track direction, and rate of change of track direction during the turn.

The first option is being studied in the current research. It does not provide estimates of groundspeed and direction during the turn, but the number of measurements and period of turning is small (there are less than six measurements for a 90° turn and most turns are smaller than 90°). It seems reasonable to try to use them to prevent transient errors and a good initial estimate along the new straight line segment.

The second option may be studied later. It is necessary to declare a model of the curved path, and it is known that it will not be circular nor at constant groundspeed when there are strong winds. It is possible to consider sending more information about the current aircraft state such as bank angle, rate of change of heading, or heading itself to augment an "aided" Turning Tracker; and for modern transport aircraft with a digital FMS, it is possible to send the onboard estimate of ground speed and track direction directly to the ground on each scan which obviates the need to implement any ground based Turning Tracker. It is not even clear that ground speed and direction during the turning maneuver is useful. Of much more value would be the intended final path direction for the turn since the future trajectory of interest probably exceeds its curving portion.

A simulation called TASIM for studying tracker performance has been created. Radar measurement errors are randomly drawn from a normal distribution of range and azimuth errors of known size. Aircraft are flown at differing airspeeds along paths which provide Radial and Tangential turns at varying distances from the radar site. The aircraft has an automatic guidance system which causes it to track these paths in the face of varying winds or navigation system errors. There is a guidance logic which initiates a turn at the appropriate point near the end of one straight segment of the path, and then transition to an acquisition of the next segment (which may have a dynamic overshoot due to winds and navigation errors). It is possible to vary the turn initiation time to occur at random times in the radar scan.

3. REFERENCES

3.1 Chi, Zhihang, A Graphic Simulation System for Adaptive, Automated Final Approach Spacing, Flight Transportation Laboratory Report 91-3, June 1991, Flight Transportation Laboratory, MIT, Cambridge, MA, 02139

3.2 Hahn, E., and Hansman, R.J., "An Experimental Study of the Effect of Automation on Pilot Situational Awareness in the Datalink ATC Environment", MIT Aeronautical Systems Report, ASL-92-1, June 1992.

3.3 Midkiff, A., and Hansman, R.J., "Analysis of the Importance of Party Line Information in ATC Operations", MIT Aeronautical Systems Report, ASL-92-2, August 1992.

3.4 Wanke, C., and Hansman, R. John, Hazard Evaluations and Operational Cockpit Display of Ground Measured Windshear Data, Journal of Aircraft, Vol. 29, No. 3 - May - June 1992

3.5 Hansman, R. John; Wanke, C.; Kuchar, James; Mykityshyn, Mark; Hahn, E.; Midkiff, A., Hazard Alerting and Situational Awareness in Advanced Transport Cockpits, Eighteenth ICAS Congress, Beijing, China, Sept. 1992

The ASLOTS Concept

An Interactive, Adaptive Decision Support Concept
for
Final Approach Spacing of Aircraft (FASA)

FAA-NASA JOINT UNIVERSITY PROGRAM

Robert W. Simpson
Flight Transportation Laboratory, MIT

This presentation outlines a concept for an adaptive, interactive decision support system to assist controllers at a busy airport in achieving efficient use of multiple runways. The concept is being implemented as a computer code called FASA (Final Approach Spacing for Aircraft), and will be tested and demonstrated in ATCSIM, a high fidelity simulation of terminal area airspace and airport surface operations.

Objectives

- PROVIDE AUTOMATED CUES TO ASSIST CONTROLLERS IN THE SEQUENCING AND SPACING OF LANDING AND TAKEOFF AIRCRAFT

- PROVIDE THE CONTROLLER WITH A LIMITED ABILITY TO MODIFY THE SEQUENCE AND SPACINGS BETWEEN AIRCRAFT, AND TO INSERT TAKEOFFS AND MISSED APPROACH AIRCRAFT IN THE LANDING FLOWS

- INCREASE SPACING ACCURACY USING MORE COMPLEX AND PRECISE SEPARATION CRITERIA WHILE REDUCING CONTROLLER WORKLOAD

- ACHIEVE HIGHER OPERATIONAL TAKEOFF AND LANDING RATES ON MULTIPLE RUNWAYS IN POOR VISIBILITY

Assumptions

1. A "metering " process is being applied to all arrivals for landing, and a Runway Operations Schedule (ROS) is being generated and updated continuously for landing and takeoff operations on each active runway.

2. Each landing aircraft has declared an IAS (Indicated Airspeed) for the final approach from the Outer Marker to the runway, and will be obligated to fly it. Each takeoff aircraft will declare itself ready for immediate takeoff as it approaches the runway.

3. A continuously updated estimate of the complete windspeed field in the terminal area is available.

4. Radar surveillance provides data on the position of all aircraft and a tracking process estimates their current speed and direction.

5. Errors of known static and transient characteristics will occur in tracking and surveillance, in wind estimation, and in pilot and aircraft response to clearances for turns and speed reductions.

System Characteristics - Adaptive and Interactive

1. ASLOTS cues are " **adaptive** " to errors in measuring position and estimating speed by the radar and its tracking process, and from piloting errors in execution of commanded turns and speed reductions. Adaptation ensures that the planned spacing schedule is consistent with the actual traffic situation. Any inconsistency will be displayed to the controller for immediate correction.

2. The ASLOTS plans are " **interactive** " with the controllers, and are displayed to them by a sequence of "slot markers" which move along the extended runway centerline. Each aircraft using the runway has a slot marker which becomes visible to the controller as its scheduled operation time approaches. By manipulating the slot markers, controllers can change landing times, change the desired sequence of landings or takeoffs, change individual spacings, set a buffer on separation criteria between particular aircraft, locally modify the desired runway acceptance rate, insert a missed approach, and insert planned takeoffs between landings (which automatically modifies landing spacings).

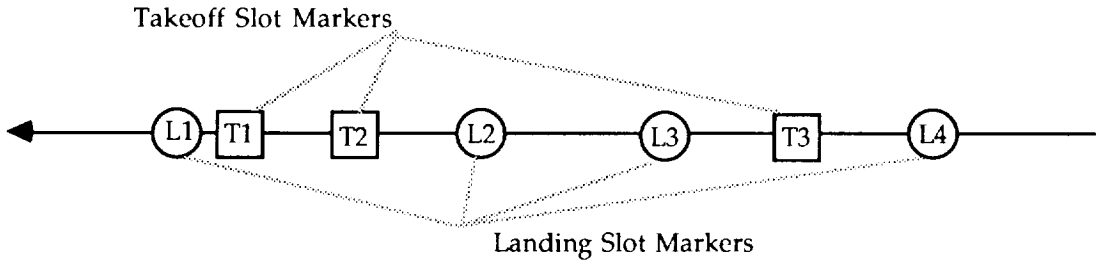

Generic Arrival Patterns for Spacing

There are two generic patterns from which all landing paths are constructed. These arrival patterns are commonly used at major airports and can be adapted easily to any airport and terminal area. There is no fixed path to the runway, but instead each pattern consists of a fixed sequence of commanded turns and speed reductions (ie., "vectors"). The feasible area for patterns is constrained to maintain independence of arrival traffic streams.

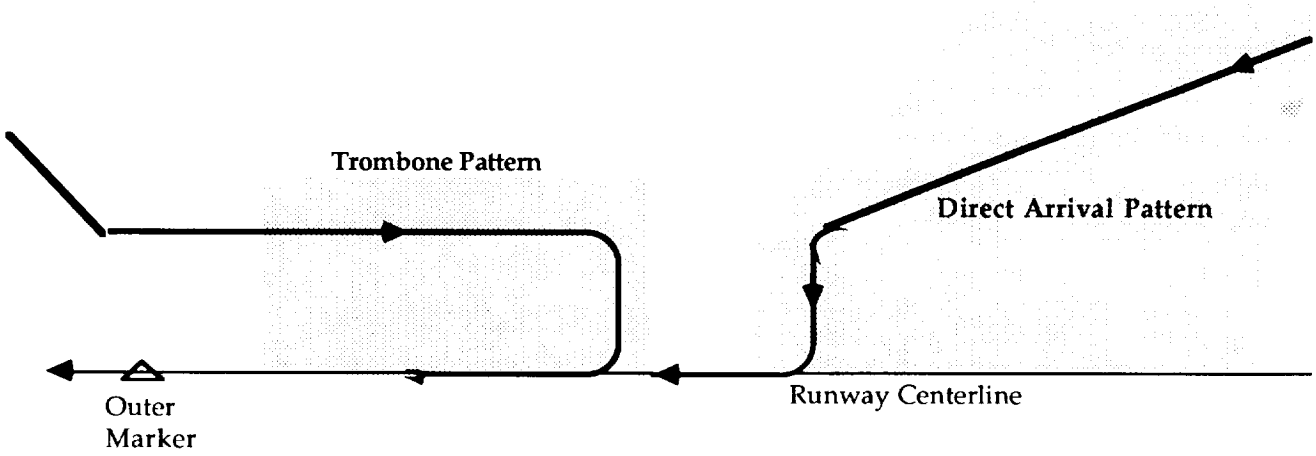

The Components of the Trombone Pattern

There are 8 Components:

1. Downwind Leg
2. Base Turn
3. Base Leg
4. Intercept Turn
5. Initial Intercept Leg
6. Reduce to Final Speed
7. Final Intercept Leg
8. Acquisition Turn

and 3 Adaptive Cues;

1. Turn to Base
2. Turn to Intercept
3. Reduce to Final Approach Speed

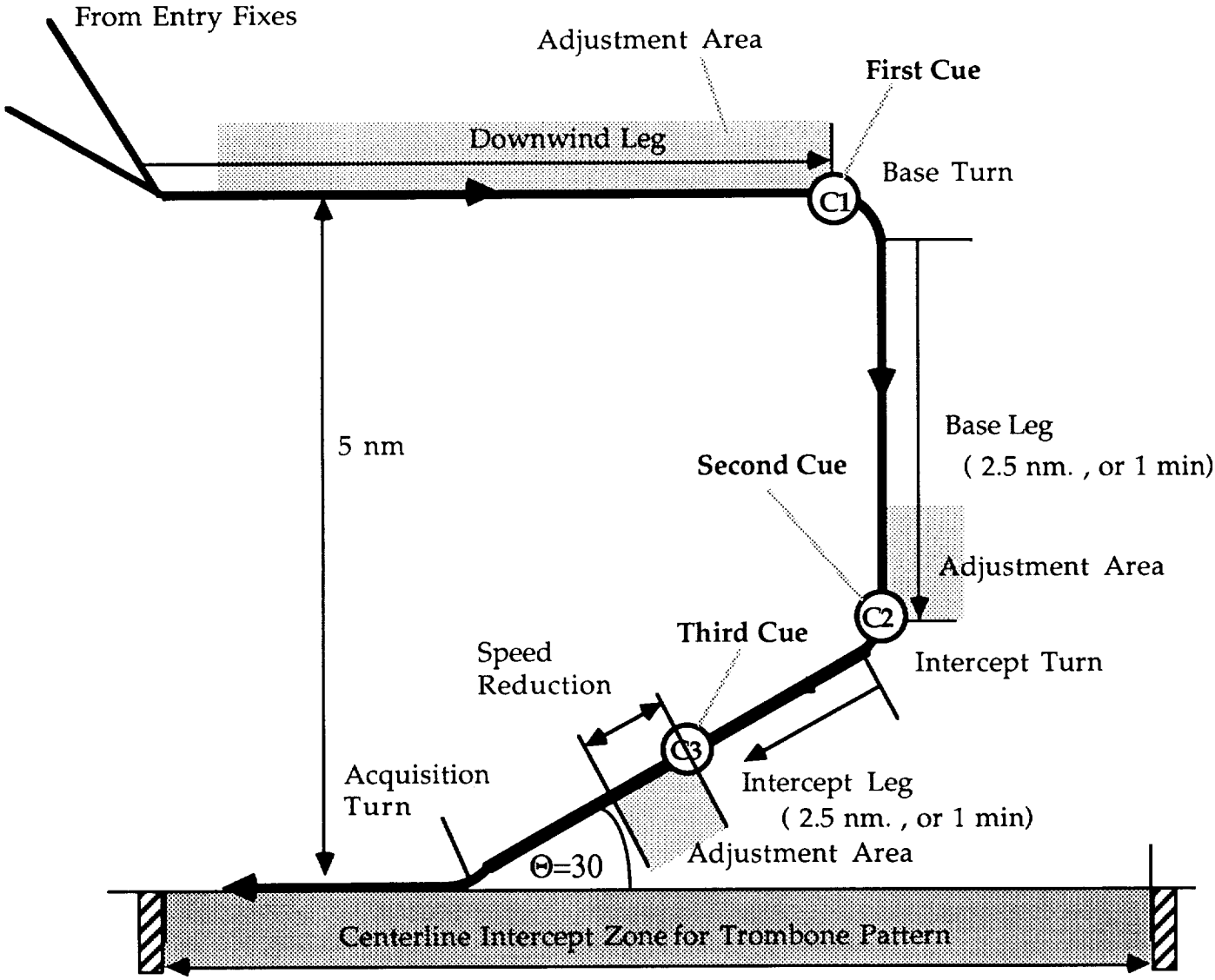

The Components of the Direct Arrival Pattern

There are 11 Components:

1. Arrival Turn
2. Initial Arrival Leg
3. Arrival Speed Reduction
4. Intermediate Arrival Leg
5. Base Turn
6. Base Leg
7. Intercept Turn
8. Initial Intercept Leg
9. Final Speed Reduction
10. Final Intercept Leg
11. Acquisition Turn

and 5 Adaptive Cues:

1. Turn to Arrival direction
2. Reduce to Arrival Speed
3. Turn to Base
4. Turn to Intercept
5. Reduce to Final Approach Speed

(not all cues may be utilized on any approach)

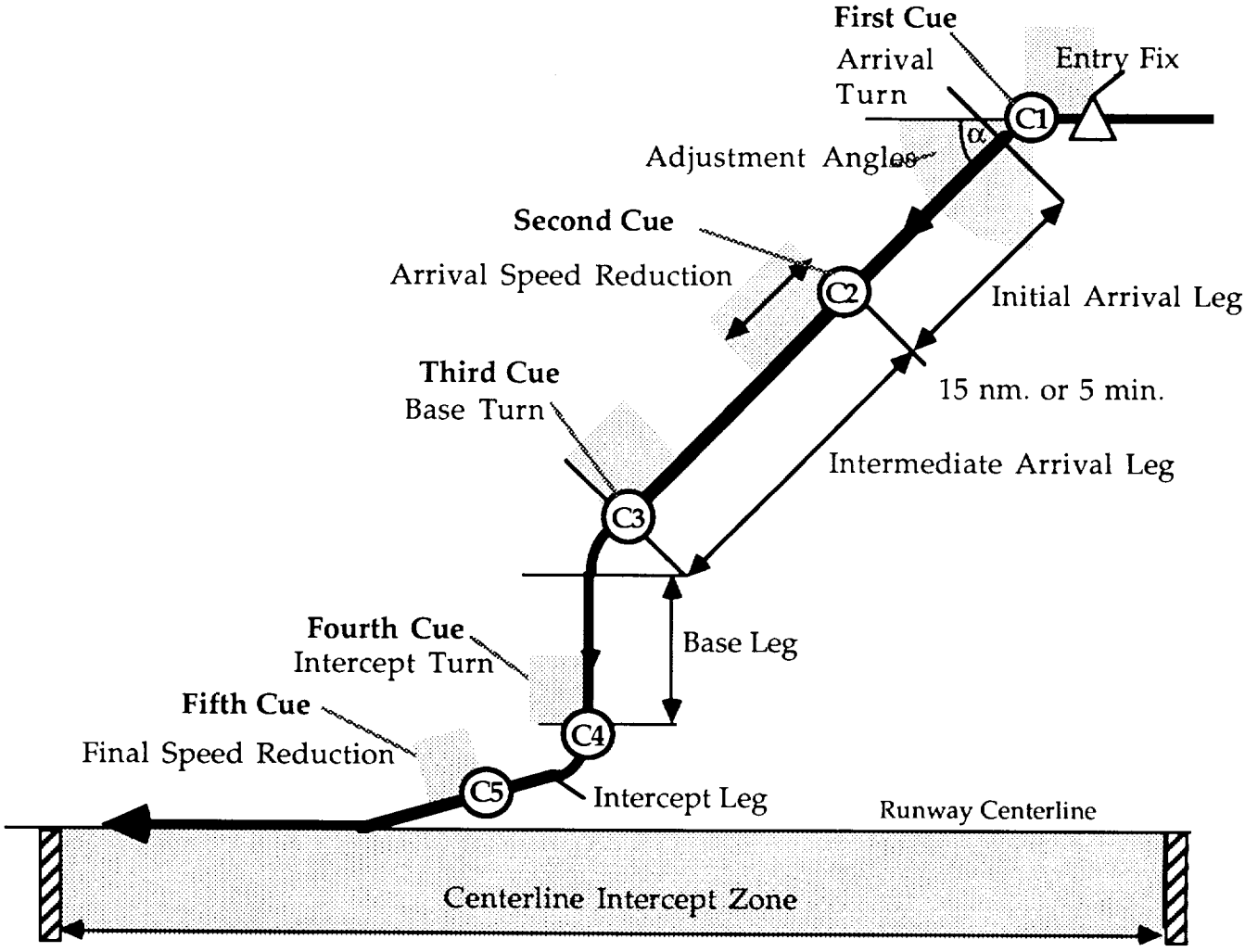

Constrained Pattern Parameters (CPP)

There are a number of constraints on the paths flown in each pattern

Trombone Pattern

1. There is a minimum length specified for Base and Intercept Legs which ensures that radar tracking processes will be stabilized in estimating speed and direction

2. The intermediate airspeed on downwind, and angle of final intercept of the runway centerline can be specified within limits.

3. The geometries can be constructed to provide non-simultaneous cues for delivery to successive, closely spaced aircraft in a pattern

4. Minimum and Maximum slot acquisition points define a Trombone Intercept Zone on the runway centerline beyond the Outer Marker.

Direct Arrival Pattern

1. There is a range of angles and distances for the arrival leg from various entry points.

2. A common intermediate airspeed can be specified, or various intermediate airspeeds for different types of aircraft.

3. Minimum and Maximum slot acquisition points define a Direct Arrival Intercept Zone on the runway centerline beyond the maximum acquisition point of the Trombone Pattern

Adaptive Cues for Controller Actions

1. At some selectable warning time (eg., 10 seconds), the icon representing an aircraft position will turn yellow, and after some further period (eg., 5 seconds) begin to blink. At the desired time of the turn or speed reduction, the icon turns red indicating lateness in executing the cue. To stop the blinking, the controller must "mouse" the icon indicating his response.

2. It is not important that the cue be issued or executed exactly on time. The cueing logic is "adaptive" and will compute the next cue for this aircraft (and others) based on the **actual achieved position and ground speed** of aircraft after they complete the maneuver.

3. If the aircraft responds so poorly that it is not possible to make the current schedule, its slot marker will turn red indicating to the controller that a schedule change is necessary. This is done by mousing the slot marker and sliding it to a feasible position. This causes an adaptation in all other spacings.

The Spacing Schedule - Slot Markers

1. Along the runway centerline, a sequence of slot markers is displayed representing the desired schedule for landing and takeoff operations. They move at a groundspeed corresponding to final approach airspeed declared by each aircraft corrected for the current estimate of the wind on final approach. Eventually, the aircraft is directed to "intercept" its slot marker.

2. A landing sequence and schedule will be automatically generated, but controllers are able to modify both the sequence and schedule within certain limits by mousing and sliding slot markers within a safe and feasible range.

3. The spacings are computed to ensure safe separations at all points on the path to the runway. Since spacings are computed, the criteria for separation can be more efficiently determined and more complex than those used presently (eg., dependent on type of aircraft or actual weather). The controller is assured that only legal separations will be allowed on the display without having to remember them .

The Feasible Slot Range - (FSR)

1. The computations for the controller cues are used to compute a range of feasible positions along the extended runway centerline for each slot marker which depend on:

    a) the current position of its aircraft and its planned speeds

    b) its planned separations from other aircraft accounting for the fact that they can be shifted rearwards within their feasible ranges

2. When the controller "mouse" is a slot marker, the extent of the feasible range is displayed along the centerline. The slot marker may then be dragged to its desired position anywhere in that range. If it is dragged beyond its range, it snaps back to the limit of its range.

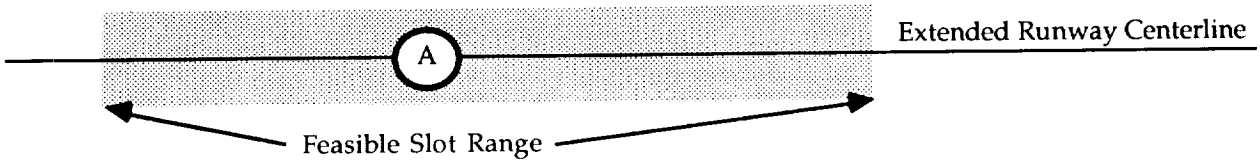

Automatic Rearward Shifting of Slots (ARS)

1. If a slot marker is shifted rearwards within its range, there may be an automatic adjustment of the positions of subsequent slot markers within their ranges. First any slack between successive aircraft is removed. The limit of rearward shifts is determined by one or more of the slot markers in the chain.

2. If a slot marker is shifted forward within its range, no other slot marker is affected. Each slot marker must be moved forward by the controller individually.

3. Having shifted a number of slot markers, there is an automatic adjustment of the cues. All cues are now based on the new positions of the slot markers.

4. By moving a slot marker rearward, space can be made for inserting a missed approach or one or more takeoff aircraft. When the controller tries to insert a new slot marker into the sequence, the new scheduled positions of subsequent slots are automatically displayed. A non-feasible insertion would be rejected, and the controller must then try a later insertion.

Automatic Rearward Shifting of Slots (ARS)

Example:

If an attempt is made to shift A rearwards, it cannot reach the limit of its feasible range because it must maintain a separation Sab from B; and when B reaches the limit of its range, A cannot be moved further and still maintain separation from B. As B moves rearward, C is also moved since it is tight in the original spacing, but when B reaches its limit, C stops moving rearward and since there still is excess spacing from D, it turns out that D does not have to be shifted. The shift range shown to the controller will instantly show how far each aircraft can be shifted in any situation so that the complexity of the shifting need not be known.

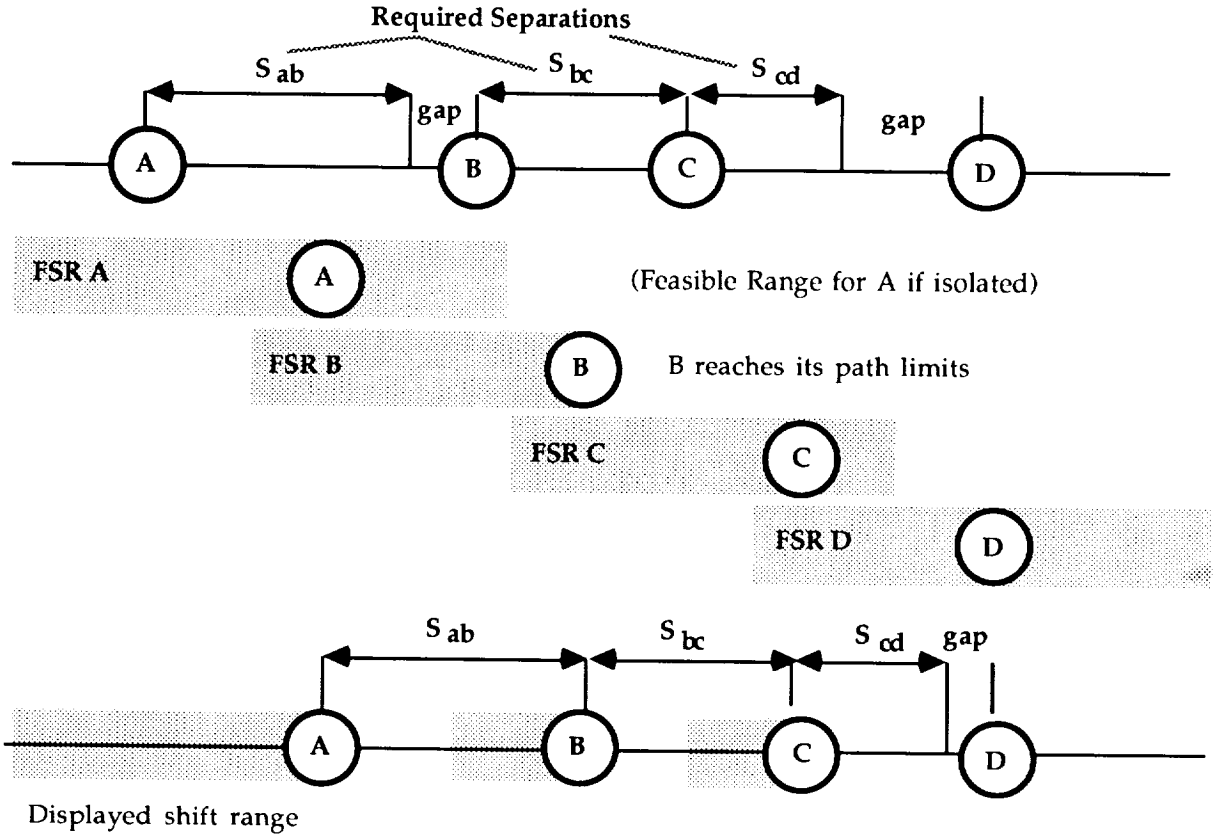

Centerline Adaptation - (CLA)

1. To prevent the actual situation from diverging from the planned situation, it is necessary to have a continuous feedback of the actual spacings achieved. This is done by **Centerline Adaptation**

2. As each aircraft approaches the runway centerline (and its slot marker), the slot marker disappears and its position is then replaced in the ASLOTS computations by the actual position of the aircraft along the centerline. Due to the operation of the Automatic Rearward Shifting, all slot markers for subsequent aircraft will then be shifted back if the aircraft is late. This maintains a safe spacing whenever an aircraft is late into its slot.

3. If the aircraft is early, it may be tight for spacing from the prior aircraft. If the earliness exceeds some buffer specified in time or distance, the aircraft icon will be turned red to advise the controller of the potential violation. Subsequent slot markers will not be moved forward. The controller can call a missed approach if it is warranted.

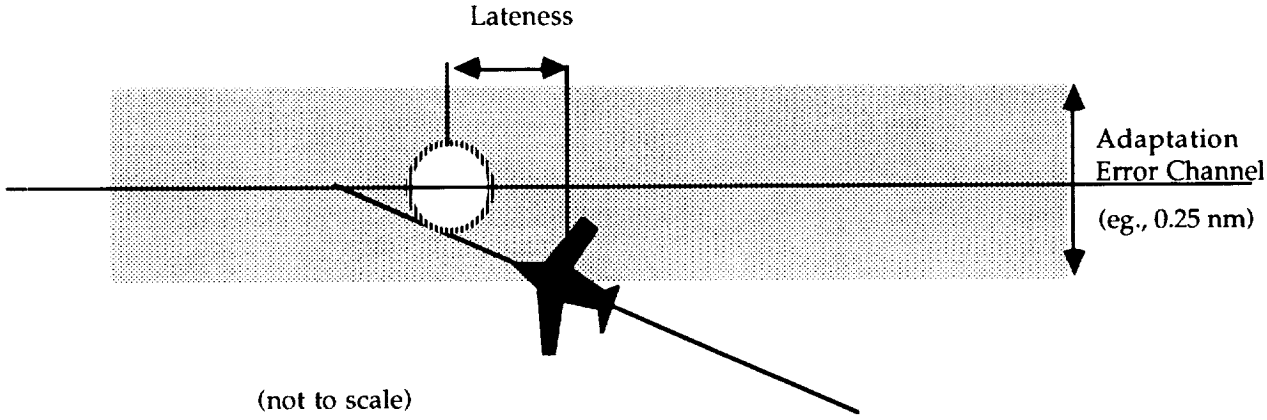

Spacing for Multiple Dependent Runways

Convergent and Parallel Runways

Dual runway operations are staggered and convergent runways are scheduled to assure safety if simultaneous missed approaches occur. Altitude Separation occurs in overlapping areas of the patterns for different runways.

The ASLOTS logic assists 3 Final Approach controllers in the situation below.

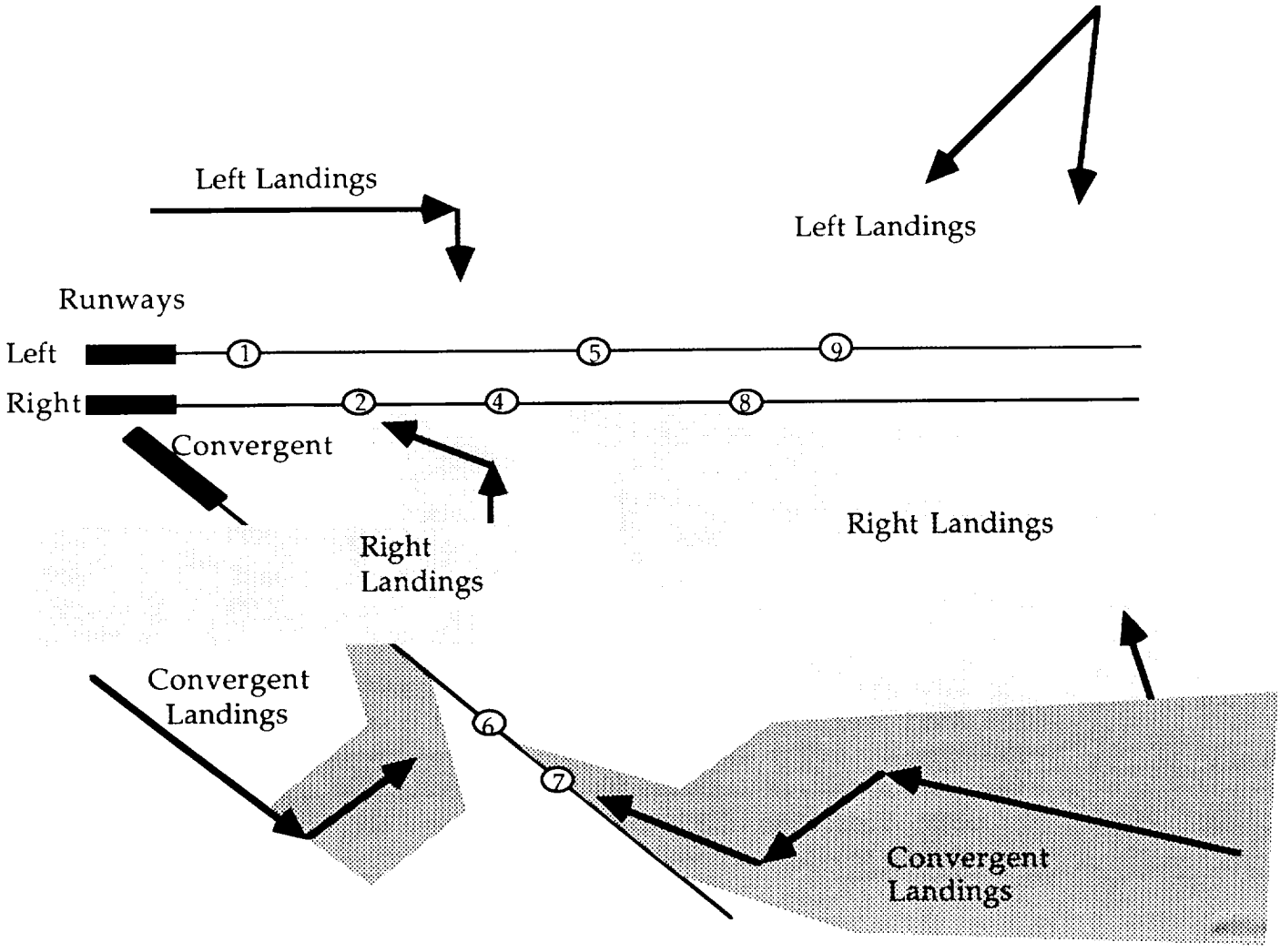

ASLOTS Research - Accomplishments

- research sponsored by FAA-NASA under the Joint-University Program has resulted in a recent S.M. Thesis at MIT/FTL.

  "A Graphic Simulation System for Adaptive Automated Final Approach Spacing", MIT/FTL Report 91-3, Z. Chi,

- a portable, desktop simulation for modern workstations has been created by writing the software in Standard C, and putting the graphics in X-Window. At FTL, it runs on an Apollo 4500, and an IBM RS-6000

Accomplishments to date

- the implementation of the following functions has been done:

  - Auto Rearward Shift (ARS)
  - Centerline Adaptation (CLA)
  - Constrained Pattern Parameters (CPP)
  - Feasible Slot Range (FSR)

Improvements in continuing research:

- the aircraft motion modeling needs improvement
- the effect of winds and a time varying wind model will be included
- the error modelling for radar and tracking is being incorporated
- the graphic representation of the cues for controller is primitive
- automated insertion of missed approaches and takeoffs will be achieved
- the system will be transferred to ATCSIM

Hazard Evaluation and Operational Cockpit Display of Ground-Measured Windshear Data

Craig Wanke* and R. John Hansman Jr.†
Massachusetts Institute of Technology, Cambridge, Massachusetts 02139

Information transfer issues associated with the dissemination of windshear alerts from the ground are studied. Two of these issues are specifically addressed: the effectiveness of different cockpit presentations of ground-measured information and assessment of the windshear hazard from ground-based measurements. Information transfer and presentation issues have been explored through pilot surveys and a part-task Boeing 767 "glass cockpit" simulation. The survey produced an information base for study of crew-centered windshear alert design, whereas the part-task simulations provided useful data about modes of cockpit information presentation for both windshear alert and ATC clearance delivery. Graphical map displays have been observed to be exceptionally efficient for presentation of position-critical alerts, and some problems with text displays have been identified. Problems associated with hazard assessment of ground-measured windshear information have also been identified.

I. Introduction

LOW-ALTITUDE windshear is the leading weather-related cause of fatal aviation accidents in the U.S. Since 1964, there have been 26 accidents attributed to windshear resulting in over 500 fatalities.[1,2] Low-altitude windshear can take several forms, including macroscopic forms such as cold-warm gustfronts down to the small, intense downdrafts known as microbursts. Microbursts are particularly dangerous and difficult to detect due to their small size, short duration, and occurrence under both heavy precipitation and virtually dry conditions. For these reasons, the real-time detection of windshear hazards is a very active field of research. Also, the advent of digital ground-to-air datalinks and electronic flight instrumentation opens up many options for implementation of windshear alerts in the terminal area environment. Study is required to determine the best content, format, timing, and cockpit presentation of windshear alerts in the modern ATC environment to best inform the flight crew without significantly increasing crew workload.

II. Ground-Based Windshear Detection and Warning

A. Ground-Based Detection Technology

Ground-based windshear detection will play a large role in near-term windshear alerting and avoidance systems. The currently operational Low-Level Windshear Alert System (LLWAS), networks of anemometers around an airport and its approaches, are being expanded at some airports and are more capable of detecting windshears that impact the ground within the network boundaries. More importantly, ground-based Doppler weather radar systems such as Terminal Doppler Weather Radar (TDWR) and Doppler processing of ASR-9 radar data are becoming available and are capable of locating and measuring windshear events throughout the terminal area. These systems will provide the core data for near-term windshear alerting systems. Airborne predictive (look-ahead) sensors currently in the R&D phase—such as infrared radiometers, airborne Doppler radars, and lidars—will supplement ground-derived data as they become available and economically feasible. Airborne in situ or reactive windshear sensing, provided through comparison of airspeed measurements with inertial accelerometer measurements, is a currently available technology that can provide flight crews with warning once windshear penetration has occurred.

B. Integrated Ground-Based Systems

Assuming the near-term (early 1990s) deployment of both ground-based Doppler weather radars and the Mode-S ground-to-air digital datalink, possible paths of information flow are illustrated in Fig. 1. In this environment, data from LLWAS and TDWR sensors can be combined with pilot reports (PIREPs) to form the current windshear database. These PIREPs may be verbal or reported automatically by an airborne inertial sensor over the digital datalink. This data then can be processed to varying degrees and transmitted to the aircraft via voice communications or digital datalink. Several issues are raised by this implementation. One of these is the degree of data processing done; this can range from transmission of essentially raw data (as in the original LLWAS implementation, for example) or complete processing of the data into an executive decision to close the runway. One consideration is purely operational: what should be the distribution of decision-making responsibility between the pilot and the ATC controller? Another consideration is technical: given the available weather information, what is the (quantitative) hazard posed by the current weather situation to a particular aircraft or aircraft type?

Another of these issues is the "crew interface," the procedure and method used to inform the crew of a hazard. An essential difficulty in presenting windshear information is the need for alerts during descent and final approach, which are high workload phases of flight. For this reason, design of the crew interface is critical; a poor interface will result in loss of information or increased crew workload. The advent of electronic cockpits and digital ground-to-air datalink opens up a variety of options for implementation of the crew interface. Some issues to be examined include information content, message format, and mode of presentation.

C. Research Focus

The specific focus of this research has been the evaluation, transmission, and presentation of ground-based Doppler

Presented as Paper 90-0566 at the AIAA 28th Aerospace Sciences Meeting, Reno, NV, Jan. 8–11, 1990; received March 1, 1990; revision received April 6, 1991; accepted for publication April 8, 1991.

*Research Assistant, Department of Aeronautics and Astronautics.

†Associate Professor, Department of Aeronautics and Astronautics. Associate Fellow AIAA.

Supported by government grant. See Acknowledgments.

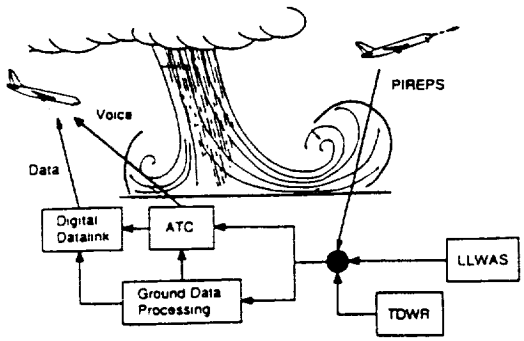

Fig. 1 Integrated ground-based windshear alerting system.

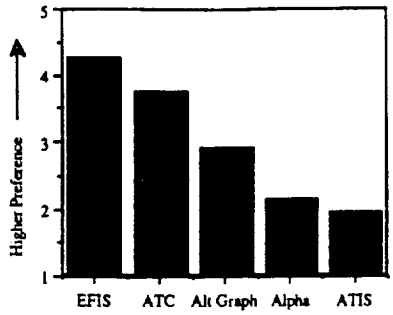

Fig. 2 Pilot rankings of possible relay/presentation modes for ground-generated wind shear alerts.

weather radar derived information through a limited bandwidth digital datalink (Mode-S). The first issue studied is the content and cockpit presentation of uplinked windshear alerts. User input was solicited through pilot opinion surveys and then used to design a part-task simulation experiment. The primary results deal with the use of electronic instrumentation for presentation of uplinked information, specifically the relative merits and disadvantages of voice, alphanumeric (textual), and graphical modes of presentation. In this context, *voice* or *verbal* mode refers to standard ATC radio communications, *alphanumeric* or *textual* mode refers to presentation (on some electronic or paper device) of the literal text of a message, and *graphical* mode refers to a combined pictorial/text presentation of the alert information on some electronic map or map-like display. Alphanumeric and graphical presentations presuppose the existence of a ground-to-air digital datalink.

The second issue examined is the evaluation of ground-measured windshear data to determine a hazard index. This hazard index should both be able to accurately quantify the windshear hazard present and be used to generate a meaningful alert for the flight crew. Overwarning must be minimized, since a large number of false or nuisance alerts can disrupt airport operations and damage pilot confidence in the alerting system. Preliminary analysis has identified some of the issues and problems involved, and further work is in progress.

III. Crew Interface Issues

A. Pilot Opinion Surveys

To obtain user input on both current windshear alert systems and requirements for future systems, a pilot opinion survey was conducted. With the cooperation of the Airline Pilots Association and United Airlines, responses were collected from 51 line pilots of transport category aircraft with autoflight systems (Boeing 757, 767, 747-400). Significantly, 51% of the respondents have had what they considered to be a hazardous windshear encounter; most of these occurred at Denver-Stapleton airport, a UAL hub and an area noted for heavy microburst activity during the summer months. It should also be noted, however, that pilots who have had a hazardous windshear encounter may have been more likely to respond to the survey. Some general results are the following:

1) Most of the pilots (90%) agreed that "microbursts pose a major safety hazard to transport category aircraft."

2) Only 15% of the respondents agreed that "currently available windshear alert data is sufficient for safe operation in the terminal area," while 44% disagreed.

3) *All but one* (98%) of the pilots felt that "a system to provide aircrews with better and more timely windshear alerts is *necessary*."

These responses clearly indicate that pilots are dissatisfied with current windshear alert data and would be receptive to improvements. The pilots were also asked to rate the usefulness of currently available windshear data. Significantly, PIREPs and visual clues were rated more useful for windshear avoidance than LLWAS. However, neither PIREPs or visual information are always available. This emphasizes the need for improved remote detection and advance warning and the importance of good PIREP collection and distribution. A digital datalink would be very useful in this application.

Another set of questions dealt specifically with the use of a ground-to-air datalink and an EFIS to display windshear (specifically microburst) alerts. Responses indicated that pilots are receptive to graphic displays (Fig. 2). The specific suggestion of integrating windshear information with an EFIS moving map display was strongly supported, ranking 4.3 out of 5. Also of interest was the high preference for ATC voice alerts (3.9/5), which is likely a result of a practiced ability to interpret radio communications. Display of wind shear alerts on some alternate graphical display (other than the EFIS moving map) was also ranked above alphanumeric displays and ATIS. Comments indicated that the low ranking of ATIS was due to the long time between updates.

Due to time limitations of VHF verbal communications and bit limitations of digital datalinks, the amount of information space available for a given alert is limited. For this reason, message content is critical. Thus, a question dealing with the message content of microburst alerts was included. The responses indicated that location and intensity of microbursts are clearly the most important items of information. Size, microburst movement, and intensity trends are of secondary importance. Ranking of this information allows design of alerts that fit within the message length constraints and still retain enough information to be useful. In this case, the data indicates that the message must include location and intensity. Later comments from the part-task simulation experiment subjects indicated that size would be desirable also, since it is in some sense related to the intensity.

The survey also addressed timing of microburst alerts. There was no consensus as to in what phase of flight (i.e., when during the descent and approach) alerts should be given; the most common response was "as soon as detected." This topic needs to be further examined, since the high workload environment during terminal area operations makes timing of the warning crucial.

A codistributed survey was specifically concerned with use of a Flight Management Computer (FMC) in concert with an EFIS and was intended to evaluate crew acceptance and use patterns of these automated systems. Regardless of flight hours with the FMC, pilots expressed a decided preference for automated aircraft over nonautomated ones, with an overall mean of 82%. In general, crews were enthusiastic about the EFIS, which supported the preference for graphical alerts expressed during the windshear survey. The complete findings from this survey are presented in Ref. 3.

B. Flight Simulator Study

The purpose of the part-task simulator study was to compare message presentation modes—verbal, alphanumeric, and graphical as defined in Sec. II. C—on a modern "glass cockpit" aircraft. This was done for both uplinked microburst windshear alerts and for ATC clearance amendments in the terminal area.

Simulator Design

The Boeing 757/767 class of aircraft with its Electronic Flight Instrumentation System (EFIS) was (approximately) simulated (Fig. 3). The primary instrumentation was displayed on an IRIS 2400T color graphics workstation. It included a good fidelity representation of the EFIS displays, including the EHSI and the Electronic Attitude Director Indicator (EADI). Airspeed and altitude were displayed as moving tapes (as in the 747-400 aircraft), and a vertical speed indicator was also included. A window for display of alphanumeric wind shear alerts was provided. A low-priority tracking sidetask was included for workload adjustment and monitoring. The EHSI display was controlled through an external control panel that allowed the pilot to change EHSI modes (MAP or ILS) and the display range and to suppress unwanted off-route information.

The Control Display Unit (CDU) for data entry into the FMC was simulated with an IBM/XT computer. It provided the necessary subset of the FMC functions required for the simulation. Non-FMC control of the aircraft was performed through an autopilot panel, similar to the glareshield panel on the 757/767. The standard autothrottle and autoflight systems were available, including FMC-programmed lateral and vertical path guidance and the various capture ("select") and hold modes for airspeed, heading, vertical speed, and altitude guidance.

An ATC workstation was located in a separate area. The controller received live audio and video of the simulation area, which were recorded. The controller monitored the experiment, controlled the timing of ATC clearances and windshear alerts, and communicated with the pilot through a voice link.

This experiment was concerned with cognitive decision-making issues rather than the details of pilot performance. Therefore, controls and instruments not related to the particular cognitive task at hand were not simulated. The lack of a copilot and imposition of a sidetask compensated for the workload loss. The subjects generally agreed that the simulation was accurate for the tasks they were asked to perform. Also, no windshear dynamics were included, in that the data of interest was the go/no-go decision and whether or not penetration occurred. The major advantages of the part-task simulator are the ease of setup and operation and the flexibility of the electronic displays. Alphanumeric and graphical message formats are easy to implement and change.

Scenario Design

Nine descent and approach scenarios into the Denver-Stapleton airport were devised. The Denver terminal area was selected for two reasons: 1) the high incidence of dry microburst activity observed there, and 2) the large number of possible descent profile and landing runway combinations. The inclusion of both ATC amendments and microburst alerts in the same scenario was useful in preventing the subject from anticipating repeated windshear alerts.

Each scenario was divided into two phases. The aircraft started at the outer limit of the terminal area with an initial flight plan, which was preprogrammed into the FMC. During descent, three amendments that required reprogramming of the FMC for compliance were given. Of these, one was "unacceptable," implying that the pilot should have taken some corrective action such as requesting clarification or a new routing. The pilot was unaware that any of the amendments were going to be unacceptable.

The second phase of the scenario began when the aircraft was vectored onto the final approach course. Windshear alerts could occur after this point. Microbursts were positioned either as a *threat* on the approach path or as a *nonthreat* on the approach or departure end of another runway. In addition, microbursts were sometimes positioned on the missed approach path. The alert was given either close in (at the outer marker, 6 to 9 n.mi. from touchdown) or further out (20 n.mi., with a second message at 10 n.mi. from the runway threshold). The microburst alerts always contained warnings for all possible approach runways, not only the one being used by the simulated aircraft. This was to measure the pilot's ability to discriminate between threatening and nonthreatening situations.

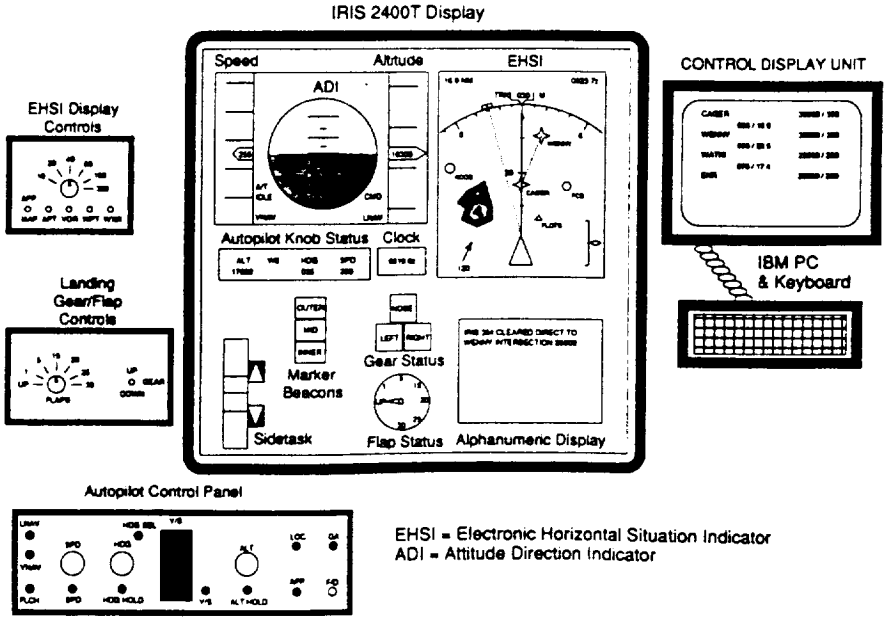

Fig. 3 Boeing 757/767 part-task simulator.

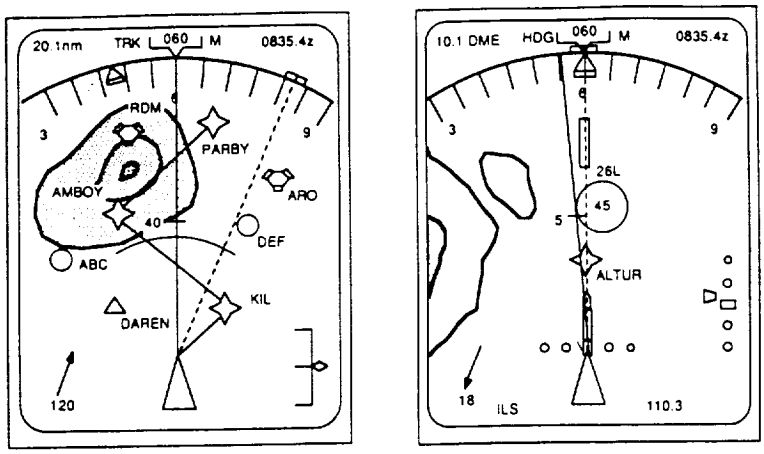

Fig. 4 Boeing 757/767 EHSI display modes: MAP (left) and ILS (right).

The nine scenarios were divided into three sets of three by presentation mode. In each block, all amendments and windshear alerts were given in the assigned mode: verbal, alphanumeric, or graphical. Verbal clearance amendments were given according to current ATC operating procedures. Alphanumeric clearance amendments were activated remotely by the controller, generating an audible alert. The text of the message appeared on the CDU screen when called up by the pilot. In the graphical mode, activated clearance amendments appeared on the EHSI as an alternate route (dashed white line). These could be accepted or rejected with a single CDU keystroke. Pilots were not required to read back text or graphical amendments.

Verbal microburst alerts were given as radio messages by the controller. Text microburst alerts appeared in an alphanumeric window just below the EHSI display. The following is a typical verbal or text alert: "IRIS 354, Microburst Alert. Expect four-zero knot loss, 2 mile final approach runway one-seven-left." Graphical microburst alerts appeared in the appropriate location on the EHSI map (in both MAP and ILS mode) as flashing white circles with the intensity (headwind-to-tailwind divergence value in knots) drawn inside them. An example is shown on the ILS mode display in Fig. 4. Verbal cues were given (i.e., "IRIS 354, Microburst alert.") in all modes, so that the method and time of initial notification were kept constant. This would not be true of an actual cockpit, where an automated audible alert would most likely be used. Over the subjects tested, all scenario blocks were tested in all the modes, and the order in which the subject encountered the modes was rotated. This process was used to attenuate learning and scenario-dependent effects.

With the approval of the Air Line Pilots' Association, eight active 757/767 line pilots volunteered for the experiment. The subjects were all male; five were captains, and three were first officers. The pilots ranged in age from 30 to 59 years, with a mean of 47 years. In addition, several other pilots of varying experience assisted in the development of the simulator and the scenarios.

Experimental Procedure

At the start of the session, the pilot was asked to complete the first stage of a NASA-designed workload evaluation,[4] which asked him to prioritize the different types of workload for the specific task of flying a 757/767 aircraft. Next, the features of the simulator were demonstrated. A sample scenario was used to demonstrate all of the three modes for both phases of flight. When the subject became comfortable with the operation of the simulator, the test scenarios began. At the start of each scenario, the pilot was given an initial clearance into Denver-Stapleton and had all the necessary charts to make the approach. Each of the nine scenarios lasted from 20 to 35 min. During the flights, one of the experimenters served as the ATC controller and one remained in the cockpit with the pilot to answer questions about physical operation of the simulator. After each scenario the pilot completed a separate subjective workload evaluation sheet for the descent phase (the clearance amendment task) and for the approach phase (when microburst alerts were given). After all of the scenarios, there was a debriefing session in which the pilot's impressions of the simulator and the presentation modes were solicited.

Results

Three forms of numerical data—pilot performance, workload, and preference—were taken. The measure of pilot performance for the microburst alerts was the percentage of "correct decisions" made in each presentation mode. An incorrect decision was scored for either 1) avoidance action taken when none was necessary, or 2) no avoidance action was taken in a clearly hazardous situation. The fewest incorrect decisions (8%) were made with graphical microburst alerts, the next fewest (17%) with verbal alerts, and the most (27%) were made with text alerts. This indicates that text alerts may actually degrade performance relative to verbal alerts, likely due to the greater comprehension time associated with reading the text message. It is also important to note that pilots are very experienced and comfortable with verbal radio communications. The positional information contained in the graphical mode actually led several pilots to request and program nonstandard missed approach procedures in advance to avoid the windshear areas completely. When the pilots were given the information in the other modes, this was generally not observed.

The NASA Task Load Index[4] was selected to assess workload for both tasks in each of the modes. This scale divides workload into six components: mental demand, physical demand, temporal demand, effort, frustration, and performance. The ratings were made along a continuum from "very low" to "very high." Weightings for each of the aforementioned six factors are obtained individually for each subject through a paired comparison task during subject orientation. The weights are simply the number of times a particular component was chosen to be a more important contributor to workload.

The overall workload ratings for each mode are plotted in Fig. 5. For both tasks, workload for the graphical mode was significantly lower than the workload for the verbal and textual modes. The six subscale ratings all showed a similar trend. The appearance of greater workload induced by the textual condition is not a significant effect.

Pilot comments and subjective evaluations of the presentation modes were obtained through loosely structured post-

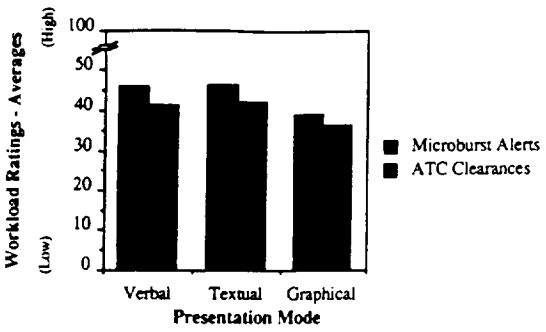

Fig. 5 Part-task simulation results—subject workload by mode.

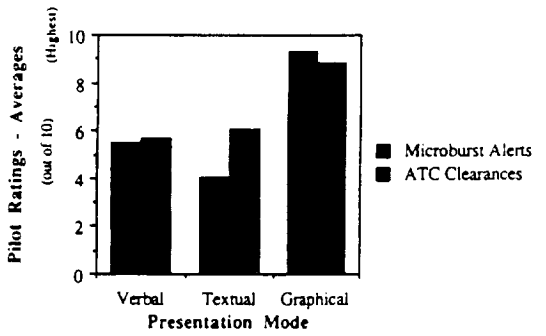

Fig. 6 Part-task simulation results—pilot preference by mode.

experiment interviews. In their evaluation of the modes, pilots overwhelmingly preferred the graphical mode of communication (Fig. 6), which is consistent with the survey results. For the windshear alerts, the text mode was consistently rated less desirable than the verbal mode. This was not the case for clearance amendments. Although the text and verbal modes seemed to be equally desirable from the averaged ratings, in fact, some pilots greatly preferred the text mode over the verbal, while others preferred the exact opposite (hence the midrange average value). All pilots indicated that they were comfortable with current verbal procedures, though, so they did not feel that the advantages of the text mode were significant.

Some further observations were taken from the experimenters' notes and pilots' comments. First, textual alerts given in time-critical situations, such as final approach, were thought to require too much head-down time. Second, digitally transmitted information in either mode, textual or graphical, leads to a loss of voice inflection information. Since controllers sometimes use voice inflection to distinguish urgent alerts from normal communications, this is in some sense a loss of information. Third, digitally transmitted information, if directed to specific aircraft, prevents pilots from hearing instructions given to other aircraft in the terminal area ("party-line" information). Some pilots stated that hearing the communications to other aircraft in the vicinity gave them a better understanding of the overall situation and enabled them to be better prepared when an alert arrived. Other pilots indicated that they could do without the information.

To obtain the benefits of graphical messages, the detailed format of such messages must be carefully designed to present only the necessary information in clear fashion without clutter or data overload. In the case of windshear alerts, the pilots identified this minimum presentation to be a simple symbol showing location, approximate size, and intensity. The proposed Mode-S datalink, for example, allows 48 bits of useful information every 4 to 12 seconds in surveillance mode. This minimum alert presentation can likely be expressed in 24 bits or less, allowing two messages per scan. Therefore, the Mode-S link can possibly be used to display and track several microbursts, while keeping up with the 1 minute update rate achieved by TDWR in the current configuration.

IV. Hazard Assessment

The successful implementation of ground-measured windshear alerts requires an effective way of quantifying the windshear hazard. This hazard criterion must provide an accurate estimate of the danger to approaching and departing aircraft that can be easily interpreted by the flight crew. To maintain pilot confidence in a ground-based windshear avoidance system, an alert must correlate with what the aircraft is experiencing or will experience. Otherwise, even an accurate measurement can be perceived as a false alarm.

The alerting criterion used in the recent TDWR operational evaluations at Denver-Stapelton and Kansas City International airports (and in current testing, as well) is based on horizontal wind measurements. When a change in low-altitude horizontal winds above a threshold is measured (radial from the radar), the area is marked and quantified by the maximum radial shear measured within it. If this area is within the segments identified in Fig. 7, an alert is issued.[5,6]

One problem with this system is that a microburst that occurs in one of the boxes may in one case never encroach on the flight path and in another be right on the center of it. In either case, the same alert is issued. This means that approaching or departing aircraft may fly through the center of a microburst or almost entirely miss it, experiencing the entire event or nothing at all. This could be perceived as a false alarm by the pilot, although the windshear is present and may even be fairly close to his position. A recent report about the 1988 TDWR Operational Evaluation indicates that this could be a major issue.[7] Data was collected from 111 pilots who landed or took off during alert periods. (Since the microburst alerting software changed over the course of the 1988 Operational Evaluation, the pilot responses included in this calculation were those pilots who not only were alerted but also would have been alerted by the final version of the warning algorithm. The earlier version of the algorithm produced more alerts than the final one.) Of this group, 34% indicated that "nothing was encountered," whereas another 31% reported something like "nothing much was encountered." A "nuisance alarm" rate this high can unnecessarily disrupt airport operations as well as damage pilot confidence in the windshear alert system.

A portion of this problem may also stem from the intensity quantity used. The windshear quantity used in the alerts is derived from the maximum change in radial velocity over the area of shear. This number is reported in the alert as an *X* ". . . knot airspeed loss." In reality, for an axisymmetric microburst, this number represents about an *X*/2 airspeed gain followed by an *X* knot loss. This is not a reporting error, but crews should be aware that the quantity being measured is the maximum horizontal wind change over the shear and that the maximum airspeed loss relative to the reference airspeed before penetration is approximately one-half of the reported value.

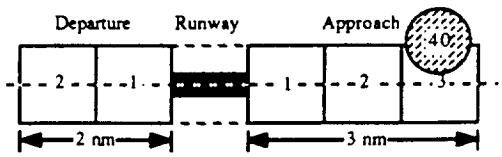

The alert corresponding to the 40 knot microburst pictured above might be:"United 226, Denver tower, threshold wind one six zero at six, expect a forty knot loss on three mile final."

Fig. 7 Windshear reporting zones for approach and departure: 1988 TDWR operational evaluation.

A more fundamental difficulty in using wind change or "airspeed loss" as the hazard criterion is that the hazard due to a microburst windfield is primarily a function of horizontal wind gradient and downdraft velocity rather than overall horizontal windshear. The critical danger is loss of aircraft total energy, which can be usefully defined as the sum of air-mass relative kinetic energy and potential energy measured with respect to ground level. The impact of the immediate windfield on the aircraft's rate of energy loss has been quantified by some researchers[8] as "F-factor"

$$F \equiv \frac{\dot{W}_x}{g} - \frac{W_h}{V} \tag{1}$$

where $\dot{W}_x$ is horizontal wind velocity (tailwind positive), g is gravitational acceleration, W_h is vertical wind velocity (updraft positive), and V is aircraft airspeed.

This quantity indicates the loss of climb rate (or effective excess thrust-to-weight ratio) due to the immediate windfield. It is clear, through examination of the windshear hazard in energy terms, that the energy loss the aircraft experiences can take the form of either airspeed or altitude loss. The proportion of these is a function of the control strategy employed. Therefore, F is a more compelling measure of the potential performance loss due to a microburst than total divergence.

Wind change, however, is convenient for intensity measurement since it can be measured directly by a ground-based Doppler radar. There are several problems with using ground-based radar measurements to estimate F. One is the inability to directly measure vertical wind velocity. A second relates to altitude variance. Microburst windfields can vary strongly over the lowest 1000 ft above ground level (AGL). A radar scan beam used for microburst detection has a finite beamwidth on the order of 0.5–1 deg. For a radar situated several miles from the airport (typical for TDWR), this implies that the radial velocity measurements are a weighted average over the lowest 500–1000 ft AGL. This makes estimation of peak horizontal shear more difficult.

A third difficulty is microburst asymmetry. For divergence estimating purposes, the asymmetry ratio of a microburst can be defined as the ratio of shear in the direction of maximum divergence to shear in the direction of minimum divergence. One study of Colorado microbursts[9] indicated an average asymmetry ratio of greater than 2 with extreme cases greater than 5; asymmetries of up to 5.5 were also measured in Oklahoma downbursts.[10] This indicates that a single Doppler measurement of one radial microburst slice (not aligned with the flight path) can significantly over or underestimate the shear along the flight path.

The problem is then estimation of F given the measurement limitations. The TDWR measurement of radial velocity also contains an estimate of microburst size (diameter along the radial slice), as well as the locations of other microbursts that may interact with the local wind field of global knowledge to identify and estimate F using characteristics. The reflectivity field is also known. The microburst itself can be modeled either with a suitable fluid dynamic model of microburst winds and/or measured statistics of naturally occurring microbursts. It should then be possible to combine the measured data with the microburst models to estimate the peak downdraft, peak horizontal shear, and hence the peak F that could be encountered within the microburst. Provided this problem can be solved, use of estimated F-factor as a hazard criterion for alert generation could reduce overwarning.

Another way to reduce "nuisance alerts," specifically in the case of microbursts laterally displaced with respect to the flight path, could be accomplished by modifications of the alert format. One possible change (proposed in Ref. 7) is to add the words "left," "right," or "center" to the alert to indicate the microburst position relative to the flight path.

Independent of changes in the hazard criterion or the alert format, the detrimental effects of nuisance alerts could be reduced by clarifying the actual meaning of the currently employed alert to flight crews. The possibility of a microburst being to the side of the flight path should be discussed, and the meaning of the microburst wind change value should be explained. Crews should also be aware of the measurement limitations of the sensing system.

V. Conclusions

A pilot opinion survey and a flight simulator experiment have been performed to examine issues related to dissemination of ground-measured windshear information to flight crews with and without a digital datalink. Survey results indicated that the currently available windshear avoidance information is not sufficient and that a better system is highly desirable. A preference for graphically presented microburst alerts was expressed, and some specific questions about the makeup and timing of microburst alerts were answered.

Simulation experimental results indicated that presentation of windshear alerts as graphical symbols on a moving-map display is significantly more effective than verbal alerts. Pilot performance improved, and pilot workload decreased. Both the survey results and comments from the simulation subjects indicated a strong pilot preference for graphical presentations. Presentation of windshear alerts as text on an electronic display proved inferior to standard verbal communications in terms of workload increase, pilot performance, and pilot preference. In the time-critical situation of windshear alerts, it was apparent that textual messages were more subject to misinterpretation than were verbal ones.

It is critical to the implementation of a ground-based windshear alerting system to quantify the windshear hazard both accurately and clearly. Overwarning can unnecessarily disrupt airport operations as well as damage pilot confidence in the windshear alert system. The system used in the 1988 TDWR Operational Evaluation was shown to result in a significant number of nuisance alerts, for which the pilots reported experiencing little or no windshear.[8] To address this problem, it is proposed that 1) a better method of assessing the windshear hazard be developed, and that 2) flight crews be better educated about the meaning of ground-generated windshear alerts.

The current method of generating windshear alerts from TDWR information has been examined, and some causes of overwarning have been identified. These causes fall into two groups: 1) the alert generation methodology, and 2) difficulties in quantifying microburst hazard from the available measurements.

Educating flight crews about the meaning of ground-generated alerts is equally as important as good hazard assessment. Some possible pilot errors in interpretation of the current alert format have been identified. By better informing flight crews about the details of the alerts and the limitations of the sensor system, the inevitable "nuisance alerts" that will be issued will not damage crew confidence in the system.

Acknowledgments

This work was supported by the MIT Lincoln Laboratory under contract BARR-10-119 and by the Federal Aviation Administration and the National Aeronautics and Space Administration under grants NGL-22-009-640 and NAG-1-690. The authors would like to thank the respondents, Rick Brown, and United Airlines for assistance with the pilot opinion surveys. The authors would also like to thank Divya Chandra, Steven Bussolari, Ed Hahn, Amy Pritchett, ALPA, and especially the pilots who volunteered their time and wisdom, all of whom contributed to the success of the simulator experiments.

References

[1]National Research Council, *Low Altitude Wind Shear and Its Hazard to Aviation*, National Academy Press, Washington, DC, 1983.

[2]Wolfson, M. M., "Characteristics of Microbursts in the Continental United States," *The Lincoln Laboratory Journal*, Vol. 1, No. 1, Spring 1988, pp. 49–74.

[3]Chandra, D., Bussolari, S. R., and Hansman, R. J., "A Comparison of Communication Modes for Delivery of Air Traffic Control Clearance Amendments in Transport Category Aircraft," 5th International Aviation Psychology Symposium, Ohio State University, Columbus, OH, 1989.

[4]Hart, S. G., and Staveland, L. E., "Development of NASA-TLX (Task Load Index): Results of Empirical and Theoretical Research," *Human Mental Workload*, edited by P. A. Hancock and N. Meshkati, Elsevier Science Publishers, Amsterdam, 1986.

[5]National Center for Atmospheric Research, "Terminal Doppler Weather Radar (TDWR): A Briefing Paper," Boulder, CO, July 1, 1988.

[6]Sand, W., and Biter, C., "TDWR Display Experiences," AIAA Paper 89-0807, Jan. 1989.

[7]Stevenson, L., "A PIREP-Based Analysis of the Candidate TDWR-Based Products and Services Evaluated at Stapelton International Airport During the Summer of 1988," Federal Aviation Administration, Project Memorandum DOT-TSC-FA9E 1-89, draft copy, May 1989.

[8]Targ, R., and Bowles, R. L., "Investigation of Airborne Lidar for Avoidance of Windshear Hazards," AIAA Paper 88-4658, Sept. 1988.

[9]Wilson, J. W., Roberts, R. D., Kessinger, C., and McCarthy, J., "Microburst Wind Structure and Evaluation of Doppler Radar for Airport Wind Shear Detection," *Journal of Climate and Applied Meteorology*, Vol. 23, April 1984.

[10]Eilts, M. D., and Doviak, R. J., "Oklahoma Downbursts and Their Asymmetry," *Journal of Climate and Applied Meteorology*, Vol. 26, Jan. 1987, pp. 69–78.

Heat Transfer on Accreting Ice Surfaces

Keiko Yamaguchi* and R. John Hansman Jr.†
Massachusetts Institute of Technology, Cambridge, Massachusetts 02139

Based on previous observations of glaze ice accretion on aircraft surfaces, a multizone model with distinct zones of different surface roughness is demonstrated. The use of surface roughness in the LEWICE ice accretion prediction code is examined. It was found that roughness is used in two ways: 1) to determine the laminar to turbulent boundary-layer transition location and 2) to calculate the convective turbulent heat-transfer coefficient. A two-zone version of the multizone model is implemented in the LEWICE code, and compared with experimental convective heat-transfer coefficient and ice accretion results. The analysis of the boundary-layer transition, surface roughness, and viscous flowfield effects significantly increased the accuracy in predicting heat-transfer coefficients. The multizone model was found to significantly improve the ice accretion prediction for the cases compared.

I. Introduction

A. Background

In rime ice accretion, which occurs at cold temperatures, there is adequate convective heat transfer to rapidly freeze the impinging supercooled water droplets. The rapid freezing results in an opaque white ice due to entrapped air bubbles. Because of the rapid freezing, rime ice shapes are determined solely by the droplet impingement behavior; efforts to model rime ice accretion have been relatively successful.

In contrast, current efforts to analytically model glaze ice accretion are hampered by insufficient knowledge of the accreting ice surface roughness. In glaze icing, which normally occurs at temperatures near freezing or at high liquid water contents, there is insufficient convective heat transfer to remove all of the latent heat of freezing from the impinging supercooled water droplets. The water freezes slowly, resulting in a strong clear ice structure. The local ice accretion rate is controlled by the ability to remove latent heat and thus the local convective heat transfer. The droplet impingement behavior also plays an important role in determining where on the surface there is sufficient impingement that the surface is wet.

The local convective heat transfer from a surface is known to be strongly dependent on the ice surface roughness.[1] Because of the importance of heat transfer on the ice accretion rate, surface roughness becomes an important factor in modeling glaze ice accretion. Current analytical models such as LEWICE generally assume that the surface roughness is uniform and the effective sand grain roughness k_s is used as an input parameter in the code.[2,3] The magnitude of k_s, the roughness parameter, is normally determined empirically by comparison of predicted and experimental ice accretions. The erratic performance of glaze ice accretion models and the empirical manner in which the surface roughness is treated indicate the need for a more deterministic treatment of the surface roughness.

B. Multizone Model

In prior experiments, detailed observations of accreting ice surface roughness were made at several icing facilities.[4-6] As a result of the detailed photographic analysis of accreting ice surfaces in these facilities, distinct regions were identified each having a characteristic roughness and identifiable boundaries. Based on these observations, a multizone model, in which the accreting ice surface is divided into two or more discrete zones with varying surface roughness and water behavior, was proposed.

1. Surface Roughness Zones

A total of three roughness zones were identified. A typical ice accretion showing the three zones is shown in Fig. 1.

1) *Smooth zone*: Close to the stagnation point, the surface was observed to be uniformly wet with a thin film of water at warm temperatures. In this "smooth zone," the surface was smooth with no distinctively visible roughness.

2) *Rough zone*: At some point downstream, there was a sudden transition to a significantly rougher zone, where there appeared to be insufficient water to maintain a uniform film, and the water tended to coalesce into the water beads first observed by Olsen and Walker.[7,8] In this "rough zone," the ice accretion rate was observed to be enhanced compared to the smooth zone. This is thought to be due to increased heat transfer resulting from the greater surface roughness.

In certain glaze ice accretions, particularly at high liquid water contents, some of the roughness elements within all or part of the rough zone were observed to grow into distinct protuberances. With higher collection efficiency and enhanced heat transfer, these protuberances tended to grow rapidly resulting in horned ice accretions.

3) *Runback or rime feather zone*: Behind the impingement region, aft of the rough zone, ice was observed to accrete by two different processes, depending on temperature. At warm temperatures, a runback zone was observed aft of the rough zone, which was characterized by areas of ice interspersed with un-iced surface. The surface water was observed to initially runback and then stagnate at the point of flow separation, where this water slowly froze as rivulets or as large coalesced water cells. At cold temperatures, rime feathers were sometimes observed to grow in the region aft of the primary accretion. The feathers were dry ice accretions, which propagated in the local upstream direction.

2. Roughness Transition Location

The angular position of the boundary between the smooth and rough zones has been experimentally observed as a function of time for cylinders. A typical example is shown in Fig. 2 for a 1 in. diameter cylinder. This data was obtained using the technique discussed in Sec. IVA. The initial location of roughness transition is believed to be caused by, and to coincide with, the location of the boundary-layer transition from

Presented as Paper 90-0200 at the AIAA 28th Aerospace Sciences Meeting, Reno, NV, Jan. 8-11, 1990; received April 6, 1990; revision received Feb. 15, 1991; accepted for publication March 5, 1991.

*Research Assistant. Student Member AIAA.
†Associate Professor. Associate Fellow AIAA.

Supported by government grant. See Acknowledgments.

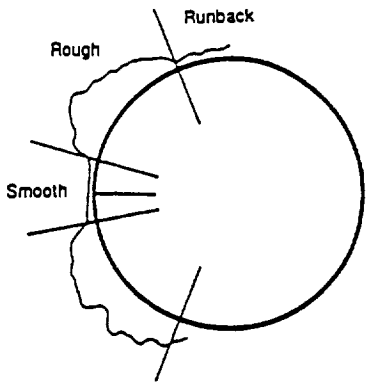

Fig. 1 Typical glaze ice shape for a 2-min exposure on a 1-in. cylinder showing the three distinct roughness zones ($T = -4.5°C$, $V = 150$ kt, liquid water content = 1.0 g/m³, and median volumetric diameter = 30 μm).

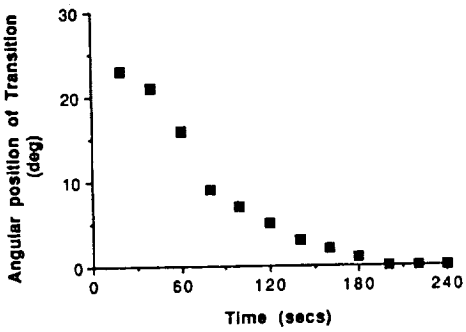

Fig. 2 The angular position vs time of smooth-rough transition location ($T = -7°C$, $V = 125$ kt, liquid water content = 0.8 g/m³, and median volumetric diameter = 12 μm).

laminar to turbulent. Experimentally, the rough/smooth transition was observed to propagate with time towards the stagnation region for a wide variety of icing conditions. The effect of icing cloud parameters on the transition location has been studied in an attempt to identify the underlying physical mechanisms that cause the rough surface to develop. It was found that higher velocity tends to move the initial location of the transition closer to the stagnation point. Warmer temperatures and higher liquid water contents tend to move the transition point more quickly towards the stagnation region.

Observations that the smooth/rough transition depends on Reynolds number indicate that the initial transition in surface roughness is caused by boundary-layer transition. In these cases, the laminar/turbulent boundary-layer transition point will also be the initial smooth/rough transition point. In the laminar region, the heat transfer is low enough that all of the latent heat cannot be removed and the surface is coated by a uniform water film. However, the enhanced heat transfer in the turbulent region can cause sufficient freezing to partially dry the surface and cause bead formation, which results in the increased roughness and the increased heat transfer observed in the rough region.

The influence of surface water flow on the smooth/rough transition location also indicates that dynamic effects are important. It is thought that the dynamic effects are caused by bead formation at the interface between the smooth and rough surface zones as shown in Fig. 3. The formation of these beads at the interface causes enhanced heat transfer within the rough zone, which tends to freeze out the downstream beads and dry the surface. As the surface dries, beads begin to form further upstream and the transition point will propagate towards the stagnation region as observed experimentally. As

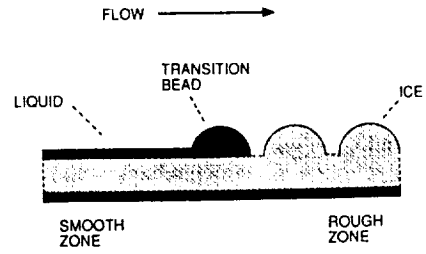

Fig. 3 Schematic representation of bead formation at the smooth-to-rough transition.

roughness moves upstream, the boundary layer is tripped and will move with the roughness transition. By increasing the surface water flux, the rate of formation and growth of the interfacial beads is increased. This causes the observed faster upstream propagation of the transition point with increased surface water flux.

Based on the experimental observation of the smooth/rough transition location, it was determined that for some cases, the initial smooth/rough transition occurs on the laminar/turbulent boundary-layer transition point. Therefore, for the purposes of ice accretion prediction, it is hypothesized that the smooth/rough transition location can be assumed to coincide with the laminar/turbulent boundary-layer transition.

3. Model Description

In contrast to the conventional techniques that assume uniform roughness over the entire ice accretion, the multizone model is divided into two or more discrete zones with varying surface roughness and surface water behavior to be consistent with experimental observations.

In the simplest version of the model, the surface is divided into two zones, the "smooth" zone and the "rough" zone. In the "smooth" zone, corresponding to the smooth region centered about the stagnation line, the surface is uniformly wet, with thin water film runback. The heat transfer is that for a laminar boundary layer and a Messinger[9] type water runback model used in the original LEWICE code appears to be valid.

In the "rough" zone, surface tension effects are important and the characteristic water beads or roughness elements appear. Here, the heat transfer is enhanced due to increased roughness and the experimental results have indicated no water runback in this region for some cases.[5-8]

II. Implementing the Multizone Model Through Boundary-Layer Transition

Based on the hypothesis that the smooth/rough transition location coincides with the laminar/turbulent boundary-layer transition, a simple more physically realistic multizone model was implemented in the LEWICE code. Basically, the smooth and rough zones were considered to coincide with the regions of laminar and turbulent boundary layer, which are treated separately when calculating heat transfer in LEWICE. In order to implement the multizone model effectively, the use of surface roughness in the LEWICE code was examined. The multizone model was then implemented in the LEWICE code through boundary-layer transition in order to evaluate the effectiveness of the model.

A. Use of Roughness in LEWICE

In the original LEWICE code, the only roughness parameter is the equivalent sand grain roughness height k_s. This parameter, which is one of the most important factors in determining the ice shape,[7,8] is used in two ways. One use is to determine the location of boundary-layer transition from laminar to turbulent, and the other is to calculate the magnitude of heat transfer in the turbulent region.

The boundary-layer transition is determined in the laminar region with reference to a critical Reynolds number based on

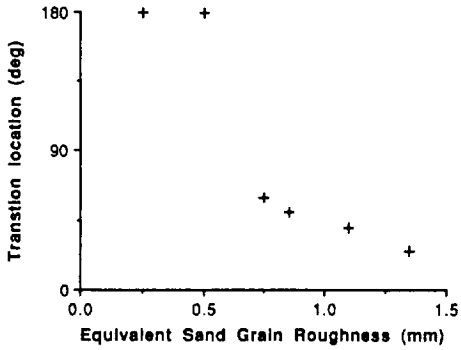

Fig. 4 Effect of k_t in the laminar region on the transition location.

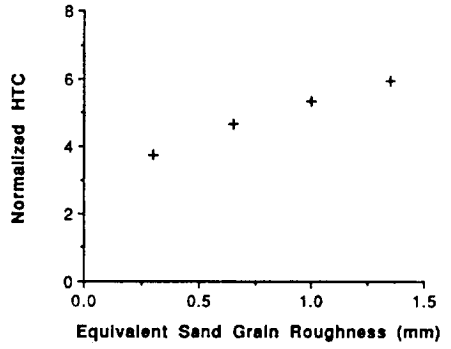

Fig. 5 Effect of k_t in the turbulent region on the magnitude of the heat-transfer coefficient (Note: Normalized $HTC = HTC/\sqrt{Nu}$).

the roughness element height and local velocity. This Reynolds number is

$$Re_t = \frac{k_t v_k}{\nu}$$

where k_t is the roughness element height in the laminar region, v_k is the air velocity at distance k_t from the surface, and ν is the kinematic viscosity of the air. When this local Reynolds number exceeds a critical value of 600, the boundary layer is transitioned to turbulent,[10] and any region downstream of this point is considered to have turbulent boundary layer. The effect of varying k_t in this region on the transition location is demonstrated in Fig. 4 by running LEWICE on a 0.15-m-diam cylinder at a velocity of 25 m/s and temperature of 0°C. It is noted that no transition occurs until a value of k_t above 0.5 mm. At higher values, the transition location propagated towards the stagnation region with increasing k_t.

In the laminar region, the heat transfer is independent of the roughness element height, assuming the roughness height is less than the boundary-layer thickness. In regions with a turbulent boundary layer, the roughness element height is used in another way. Here, roughness plays an important role in the heat transfer. Calculation of the heat-transfer coefficient in the turbulent region involves a complicated set of equations based on flow parameters, roughness, and the geometry of the accreting body, including the roughness element height.[3] Because of the complexity of these equations, it is very difficult to determine the effects of the equivalent sand grain roughness k_t on the turbulent heat transfer analytically. However, these effects of k_t on heat transfer were observed numerically using the LEWICE code. An example is shown in Fig. 5 where the convective heat-transfer coefficient (HTC) normalized by the square root of the Nussult number (i.e., normalized $HTC = HTC/\sqrt{Nu}$) is plotted against k_t, for a 0.15-m-diam cylinder at a velocity of 33 m/s and temperature of 0°C. It was found that increasing k_t significantly increased the heat transfer in the turbulent region.

Because of the manner in which roughness is treated in the LEWICE code, it is possible to separate the surface roughness in the laminar and turbulent regions. The laminar roughness value is then used to determine the laminar to turbulent boundary-layer transition location. The turbulent roughness is used to calculate the heat-transfer coefficient in the turbulent region.

B. Implementation of the Multizone Model

In order to evaluate the effectiveness of the multizone model, a simple two-zone version was implemented in the LEWICE code. For the first time step, different roughness are used for the laminar and the turbulent regions. In subsequent time steps, the boundary-layer transition point is made to propagate towards the stagnation line in a manner consistent with experimental observations of the smooth/rough transition. In order to avoid errors due to improper boundary-layer transition placement in these initial evaluations, the transition location was input to the code from the experimental measurements of smooth/rough transition migration such as those shown in Fig. 2. It should be noted that a deterministic prediction of the smooth/rough transition migration valid for all geometries and based on nominal code inputs is necessary for a full implementation of the multizone model.

For the initial time step, the user can input two different roughness element sizes, one for the laminar region k_t and another for the turbulent region k_t. As explained in Sec. IIB, the roughness element height is used in LEWICE for different purposes in the two regions. By separating the two, it is possible to control the transition location and the turbulent heat transfer independently. This method more closely emulates the physical situation where two different roughness element heights have been observed in the smooth and rough regions. In the laminar region, a roughness height k_t corresponds to the roughness of the uniform water film found in the experimental observations. In the turbulent region, the roughness height k_t corresponds to the roughness size observed in the rough zone. This method is valid only for the first time step where the transition location is determined mainly from the boundary-layer instability and the dynamic effects of surface water are negligible.

For subsequent time steps, the angular locations of the laminar to turbulent transition point as a function of time are specified based on the experimental data. The roughness element height k_t for the turbulent region still needs to be specified. For some cases, however, the experimental results have indicated that freezing fraction is unity (i.e., all impinging water freezes) in this region. For these cases, the ice shape is not dependent on the roughness element height that user chooses, since k_t is large enough to ensure that there is enough heat transfer to remove all of the latent heat.

III. Ice Shape Comparisons on Cylinders

A. Comparison with Original LEWICE

In order to investigate the discrepancy that had been observed between the experimentally observed roughness element sizes and the recommended roughness element size in LEWICE,[4] several original LEWICE runs were compared to the experimental heat-transfer coefficient data of Achenbach for rough 0.15-m-diam cylinders.[1] The measurements provide convective heat transfer coefficient data for cylinders with known surface roughness sizes at various Reynolds numbers. In the following figures, θ indicates the angular position along the cylinder, where 0 deg is the stagnation point. The vertical axis indicates the heat transfer coefficients normalized by the square root of the Nussult number.

A typical heat transfer comparison is shown in Fig. 6 for a case with $Re = 1.27 \times 10^5$ and a moderate roughness element

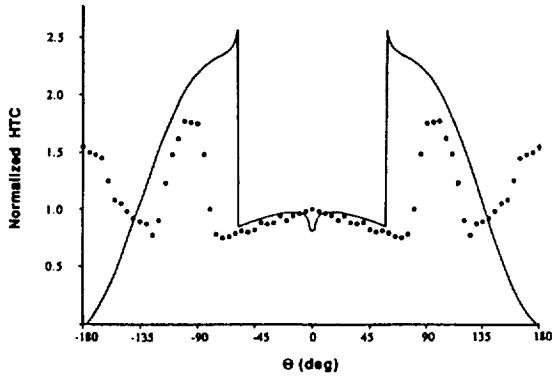

Fig. 6 LEWICE predicted and Achenbach measured heat-transfer coefficients for a cylinder with equivalent sand grain roughness k_s = 0.115 mm and Re = 5.9 × 10^5 (Note: Normalized HTC = $HTC/\sqrt{Nu}$).

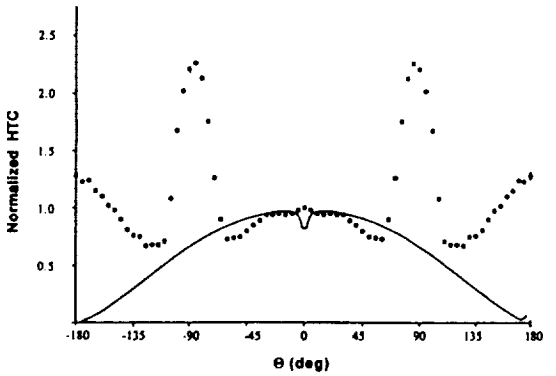

Fig. 7 LEWICE predicted and Achenbach measured heat-transfer coefficients for a cylinder with equivalent sand grain roughness k_s = 0.45 mm and Re = 1.27 × 10^5 (Note: Normalized HTC = $HTC/\sqrt{Nu}$).

size k_s of 0.45 mm. In this case, the heat transfer is well-predicted in the laminar region. However, where the transition to a turbulent boundary layer is indicated by a rise in the Achenbach heat transfer data at 75 deg, LEWICE predicts transition further forward at 57 deg. This discrepancy can be explained by one of the following hypotheses. One is that the roughness element height k_s used to calculate the critical transition Reynolds number is not correct. The other is that the transition model, based on the critical roughness element Reynolds number of 600, is not valid for this case.

The comparisons shown in Fig. 6 also indicate a difference in the magnitude of heat transfer predicted in the turbulent region. LEWICE can be seen to clearly overpredict the heat transfer in this region. This result indicates the need to further investigate the effect of roughness on heat transfer in the turbulent region.

Another comparison is shown in Fig. 7 for a case with Re = 5.9 × 10^5 and a small roughness element height k_s of 0.115 mm. Here, LEWICE does not predict transition at all, where the experimental result indicates a transition at 63 deg. For this case of very small roughness element size, the transition model is clearly not valid, since it fails to predict transition at all, indicating a limit of the critical transition Reynolds number theory.

B. Effect of External Flowfield Model

Because the local convective heat transfer coefficient is strongly dependent on the external flow velocity on the surface, errors in the velocity field will manifest as errors in the convective heat transfer coefficient. This can be seen in Fig. 6. Because LEWICE uses an inviscid flow model, it cannot accurately calculate the flowfield in the separation region behind the cylinder. This is thought to be the cause of the large discrepancy between LEWICE and the experimental results in Fig. 6 for angles greater than 135 deg.

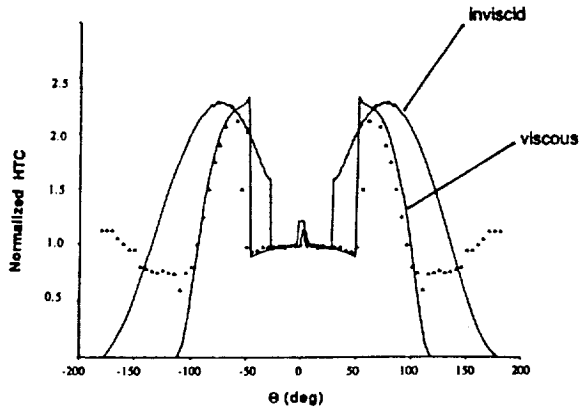

Fig. 8 A comparison of normalized heat-transfer coefficients calculated viscous and inviscid flowfields (Re = 7.3 × 10^4 and k_s = 1.35 mm).

The inability of LEWICE to accurately calculate heat transfer in separation and recirculation zones may be significant for glaze ice modeling where such regions are common behind "horn-shaped" ice accretions. It should be noted, however, that there is very little droplet impingement in the recirculation regions and that the heat transfer discrepancies will be most apparent in ice accretions where there is surface water runback into the recirculation region.

In order to verify that it is possible to predict heat transfer more accurately using the LEWICE methodology with a more accurate velocity field, the potential flowfield was replaced with a well-documented empirical formula for cylinders.[11] The heat transfer was calculated using the empirical flowfield and an example is shown in Fig. 8. In this comparison, the critical Reynolds number was set at 975 to match the boundary-layer transition location based on the known roughness element height of 1.35 mm. It can be seen that the heat-transfer prediction was significantly improved by the use of the viscous flowfield and a more accurate prediction of boundary-layer transition location.

IV. Comparison with Experimental Ice Accretion Data

A. Experimental Setup

In order to obtain roughness transition locations as a function of time on well-defined ice shapes for comparison with the multizone model, detailed observations of accreting ice shapes on cylinders at various cloud conditions were made at the B. F. Goodrich Ice Protection Research Tunnel. A series of 1-in.-diam cylinders were observed at a freestream velocity of 125 kt. The liquid water content (LWC) ranged from 0.4–1.5 g/m^3 with median volumetric diameter (MVD) of 11–40 μm. The tunnel total air temperatures varied from 0°C to −15°C.

The photographic setup used in the tunnel is shown in Fig. 9. The cylinders horizontally spanned the test section. The test section walls had heated glass windows to provide photographic access. Two charge-coupled device (CCD) high-magnification microvideo cameras were used to obtain a graz-

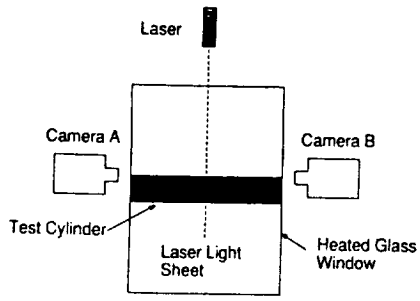

Fig. 9 Schematic diagram of the photographic setup in the icing wind tunnel.

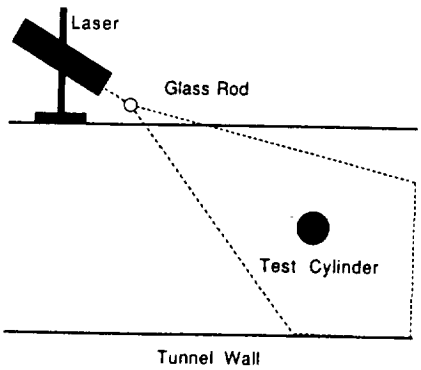

Fig. 10 Schematic diagram of the fan laser beam setup in the icing wind tunnel.

ing angle view of the ice accretion. The cameras were focused at the central region of the tunnel where the cloud was most uniform.

A laser light sheet was used to illuminate a plane perpendicular to the test cylinders to accurately identify the plane of focus (Fig. 10). With the laser sheet, it was possible to record on video and still cameras the details of accreting ice shapes and roughness at a single spanwise location. Because the rougher surface in the rough region increased the internal reflection, the ice shape appeared brighter in the rough region, which allowed an accurate identification of smooth to rough transition point. The external light inside the tunnel was turned off at a specific time interval, usually 20 s, providing enhanced details in the laser illuminated ice shape.

B. Comparison of Actual and Predicted Ice Shapes

An example of actual and predicted ice shapes using the multizone LEWICE code and the original LEWICE code values for a 4-min ice accretion at 20-s intervals is shown in Fig. 11. The icing cloud condition was −7°C, 125 kt, LWC of 0.8 g/m³, and a MVD of 12 μm. The angular position of transition was measured from the video recordings at 20-s intervals and is shown in Fig. 2. Characteristically, the transition was observed to migrate towards the stagnation region with time. For the original LEWICE case which used a recommended[3] roughness height value of 0.04 mm, a relatively thin conformal ice accretion was predicted. However, for the multizone case, the smooth and rough ice accretion zones significantly improved the prediction of the overall ice shape, showing a good correlation between the experimental ice accretion and predicted ice accretion using the multizone version of LEWICE. Although additional validation cases must be run, the initial improvement of the multizone prediction is encouraging.

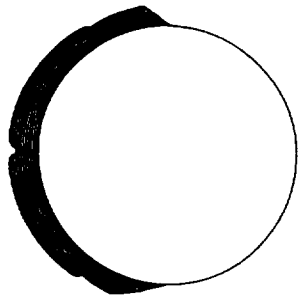

a) Original LEWICE prediction

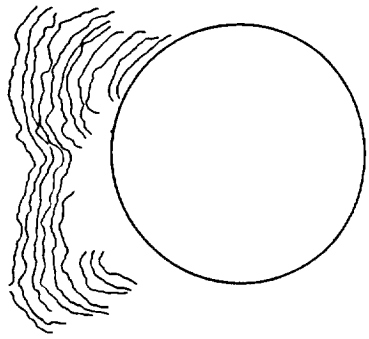

b) Experimental ice shape

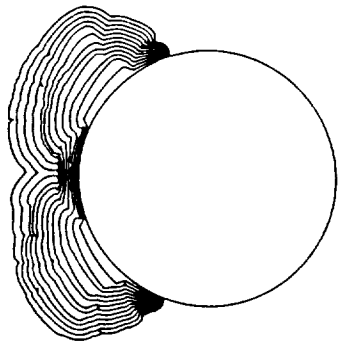

c) Multizone LEWICE prediction

Fig. 11 Comparison of original and multizone LEWICE predictions with the experimental ice shapes for a 1-in. cylinder at 20-s intervals ($T = -7°$, $V = 125$ kt, liquid water content = 0.8 g/m³, and median volumetric diameter = 12 μm).

V. Conclusions

The investigation of the heat transfer on accreting ice surfaces has resulted in the following conclusions:

1) The use of roughness element height in LEWICE has been investigated. The roughness influences the location of the laminar to turbulent boundary-layer transition and the convective heat transfer in the turbulent boundary-layer region. The convective heat transfer in the laminar region is independent of the roughness element height.

2) Increasing the roughness height in the laminar region was observed to move the laminar to turbulent boundary-layer transition location closer to the stagnation region. Increasing the roughness height in the turbulent region increased the turbulent heat transfer.

3) The heat transfer predicted by the multi-zone version of LEWICE was compared with known data on cylinders. It was found that by using a viscous flowfield and appropriate

boundary-layer transition criteria, it was possible to predict the heat transfer quite accurately. This indicated the importance of having a viscous flowfield model in regions of separation and recirculation.

4) A laser fan beam technique was used to obtain high-resolution profiles of ice accretions and to highlight the smooth-to-rough surface transition location. This technique significantly improved the ease and accuracy of ice accretion photography.

5) An initial multi-zone version of the multizone model was implemented in the LEWICE ice accretion prediction code. For the first time step, different roughness heights for laminar and turbulent regions were used. For the subsequent time steps, an experimentally observed smooth-to-rough transition location was used to impose laminar to turbulent boundary-layer transition. The experimental observations were used to verify the concept of the multizone model. The multizone model significantly improved the prediction of the glaze ice accretion. However, further work is required to validate the approach and to develop a deterministic prediction of the rough-to-smooth transition dynamics.

Acknowledgments

This work was supported in part by the National Aeronautics and Space Administration and the Federal Aviation Administration under Grants NAG-3-666 and NGL-22-009-640. The work was also supported by the National Science Foundation Presidential Young Investigators Program, Award No. 8552702. Use of the icing wind-tunnel facilities were provided courtesy of B. F. Goodrich De-Icing Systems.

References

[1]Achenbach, E., "The Effect of Surface Roughness on the Heat Transfer from a Circular Cylinder to the Cross Flow of Air," *International Journal of Heat and Mass Transfer*, Vol. 20, 1977, pp. 359–369.

[2]MacArthur, C. D., "Numerical Simulation of Airfoil Ice Accretion," AIAA Paper 83-0112, Reno, NV, Jan. 1983.

[3]Ruff, G. A., and Berkowitz, B., "User's Manual for the NASA Lewis Ice Accretion Prediction Code (LEWICE)," NASA-CR-185129, May 1990.

[4]Hansman, R. J., Yamaguchi, K., Berkowitz, B., and Potapczuk, M., "Modeling of Surface Roughness Effects on Glaze Ice Accretion," AIAA Paper 89-0734, Reno, NV, Jan. 1989.

[5]Hansman, R. J., and Turnock, S., "Investigation of Surface Water Behavior During Glaze Ice Accretion," AIAA Paper 88-0115, Reno, NV, Jan. 1988.

[6]Hansman, R. J., and Turnock, S., "Investigation of Microphysical Factors Which Influence Surface Roughness During Glaze Ice Accretion," *Proceedings of the 4th International Workshop on the Atmospheric Icing of Structures*, Academie National de l'Aires l'Espace, Touloose, FR, Sept. 1988.

[7]Olsen, W., and Walker, E., "Close-Up Motion Pictures of the Icing Process," NASA Lewis Research Center Film, 1983.

[8]Olsen, W. A., and Walker, E., "Experimental Evidence for Modifying the Current Physical Model for Ice Accretion on Aircraft Structures," NASA TM 87184, 1987.

[9]Messinger, B. L., "Equilibrium Temperature of an Unheated Icing Surface as a Function of Airspeed," *Journal of the Aeronautical Sciences*, Jan. 1953, pp. 24–42.

[10]von Doenhoff, A. E., and Horton, E. A., "A Low-Speed Experimental Investigation of the Effect of Sandpaper Type of Roughness on Boundary-Layer Transition," NACA TN 3858, 1956.

[11]Zukauskas, A., and Ziugzda, J., *Heat Transfer of a Cylinder in Crossflow*, Hemisphere Publishing Corporation, Washington, DC, 1985.

Hazard Alerting and Situational Awareness in Advanced Air Transport Cockpits

R. John Hansman,* Craig Wanke,** James Kuchar,** Mark Mykityshyn,** Edward Hahn,** and Alan Midkiff**
Aeronautical Systems Laboratory
Department of Aeronautics and Astronautics
Massachusetts Institute of Technology
Cambridge, Massachusetts USA

Abstract

Advances in avionics and display technology have significantly changed the cockpit environment in current "glass cockpit" aircraft. Recent developments in display technology, on-board processing, data storage, and datalinked communications are likely to further alter the environment in second and third generation "glass cockpit" aircraft. The interaction of advanced cockpit technology with human cognitive performance has been a major area of activity within the MIT Aeronautical Systems Laboratory. This paper presents an overview of the MIT Advanced Cockpit Simulation Facility. Several recent research projects are briefly reviewed and the most important results are summarized.

1. Introduction

The implementation of advanced technology has significantly changed the cockpit environment in current "glass cockpit" aircraft. Recent developments in display technology, on-board processing, data storage, and datalinked communications are likely to further alter the environment in second and third generation "glass cockpit" aircraft. It is, however, important that these technologies be implemented in a manner which will enhance both the human and systems performances, in terms of both safety and efficiency. Because many of the changes in cockpit technology center around information management, proper design of advanced cockpit systems requires careful consideration of the human performance issues, particularly in the cognitive domain.

The interaction of advanced cockpit technology with human cognitive performance has been a major area of activity within the MIT Aeronautical Systems Laboratory. This paper presents an overview of the MIT Advanced Cockpit Simulation Facility. In addition, several recent research projects are briefly reviewed and the most important results are summarized. It should be noted that the experimental programs are summarized and that the authors or references should be consulted for complete details on the experimental methods and results.

2. The MIT Advanced Cockpit Simulator[1]

The principal experimental facility used by he MIT ASL for studies of advanced information management issues is the MIT ASL Advanced Cockpit part-task simulator shown in Figure 1. The facility is a part task simulator which replicates the automatic flight components of a modern "glass cockpit" transport category aircraft. The simulator is implemented on a series of graphical workstations. This allows rapid prototyping of advanced displays, digital communications systems, and information management systems.

The MIT ASL Advanced Cockpit Simulator is a part-task facility based on Boeing 757/767 and 747-400 flight displays. The facility utilizes two computers and several control panels to emulate aircraft autoflight systems. In addition, a third computer is linked to the cockpit simulation which can be used either as an ATC station or for experiment control.

A Silicon Graphics 4D-25G graphics workstation is used to simulate the aircraft dynamics and present the primary flight displays. Airspeed, altitude, and vertical speed are indicated using tape displays similar to those found on the 747-400. An Electronic Attitude Director Indicator (EADI) is provided, and is used to display the artificial horizon, ground speed, radio altitude, and Instrument Landing System (ILS) localizer and glideslope deviations.

The flexibility of the graphical workstation allows rapid prototyping of new display concepts. Prototype displays can be implemented in a matter of days and the primary flight displays can be configured to accommodate new displays for experimental evaluation.

---

* Associate Professor
** Research Assistant

Preprint, 18th ICAS Congress, Beijing, China, Sept. 1992.

Supported by government grant. See Acknowledgments.

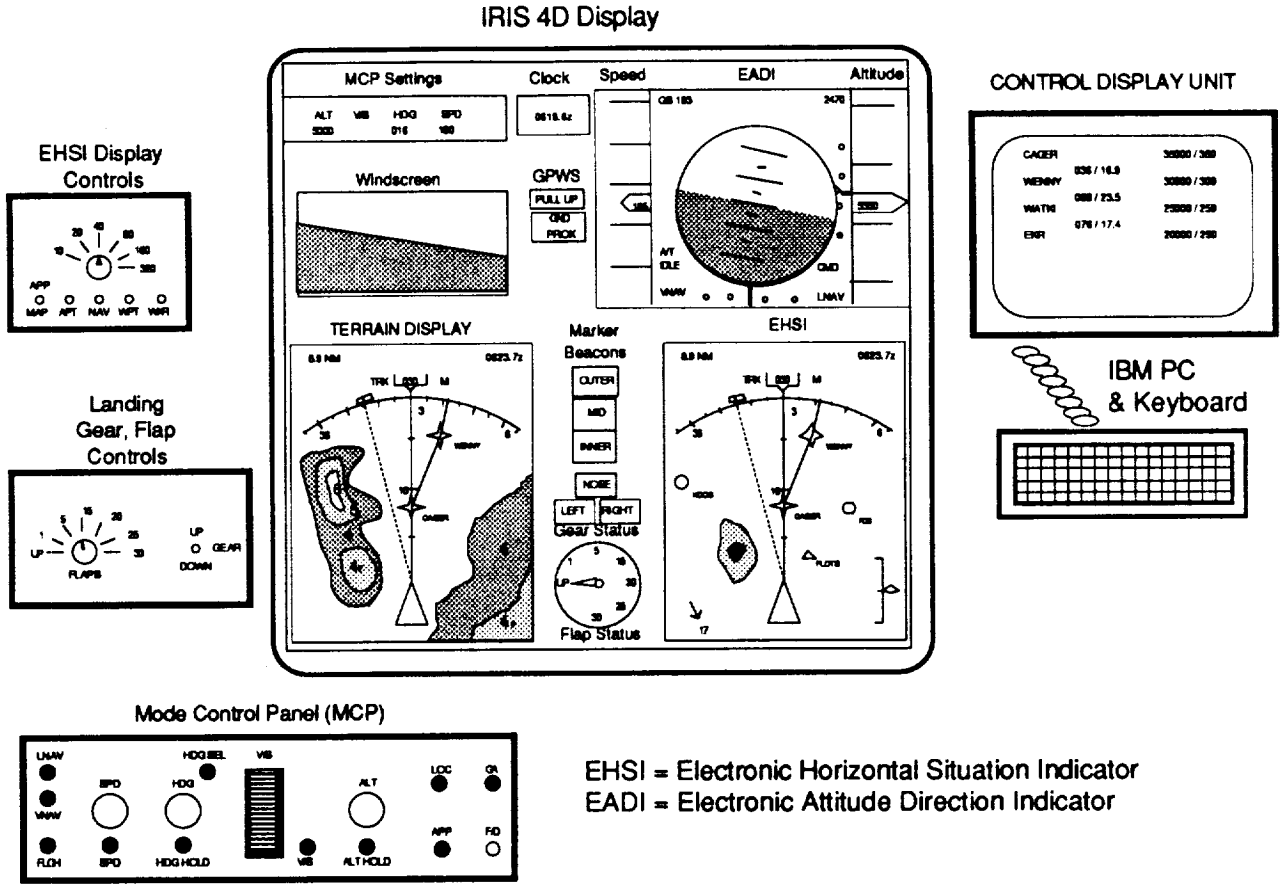

Figure 1. MIT Advanced Cockpit Simulator.

In the nominal display configuration, the Electronic Horizontal Situation Indicator (EHSI) is located below the EADI, as in the 757 or 767. The EHSI displays the 757/767 map mode, including aircraft heading, ground track, and programmed route.

A control panel is provided to allow the pilot to configure the EHSI in a manner similar to the actual aircraft. The pilot can select and de-select airports, navaids, intersections, and weather information, as well as scale the map display from 10 to 360 nautical mile range.

Flap, gear, and marker beacon light displays are provided to the left of the EHSI. Controls are provided to allow the pilot to set the flaps and lower or raise the landing gear during the approach. Additional controls such as a manual pressurization valve can be added to the simulation if a side task is necessary to increase the ambient crew workload.

A simple perspective out-the-window view is provided as a means by which to cue the pilot that the aircraft has descended below the cloud deck. While in instrument conditions, the display appears gray. When descending out of the cloud deck a single runway appears, representing the airport.

The Control Display Unit (CDU) for data entry into the FMC is simulated with an IBM/XT computer. It provides the necessary subset of the FMC functions required for the simulation, including basic route programming and destination selection.

Non-FMC control of the aircraft is performed through an autopilot Mode Control Panel (MCP), similar to the one used on the Boeing 757/767. A standard set of autothrottle and autoflight modes are available, including LNAV/VNAV flight (i.e. following FMC-programmed lateral and vertical flight paths) and the various capture ("select") and hold modes for airspeed, heading, vertical speed, and altitude.

In a typical experimental set up, an experimenter acting as air traffic controller is stationed at the ATC/Experimental Control Station and is in contact with the pilot through a simulated VHF link. The controller monitors the progress of the flight and

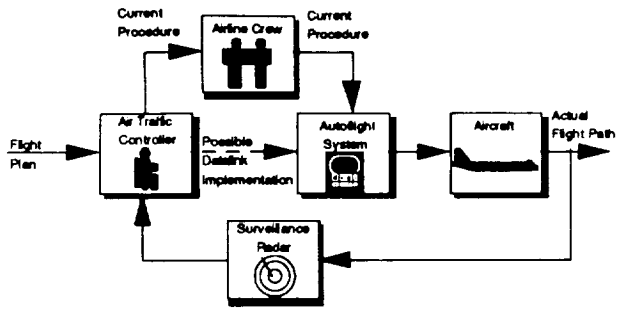

Figure 2. The ATC-to-Aircraft Communications Loop.

issues vectors and approach clearance amendments according to a script for each scenario.

A second experimenter, acting as the Pilot Not Flying (PNF), is seated next to the subject pilot. In most experiments, the PNF experimenter handles ATC communications and is available to answer any questions about the simulator that occur during the experiment.

The cockpit is videotaped during the experiment to record ATC and intra-cockpit communications and actions. In addition, the simulator records all flight data and control input parameters for the entire experimental run.

In order to maximize the validity of the results and minimize simulator training requirements, the subject pool is normally limited to professional air carrier pilots currently qualified on autoflight aircraft.

3. Datalink Delivery of ATC Clearance Amendments[2,3]

Motivation

The Federal Aviation Administration (FAA) has mandated the use of digital ground-to-air datalink for Air Traffic Control (ATC) services in the mid-1990's time frame. The delivery of ATC clearance amendments in-flight holds the potential to reduce voice congestion and information transfer errors associated with VHF radio communications.[4,5] However, there is some concern that datalink, especially when combined with automation, may actually decrease the crew's level of situational awareness.[6]

The FAA and the National Aeronautics and Space Administration (NASA) are studying systems which would automatically gate clearance amendment information into the onboard Flight Management System (FMS). While all proposed datalink systems would require pilot authorization before the aircraft would execute a new clearance automatically, there is some concern that pilots will become less involved in the clearance amendment processing loop and therefore may not be fully aware of the consequences of new amendments. Figure 2 shows the ATC-to-aircraft communications loop, which currently requires all clearance information to be processed by the crew. However, automation of datalink may inadvertently exclude the crew from the loop because they would assume a supervisory rather than participatory role in clearance communication.

Prior studies on automatic gating of clearance information using the MIT ASL Advanced Cockpit Simulator had shown that pilots preferred this option over voice or textual datalink delivery because of the advantages of the graphical presentation of the clearance information.[7,8] In these experiments, situational awareness was tested by issuing erroneous clearances and measuring the ability of the crews to detect these errors. This preliminary study was inclusive, however, there were indications that incorrect implementation of automatic clearance delivery could decrease situational awareness.

Approach

A simulation study was conducted to study the effect of automated clearance delivery on situational awareness as measured by pilots ability to detect errors in clearance amendments. The testing protocol was that the subject pilot was occasionally presented with nominally unacceptable ATC clearance amendments during terminal area operations. The ability of the pilot to recognize the errors was recorded as the dependent variable. Additionally, subjective ratings and comments by the subjects were collected.

The independent variables in the experiment were; automated verses manual programming of the datalinked clearance amendments into the FMS, procedural readback of the clearance amendment, and the mode of display of the information (verbal, textual, or graphical).

The experiment was a "within subject" design. Each subject flew the 10 scenarios required to fill the entire test matrix to control for differences between subjects. To ensure uniformity in notification, each amendment was enunciated using aural and visual alerts regardless of delivery mode or procedure. Each experimental run began during descent, approximately 120 nautical miles from the destination airport (thus requiring approximately twenty minutes to complete). After each scenario, subjects were asked for comments on the preceding scenario.

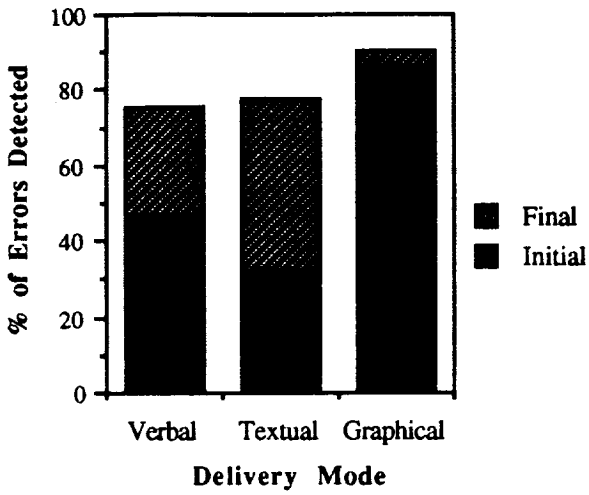

Figure 3. Detection of All Events by Delivery Mode.

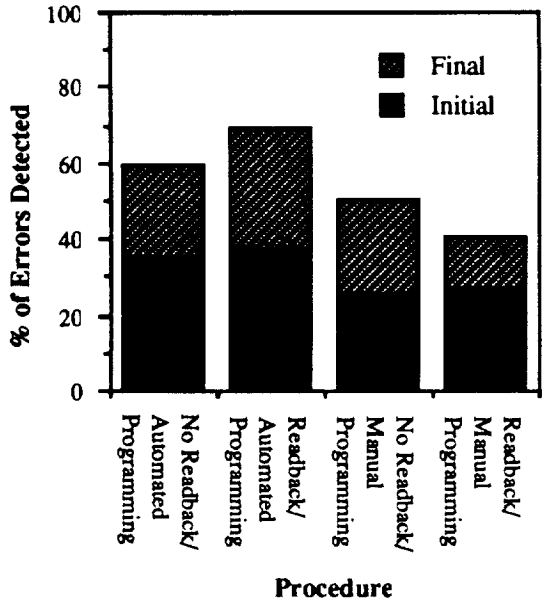

Figure 4. Detection of Routing Events by Procedure.

The scenarios were designed to represent the Northeast Corridor of the United States (i.e. the airspace between Washington DC, New York City, and Boston), with heavy traffic and weather in the entire region. Each scenario included a total of five clearance amendments, of which two were nominally unacceptable (i.e. an "error"). One error in each experimental run involved a clearance into weather, while the other was related to routing. During unacceptable routing clearances, pilots were given one of the following types of errors: 1) clearance to an incorrect initial fix to an approach for landing, 2) clearance to an incorrect destination, or 3) an illogical routing which headed the aircraft in a direction opposite to the intended flight path.

Results

Nine male B-757/767 qualified air transport pilots participated in the study. It should be noted that the subjects were volunteers. Because of this and the small sample size, the sample population may be biased towards favoring new technology when compared with the mean pilot population.

As shown in Figure 3, the graphical delivery mode yielded the best performance in detecting unacceptable clearances. In addition to the best apparent situational awareness, it also had the advantage that the vast majority of events were detected rapidly upon initial review of the clearance. In addition, graphical was outstanding in the detection of clearances into weather, with 100% of weather events detected immediately upon receipt of the clearance. This may illustrate the possible benefit of having a display which is simultaneously displays both the clearance routing and the location of potential hazards.

As shown in Figure 4, automated FMC programming appeared to aid in the ability to detect unacceptable routing amendments. This was supported by subjective opinions as the majority of subject pilots preferred automated programming with datalink. It was also clear from subjective comments that manual programming does not appear to aid in situational awareness even though each component of the clearance was entered into the FMS. In contrast, automated programming appears to allow the pilot to concentrate on evaluating the clearance on the strategic level.

Based on this study, automated FMS programming does not appear to adversely affect situational awareness and should be considered for the datalinked delivery of ATC clearances.

In contrast, no clear effect of readback performance was measured. Clearance readback showed a small improvement in error detection with automated programming. However, this effect was not statistically significant. Additionally, pilots rated the procedures with readback and automated FMS programming higher, on average, than any other procedure in terms of subjective situational awareness. Taken together, there is an indication that readback may have a benefit when used with automated FMS programming. While it is recommend that readback be retained on this basis,

further study on the effectiveness of readback is warranted.

The primary advantage of the graphical delivery mode was in the rapid evaluation of clearances. However, details of the clearance can sometimes be difficult to interpret in most likely graphical implementations such as the one tested. Textual delivery has the advantage of having all the information in one place in a concise format. Nevertheless, textual delivery seems to have few decision-aiding advantages over the current verbal delivery. It seems likely that a simultaneous presentation in both text and graphics will combine the advantages of the individual modes, and eight of nine subject pilots desired this. This is also consistent with the current dual representation of information in existing FMS/EFIS Systems. Further investigation into this possible "mixed" delivery mode is warranted.

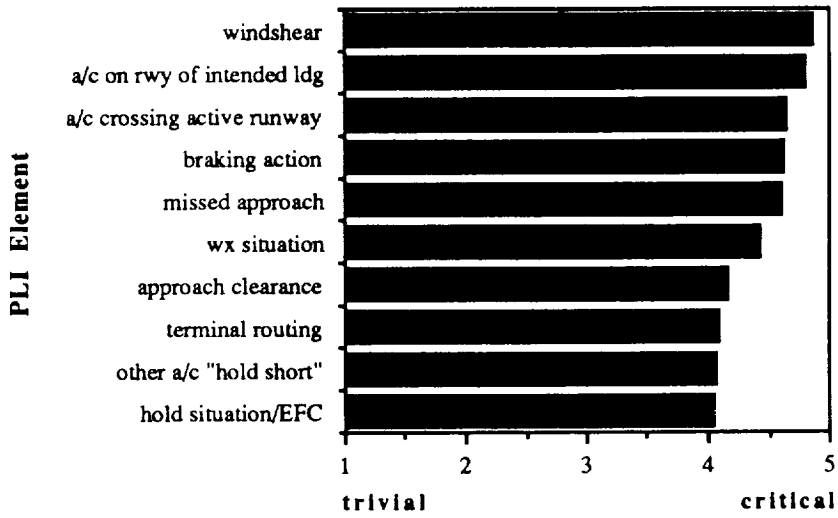

Figure 5. Importance of Specific PLI Elements.

4. "Party Line" Information Studies[9,10]

Motivation

Air/ground digital datalink communications are an integral component of the FAA's Air Traffic Control (ATC) modernization strategy.[11] With the introduction of datalink into the ATC system, there is concern over the potential loss of situational awareness by flight crews due to the reduction in the "party line" information available to the pilot.[4,5,12] "Party Line" Information (PLI) is gleaned by flight crews overhearing communications between ATC and other aircraft. In the datalink environment, party line information may not be available due to the use of discrete addressing.

Approach

Information concerning the importance, availability, and accuracy of party line elements was explored through an opinion survey of 187 active air carrier flight crews. Specific party line information elements were ranked for importance, availability, and accuracy for various phases of flight. The survey identified numerous important party line elements. These elements were scripted into a full-mission flight simulation using the "Advanced Cab" in the NASA-Ames Man-Vehicle System Research Facility. The flight simulation experiment examined the utilization of party line information by studying subject responses to the specific information elements. The pilot responses to the PLI stimuli were rated according to level of awareness and action taken.

Results

The mean values of importance, availability and accuracy of the surveyed party line information elements were high. An example is shown in Figure 5 where information elements perceived as most important are shown. It is interesting to note that the most important elements occur during operations on or near the airport. This indicates that consideration of party line information should be given if datalink is to be implemented in near airport control sectors.

The results from flight simulation study of the important information elements are presented in Table 1. The scripted Party Line Events are presented in rank order by action taken and level of crew awareness of the Party Line Event. Some party line elements perceived as important, such as windshear or holding EFC validity, were effectively utilized by flight crews in the simulated operational environment. However, other party line elements stimulated little or no increase in situational awareness. The ability to assimilate and use party line information appeared to be dependent on workload, time availability and the tactical/strategic nature of the situations. For example, the aircraft crossing the active runway event occurred during takeoff roll where the crew was fully occupied with other critical tasks.

In addition, the results of both the survey and the simulation indicated that the importance of party line information appeared to be greatest for operations near or on the airport. This indicates that caution must be exercised when implementing datalink communications in these high workload, tactical sectors.

Table 1. Ranked PLI Event Results

PLI EVENT #	NOT AWARE	AWARE	ACTION TAKEN
Windshear	0	0	6
Holding EFC	0	1	6
Turbulence and weather	1	1	5
Aircraft hold short at taxiway	1	4	2
Aircraft on runway	0	7	0
Traffic watch/climb	1	6	0
Aircraft Sequencing	1	5	0
Traffic watch/holding	5	2	0
Aircraft crossing active runway	6	0	0

5. Hazardous Wind Shear Alerts[8,13,14]

Motivation

In the past few years, systems for the detection of low altitude wind shear hazards, particularly microbursts, have been under steady development. These include ground-based systems such as Terminal Doppler Weather Radar (TDWR) and an enhanced version of the anemometer-based Low Level Windshear Alert System (LLWAS), as well as airborne forward-looking systems such as infrared radiometers, doppler radar, and doppler lidar. In order to incorporate these new sensors into an effective alert system, the problem of dissemination to flight crews must also be addressed. The variety of systems under development for both wind shear detection and ground-to-air datalink, combined with the advent of electronic cockpit instrumentation, allow many options for alert generation and dissemination. A critical part of the dissemination task is presentation of alerts to the flight crew in an easily understood and timely manner.

Approach

Two piloted flight simulator experiments have been conducted at MIT to study this issue. The first experiment focused on comparing verbal, alphanumeric, and graphical modes of presentation in the context of both ATC amendments and microburst alerts.[8,13] Eight active 757/767 pilots volunteered for the experiment.

In this experiment, pilots were asked to fly nine descent and approach scenarios under weather conditions conducive to wind shear. During the descent, ATC clearance amendments were given in the various modes; this portion of the experiment is discussed in detail in Reference 8. When the aircraft was vectored onto the final approach course, microburst alerts were issued in one of the presentation modes. Microbursts were positioned either as a threat on the approach path or as a non-threat on the approach or departure end of another runway. In addition, microbursts were sometimes positioned on the missed approach path.

Microburst alerts always contained warnings for all possible approach runways, not only the one being used by the simulated aircraft. This was to ensure that all modes had the same information content, and to allow measurement of the pilot's facility to discriminate between threatening and non-threatening situations.

Verbal microburst alerts were given as radio messages by the controller. Text microburst alerts appeared in an alphanumeric window just below the EHSI display. A typical verbal or text alert: "IRIS 354, Microburst Alert. Expect four-zero knot loss, 2 mile final approach runway one-seven-left." Graphical microburst alerts appeared in the appropriate location on the EHSI as flashing white circles with the intensity (headwind-to-tailwind change, in knots) drawn in red inside them.

Verbal cues were given (i.e. "IRIS 354, Microburst alert.") in all modes, so that the time of notification was kept constant. This would not be true of an actual cockpit, where an automated audible alert would most likely be used. Over the subjects tested, all scenario blocks were tested in all the modes, and the order in which the subjects encountered the modes was rotated. This process was used to attenuate learning and scenario-dependent effects.

Results

The results demonstrated that graphical alerts have significant benefits. The measure of pilot performance for the microburst alerts was the percentage of "correct decisions" made in each presentation mode. An incorrect decision was scored for either: (1) avoidance action taken when none was necessary, (2) no avoidance action was taken in a clearly hazardous situation. The data in Figure 6 show that the highest percentage of correct decisions

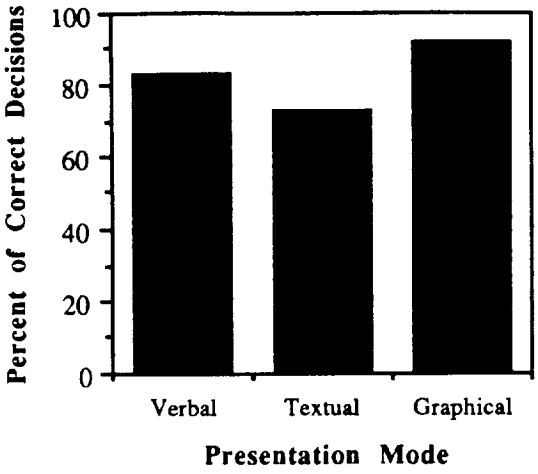

Figure 6. Decision-making performance for microburst alerts by mode of alert presentation.

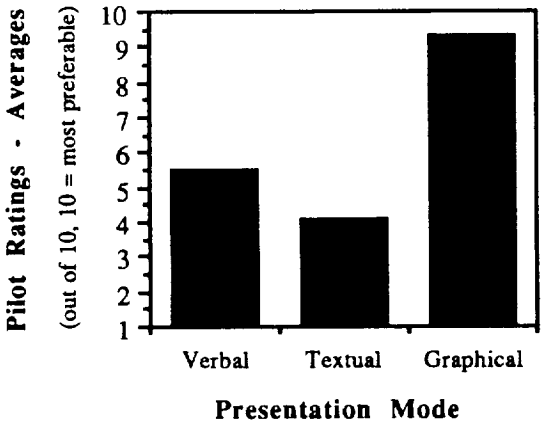

Figure 7. Pilot preference ratings for modes of microburst alert presentation.

were made with graphical microburst alerts, and the largest number of errors were made with textual alerts. When asked to rate the desirability of the three modes, pilots overwhelmingly preferred the graphical mode of communication (Figure 7). In addition, the text mode was consistently rated less desirable than the verbal mode. Pilots disliked in particular the additional head-down time required to read textual information.

Based on these demonstrated advantages of graphical alerts, a second piloted simulator experiment was designed to evaluate specific format and implementation issues associated with graphical microburst alert displays.[14] Issues addressed included display clarity, usefulness of multi-level microburst intensity information, and whether information from multiple sensors should be presented separately or

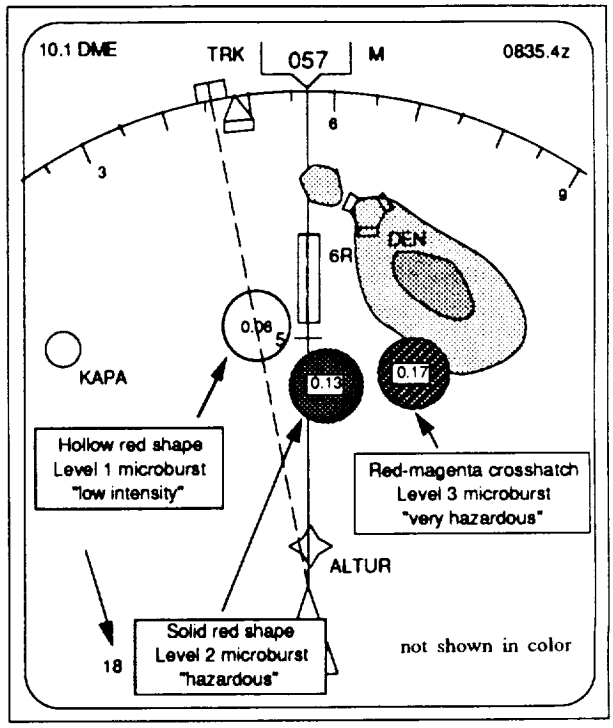

Figure 8. Example multi-level microburst alert display on the EHSI.

"fused" into combined alerts. Three different candidate graphical alert formats were tested. Nine active airline pilots of EFIS-equipped aircraft participated in the study.

Pilots found that graphical presentation of microburst alerts on a moving map display (the EHSI) was visually clear and useful and did not induce unacceptable display clutter. Also, multi-level intensity information coded by colors or patterns was found to be important for decision-making purposes, and was strongly preferred to displaying only "hazardous" microbursts in a single intensity level format. The intensity levels were defined using the "F-factor" hazard criterion,* which was found to be acceptable by the pilots.

A sample multi-level display format (including F-factor values) is illustrated in Figure 8. Also, the positional information included in the graphical alert presentation was found useful by the pilots for planning lateral missed approach maneuvers, but may result in deviations which could interfere with normal

* F-factor is a hazard criterion, including both headwind loss and downdraft components, which indicates the instantaneous loss of aircraft available climb rate due to the immediate windfield. It is described in detail in Reference 15.

airport operations. This experiment is described in detail in Reference 14.

6. Electronic Instrument Approach Plates[16]

Motivation

This study investigated the systems and human engineering design issues of electronic approach chart systems. Currently, IAP information is presented in paper format only. Information for all user groups and situations is normally contained on a single chart for each approach because it is too expensive to produce separate charts for different user groups. The small size of the charts (8.5 x 5 in.) forces the symbology and text to be quite small in order to accommodate all the information; consequently, current IAPs tend to be information dense.

Electronically based Instrument Approach Plates (EIAPs) offer a more flexible medium to present approach information to the pilot, as well as an opportunity to re-evaluate and modify conventional IAP design parameters. However, electronic display limitations require increases in minimum display element size to avoid aliasing problems. Methods are required to avoid display clutter problems which occur as a result.

Approach

An experimental study using the MIT ASL Advanced Cockpit Simulator was conducted in order to evaluate several Electronic Instrument Approach Plate (EIAP) formats. Two groups of three IAP formats were used in the experimental study. Paper, Monochrome, and Color formats comprised the first group of three. They were constructed in order to investigate the transition from paper to electronic IAP formats. Since the complete information set was always present on these charts, they were referred to as "non-selectable".

North-Up (Static), Track-Up (Moving Map), and EFIS Integrated formats comprised the second group of three. They were all color, and were constructed in order to evaluate potential EIAP design features and investigate decluttering issues. Since these three charts provided pilots with a prototypical decluttering capability, they were referred to as "selectable". These IAP formats were constructed in increasing technical levels toward more advanced electronically based IAPs. Each EIAP was based on the current paper IAP format and current EHSI, and was designed to utilize the format flexibility provided by electronic systems.

During the approach scenarios, each pilot responded to a total of 45 performance questions that were scripted into each approach in order to explicitly measure the efficacy of each format. Response time and error rate were used as an indicator of the ease and accuracy with which information could be extracted from the chart. Display order was counterbalanced across subjects in order to minimize learning effects.

Four of the twelve approaches that were flow by each subject entailed a scripted ATC clearance into terrain in order to implicitly measure the efficacy of terrain information depiction by spot elevations. In each case, the erroneous vector required no course deviation and entailed a premature descent clearance. Prior to commencing the approach , the pilot had ample time to orient himself to the heading assigned by ATC and to study the situation. If the pilot accepted the erroneous descent clearance without noting the hazardous terrain, a "terrain fly-through" event was recorded. If the pilot correctly identified the hazardous terrain, ATC immediately complied with his request for a climb to a safe altitude or a vector clear of terrain.

Twelve pilots who averaged 10,300 total flight hours, including 1,850 hours in autoflight equipped aircraft participated in this experimental study.

Results

Pilots ranked all six chart formats that were used in the experiment from the most desirable (1) to the least desirable (6). Results from this procedure are depicted in Figure 9. The general preference for the "selectable" formats indicates the desirability of color, information selectability and the depiction of real-time aircraft position information.

The subjects consistently indicated that the pilot selectable IAP decluttering capability helped to reduce clutter problems. Those who used the prototypical decluttering technique in the experiment unanimously agreed that it was desirable. Pilots unanimously agreed that the decluttering capability was desirable, and helped to reduce clutter problems.

Information retrieval response times and error rates indicate that there appears to be no loss in performance, and possibly a limited gain in information retrieval performance when IAP information was presented in electronic format. Response times to the performance question concerning the location of the highest obstacle on the chart were considerably faster when this information was presented in Color format.

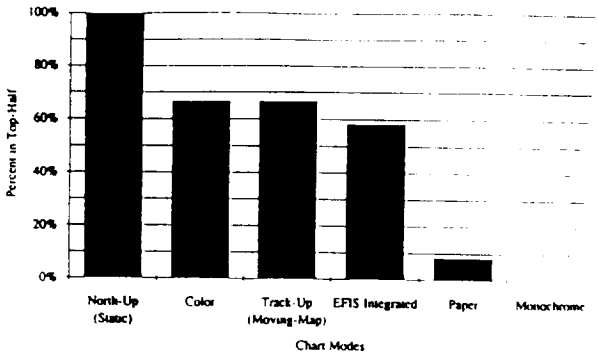

Figure 9. Preference Ranking For All Formats.

The ability of the flight crews to identify the hazard associated with terrain was found to be low. When using the "non-selectable" charts, pilots accepted the erroneous ATC clearances and penetrated hazardous terrain without question 38 times out of 39 opportunities, generating a hazard recognition rate of only 3%. When using the "selectable" charts, pilots accepted an erroneous ATC clearance and penetrated hazardous terrain 11 times out of 13 opportunities, generating a terrain penetration rate of 15%.

The extremely high number of recorded terrain "fly-through" events indicates that the current methods of terrain depiction were not being used to their full potential. While adequate terrain information was available on the IAP or EIAP format, pilots did not appear to have been aware that a hazard existed. The fact that pilots often accepted ATC clearances without checking the IAP to confirm adequate terrain separation indicates a general tendency to rely on ATC for terrain clearance.

7. Advanced Terrain Depiction[17]

Motivation

Controlled flight into terrain is the leading cause of Air Carrier fatal accidents world wide resulting in 47% of the fatal accidents from 1979 to 1989 [18]. This, along with the low hazard recognition rates found in the EIAP experiment discussed in Section 6, motivated a study to investigate the effectiveness of two methods of terrain depiction. Two primary methods of terrain presentation are currently used on paper Instrument Approach Charts. The first method depicts hazardous obstacles using spot elevation symbols on the chart. These symbols provide detailed terrain or obstruction altitude information at the specific locations of high points on the chart. However, the pilot must interpolate the terrain altitude in areas between the spot elevation symbols.

The second method of terrain depiction is smoothed contour depiction. Contours offer an advantage over spot elevation symbols in that terrain information is depicted throughout the chart, providing a continuous representation of the terrain near the airport.

Approach

An experimental study was conducted using the MIT ASL Advanced Cockpit Simulator to investigate the relative effectiveness of the two current terrain presentation methods. Each subject flew 12 approaches on the simulator while viewing a prototypical electronic terrain display. A Spot Elevation Display was used in six of the approaches, and a Smoothed Contour Display was used in the remaining six approaches. Display order was counterbalanced across subjects to minimize learning effects to the extent possible. Nine subjects participated in this study, with an average of 6400 hours of civil flight experience, of which 1275 hours were in autoflight aircraft.

Four of the twelve approaches flown by each subject included a scripted ATC clearance into terrain. In each case, the clearance was issued near the start of the scenario, at a point when the pilot had ample time to evaluate the situation. The erroneous clearance involved vectoring the aircraft close enough to terrain (i.e., within 1000') such that the simulator's Ground Proximity Warning System would activate. If the pilot did not recognize the terrain threat, the simulator's GPWS system would alert the pilot, and a terrain proximity event was recorded.

If the pilot recognized the terrain hazard and requested a new clearance to avoid the terrain, an appropriate clearance was immediately issued by ATC.

Results

The results are given in terms of the *hazard recognition rate*, which is defined as the ratio of incidents in which pilots determined that a hazard existed, to the total number of erroneous clearances given with a display format.

Figure 10 shows the hazard recognition rates for both terrain display types broken down into each terrain proximity scenario. In the first terrain proximity scenario, when the pilots may have assumed ATC was providing terrain clearance, pilots had a low hazard recognition rate (20-25%). In

addition, there was little difference between the Spot Elevation and the Smoothed Contour display formats. Once the subjects became aware that erroneous vectors were possible, they appeared to assume more responsibility for terrain clearance and there was an acute improvement in display effectiveness and a difference in performance between the two formats. When averaged over both display formats, hazard recognition rates increased from 22% for the first scenario to 78% for the subsequent scenarios (when the pilots were aware that erroneous vectors might be issued). This increase in hazard recognition is statistically significant ($p < 0.01$).

Hazard recognition rates improved from 20% to 62% (averaged over the last three scenarios) when using the Spot Elevation Display once the pilots apparently assumed more responsibility for terrain separation. A greater improvement was observed with the Contour Display: recognition rates increased from 25% to an average of 93%. However, the difference in performance between the two display formats when pilots appeared to assume terrain separation responsibility (62% vs. 93%) is not statistically significant ($p > 0.05$).

The high rate of terrain proximity incidents by qualified active air crews in this experiment indicates that current methods of terrain depiction were not being used to their full potential. Although the necessary information to depict hazards was available, the fact that a hazard existed was not always readily evident.

The combination of high workload levels, reliance on ATC, and the fact that pilots do not have access to intuitively presented terrain information appear to be primary factors in the low hazard recognition rates observed in this study. The lack of effective terrain information in the cockpit and the excellence of ATC in providing safe terrain clearance appear to have led pilots to implicitly transfer the responsibility for terrain separation to ATC.

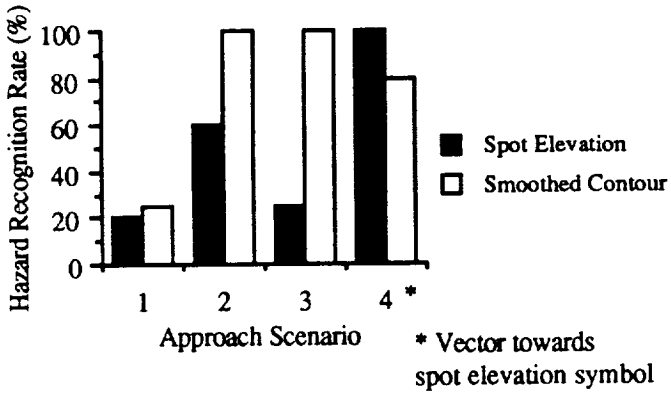

Figure 10. Scenario Hazard Recognition Rates.

When pilots appeared to depend on ATC for terrain separation, the type of terrain display did not make a difference in performance. However, in situations where pilots assume more responsibility for terrain clearance, it appears terrain situational awareness is improved when using a Smoothed Contour Display instead of a Spot Elevation Display.

8. Conclusion

The results presented above indicate that part task simulation studies using facilities such as the MIT ASL Advanced Cockpit Simulator can be effective in identifying important issues for cockpit information systems. While detailed results depend in the specific implementation, graphical presentation of alert and flight control information has generally been found to be effective for situational awareness and subjectively preferred by flight crews. Graphical display is most effective when it is consistent with the pilots cognitive map of the situation or process being displayed.

Acknowledgments

Support for the research activities discussed above was received from the Federal Aviation Administration, National Aeronautics and Space Administration, DOT Volpe National Transportation Systems Center, Lincoln Laboratory, and the National Science Foundation Presidential Young Investigator Award Program under the following grants; MSS-8552702, NGL-22-009-640, BARR-10-119, NAG 2-12, NAG 2-716, DTRS 57-88-C-0078TD39, NAG-1-690. The survey and simulation activities were aided by cooperation of the Air Line Pilots Association, the Allied Pilots Association, American Airlines, and United Airlines. The authors would also like to thank the many subject pilots who participated in the survey and experimental efforts.

References

[1] Wanke, C., Kuchar, J., Hahn, E., Pritchett, A., and Hansman, R.J., "Design of a Graphical Workstation Based Part-Task Flight Simulator for User-Centered Evaluation of Advanced Electronic Flight Displays," SAE Aerospace Technology Conference and Exposition '92, Anaheim, CA, (to be presented October 1992).

[2] Hahn, E., and Hansman, R.J., "An Experimental Study of the Effect of Automation on Pilot Situational Awareness in the Datalink ATC Environment," MIT Aeronautical Systems Laboratory Report, ASL-92-1, (expected June 1992).

[3] Hahn, E. and Hansman, R.J., "Experimental Studies on the Effect of Automation on Pilot Situational Awareness in the Datalink ATC Environment," SAE Aerospace Technology Conference and Exposition '92, Anaheim, CA, (to be presented October 1992).

[4] Knox, Charles E., and Charles H. Scanlon, "Flight Tests Using Data Link For Air Traffic Control and Weather Information Exchange," SAE Aerospace Technology Conference and Exposition '90, SAE 901888, Long Beach, CA, October 1990.

[5] Waller, Marvin C., and Lohr, Gary W., "A Piloted Simulation Study of Data Link ATC Message Exchange," NASA Technical Paper 2859, Hampton, VA, 1989.

[6] Wickens, Christopher D., Engineering Psychology and Human Performance, Harper-Collins, Champaign-Urbana, IL, (no information on publication date provided).

[7] Chandra, Divya, "An Evaluation of Automation for Flight Path Management in Transport Category Aircraft," MIT Man-Vehicle Laboratory, Cambridge, MA, August 1989.

[8] Wanke, Craig, Divya Chandra, R. John Hansman, and Steven R. Bussolari, "A Comparison of Voice and Datalink For ATC Amendments and Hazardous Wind Shear Alerts," 4th International Symposium on Aviation and Space Safety, Toulouse, France, November 1990.

[9] Midkiff, A., and Hansman, R.J., "Analysis of the Importance of Party Line Information in ATC Operations," MIT Aeronautical Systems Laboratory Report, ASL-92-2, (expected June 1992).

[10] Midkiff, A., and Hansman, R.J., "Identification of Important 'Party Line' Information Elements for Situational Awareness in the Datalink Environment," SAE Aerospace Technology Conference and Exposition '92, Anaheim, CA, (to be presented October 1992).

[11] FAA AC-20-XX, "Airworthiness Approval of Airborne Data Link Systems," March 1990.

[12] Boucek, G.P., "Human Engineering Issues for Datalink Systems," SAE G-10 Flight Deck Information Management Subcommittee (Seq No. BA010), February 1990.

[13] Wanke, C., and Hansman, R. J., "Hazard Evaluation and Operational Cockpit Display of Hazardous Windshear Information," AIAA Paper 90-0566, 28th Aerospace Sciences Meeting, Reno, NV, January 1990.

[14] Wanke, C., and Hansman, R. J., "Experimental Evaluation of Candidate Graphical Microburst Alert Displays," AIAA Paper 92-0292, 30th Aerospace Sciences Meeting & Exhibit, Reno, NV, January 1992.

[15] Bowles, R. L., "Reducing Windshear Risk Through Airborne Systems Technology," 17th Congress of the International Council of the Aeronautical Sciences, Stockholm, Sweden, September 1990.

[16] Mykityshyn, M. and Hansman, R.J., "An Exploratory Survey of Information Requirements For Instrument Approach Charts," MIT Aeronautical Systems Laboratory Report ASL-90-1-2, November 1990.

[17] Kuchar, J., and Hansman, R.J., "Advanced Terrain Displays for Transport Category Aircraft," MIT Aeronautical Systems Laboratory Report, ASL-91-3, August 1991.

[18] Bateman, D., "Past, Present and Future Efforts to Reduce Controlled Flight Into Terrain Accidents," 43rd Annual International Air Safety Seminar, Rome, Italy, November 1990.

OHIO UNIVERSITY

INVESTIGATION OF AIR TRANSPORTATION TECHNOLOGY AT OHIO UNIVERSITY 1991-1992

Robert W. Lilley
Avionics Engineering Center
Department of Electrical and Computer Engineering
Ohio University
Athens, Ohio

SUMMARY OF RESEARCH

This twenty-first year of the Air Transportation Technology Program at Ohio University saw continued progress by students, faculty and staff in three major areas. Brief reports are given in this section.

- The study of spectrum-efficient methods for transmitting weather information to aircraft has resulted in the design and implementation of an improved amplitude and phase modulation process. This technique permits re-utilization of voice channels for both voice and data. Efforts continue on the design of a receiver which will not be affected by the Doppler frequency shift present in the received radio frequency signal.

- Fault Detection and Isolation (FDI) algorithms for integrated navigation systems have been developed and flight tested. The FDI algorithm provides the integrity function required for navigation. Current research is focussed on two areas: 1) the design of a baseline FDI algorithm which could be used as a minimum standard for civil aviation receivers; and 2) FDI algorithms for integrated systems using both satellite navigation and inertial reference systems.

- Operation of the satellite-based Global Positioning System (GPS) in an interferometric mode permits real time relative positioning with centimeter-level accuracy. The first known real time flight tests of an interferometric GPS attitude and heading determination system were completed during this year. Multipath, the largest error source, was studied in great detail. The development of core GPS interferometry technology continues, as well as the application of this technique to flight reference systems.

The 1991-1992 research resulted in several conference papers, a journal paper, a M.S. thesis, and a Ph.D. dissertation. An annotated bibliography of these publications can be found on the following pages.

ANNOTATED BIBLIOGRAPHY OF 1991-92 PUBLICATIONS

1. Braasch M. S. and Van Graas, F.: Guidance Accuracy Considerations For Real Time GPS Interferometry. Proceedings of ION GPS-91, Albuquerque, NM, September 11-13, 1991.

During April and May of 1991, the Avionics Engineering Center at Ohio University completed the first set of real time flight tests of a GPS interferometric attitude and heading determination system. This technique has myriad applications for aircraft and spacecraft guidance and control. However, before these applications can be further developed, a number of guidance accuracy issues must be considered. Among these are signal degradation due to multipath and shadowing, effects of structural flexures, and system robustness during loss of phase lock. This paper addresses these issues with special emphasis on the information content of the GPS signal, and characterization and mitigation of multipath encountered while in flight.

2. Braasch M. S. and Van Graas, F.: Mitigation Of Multipath In DGPS Reference Stations. Proceedings of the ION National Technical Meeting, San Diego, CA, January 27-29, 1992.

Multipath represents one of the most serious threats to accuracy in Differential GPS (DGPS). However, over the past few years a number of techniques have been developed to combat this problem. The theoretical foundations of multipath are presented and several multipath mitigation techniques are reviewed. Special emphasis is placed on signal diffraction methods. Diffraction from, for instance, antenna ground plane edges induces significant distortions in the radiation pattern of the antenna. Although this would seem to be undesirable, it can actually be used to mitigate the errors caused by signals reflecting from nearby objects. The process is known as multipath randomization and it simply involves jittering the antenna and ground plane with respect to the reflecting surfaces. Reflections enter peaks and nulls in the distorted antenna patter in a random manner. This coupled with the oscillations in relative phase (with respect to the direct signal) result in a multipath error signature which is noise-like. Since it is noise-like it may be significantly reduced by averaging the code phase measurements against the more stable carrier-phase measurements. Exploitation of this effect to reduce multipath error represents a significant increase in accuracy for real time DGPS. Experiments have been performed which verify these conclusions.

3. Van Graas, F. and Braasch, M. S.: Real-Time Attitude And Heading Determination Using GPS. GPS World, March 1992.

Differential carrier-phase tracking, also known as GPS interferometry, can be used to determine position with millimeter accuracy. This article describes the results from an evaluation of the technique for determining attitude and heading in real time on the ground and in flight.

4. Van Graas, F. and Braasch, M. S.: GPS Interferometric Attitude And Heading Determination: Initial Flight Test Results. Navigation: Journal of The Institute of Navigation, Vol. 38, No. 4, Winter 1991-92.

Attitude and heading determination using GPS interferometry is a well-understood concept. However, efforts have been concentrated mainly in the development of robust algorithms and applications for low-dynamic, rigid platforms (e.g. shipboard). This paper presents results of what is believed by the authors to be the first real-time flight test of a GPS attitude and heading determination system. Signals from four antennas are processed by a 24-channel GPS receiver. Data from the receiver are sent to a microcomputer for storage and further computations. Attitude and heading data are sent to a second computer for display on a software-generated artificial horizon. Demonstration of this technique proves its candidacy for augmentation of aircraft state estimation for flight control and navigation, as well as for numerous other applications.

5. Braasch, M. S.: On The Characterization Of Multipath Errors In Satellite-Based Precision Approach and Landing Systems. Ph.D. Dissertation, Ohio University, Department of Electrical and Computer Engineering, Athens, OH, June 1992.

This paper addresses the characterization of multipath errors in satellite-based precision approach and landing systems. Satellite-based navigation systems such as the NAVSTAR Global Positioning System (GPS) are currently being considered for use as precision approach aids. However, before these systems can reach full maturity the issue of multipath must be addressed. Multipath represents the dominant error source for the precision approach application.

The work presented in this dissertation provides insight into the range and behavior of multipath errors in satellite-based precision approach and landing systems. Multipath error has been shown to be a function of multipath strength, delay, phase and phase rate-of-change relative to the direct signal. These parameters have been characterized for the precision approach environment and have been shown to be capable of producing severe multipath error. In the absence of pathological multipath-producing obstacles, collected data reveals the Earth's surface to be the major multipath source.

6. Van Graas, F.: Toward Achieving Global Sole Means of Navigation Systems. NATO AGARD Guidance and Control Panel Navigation Specialists' Meeting, Ottawa, Canada, May 14-15, 1992.

This paper briefly reviews tentative requirements for global, earth-referenced sole means of navigation systems with emphasis on integrity and availability. These requirements can be allocated to integrated navigation system architectures based on for instance GPS, GLONASS, VOR/DME, TACAN, Omega, Chayka, and Loran-C. Fault detection and isolation techniques (FDI) for integrated radio navigation systems are

presented. The FDI algorithm provides a protection radius with a specified confidence level as a function of measurement geometry and algorithm requirements. This is followed by a case study of integrated GPS/Loran-C.

7. Kline, P. A.: Fault Detection And Isolation For Integrated Navigation Systems Using the Global Positioning System. M.S. Thesis, Ohio University, Department of Electrical and Computer Engineering, Athens, OH, November 1991.

A Fault Detection and Isolation (FDI) algorithm is presented which is capable of providing the integrity function of an integrated radio navigation system. Next, it is shown that the satellite-based Global Positioning System (GPS) alone cannot meet sole means navigation requirements. The FDI algorithm is then applied to an integrated navigation system combining GPS and Loran-C. Using real flight data, artificial failures are injected to study the performance of the FDI algorithm. The algorithm performance is independent of measurement geometry and the output of the algorithm also provides a confidence level for the navigation solution.

A HYBRID VOICE/DATA MODULATION FOR THE VHF AERONAUTICAL CHANNELS

Dennis M. Akos
Ohio University
Athens, Ohio

SUMMARY

A method of improving the spectral efficiency of the existing Very High Frequency (VHF) Amplitude Modulation (AM) voice communication channels is proposed. The technique is to phase modulate the existing voice amplitude modulated carrier with digital data. This allows the transmission of digital information over an existing AM voice channel with no change to the existing AM signal format. There is no modification to the existing AM receiver to demodulate the voice signal and an additional receiver module can be added for processing of the digital data. The existing VHF AM transmitter requires only a slight modification for the addition of the digital data signal. The past work in the area is summarized and presented together with an improved system design and the proposed implementation.

INTRODUCTION

A system for weather data dissemination to aircraft was developed at Ohio University to improve weather uplink service to general aviation aircraft. This system obtained weather radar reflectivity patterns from the National Weather Service via telephone lines. This image is digitized, the data is compressed, modulated using Quadrature Phase Shift Keying (QPSK), and transmitted over a VHF aeronautical channel. In the aircraft, data is demodulated and processed so that the image can be displayed (ref. 1).

This system offers a potential improvement over the inadequate weather uplink service now in use. The remaining obstacle is in finding a channel in the already overcrowded frequency spectrum. A possible solution may be obtained through the use of a hybrid modulation, utilizing both amplitude and phase modulation on the same channel. Currently, voice communication between the ground and aircraft is accomplished using amplitude modulation of a VHF carrier. This carrier can be phase modulated with digital data such that minimal interference results between the two modulations. This allows reception of the existing AM voice signal with no receiver modification since the signal is transmitted on the carrier in the existing modulation format. The digital data can be extracted using the appropriate processing of this signal.

HYBRID MODULATION

A signal using both amplitude and phase modulation can be expressed by:

$$s(t) = A_c \cdot [1 + k_v \cdot m(t)] \cdot \cos\,[2\pi f_c t - \Phi(t)] \qquad (1)$$

where m(t) is the AM signal, $\Phi(t)$ is the phase modulation (PM) signal, A_C is the amplitude of the carrier, f_C is the carrier frequency, and k_V is the amplitude modulation index. Ideally, these two modulations are independent of one another. However, due to the band limiting necessary for transmission, an interference mechanism is introduced. A phase-modulated signal normally retains a constant amplitude. When this signal is filtered, removing the out-of-band spectral energy,

envelope variations result which will directly interfere with an AM signal (ref. 2). This can be verified by filtering a phase-modulated signal and comparing the envelope of the carrier of the pre-filtered and post-filtered signal. Figure 1 shows a phase modulated carrier while figure 2 shows this signal after filtering with a Butterworth band-pass filter. The plot represents a 10.2-kHz carrier, 200-kHz sampling frequency, Minimum Shift Keying (MSK) phase modulation at a data rate of 2400 bits/seconds, and a tenth order Butterworth filter with a passband extending from 9.0 kHz to 11.4 kHz (All filter transient effects have been truncated for clarity).

The filtered signal experiences envelope variations which would severely distort any additional amplitude modulation. It is necessary to examine further the degradation introduced so that it can be minimized for the implementation of the hybrid modulation.

CHANNEL STUDIES

The hybrid modulation was first studied by Benelli and Fantacci in 1982 and 1983 (refs. 3 and 4) to determine if it could be used to transmit digital information concerning air traffic control to enroute aircraft. A computer simulation was developed to test implementation of the hybrid modulation. The simulation consisted of phase modulating a carrier using random data bits and then amplitude modulating this same carrier with a simulated voice waveform. The signal was then filtered using specifications consistent with typical transmission and reception filters; that is a fourth-order Butterworth with a 3-dB bandwidth of ±7.5 kHz and an eight-order Butterworth with a 3-dB bandwidth of ±5 kHz, respectively. Filtering was performed in the frequency domain, with the nonlinear operations, such as modulation and demodulation, simulated in the time domain.

The simulation tested three digital phase modulations: Binary Phase Shift Keying (BPSK), QPSK, and MSK, at data rates between 300 and 2400 bits/second. The results concluded that MSK was the best choice for phase modulation in a hybrid signal. They also concluded that the combination AM-PM MSK provides acceptable performance with an AM signal-to-noise ratio (SNR) of at least 30 dB, up to a data rate of 2400 bits/seconds. The limiting factor on the data rate is the degradation of the voice SNR due to the envelope variation introduced by the removal of the high-frequency energy of the phase modulation. In the case of AM-PM BPSK, the maximum achievable data rate is 600 bits/second and with AM-PM QPSK the maximum is 1200 bits/second. This can be explained by examining the theoretical baseband power spectral densities (PSD) for each of the tested phase modulation methods, shown in figure 3.

As seen in the figure, the power in MSK is concentrated in a more narrow bandwidth than is the case for BPSK or QPSK. As a result, the filtering process eliminates less spectral energy and therefore yields less envelope variation. Likewise, the PSD is more compact for QPSK when compared to BPSK which explains why QPSK outperforms BPSK at equal data rates. Therefore the spectral efficiency of the digital phase modulation is a primary concern in the hybrid signal.

The main criteria used in judging the performance of a system is the degradation of the existing voice signal. This is the principle consideration since the addition of the digital data should be transparent to those using the AM communication channel. It is, however, important to evaluate the bit error rate (BER) of the possible combinations of AM and PM methods. This also was included in the initial work by Benelli and Fantacci (refs. 3 and 4). They concluded that the performance of the data channel is naturally degraded by the presence of the amplitude modulation. This is caused by the need to hard limit the hybrid signal and then filter the resulting waveform to remove the amplitude modulation for recovery of the digital data. They found that using an AM-PM MSK system, the BER degradation for the data channel shows a 2-4 dB loss as compared to the infinite bandwidth and constant envelope case. The 2-4 dB loss was considered an acceptable degradation. It should be noted that their model did not account for possible effects from the

Doppler shift of the carrier due to aircraft dynamics. This Doppler effect will introduce a frequency shift into the carrier which must be considered to ensure the feasibility of the hybrid modulation.

This hybrid modulation concept was also studied by Parker (ref. 1) for its potential as a method to uplink graphical weather information to enroute aircraft. Through analytical and simulation work, he also concluded that acceptable performance could be obtained for a hybrid modulation under the following conditions: (1) digital data transmitted using MSK at a maximum of 2400 bits/second, (2) voice signal transmitted using AM with an index of modulation limited to 0.7, (3) subject to Additive White Gaussian Noise (AWGN), and (4) transmitted and received by VHF AM communication equipment.

IMPROVEMENTS TO THE PROPOSED HYBRID MODULATION

Subsequent to the initial work by Benelli and Fantacci, a number of new continuous constant-amplitude phase modulation methods have been introduced (ref. 5). These methods improve upon MSK with a narrower power spectrum, lower spectral sidelobes, and reduced error probabilities. All of these properties would yield improved system performance in a hybrid modulation.

One such modulation which is becoming increasingly popular is Gaussian Minimum Shift Keying (GMSK), developed by Murota and Hirade for digital mobile radio applications (ref. 6). GMSK incorporates a Gaussian low-pass filter in order to smooth the phase transitions of MSK, thus yielding a narrower PSD by introducing memory into the bit transitions. The roll-off of the filter is adjusted using a parameter known as B_bT, where T is the bit period, and B_b is the 3 dB bandwidth of the Gaussian premodulation filter. Choosing a B_bT value is a tradeoff between spectral economy and receiver complexity. A high B_bT value will result in a very sharp transition band and will confine the phase transition for a single bit to slightly more than a single bit period. It can be shown that as B_bT increases to infinity, the GMSK system actually approaches MSK. A small B_bT value spreads a single phase transition over multiple bit periods, introducing a high degree of intersymbol interference, which requires a complex receiver structure to demodulate. Values of 0.25 and 0.5 for B_bT are becoming standard for the majority of GMSK implementations. The infinite response of the Gaussian filter must be truncated to an integer number of bit periods to provide a functional system.

Figures 4 through 7 compare a MSK signal and phase transitions to the equivalent GMSK signal and phase transition. The parameters for the plots are: carrier frequency of 2 Hz, bit rate of 2 bits/second, B_bT of 0.25 truncated to four bit periods, and the modulating bits 0100110. Both methods require a knowledge of bits beyond the seven modulating bits due to memory requirements. The additional bits are set to binary ones. The GMSK phase path has removed the discontinuities present in the phase path of the MSK signal and thus the spectral efficiency of GMSK is superior to MSK. A closed-form expression for the PSD of GMSK has not yet been derived due to the complexity of the modulation. It is, however, possible to sample a GMSK waveform and estimate the power spectral density using numerical techniques. Applying this to both a MSK and GMSK waveform will allow a comparison to be made. The PSDs are presented in figures 8, 9 and 10 with 95% confidence intervals shown as dashed lines. The plots were produced using a sampling frequency of 19.2 kHz, a carrier frequency of 4.8 kHz, approximately 500 equally likely random data bits, and a bit rate of 2400 bits/second. It is obvious that the spectral efficiencies of GMSK are superior to MSK at both B_bT equal to 0.5 and 0.25. Based on the spectral properties of the digital phase modulations, it would appear that GMSK would be a superior choice for use in the hybrid signal.

A possible problem, not previously considered in the implementation of an AM-PM MSK system, is the ability to maintain a constant carrier frequency in the transmitter. One requirement of a MSK signal is that the carrier frequency must be an exact integer multiple of one-quarter the bit rate ($f_c = n*B_r/4$, where n is an integer). If this requirement is not met, the phase will not be continuous at bit transitions (ref. 7). Using an in-phase/quadrature modulation method to generate the MSK signal will force phase continuity, but will introduce envelope variations which will directly interfere with the AM signal. This is demonstrated in figures 11 and 12 where an MSK signal is generated with a bit rate of 2400 bits/second and carrier frequency of 9 kHz (n = 15) and 9.1 kHz (n = 15.33).

It follows that the transmitter in an AM-PM MSK must generate a constant carrier frequency to ensure a constant envelope for the AM modulation. For the case of a VHF channel phase modulated using MSK at 2400 bits/second (n = 600), the transmitter must hold a stable frequency within ± 50 Hz to ensure acceptable envelope variations. This would require a modification to the existing transmitters which are in use today due to their relaxed stability specifications.

An AM-PM GMSK system is not subject to such strict requirements since the phase transitions for GMSK are continuous due to the memory introduced through filtering. As a result, GMSK is not only more spectrally efficient than MSK, but it is tolerant of typical transmitter drift as well.

AM-PM GMSK SIMULATION

In order to demonstrate the superiority of the AM-PM GMSK system, a computer simulation was developed. Initial work on the GMSK system was concentrated on studying the degradation to the existing voice signal. This is the primary concern for two reasons: 1) the modification to the channel should appear transparent to existing AM users and 2) the BER of the data channel is closely associated with the receiver implementation.

The simulation was based on calculating the mean squared error introduced into the AM voice data by the bandlimiting necessary for transmission of the hybrid signal. The simulation was performed at baseband since the unmodulated carrier is not affected by the filtering process. The hybrid modulated signal given by equation (1) can be transformed into the in-phase and quadrature representation using trigonometric identities:

$$s(t) = A_c [1 + k_v m(t)] [\cos (\Phi(t)) \cos (2\pi f_c t) + \sin (\Phi(t)) \sin (2\pi f_c t)] \quad (2)$$

Again, since the filters are centered about the carrier frequency and no distortion is introduced into the AM signal through the filtering of the carrier, it can be excluded from the simulation. It is, however, important to note that AM interference will be introduced when the carrier frequency is not matched to the bit rate when using MSK to generate $\Phi(t)$. It is now possible to conduct the simulation at the sampling frequency necessary for the AM signal provided the filters are modified accordingly. The resulting baseband signal to be used in the simulation is expressed in equation (3).

$$s_b(t) = A_c [1 + k_v m(t)] [\cos (\Phi(t)) + \sin (\Phi(t))] \quad (3)$$

In addition to the reduced complexity, the removal of the carrier also allows the AM signal, m(t), to be extracted exactly after processing. First, the signal must be factored into the in-phase and quadrature components.

$$s_I(t) = A_c [1 + k_v m(t)] [\cos (\Phi(t))] \quad (4)$$

$$s_Q(t) = A_c\,[1 + k_v\, m(t)]\,[\sin(\Phi(t))] \quad (5)$$

$$s_b(t) = s_I(t) + s_Q(t) \quad (6)$$

The individual components now can be processed separately as each will add distortion to the AM signal. After processing, the resulting AM portion of the signal can be extracted exactly by applying a trigonometric identity, shown in equation (7).

$$A_c\,[1 + k_v\, m(t)] = \sqrt{(s_I(t))^2} + \sqrt{(s_Q(t))^2} \quad (7)$$

Although not true demodulation, the AM signal is recovered with degradation caused only by the addition and filtering of the phase modulation.

It has been determined previously that AM degradation due to MSK is acceptable up to a bit rate of 2400 bits/second. Thus, this system can be used as a reference for testing. The simulation program measures distortion by calculating mean squared error. MSK, GMSK 0.5, and GMSK 0.25 are evaluated at bit rates ranging from 1200 to 5000 bits/second with the results plotted in figure 13. The reference point of 2400 bit/second is marked on the MSK curve as well as the data rates for GMSK 0.5 and GMSK 0.25 which would introduce the same error into the AM signal. The results clearly show that GMSK with either B_bT values is superior to MSK for minimal voice degradation.

PROPOSED IMPLEMENTATION OF A HYBRID SYSTEM

As discussed earlier, existing AM transmitters must be modified to allow for the transmission of the hybrid signal. The required modification is straight-forward, provided that the phase modulation is implemented in the in-phase and quadrature format as presented in equation (2). Using this methodology, the phase modulation can be accomplished by adding an additional component between the generation of the carrier and the amplitude modulation, as presented in figure 14. The boxed component is available on the market as a standard vector modulator . The difficulty remaining is the generation of the $\cos(\Phi(t))$ and $\sin(\Phi(t))$ signals. A similar modulator is presented by Davarian and Sumida (ref. 8) where the actual phase modulation signals, $\cos(\Phi(t))$ and $\sin(\Phi(t))$, are generated using a digital signal processor (DSP) and D/A converters. This is necessary due to the complexity of the phase transitions for GMSK. Currently, an existing VHF AM transmitter at Ohio University is being modified to produce the VHF AM/PM transmitter. The vector modulator is being used with a programmable floating-point DSP to perform the modification. The current DSP program generates approximately 25 data points per bit of the phase modulation signals. This digital signal is processed using an D/A which then supplies the analog signal to the vector modulator.

The BER for the data channel is highly dependent upon receiver design. Although a simple MSK demodulation method will work, the BER can be improved by applying a more sophisticated receiver structure. Receiver design for GMSK has been and continues to be an active area of research. A major reason for this is that GMSK has been chosen by the European Conference of Postal and Telecommunication Administration as the modulation method for the Pan-European Cellular Radio System. Various receiver structures have been proposed and are currently under investigation as to their performance in the hybrid modulation. It is expected that the AM-PM GMSK system should provide superior BER performance. This reasoning is based on the fact that much less of the spectral energy of the phase modulated signal is lost through the filtering process. The GMSK receiver should also prove its superiority in dealing with the presence of a Doppler shift in the receiver carrier, a source of error not fully investigated in the AM-PM MSK model. The receiver models being tested for implementation in the hybrid system are based on those designed for the Pan-European Cellular Radio System which are designed for mobile communications

(refs. 9 and 10). The effects of Doppler shift are minimized through incoherent detection and differential detection. These techniques can be applied to the hybrid system to improve performance.

CONCLUSIONS

The proposed AM-PM GMSK system has shown significant improvements over an AM-PM MSK system in terms of degradation to the existing voice signal and ability to deal with Doppler shift. Current work involves the actual modification of an existing VHF AM transmitter for testing of the hybrid signal in both time and frequency domains. Work has also been initiated on the testing of various receiver models to determine achievable BER for the signal. The AM-PM GMSK system should allow for the transmission of digital data over an existing voice channel. The primary advantage of this system is that the AM signal format is undisturbed and will be transparent to those using the channel only for the reception of the AM signal. The data can be demodulated using a second receiver which will process the same signal to extract the digital information. This not only offers a solution to the placement of the digital weather information channel in the existing spectrum, but opens up a wide range of applications for the transmission of digital data over existing AM channels.

REFERENCES

1. Parker, Craig B.: Weather Data Dissemination to Aircraft. NASA Conference Publication 3063, 1990.

2. Mathwich, H. Robert, Balcewicz, Joseph F., and Hecht, Martin: The Effect of Tandem Band and Amplitude Limiting on the Eb/No Performance of Minimum Shift Keying. IEEE Transactions on Communications, Vol. COM-22, No. 10, October 1974.

3. Benelli, G.: VHF Radio Link for Ground-Air-Ground Communications Using an Integrated Voice-Data Modulation. Electronic Letters, Vol. 18, No. 13, June 24, 1982.

4. Benelli, G. and Fantacci, R.: An Integrated Voice-Data Communication System for VHF Links. IEEE Transactions on Communications, Vol. COM-29, No. 7, December 1983.

5. Sundberg, Carl-Erik: Continuous Phase Modulation. IEEE Communications Magazine, Vol. 24, No. 4, April 1986.

6. Murota, Kazuaki and Hirade, Kenkichi: GMSK Modulation for Digital Mobile Radio Telephony. IEEE Transactions on Communications, Vol. COM-29, No. 7, July 1981.

7. Pasupathy, Subbarayan: Minimum Shift Keying: A Spectrally Efficient Modulation. IEEE Communication Magazine, Vol. 17, No. 4, July 1979.

8. Davarian, Faramaz and Sumida, Joe T.: A Multipurpose Digital Modulator. IEEE Communications Magazine, Vol. 27, No. 2, February 1989.

9. Cavers, James K.: Decision Directed Timing Recovery for Incoherent Detection of GTFM/GMSK. IEEE Vehicular Technology Conference 37th, June 1987.

10. Yongacoglu, A., Makrakis, D., Ohnishi, H., and Feher, K.: New Receiver for Differential Detection of GMSK. IEEE Global Telecommunications Conference, December 1986.

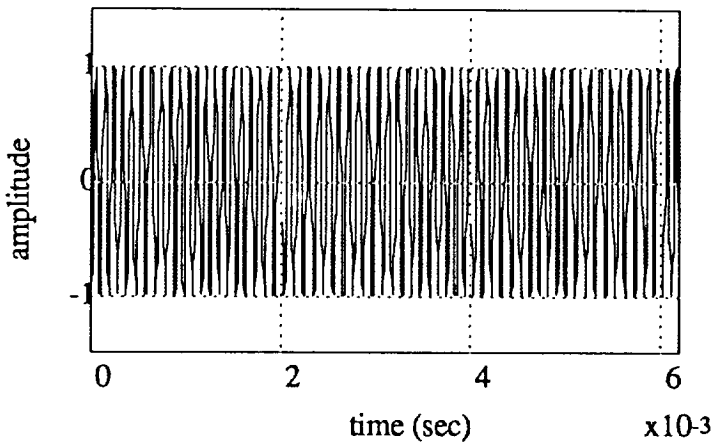

Figure 1. Constant envelope of an unfiltered MSK waveform.

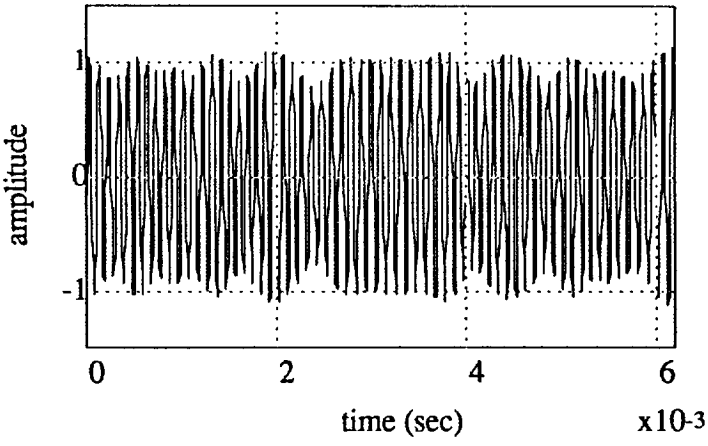

Figure 2. Envelope variations in a MSK waveform as a result of filtering.

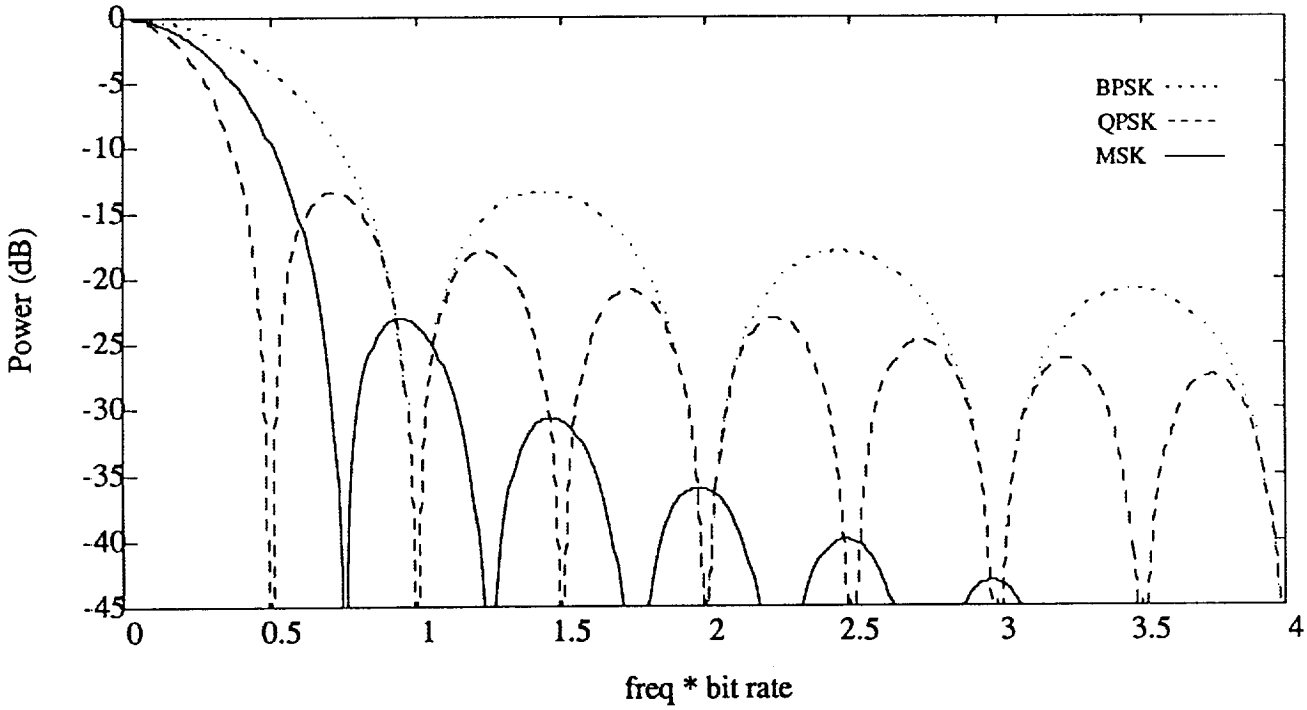

Figure 3. Power spectral densities for BPSK, QPSK, & MSK.

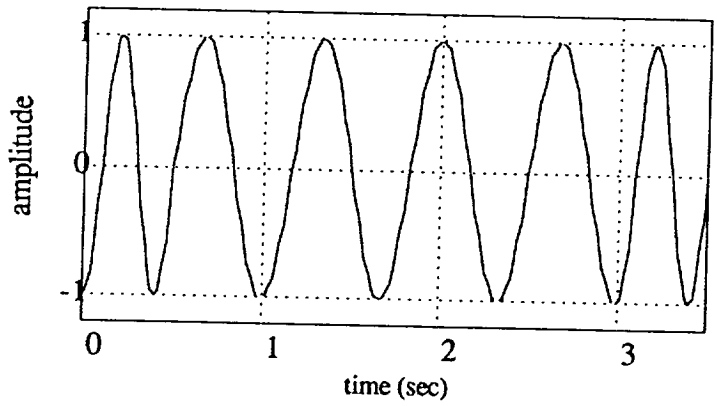

Figure 4. MSK waveform.

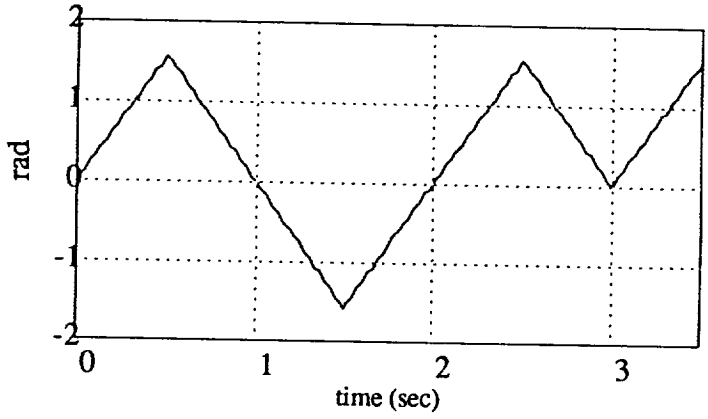

Figure 5. MSK phase transitions.

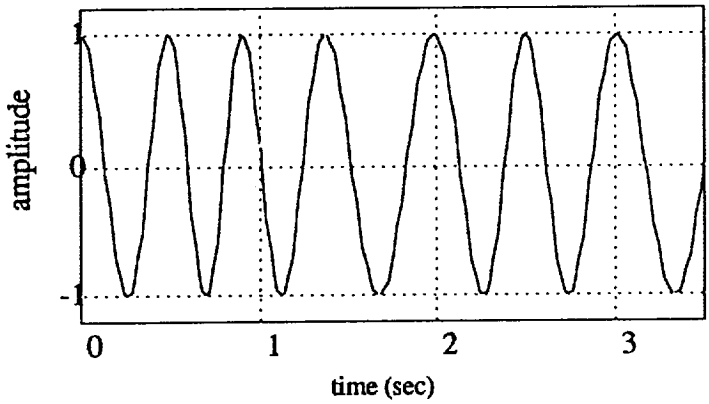

Figure 6. GMSK-0.25 waveform.

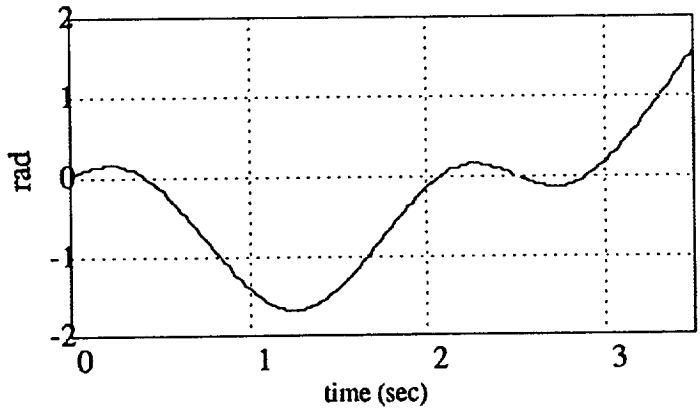

Figure 7. GMSK-0.25 phase transitions.

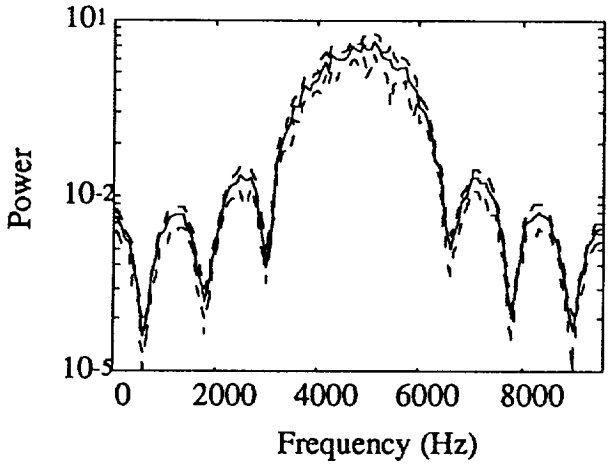

Figure 8. Numerical representation of the PSD for MSK.

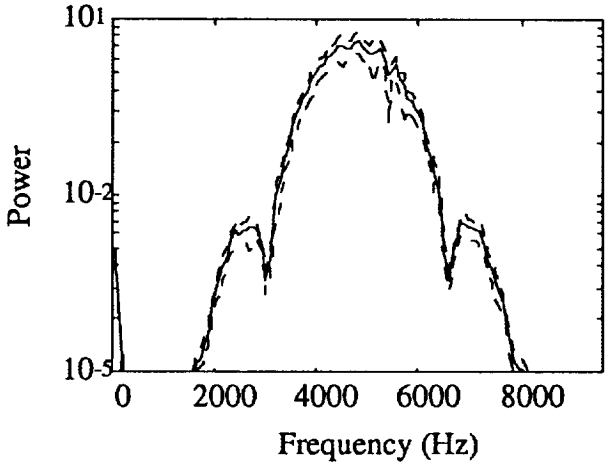

Figure 9. Numerical representation of the PSD for GMSK-0.50.

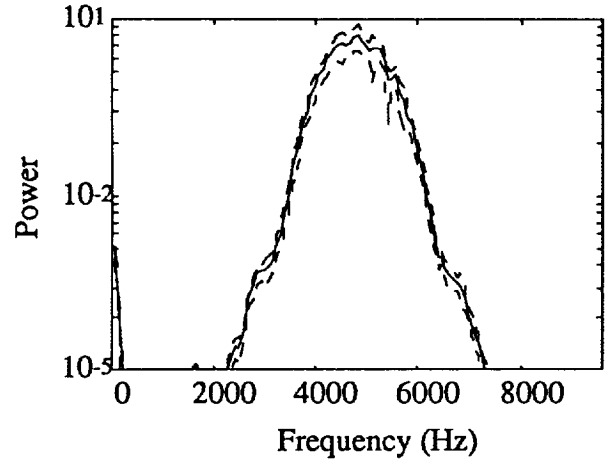

Figure 10. Numerical representation of the PSD for GMSK-0.25.

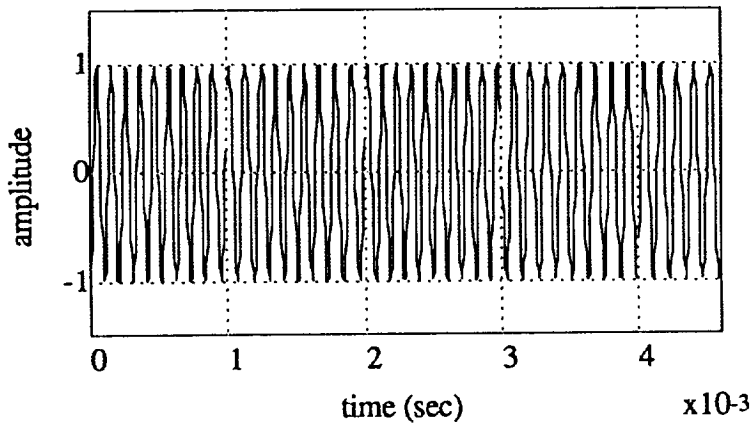

Figure 11. MSK waveform with fc = 9 kHz.

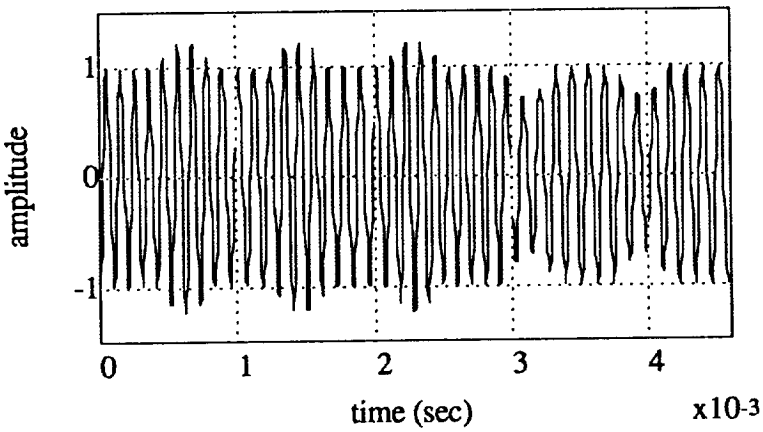

Figure 12. MSK waveform with fc = 9.1 kHz.

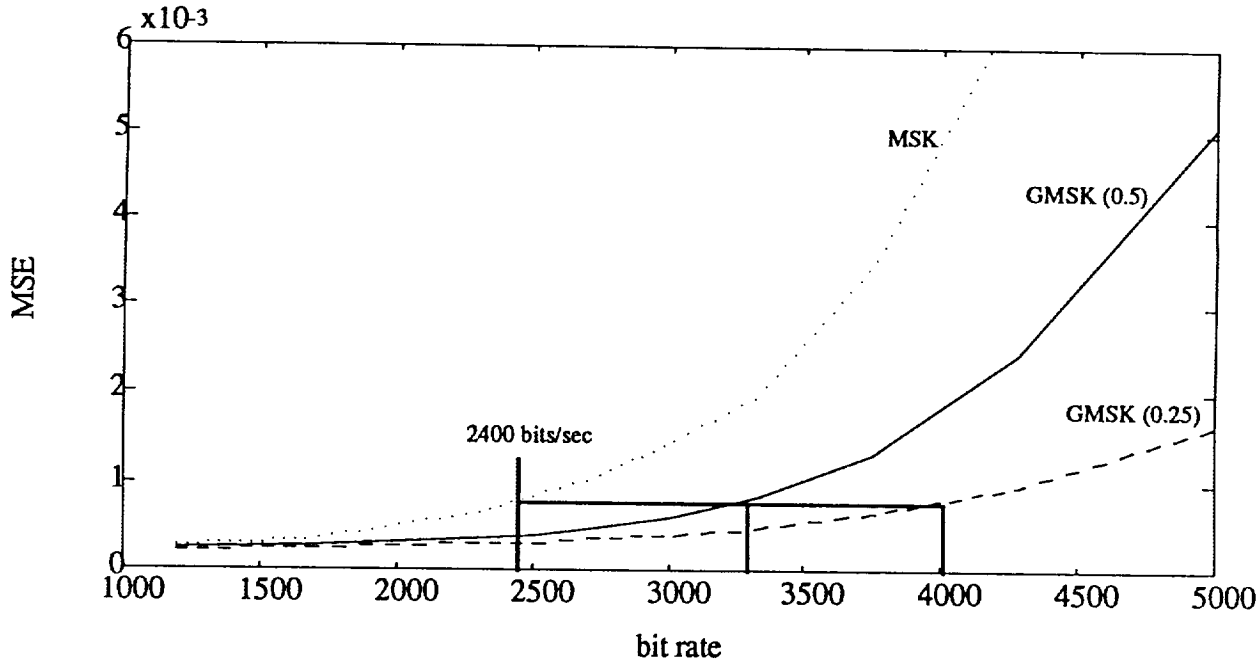

Figure 13. Mean squared error introduced into the AM signal.

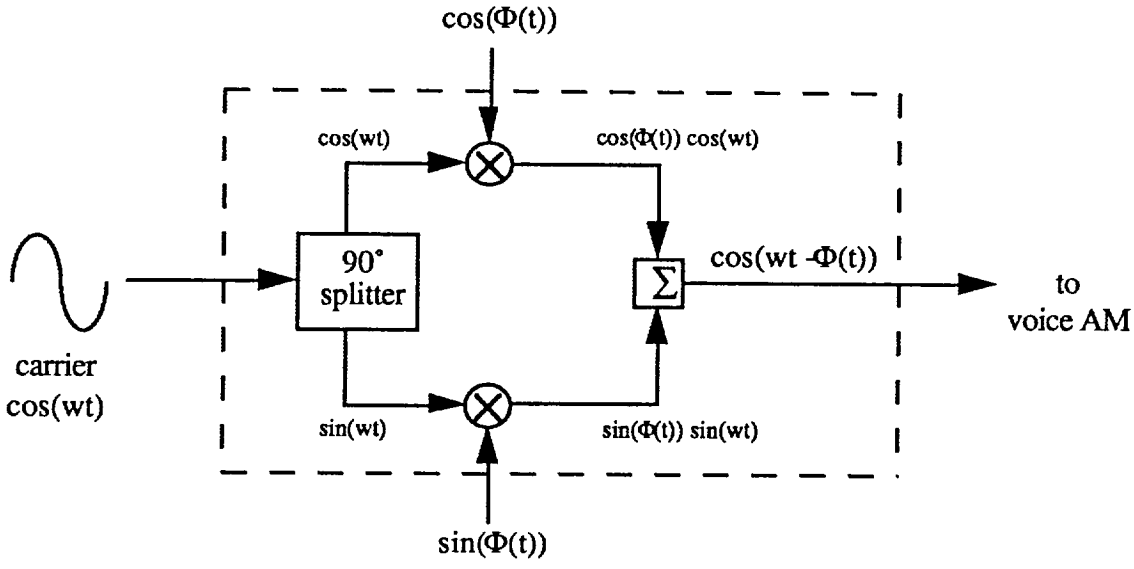

Figure 14. Transmitter modification for hybrid signal generation.

N93-22568

FAULT DETECTION AND ISOLATION

Greg Bernath
Ohio University
Athens, Ohio

SUMMARY

Erroneous measurements in multisensor navigation systems must be detected and isolated. A recursive estimator can find fast growing errors; a least squares batch estimator can find slow growing errors. This process is called fault detection. A protection radius can be calculated as a function of time for a given location. This protection radius can be used to guarantee the integrity of the navigation data. Fault isolation can be accomplished using either a snapshot method or by examining the history of the fault detection statistics.

BACKGROUND

The objective of fault detection and isolation is to use inconsistencies in redundant sensor measurement data to detect and isolate sensor malfunctions. One criterion for determining whether a system can be used as a sole means of navigation is the percentage of time that the position error is greater than a given maximum. If a given single measurement is in error, it will cause the navigation solution to be in error, possibly outside the allowable error threshold. Outside sources may not be able to broadcast in a timely manner that the signal is in error. For instance, if a single GPS satellite starts to broadcast erroneous signals, it could be from 15 minutes to several hours before this is broadcast in the satellite health data. Therefore, it is imperative for Fault Detection and Isolation (FDI) algorithms to be able to detect and isolate instrument errors using only data from the instruments themselves.

Previous work in FDI has mainly centered around inertial navigation systems (refs. 2 through 4). However, FDI can be implemented in any multisensor navigation system with redundant measurements. Current work is focusing on satellite navigation using the Global Positioning System (GPS), along with hybrid systems such as GPS integrated with the Long Range Navigation System (Loran-C) or GPS integrated with an Inertial Reference System (IRS) (ref. 6). FDI used specifically with GPS is also known as Receiver Autonomous Integrity Monitoring (RAIM) (ref. 7).

Kalman filters are becoming standard as part of the navigation solution in most GPS receivers. The Kalman filter can look at the difference between a predicted state

estimate and the actual measured state, and declare a fault if this difference is too large. This works well for detecting step errors or fast growing ramp errors. However, this will not detect a slow growing ramp error, such as might be caused by a GPS satellite clock drift. To detect slow growing errors, the Kalman filter algorithm must be run in parallel with a least squares estimator algorithm. The least- squares algorithm requires at least one redundant measurement for fault detection, and at least two redundant measurements for isolation.

PARITY SPACE AND ESTIMATION SPACE

Estimation space contains the actual horizontal measurement error and the alarm threshold for a given positioning error. However, actual positions and actual errors cannot be known given that the only measurement data is coming from imperfect sensors. Therefore, the work of detecting and isolating errors is done in parity space. Parity space is a mathematical tool where measurement noise and biases are used to create a parity vector. The parity vector determines a detection statistic, d, which is compared to a detection threshold, T_D, in order to determine whether an alarm condition exists. The parity vector is also used as a tool for fault isolation.

Errors and biases in parity space and estimation space are related, but it is not a one to one correspondence. The exact correspondence will be determined by measurement geometries. For instance, with a good geometry, a large measurement error (parity space) will result in only a small position error (estimation space). The reverse can also be true. Figure 1 illustrates two different slow growing ramp errors plotted in parity space versus estimation space. In case I, the detection threshold is crossed before the alarm threshold is reached, yielding a false alarm. As the error continues to grow, the alarm threshold is crossed, turning it into a correct fault detection. In case II, the alarm threshold is crossed before the detection threshold is reached, resulting in a missed detection. As the error continues to grow, the detection threshold is crossed, turning it into a correct fault detection. An ideal algorithm would minimize both the number of false alarms and missed detections.

LEAST SQUARES ESTIMATOR ALGORITHM

In a least-squares approach to fault detection, the relationship between the measurements and the user state (position) is given by:

$$\underline{y} = H\underline{\beta} \tag{1}$$

where: $\underline{y}$ = measurement vector (n-by-1)
H = data matrix (n-by-m)
$\underline{\beta}$ = user state vector (m-by-1)

$\underline{y}$ is a vector containing n measurements, one from each instrument. In the case

of using only GPS satellites, it would consist of the pseudoranges. $\underline{\beta}$ is the m-element user state vector, consisting of the user position coordinates and other navigation state elements such as clock offset with respect to GPS time. H is an n-by-m matrix which relates the measurements to the user states.

There are three possible cases:

1) $n < m$: Underdetermined system
2) $n = m$: Exactly determined system
3) $n > m$: Overdetermined system

In the underdetermined case, a navigation solution is not possible. In the exactly-determined case, a navigation solution is possible, but fault detection is not.

Algorithms for managing the redundant measurements in an overdetermined system form the basis of fault detection. A parity equation can be derived from equation (1), starting with a mathematical manipulation called the QR factorization on the data matrix H (ref. 4):

$$H = QR \tag{2}$$

H is factored into an n-by-n orthogonal matrix Q ($Q^TQ = I$) and an n-by-m upper triangular matrix R. R contains (n-m) rows of zeros along the bottom, due to the n-m redundant measurements in H. Substituting QR for H in equation (1) gives:

$$\begin{aligned} \underline{y} &= QR\underline{\beta} \\ Q^T\underline{y} &= Q^TQR\underline{\beta} \\ Q^T\underline{y} &= R\underline{\beta} \end{aligned} \tag{3}$$

Next partition R into an m-by-m upper triangular matrix U and (n-m) rows of zeros, denoted by 0. Similarly, partition Q^T into Q_1 (m-by-n) and Q_2 ((n-m)-by-n rows).

$$\begin{pmatrix} Q_1 \\ \hline Q_2 \end{pmatrix} \begin{pmatrix} y_1 \\ \vdots \\ y_n \end{pmatrix} = \begin{pmatrix} U \\ \hline 0 \end{pmatrix} \begin{pmatrix} \beta_1 \\ \vdots \\ \beta_m \end{pmatrix} \tag{4}$$

The least squares navigation state solution is:

$$\underline{\beta} = U^{-1}Q_1\underline{y} \tag{5}$$

The parity equation is:

$$Q_2 \underline{y} = 0 \tag{6}$$

The measurement vector $\underline{y}$ contains noise ($\underline{e}$) and measurement biases ($\underline{b}$). If $\underline{y}$ is replaced by ($\underline{y} - \underline{e} - \underline{b}$), the 0 in equation (6) can be replaced by the parity vector $\underline{p}$.

$$\begin{aligned} \underline{p} &= Q_2 \underline{y} - Q_2 \underline{e} - Q_2 \underline{b} \\ \underline{p} &= -Q_2 \underline{e} - Q_2 \underline{b} \end{aligned} \tag{7}$$

Thus, a parity vector will be determined by the noise and bias errors. From the parity vector, it can be determined which instrument is in error and whether or not to raise an alarm.

PARITY SPACE AND DETECTION PROBABILITIES

Consider a situation with one redundant measurement. In this case, the parity vector will be reduced to a scalar, and the detection statistic reduces to the absolute value of the scalar. In the case where no measurement bias exists, figure 2 shows the distribution of the parity scalar. Since there is no bias error, position error is definitely under the alarm threshold and the system is either in normal operation or a false alarm exists. The probability of a false alarm (P_{FA}) is obtained by integrating the areas outside of T_D. For noise having a normal distribution (generally a good assumption), this integral is a standard Gaussian function.

Figure 3 illustrates the case where a large measurement bias exists, making the position error larger than the alarm threshold. In this case the system is either correctly detecting a fault or a missed detection is present. The probability of a missed detection (P_{MD}) is the integral of the area inside T_D. Again, if Gaussian noise is assumed, this is a standard Gaussian function.

PROTECTION RADIUS

The above example uses a detection threshold, measurement noise, and measurement bias error as parameters to find P_{FA} and P_{MD}. Accuracy requirements are stated in a form like "the probability of exceeding 100 meters accuracy is no greater than 0.05". In order to compare FDI results with such specifications, it helps to rearrange the procedure. This means using the above parameters to determine the protection radius, which is the largest horizontal position error that is guaranteed to be detected with the required probabilities of alarm and missed detection. If all parameters are kept constant, the protection radius will vary only as a function of satellite geometry.

One way of finding the protection radius is to use all satellites in view and go through the full parity space/parity vector derivation. Another possibility is to take only

the best 5 satellites (geometry wise) in view and use only those for the calculation. The second method has the advantage that, since there is only one redundant measurement, the parity vector is reduced to a scalar and the algorithm is simpler. Also, a receiver would only be required to track five satellites.

A comparison of the two methods is shown in figures 4 and 5. These are plots of the protection radius as satellite positions change over one day at a single location. Many different locations were tested (with simulated satellite data) worldwide; figure 4 shows the best case result, figure 5 the worst case. As expected, the all-in-view method always gives a better result than the best-of-five.

FAULT ISOLATION

In the case with one redundant measurement, faults can be detected but not isolated. Isolation requires two or more redundant measurements. Consider the case of two redundant measurements. The parity vector now has two elements, making parity space two dimensional. Each measurement in parity space can be represented by an axis extended radially outward from the origin, in both (positive and negative) directions. The exact orientation of each axis depends on satellite geometry; thus each axis will rotate over time. The basic premise of fault isolation in parity space is that a bias error in measurement i will lie along measurement axis i in parity space. A growing bias error will move outward along a line parallel to the measurement axis.

Figure 6 illustrates a case of flight test data consisting of 4 GPS and 3 Loran-C measurements. There are 5 unknowns, which are the 3 user coordinates, the user clock offset from GPS time, and the user clock offset from Loran-C time. This leaves 2 redundant measurements, so parity space is 2 dimensional and it contains 7 axes, 1 for each measurement. The irregular plots are the traces over time of the end of the parity vector, as a slow growing ramp error is being artificially injected into each of the measurements. Each growing error runs parallel to the parity axis for that measurement. Measurement 2 seems to violate this rule, but what could not be shown on one graph is that axis 2 rotated significantly (as compared to the others) over the course of the data run; thus, the plot for instrument 2 ends up curved as it attempts to stay parallel with the axis as it rotates. Also note that the actual unaltered measurements contained a bias on instrument 4, as shown by the tracks originating a small distance out on axis 4.

The simplest method for isolating the faulty instrument is the "snapshot" batch estimator. This method, upon detecting a fault, looks for the parity axis that is closest to the parity vector, and assumes that the measurement belonging to that axis is faulty. The history method, on the other hand, determines which axis is parallel to the track traced out by the parity vector over time. The history method is more accurate, but requires more computation, has a built in delay and must restart if any measurements are lost.

CONCLUSIONS

A fault detection algorithm for a multisensor navigation system has been presented. A protection radius has been calculated using the all-in-view and the best-of-five methods, with the all-in-view proving significantly superior. Fault isolation methods have also been shown, using both snapshot and continuous tracing methods. Efforts continue on exploring the tradeoffs between algorithms, with the goal of determining whether minimum navigation system requirements can be satisfied using fault detection and isolation.

REFERENCES

1. Kline, P. A. and Van Graas, F.: Fault Detection and Isolation for Multisensor Navigation Systems. NASA Conference Publication 3131, Joint University Program for Air Transportation Research 1990-1991.

2. Daly, K. C., Gai, E. G., and Harisson, J. V.: Generalized Likelihood Test for FDI in Redundant Sensor Configurations. Journal of Guidance and Control, Vol. 2, Jan.-Feb. 1979.

3. Gai, E. G., Adams, M. B., and Walker, B. K.: Determination of Failure Thresholds in Hybrid Navigation. IEEE Transactions on Aerospace and Electronic Systems, Vol. AES-12, Nov. 1976.

4. Morrell, F. R., Bailey, M. L., and Motyka, P. R.: Flight Demonstration of Redundancy Management Algorithms for a Skewed Array of Inertial Sensors. Proceedings of the AIAA/AHS/ASEE Aircraft Design and Operations Meeting, AIAA Paper 88-4434, Atlanta, GA, September 7-9, 1988.

5. Golub, G. H., and Van Loan, C. F.: Matrix Computations, Second Edition. The Johns Hopkins University Press, Baltimore, MD, 1989.

6. Brenner, M.: Implementation of a RAIM Monitor in a GPS Receiver and an Integrated GPS/IRS. Proceedings of the Third International Satellite Division Meeting of the Institute of Navigation, September 1990.

7. Van Graas, F. and Farrell, J. L.: Receiver Autonomous Integrity Monitoring (RAIM): Techniques, Performance and Potential. Proceedings of the 47th Annual Meeting of the Institute of Navigation, Williamsburg, VA, June 10-12, 1991.

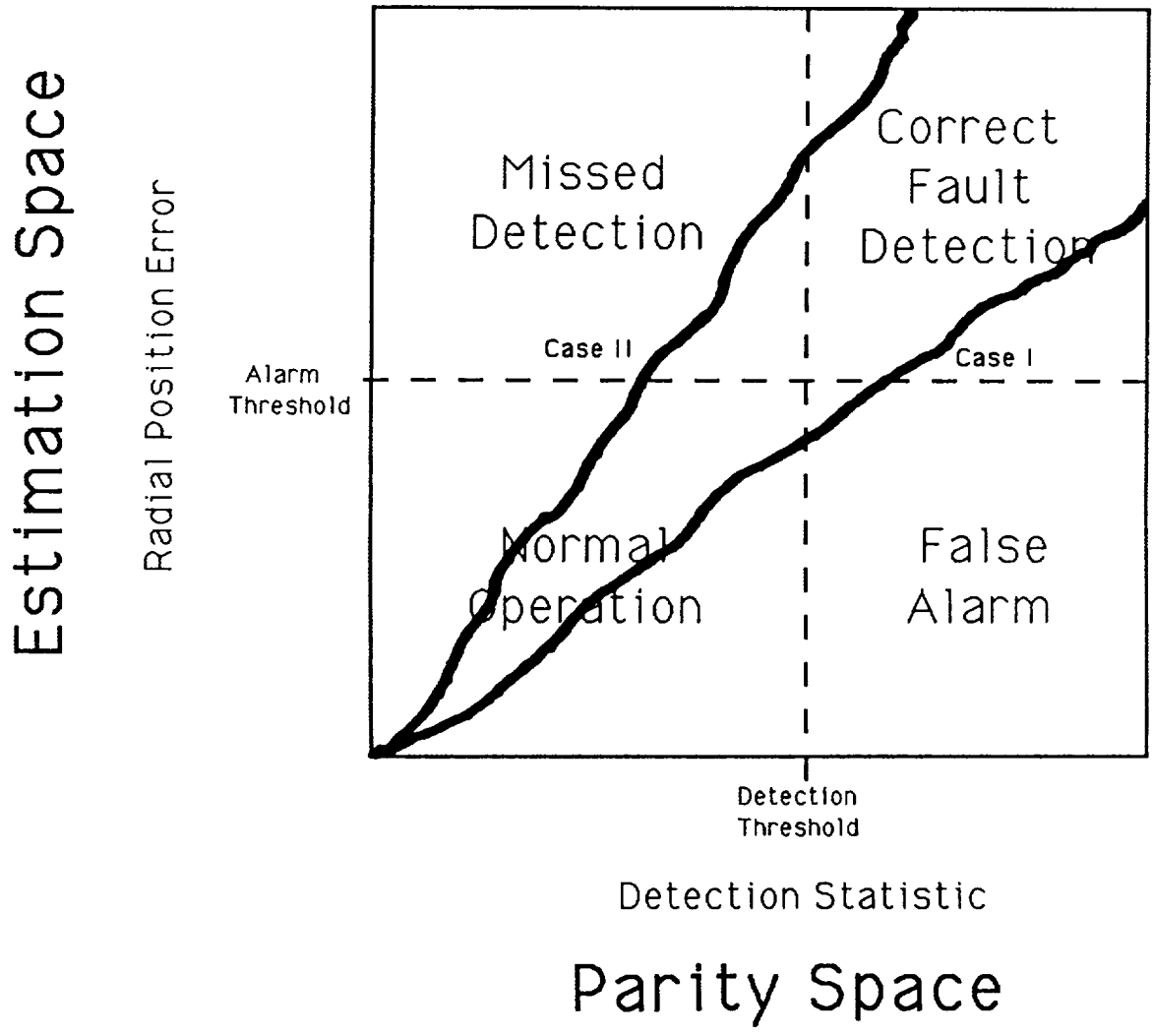

Figure 1. Two slowly growing measurement errors plotted in parity space versus estimation space.

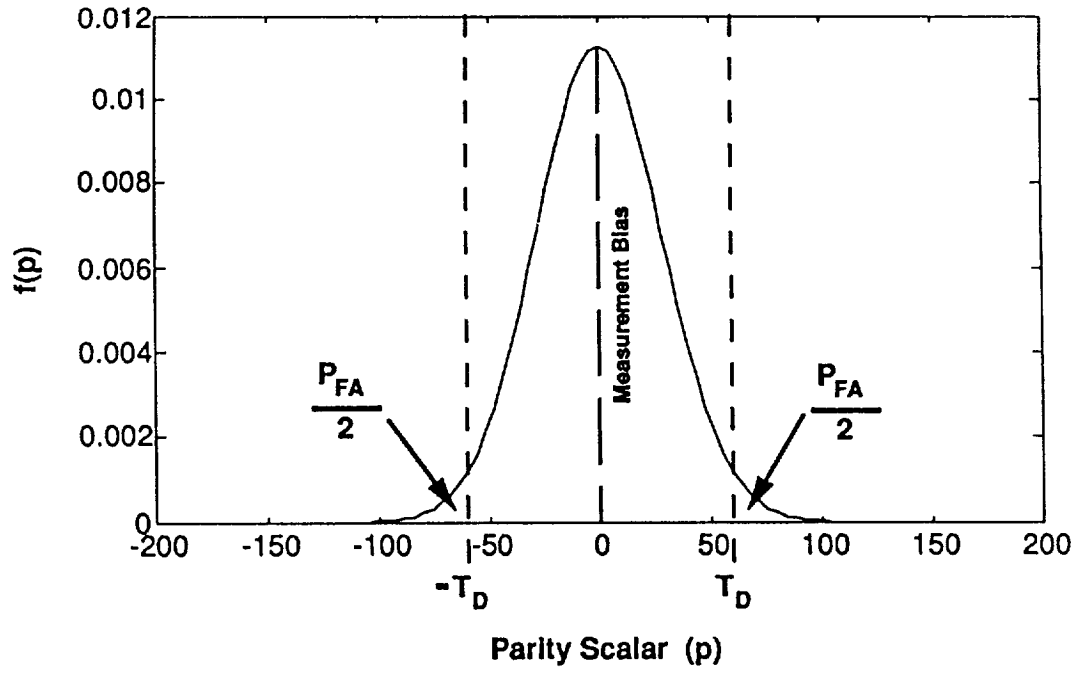

Figure 2. Probability density function for the parity scalar in the absence of a measurement bias error.

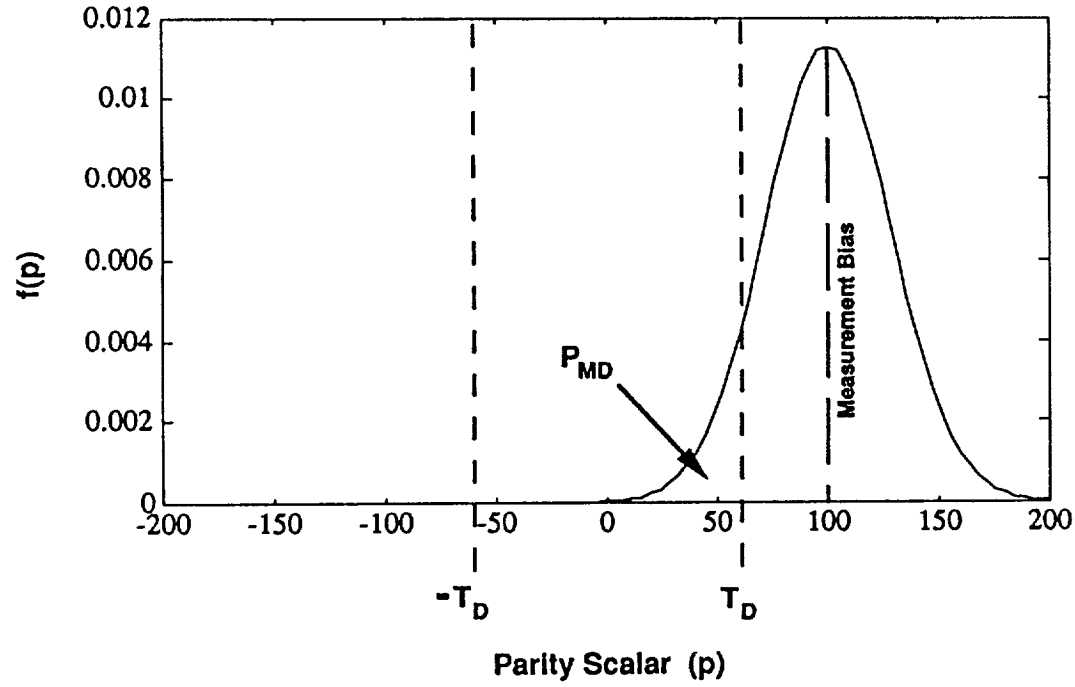

Figure 3. Probability density function for the parity scalar in the presence of a measurement bias error.

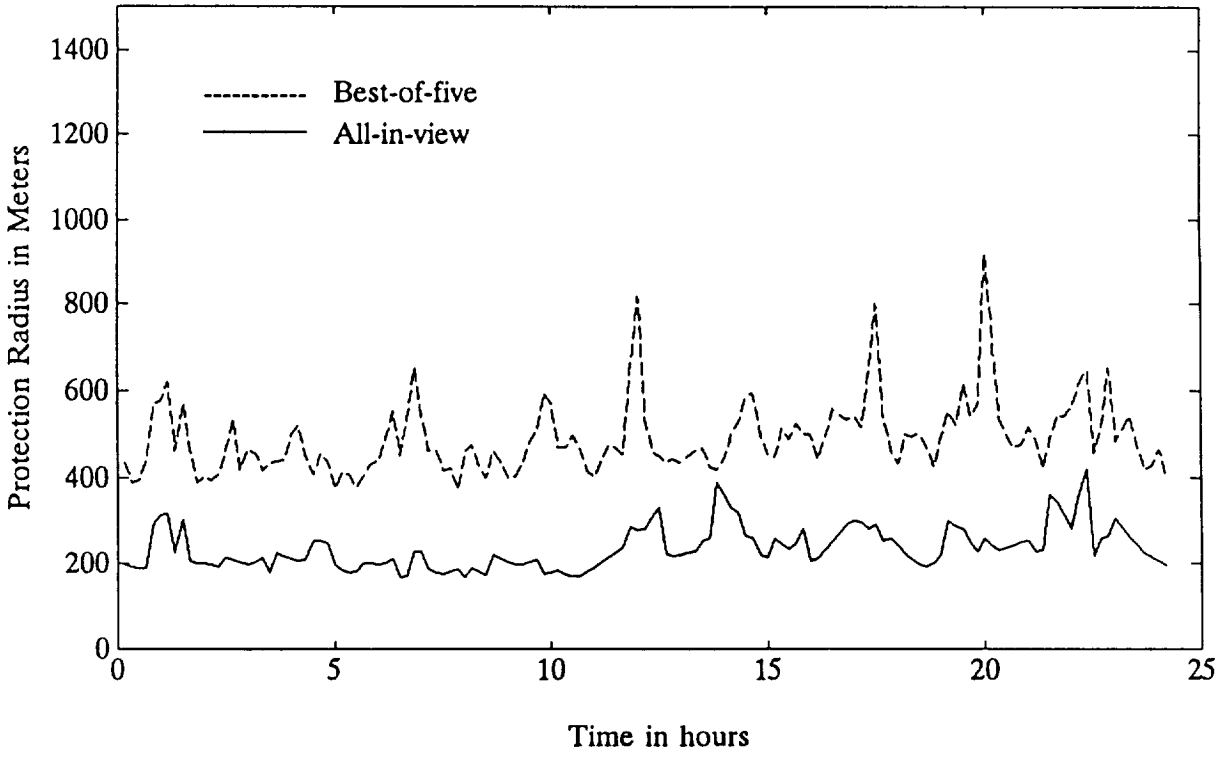

Figure 4. Best case protection radius (location: S3 W80).

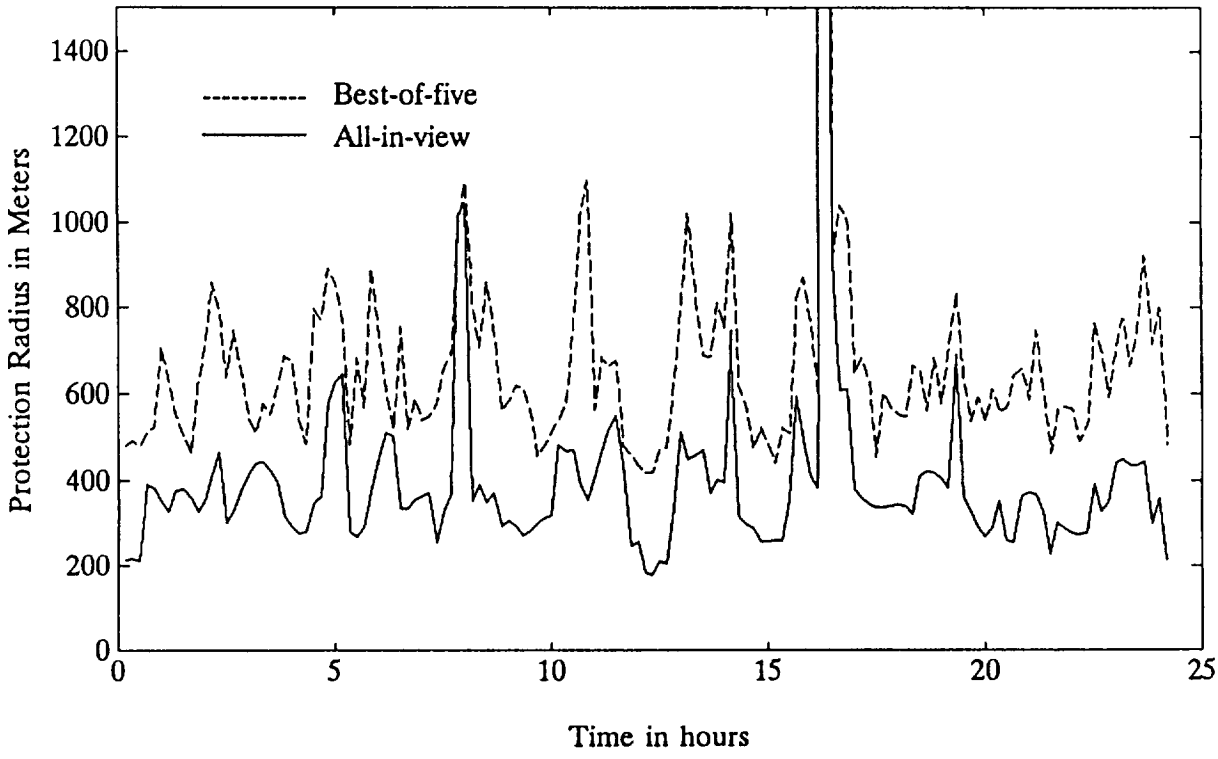

Figure 5. Worst case protection radius (location: N36 E140).

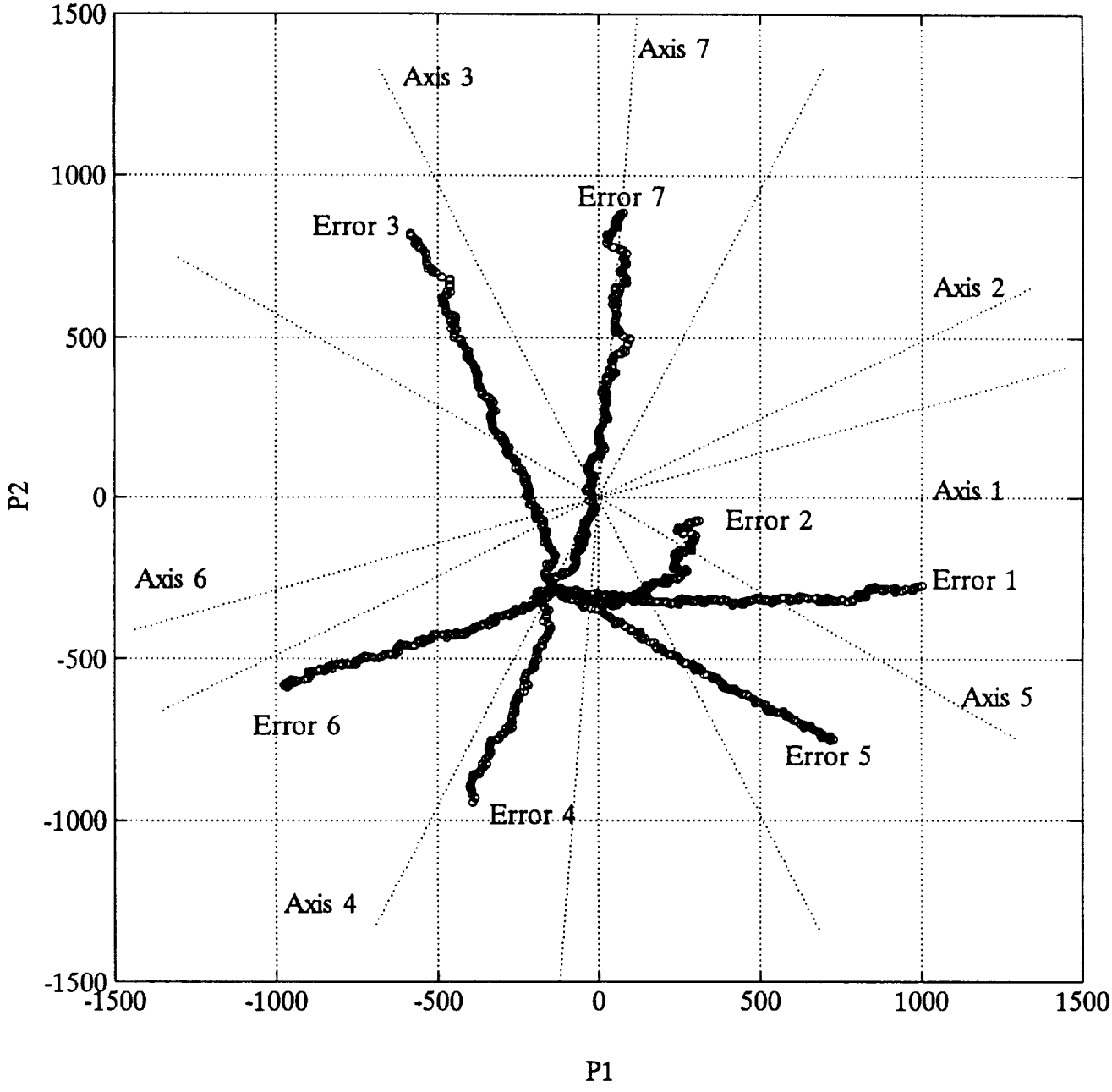

Figure 6. Parity vector trajectories as a function of time.

GPS MULTIPATH ERRORS IN THE PRECISION LANDING ENVIRONMENT

James D. Waid
Ohio University
Athens, Ohio

SUMMARY

Aircraft guidance and positioning during the final approach and landing phases of flight requires a high degree of accuracy. The Global Positioning System operating in differential mode (DGPS) is being considered for this application. Prior to implementation, all sources of error must be considered. Multipath has been shown to be the dominant source of error for DGPS. Theoretical studies have verified the severity of multipath within the final approach and landing regions. This paper presents a study of GPS multipath errors during these critical phases of flight. A discussion of GPS multipath error characteristics will be presented along with actual multipath data. The data was collected using P-code and C/A-code receiver architectures. Data was collected onboard a dual-engine fixed-wing research aircraft. Aircraft dynamics are considered in the data analysis.

INTRODUCTION

GPS soon will have the capability to provide position information to users anywhere in the world nearly 24-hours per day. For applications requiring precise positioning (better than one meter), a stand alone installation is not sufficient to provide adequate positioning accuracy. However, differential GPS (DGPS) can provide users with sub-meter level accuracies. Aircraft guidance and positioning in the final approach and landing phases of flight is a prime example of an application for DGPS.

At Ohio University's Avionics Engineering Center, the use of DGPS for aircraft guidance and positioning during final approach and landing is being investigated. GPS by itself has many sources of error including Selective Availability (SA), ionospheric delay, tropospheric delay, receiver hardware errors, receiver noise and multipath. DGPS eliminates those errors which are common to both receivers. The single largest source of error that remains is the error due to multipath (ref. 1). If DGPS is to be used for final approach and landing, the effects that multipath has on the GPS range measurements must be characterized and controlled to meet the required error budgets. This paper will present a discussion of multipath characteristics and multipath errors observed during the final approach and landing phases of flight. Aircraft dynamics are considered in the data analysis.

BACKGROUND

The accuracy of GPS positioning depends on the accuracy of the pseudorange measurements. There are many error sources which cause erroneous range measurements. The major error sources are as follows:

- signal delay due to propagation through the troposphere
- signal delay due to propagation through the ionosphere
- error due to satellite clock offset and orbit uncertainty
- Selective Availability (SA)
- receiver inter-channel biases
- receiver measurement errors
- dynamics
- thermal noise
- specular multipath
- diffuse multipath

Although differential carrier phase measurement accuracies are typically better than two centimeters, the code phase measurements are still required for ambiguity resolution. Therefore, this paper focuses on the code phase measurement error. The signal at the receiver is a combination of different types of signals: direct and non-direct. The direct signal is the signal received that travels the geometric distance from the satellite to the receiver. The non-direct or multipath signal is a signal that has been reflected or diffracted off an object and arrives at the receiver after the direct signal. In most cases the multipath signal is weaker than the direct signal. When the direct and the multipath signals combine, the result is a signal with the same frequency but having a relative phase difference with respect to the original direct signal. This phase error effects both the code measurement and the carrier phase measurement.

DGPS eliminates the errors in the measurements that are common to both receivers. Multipath has a different effect on each receiver. This is because multipath depends on the GPS antenna environment. For a typical DGPS system, the receivers are not close enough to each other to possess the same multipath characteristics. Three categories of multipath for the final approach and landing environment are (ref. 2):

- Obstacle-based at the airborne receiver.
- Airframe-based at the airborne receiver.
- Obstacle-based at the ground reference station receiver.

The air and ground system obstacle-based multipath originates from the ground itself as well as from buildings or other structures on or near the ground. The airframe-based multipath radiates from the airplane's wings and fuselage.

DATA COLLECTION

GPS multipath data collection was performed in the vicinity of the Ohio University Airport (UNI) located near Albany, Ohio. The grounds surrounding UNI are relatively flat and free of clutter. There are two large fixed structures (hangars) that are capable of generating significant multipath. Overall, UNI can be considered a benign multipath environment with the leading contributor being the ground itself. The GPS antenna used during the data collection was a duel frequency microstrip antenna.

A 12-channel GPS receiver was used for the data collection. The receiver is capable of continuous tracking the C/A-code on the L1 carrier (1575.42 MHz) and the P-code on both the L1 and the L2 carrier (1227.6 MHz). The measurement data from the GPS receiver was collected and recorded in real time using a 386-based notebook computer.

Data was collected over a 70 minute time period. The flight path is shown in figure 1. The aircraft remained stationary on the taxiway for 15 minutes and then proceeded to the end of the runway for takeoff. The airborne portion of the flight was approximately 40 minutes. After takeoff, a 180-degree left turn was executed and the aircraft climbed to 4000 feet. Then the aircraft flew out 15 miles and executed another 180-degree left turn. Completing the race track maneuver, the DC-3 flew over the runway at 600 feet. The aircraft then executed a 180-degree left turn while climbing to 1500 feet and then traveled 6 miles at level flight. At that time a tear drop maneuver was performed. After the tear drop maneuver, a 90-degree left turn was completed that aligned the aircraft for the final approach into UNI. After landing the airplane taxied and then remained stationary for another 15 minutes.

DATA PROCESSING TECHNIQUES

The combination of multipath, thermal noise, unknown bias and receiver error was extracted from the data using the standard code-minus-integrated Doppler technique (refs. 3 and 4). Equation (1) shows the result:

$$\begin{aligned} d_{code} - d_{phase} &= 2d_{iono} + d_{code\text{-}meas} \\ &- d_{phase\text{-}meas} + d_{code\text{-}noise} \\ &- d_{phase\text{-}noise} + d_{code\text{-}mp} \\ &- d_{phase\text{-}mp} - \Delta + d_{other} \end{aligned} \tag{1}$$

where:

d_{code}	is the code phase measurement
d_{phase}	is the carrier-phase (integrated doppler) measurement
$_{iono}$	is the signal delay due to propagation through the ionosphere

$d_{code\text{-}noise}$	is a combination of thermal noise and diffuse multipath on the pseudorange
$d_{phase\text{-}noise}$	is a combination of thermal noise and diffuse multipath on integrated carrier phase
$d_{code\text{-}meas}$, $d_{phase\text{-}meas}$	is receiver measurement noise for code and phase measurements
$d_{code\text{-}mp}$, $d_{phase\text{-}mp}$	is specular multipath on the code and phase
Δ	is an integer wavelength ambiguity
d_{other}	includes receiver measurement error and dynamics

For situations where the strength of the multipath is less than the direct signal, the carrier-phase multipath term will not exceed 4.8 centimeters (ref. 2). It has been shown that state-of-the-art receivers exhibit phase-noise values on the order of 0.1 millimeter (1-sigma) (ref. 5) allowing this term to be neglected as well. The receiver phase measurement error is also negligible (ref. 6). The carrier-phase multipath, the noise and the receiver phase measurement terms can all be dropped from equation (1) because the code-multipath error is usually on the order of meters and they are very small compared to that term. The integer ambiguity is a constant bias for the duration of the data collection, which is not of interest for this study. Equation (1) can be approximated by:

$$(d_{code} - d_{phase})' = 2d_{iono} + d_{code\text{-}meas} + d_{code\text{-}noise} + d_{code\text{-}mp} + d_{other} \tag{2}$$

The error due to the propagation delay through the ionosphere can be removed through the standard dual-frequency correction (refs. 2 and 7):

$$d_{iono_{f1}} = \left(\frac{f2^2}{f2^2 - f1^2}\right)\left(d_{code_{f1}} - d_{code_{f2}}\right) \tag{3}$$

Noise is reduced by averaging (filtering) the code measurements against the stable carrier measurements. This is done using a Hatch filter. The Hatch filter implementation for this application averaged over 100 seconds of data (ref. 8). After applying the ionospheric correction and the Hatch filter, we arrive at the following:

$$(d_{code} - d_{phase})'' = d_{code\text{-}meas} + d_{code\text{-}mp} + d_{other} \tag{4}$$

The next section presents the results of the data collection and data analysis.

DISCUSSION OF RESULTS

The results are presented in figures 2 through 10, and table 1. The code-minus-carrier for satellites 2, 6, 11, 15 and 19 are shown in figures 2 through 6 respectively. Figure 7 shows the elevation angles for the satellites during the flight test. As anticipated, the larger error levels are correlated to the lower elevation angles. Table 1 shows the root mean squared (rms) of the multipath error in meters for the C/A-code and the P-code for each satellite for four dynamic conditions: static, taxing at airport, airborne and the final approach. The last row in the table represents the average for all the satellites for both the C/A-code and the P-code for each phase of flight. The smallest average errors are encountered during the final approach phase of flight which had relatively low dynamics with respect to the other flight phases.

With respect to the in-flight data, preliminary analysis indicates that the dynamics seem to correlate with the excursions found in the code-minus-carrier traces. Figures 8 through 10 show the aircraft velocities for the data collection in the east, north and up directions. Clearly, the changes in velocity are correlated with some of the excursions in the multipath data, especially satellite 2. The excursions seen in the multipath plots could be a result of either the dynamics affecting the receiver tracking loops or the banking of the aircraft causing the antenna to be exposed to additional multipath from the wing or the ground. The errors are more predominant during low-altitude turns. This may lead one to conclude that the excursions are indeed a result of multipath. However, this cannot be certain, more study is required to determine the exact cause of the excursions. The data shown in figures 2 through 6 represent the data used for the ambiguity resolution. It is important to understand these deviations to achieve reliable in-flight ambiguity resolution.

CONCLUSIONS

From the data presented in this paper, we conclude that even in a benign environment, measurable multipath error exists. We also found that dynamics have a noticeable effect on multipath errors. Much work is needed in the area of multipath mitigation. Although the P-code represents a tremendous improvement over the standard C/A-code in multipath performance, total immunity has not been achieved. This must be done if DGPS is to be implemented for final approach and landing of aircraft.

ACKNOWLEDGEMENTS

This work was supported by the FAA/NASA Joint University Program for Air Transportation Research (Grant NGR-36-009-017) and NASA Langley Research Center (Grant NAG1-1423). The P-12 GPS receivers were provided by Ashtech, Inc. The author would like to thank Dr. Frank van Graas and Dr. Michael S. Braasch for their helpful suggestions during the writing of this paper. The author would also like to thank

the DC-3 flight crew, Dr. Richard McFarland, Mr. Dennis Atkeson, and Mr. Richard Zoulek.

REFERENCES

1. Lachapelle, G., Falkenberg, W., Neufeldt, D., and P. Keilland: Marine DGPS Using Code and Carrier in a Multipath Environment. Proceedings of the Second International Technical Meeting of the Institute of Navigation Satellite Division, ION GPS-89, Colorado Springs, CO, September 1989.

2. Braasch, M.: On the Characterization of Multipath Errors In Satellite-Based Precision Approach and Landing Systems. Ph.D. Dissertation, Ohio University, Athens, OH, June 1992.

3. Evans, A.: Comparison of GPS Pseudorange and Biased Doppler Range Measurements to Demonstrate Signal Multipath Effects. International Telemetering Conference, Las Vegas, NV, October 1986.

4. General Dynamics, Electronics Division: Final User Field Test Report for the NAVSTAR Global Positioning System Phase I, Major Field Test Objective No. 17: Environmental Effects, Multipath Rejection. Report GPS-GD-025-C-US-7008, San Diego, CA, March 28, 1979.

5. Ferguson, K., Kosmalska, J., Kuhl, M., Eichner, J., Kepski, K., Abtahi, R.: Three-Dimensional Attitude Determination with the Ashtech 3DF 24-Channel GPS Measurement System. Proceedings of the Institute of Navigation's National Technical Meeting, Phoenix, AZ, January 1991.

6. van Graas, F. and Braasch, M.: GPS Interferometric Attitude and Heading Determination: Initial Flight Test Results. NAVIGATION: The Journal of the Institute of Navigation, Vol. 38, No. 4, Winter 1991.

7. Spilker, Jr., J.: GPS Signal Structure and Performance Characteristics. NAVIGATION: The Journal of the Institute of Navigation, Vol. 25, No. 2, Summer 1978.

8. Hatch, R.: The Synergism of GPS Code and Carrier Measurements. Proceedings of the Third International Standards Geodetic Symposium on Satellite Doppler Positioning, Las Cruces, NM, February 1982.

TABLE 1.- SUMMARY OF MULTIPATH ERRORS

	Static		Taxi		Flight		Final Approach	
	C/A rms (meters)	P rms (meters)	C/A rms (meters)	P rms (meters)	C/A rms (meters)	P rms (meters)	C/A rms (meters)	P rms (meters)
SV2	1.127	0.749	0.721	0.233	0.640	0.362	0.315	0.075
SV6	1.272	0.339	0.607	0.161	0.435	0.360	0.367	0.291
SV11	1.040	0.643	0.768	0.547	0.570	0.287	0.883	0.385
SV15	0.679	0.359	0.570	0.370	0.610	0.367	0.405	0.261
SV19	0.708	0.189	0.762	0.179	0.695	0.156	0.932	0.182
average	0.96	0.46	0.69	0.30	0.59	0.31	0.58	0.24

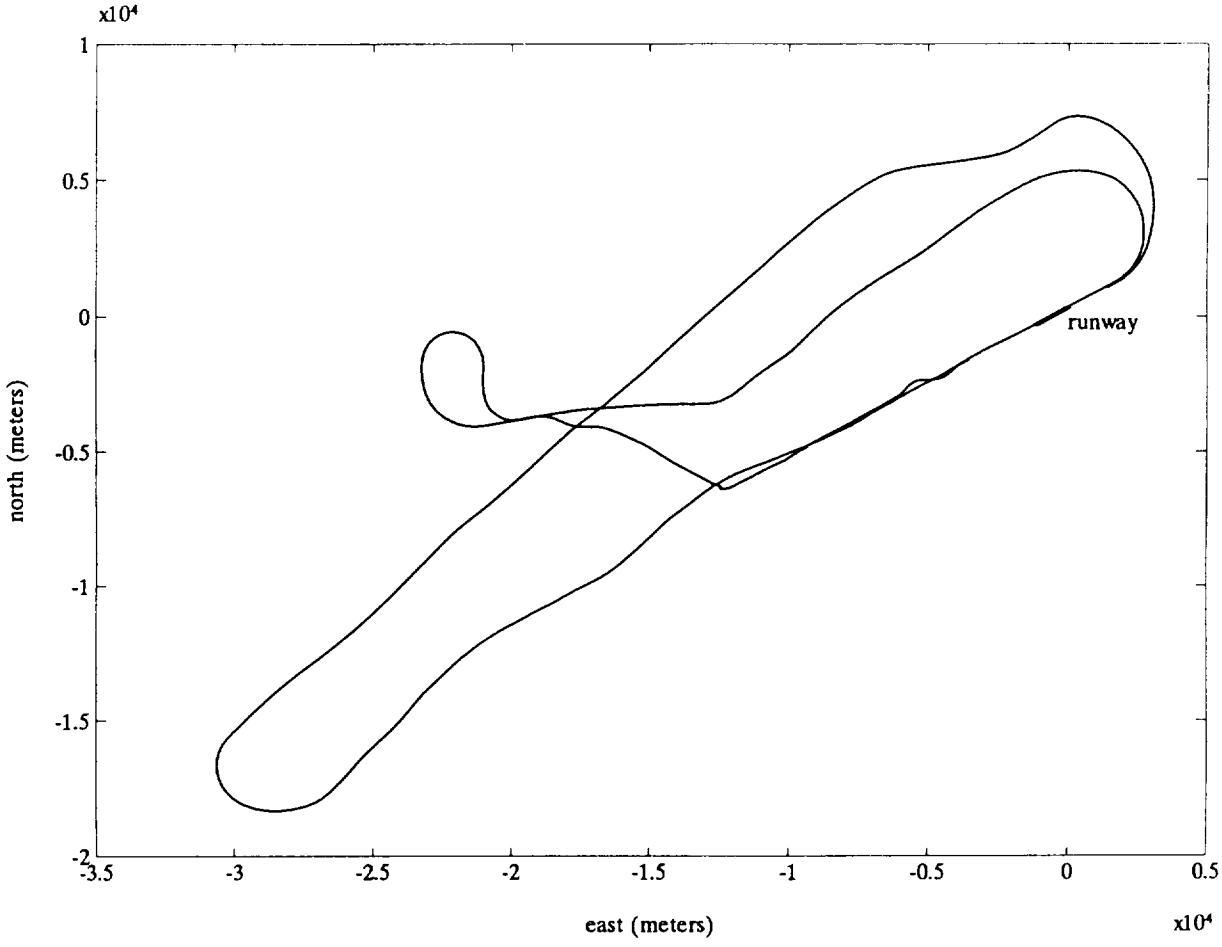

Figure 1. Aircraft flight path in East-North coordinates.

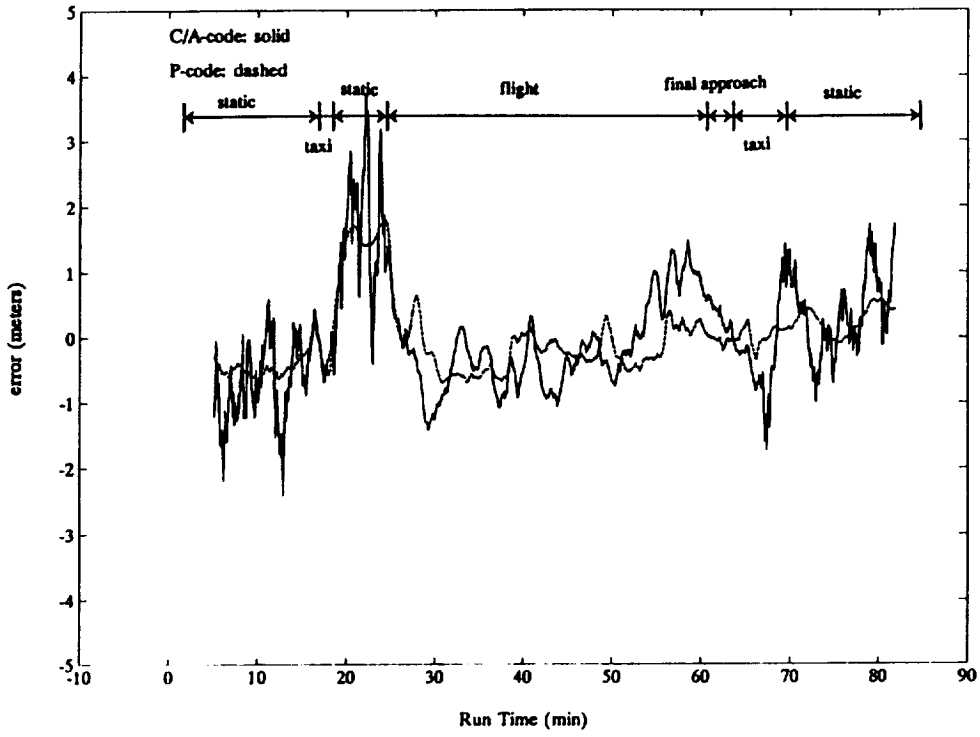

Figure 2. Satellite 2 multipath, thermal noise, unknown bias, and receiver error.

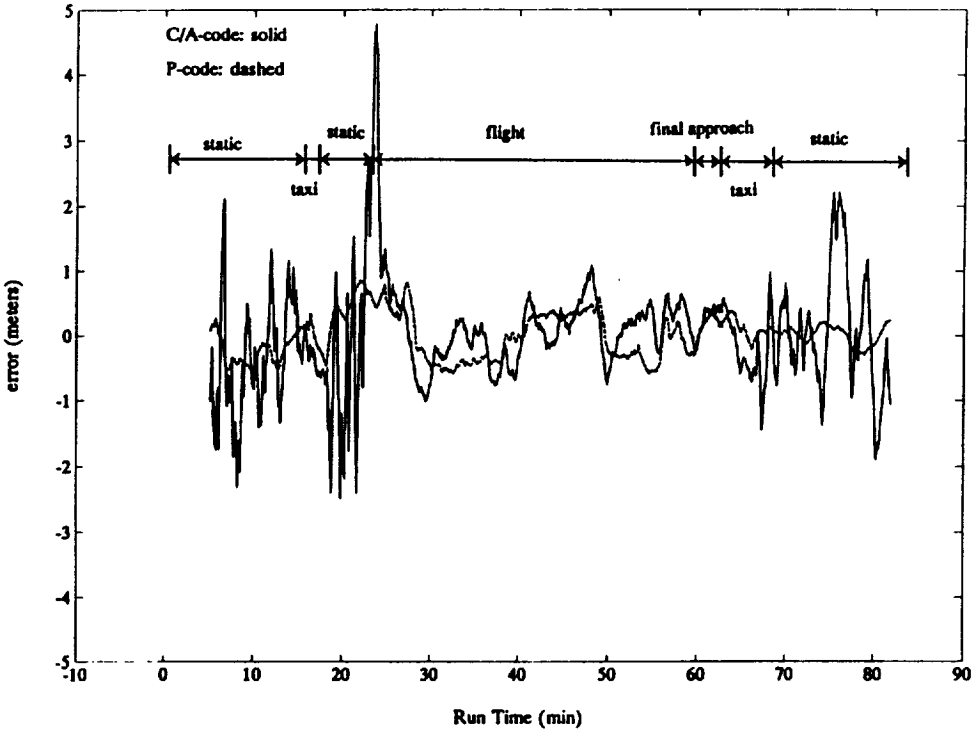

Figure 3. Satellite 6 multipath, thermal noise, unknown bias, and receiver error.

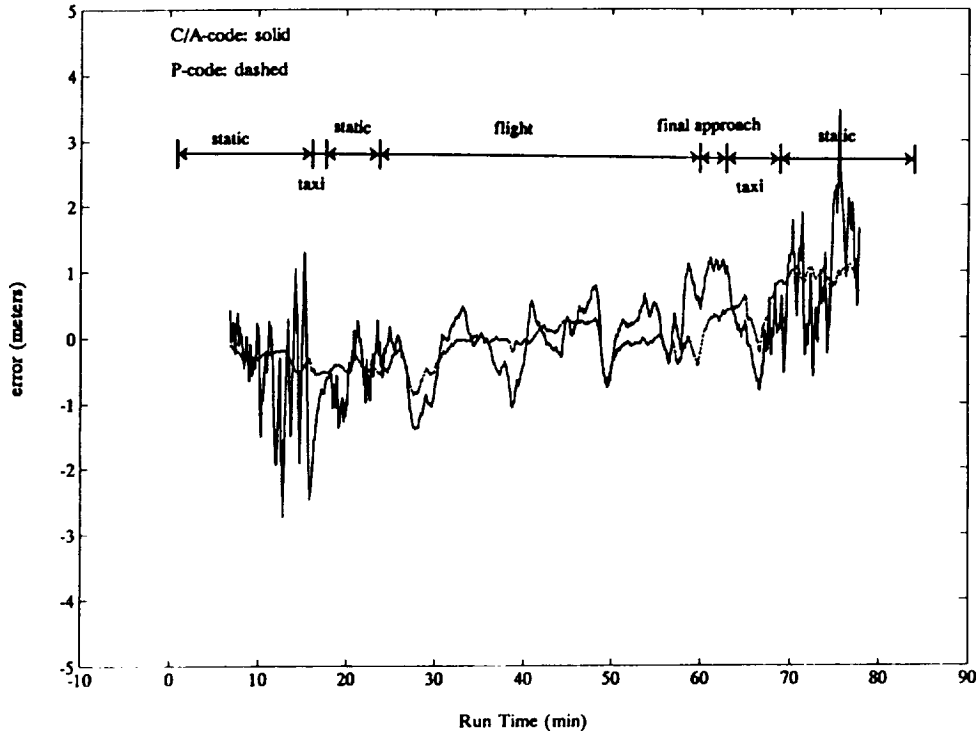

Figure 4. Satellite 11 multipath, thermal noise, unknown bias, and receiver error.

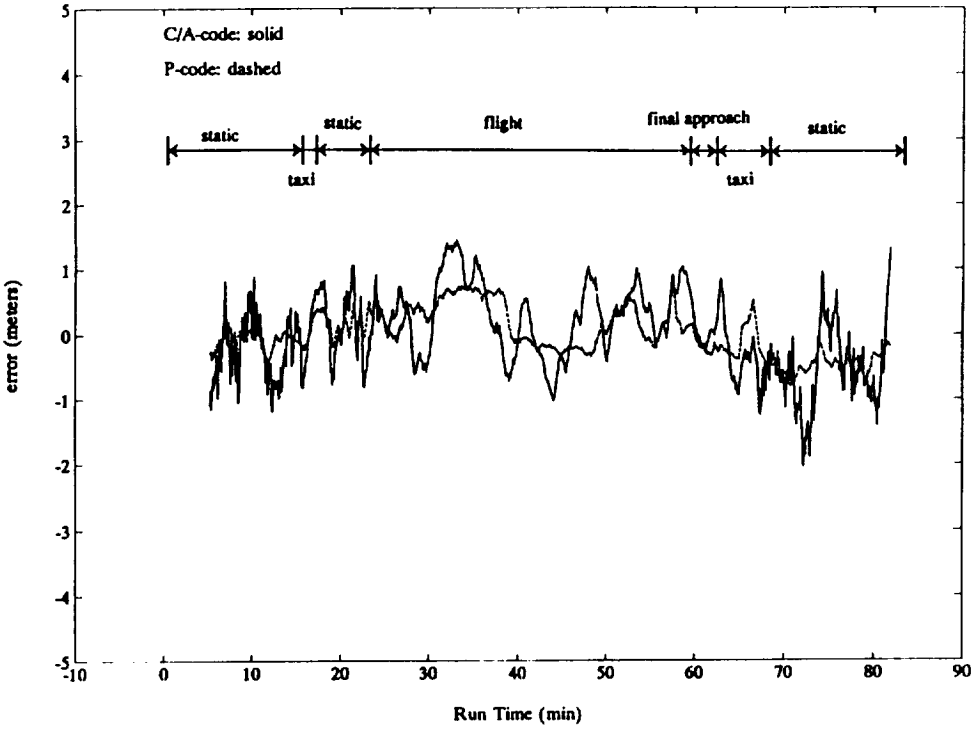

Figure 5. Satellite 15 multipath, thermal noise, unknown bias, and receiver error.

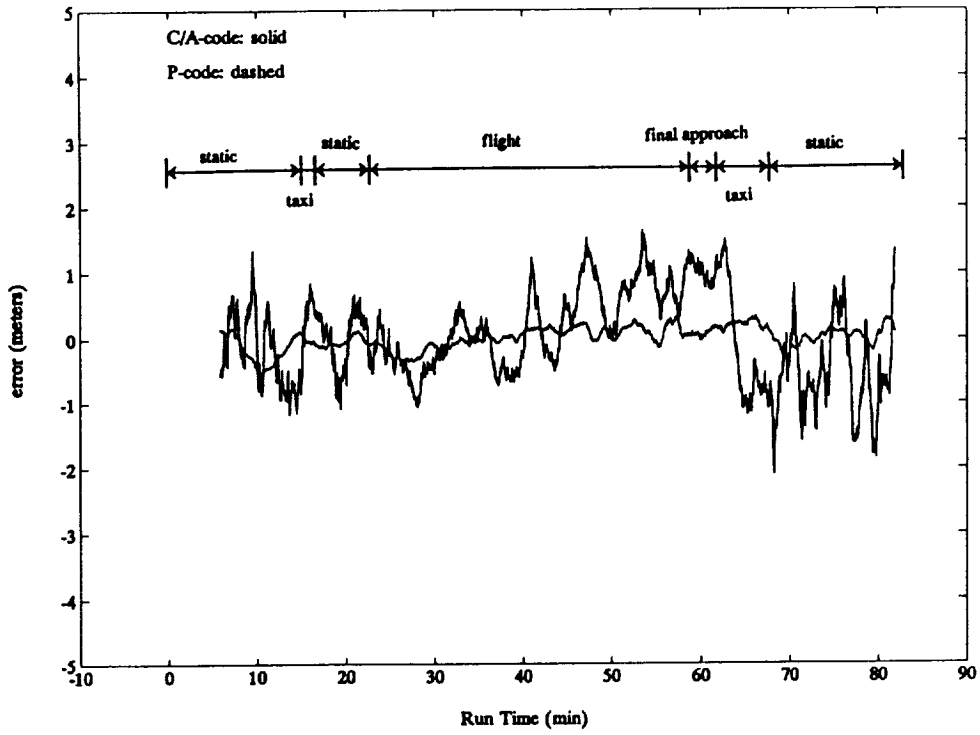

Figure 6. Satellite 19 multipath, thermal noise, unknown bias, and receiver error.

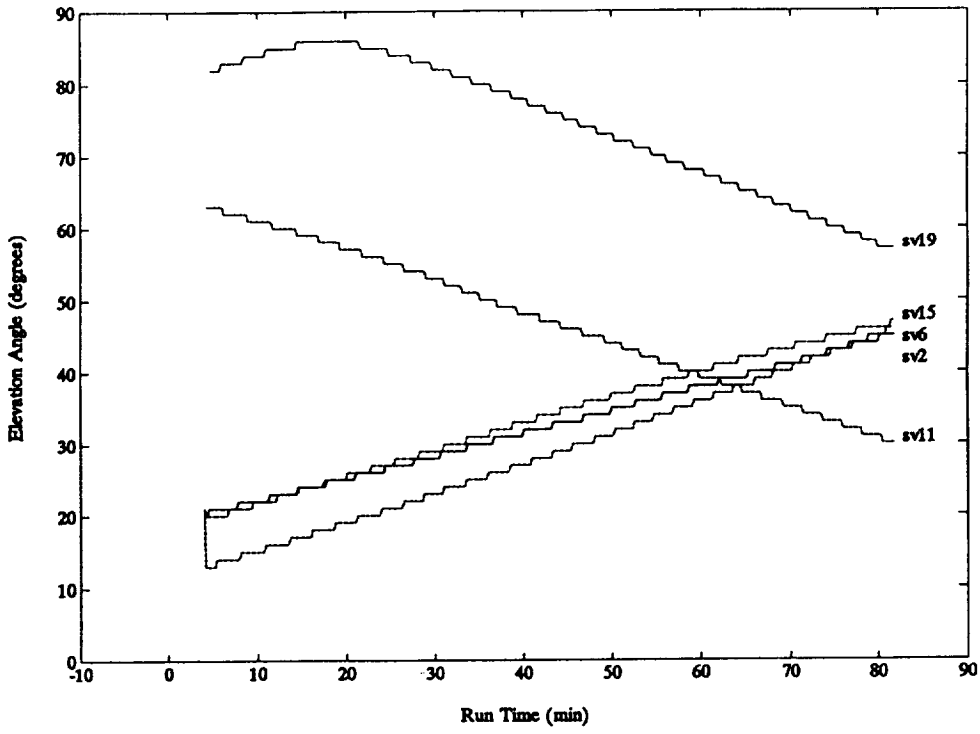

Figure 7. Satellite elevation angles as a function of time.

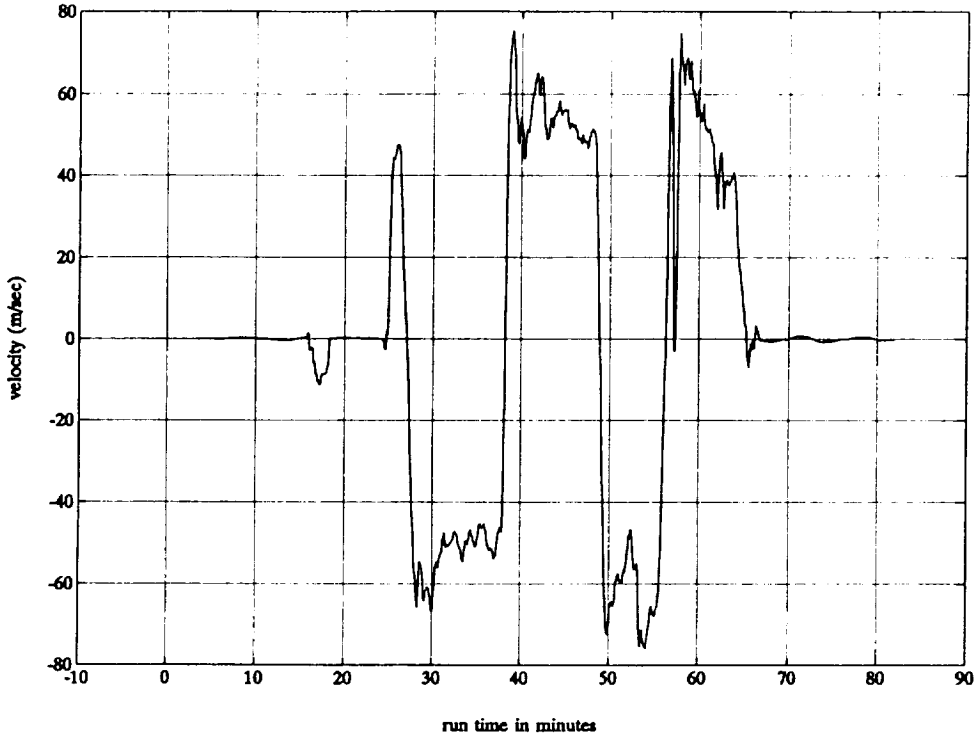

Figure 8. Aircraft velocity in the East direction as a function of time.

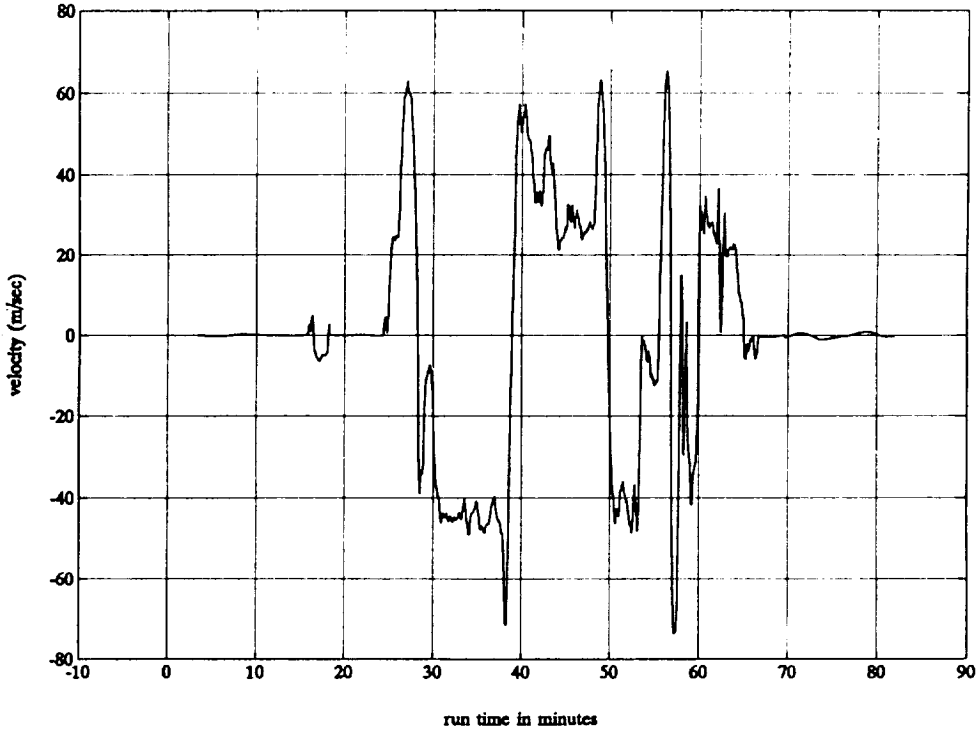

Figure 9. Aircraft velocity in the North direction as a function of time.

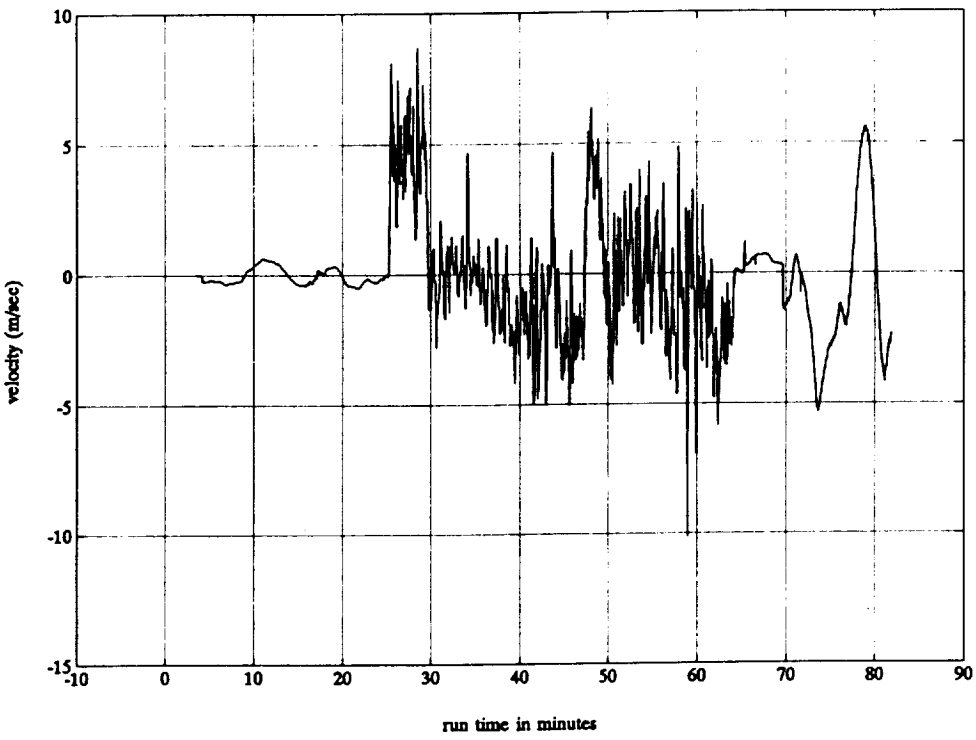

Figure 10. Aircraft velocity in the Vertical direction as a function of time.

PRINCETON UNIVERSITY

INVESTIGATION OF AIR TRANSPORTATION TECHNOLOGY AT PRINCETON UNIVERSITY, 1991-1992

Robert F. Stengel
Department of Mechanical and Aerospace Engineering
Princeton University
Princeton, New Jersey 08544

SUMMARY OF RESEARCH

The Air Transportation Research Program at Princeton University proceeded along six avenues during the past year:

- Intelligent Flight Control
- Computer-Aided Control System Design
- Neural Networks for Flight Control
- Stochastic Robustness of Flight Control Systems
- Microburst Hazards to Aircraft
- Fundamental Dynamics of Atmospheric Flight

This research has resulted in a number of publications, including archival papers and conference papers. An annotated bibliography of publications that appeared between June 1991 and June 1992 appears at the end of this report. The research that these papers describe was supported in whole or in part by the Joint University Program, including work that was completed prior to the reporting period.

Human pilots traditionally have provided the intelligence to fly manned aircraft in numerous ways, from applying manual dexterity through informed planning and coordination of missions. As aircraft characteristics have changed, and more importantly as the technology has allowed, an increasing share of the aircraft's intelligent operation has relied on proper functioning of electro-mechanical sensors, computers, and actuators. It has become possible to apply machine intelligence to flight control.

It can be argued that any degree of feedback from sensed motions to control actions instills intelligent behavior because control actions are shaped by knowledge of the system's response. In a contemporary context, intelligent flight control has come to represent even more ambitious plans to

- make aircraft less dependent on proper human actions for mission completion,
- enhance the mission capability of aircraft,
- improve performance by learning from experience,
- increase the reliability and safety of flight, and
- lower the cost and weight of aircraft systems.

The goal of Ref. 1 is to present concepts for intelligent flight control in the contemporary context, and it forms a basis for future research to be conducted in this program. Control functions are distinguished according to a cognitive/biological hierarchy that is bounded on one end by *declarative functions*, which typically involve decision-making, and on the other by *reflexive functions*, which are more-or-less spontaneous reactions to external or internal stimuli.

In a classical flight control context, declarative functions are performed by the control system's *outer loops*, and reflexive functions are performed by its *inner loops*. We may also define an intermediate level of *procedural functions*, which -- like reflexive functions -- have well-defined input-output characteristics but of a more complicated structure. Traditional design principles suggest that the outer-loop functions should be dedicated to low-bandwidth, large-amplitude control commands, while the inner-loop functions should have high bandwidths and relatively lower-amplitude actions. There is a logical progression from the sweeping, flexible alternatives associated with satisfying mission goals to more local concerns for stability and regulation about a desired path or equilibrium condition.

We have begun to examine the application of these concepts to advanced systems for air traffic management. Graduate student John Wangermann is setting the groundwork for an Intelligent Aircraft/Airspace System (IAAS). The goal is to identify means by which ground-based and airborne flight management systems can cooperate to produce a net gain in the efficiency and robustness of air transportation.

Earlier research focused on intelligent failure-tolerant control, resulting in a journal paper that appeared during the reporting period [2]. Failure-tolerant control systems can be characterized as robust, reconfigurable, or some combination of the two. A controlled system that retains satisfactory performance in the presence of variations from an assumed model without changes in the control system's structure or parameters is said to be *robust*. The degree of failure that can be accommodated by a fixed control structure is more restricted than that of a variable control structure. If the control system's structure or parameters can be altered in response to system failure,

it is said to be *reconfigurable*. In the latter case, the control system detects, identifies, and isolates failures, and it modifies control laws to maintain acceptable performance. A reconfigurable, failure-tolerant control system must be robust enough to preclude controlled system failure while adaptation is taking place.

Graduate student Subrata Sircar has begun to examine concepts for the next generation of computer-aided flight control system design through development of a comprehensive computer program called *FlightCAD* [3], and graduate student Frank Stoner is continuing this research. The program contains a variety of modeling, synthesis, simulation, and evaluation alternatives. It is organized around a desktop metaphor that takes advantage of unique capabilities of the NeXT Computer. A direct digital synthesis technique is employed; it will produce a proportional-integral-filter controller with scheduled linear-quadratic-Gaussian gains. Tight following of pilot commands will be assured by a forward-loop command generator tracker, and the controller will be sufficiently robust to account for specified levels of parameter uncertainty. A principal feature of the control design package is the enhanced ability to iterate and search during the modeling, design, and analysis process.

We are investigating the use of neural networks for system identification and adaptive control. We envision an aerodynamic model that spans the entire flight envelope of an aircraft, including post-stall and spinning regions. The model contains six neural networks with multiple inputs and scalar outputs, three for force coefficients and three for moment coefficients (for example, the pitch moment network takes the form $C_m = g(\mathbf{x},\mathbf{u})$, where $\mathbf{x}$ represents the state and $\mathbf{u}$ the control). If input variables are not restricted to those having plausible aerodynamic effect, false correlations may be created in the network; hence, attitude Euler angles and horizontal position should be neglected, while physically meaningful terms like elevator deflection, angle of attack, pitch rate, Mach number, and dynamic pressure should be included.

Neural networks can be trained using backpropagation or extended Kalman filtering. Backpropagation typically involves a gradient search that minimizes the mean-square output error between desired and network outputs. Search rate can be modified by adding momentum or conjugate-gradient terms to the algorithm. Learning speed and accuracy can be further improved using an extended Kalman filter. If the network has a scalar output, the extended Kalman filter minimizes the fit error between the training hypersurface and that produced by the network. In an examination of the nonlinear aerodynamics of a twin-jet transport aircraft, graduate student

Dennis Linse has found that the fit error can be dramatically reduced by considering the *gradients* of the surfaces as well [4]. The relative significance given to function and derivative error during training can be adjusted through the measurement-error covariance matrix used in filter design.

Control system robustness is defined as the ability to maintain satisfactory stability or performance characteristics in the presence of all conceivable system parameter variations. While assured robustness may be viewed as an alternative to gain adaptation or scheduling to accommodate known parameter variations, more often it is seen as protection against uncertainties in plant specification. Consequently, a statistical description of control system robustness is consistent with what may be known about the structure and parameters of the plant's dynamic model. Graduate student Laura Ryan Ray completed her Ph.D. thesis on this topic and co-authored a number of related papers, the most recent of which is Ref. 5. Graduate student Chris Marrison has applied *Stochastic Robustness Analysis* to ten controllers designed in response to the 1990 American Control Conference Benchmark Control Problem challenge, and he has extended the analysis approach to develop a search procedure that synthesizes controllers with superior robustness [6]. A particular finding is that there is no single "most robust" controller, as design tradeoffs must inevitably be considered. In the present case, stability, settling time, and control usage all are of concern; controllers that favor one criterion over the other two have dramatically different characteristics.

Severe downdrafts and resulting high velocity outflows caused by microbursts present a significant hazard to aircraft on takeoff and final approach. *Microbursts*, which are often associated with thunderstorm activity, also can occur in the vicinity of dissipating convective clouds that produce no rainfall at ground level. Microburst encounter is a rare but extremely dangerous phenomenon that accounts for one or two air carrier accidents and numerous general aviation accidents each year (on average). Conditions are such that an aircraft's performance envelope may be inadequate for safe penetration unless optimal control strategies are known and applied.

Our current wind shear research focuses on avoiding wind shear during transport aircraft operations, as well as on developing cockpit strategies for wind shear recovery. Graduate student Alex Stratton has developed an expert system for wind shear avoidance that extends the FAA Microburst Windshear Guidelines to account for temporal and spatial variations in the evidence that wind shear is present [7-9]. A Bayesian Belief Network relates information gathered from many sources to determine the probability

of encountering a microburst on the intended flight path. Measurements made by a look-ahead sensor (e.g., Doppler radar or lidar) are processed by a bank of extended Kalman filters to develop a head-tailwind profile estimate that helps determine the likelihood of hazardous microburst encounter.

Graduate student Sandeep Mulgund is investigating alternatives for real-time guidance for the case in which wind shear encounter has not been avoided. He has compared optimal (constant) target-pitch-angle guidance with time-varying optimal control histories for a propeller-driven commuter-type aircraft. Results show the significant differences between best target pitch angles for head-tailwind shear and downdraft encounters. (Although the best single angle of attack for wind shear encounter is essentially the same for equivalent horizontal shears and vertical downdrafts, the corresponding pitch angles are decidedly different.) Time-varying optimal control produces additional altitude margin, which could make the difference between escape and impact in critical encounters. (See ref. 10.)

Graduate student Darin Spilman has analyzed the dynamics of a twin-jet transport encountering an intense wind "rotor", finding that a physically realizable rotor could roll the aircraft to inverted attitude if left unopposed by lateral control. Similarly, unopposed full rudder deflection could invert the aircraft in its landing configuration. This analysis will provide a better understanding of possible hazards to aircraft during the approach phase.

Elements of an aircraft's phugoid motion, the long-period interchange of kinetic and potential energy, were presented in a technical comment [11]. This comment clarified the effects of thrust sensitivity to airspeed on the mode, with particular attention to supersonic flight. It also was noted that pitching moment/speed sensitivity is likely to have an effect of comparable magnitude and should not be neglected.

An archival paper describing research conducted by Brenda Belkin appeared during the reporting period [12]. In her M.S.E. thesis, Ms. Belkin used the paradigm of a hypothetical aircraft crew to facilitate the assignment of tasks, rules, and data within parallel knowledge bases. Ms. Belkin was the recipient of the 1990 William E. Jackson Award of the Radio Technical Commission for Aeronautics for her thesis.

ANNOTATED BIBLIOGRAPHY OF 1991-1992 PUBLICATIONS

1. R. F. Stengel, Toward Intelligent Flight Control, presented at the AGARD Guidance and Control Panel Workshop, *Stability in Aerospace Systems*, Toulouse, France, June 1992.

Flight control systems can benefit by being designed to emulate functions of natural intelligence. Intelligent control functions fall in three categories: declarative, procedural, and reflexive. Declarative actions involve decision-making, providing models for system monitoring, goal planning, and system/scenario identification. Procedural actions concern skilled behavior and have parallels in guidance, navigation, and adaptation. Reflexive actions are more-or-less spontaneous and are similar to inner-loop control and estimation. Intelligent flight control systems will contain a hierarchy of expert systems, procedural algorithms, and computational neural networks, each expanding on prior functions to improve mission capability, to increase the reliability and safety of flight, and to ease pilot workload.

2. R. F. Stengel, Intelligent Failure-Tolerant Control, *IEEE Control Systems Magazine*, Vol. 11, No. 4, June 1991, pp. 14-23.

An overview of failure-tolerant control is presented, beginning with robust control, progressing through parallel and analytical redundancy, and ending with rule-based systems and artificial neural networks. By design or implementation, failure-tolerant control systems are "intelligent" systems. All failure-tolerant systems require some degree of robustness to protect against catastrophic failure; failure tolerance often can be improved by adaptivity in decision-making and control, as well as by redundancy in measurement and actuation. Reliability, maintainability, and survivability can be enhanced by failure tolerance, although each objective poses different goals for control system design. Artificial intelligence concepts are helpful for integrating and codifying failure-tolerant control systems, not as alternatives but as adjuncts to conventional design methods.

3. R. F. Stengel and S. Sircar, Computer-Aided Design of Flight Control Systems, *Proceedings of the 1991 AIAA Guidance, Navigation, and Control Conference*, New Orleans, Aug. 1991, pp. 677-683.

A comprehensive computer program for designing and evaluating multidisciplinary aircraft flight control systems is described. The *FlightCAD* program contains a variety of modeling, synthesis, analysis, and simulation alternatives. *FlightCAD* ultimately will implement a number of control design techniques; here it uses direct digital synthesis to produce a robust,

proportional-integral-filter controller with scheduled linear-quadratic-Gaussian gains and command generator tracking of pilot inputs. The *FlightCAD* design approach is reviewed, and a status report is presented.

4. D. Linse and R. F. Stengel, Identification of Aerodynamic Coefficients Using Computational Neural Networks, *AIAA 30th Aerospace Sciences Meeting*, AIAA Paper No. 92-0172, Reno, Jan. 1992.

Precise, smooth aerodynamic models are required for implementing adaptive, nonlinear control strategies. Accurate representations of aerodynamic coefficients can be generated for the complete flight envelope by combining computational neural network models with an Estimation-Before-Modeling paradigm for on-line training. A novel method of incorporating first-partial-derivative information is employed to estimate the weights in individual feedforward networks for each coefficient. The method is demonstrated by generating a model of the normal force coefficient of a twin-jet transport aircraft from simulated flight data, and promising results are obtained.

5. L. R. Ray and R. F. Stengel, Application of Stochastic Robustness to Aircraft Control, *J. Guidance, Control, and Dynamics*, Vol. 14, No. 6, Nov.-Dec. 1991, pp. 1251-1259.

Stochastic robustness, a simple numerical procedure for estimating the stability robustness of linear, time-invariant systems, is applied to a forward-swept-wing aircraft control system. Based on Monte Carlo evaluation of the system's closed-loop eigenvalues, this analysis approach introduces the *probability of instability* as a scalar stability robustness measure. The related *stochastic root locus* provides insight into robustness characteristics of the closed-loop system. Three linear-quadratic controllers of increasing robustness are chosen to demonstrate the use of stochastic robustness to analyze and compare control designs. Examples are presented illustrating the use of stochastic robustness analysis to address the effects of actuator dynamics and unmodeled dynamics on the stability robustness of the forward-swept-wing aircraft.

6. R. F. Stengel and C. I. Marrison, Stochastic Robustness Synthesis for a Benchmark Problem, *Proceedings of the 1992 American Control Conference*, Chicago, June 1992, pp. 2421-2422.

Stochastic Robustness Analysis guides the synthesis of robust LQG regulators for a Benchmark Control Problem. Probabilities of exceeding allowable design limits, including stability, settling time, and control usage,

are estimated by Monte Carlo evaluation. Robust, low-gain compensators that fulfill objectives are designed by numerically minimizing quadratic functions of these probabilities. The method is straightforward and makes use of uncomplicated design principles.

7. D. A. Stratton and R. F. Stengel, Probabilistic Reasoning for Intelligent Wind Shear Avoidance, *J. Guidance, Control, and Dynamics*, Vol. 15, No. 1, Jan.-Feb. 1992, pp. 247-254.

Avoiding severe wind shear challenges the ability of flight crews, as it involves assessing risk from uncertain evidence. A computerized intelligent cockpit aid can increase flight crew awareness of wind shear, improving avoidance decisions. A primary task in the development of such a cockpit aid is providing a means of assessing risk from evidence of wind shear from sources with varying reliability. The Federal Aviation Administration's Windshear Training Aid provides guidelines for assessing the risk of wind shear encounter from meteorological evidence. Use of these guidelines in the cockpit is complicated by uncertainty surrounding meteorological knowledge of wind shear. Bayesian network representation is discussed as a means of modeling this uncertain knowledge in a computer. A probabilistic model of the Windshear Training Aid guidelines using Bayesian network representation is presented. This model combines evidence from sources of varying reliability and incorporates results from meteorological studies of wind shear. The probabilistic model can provide flight crews with meaningful estimates of risk to aid their decisions, using evidence from a variety of sources and a base of meteorological knowledge.

8. D. A. Stratton and R. F. Stengel, Robust Kalman Filter Design for Predictive Wind Shear Detection, *Proceedings of the 1991 AIAA Guidance, Navigation, and Control Conference*, New Orleans, Aug. 1991, pp. 1549-1556.

Severe, low-altitude wind shear is a threat to aviation safety. Airborne sensors under development measure the radial component of wind along a line directly in front of an aircraft. In this paper, optimal estimation theory is used to define a detection algorithm to warn of hazardous wind shear from these sensors. To achieve robustness, a wind shear detection algorithm must distinguish threatening wind shear from less hazardous gustiness, despite variations in wind shear structure. This paper presents statistical analysis methods to refine wind shear detection algorithm robustness. Computational methods predict the ability to warn of severe wind shear and avoid false warning. Comparative capability of the detection algorithm as a function of

its design parameters is determined, identifying designs that provide robust detection of severe wind shear.

9. D. A. Stratton and R. F. Stengel, Real-Time Decision Aiding: An Application to Wind Shear Avoidance, *AIAA 30th Aerospace Sciences Meeting*, Reno, AIAA Paper No. 92-0290, Jan. 1992.

Modern control theory and artificial intelligence are applied to the Wind Shear Safety Advisor, a conceptual airborne advisory system to help flight crews avoid or survive encounters with hazardous low-altitude wind shear. Numerical and symbolic processes fuse diverse, time-varying data from ground-based and airborne measurements. Simulated wind-shear-encounter scenarios illustrate the need to consider a variety of factors for optimal decision reliability. Simulations show the potential for effectively integrating available information, highlighting the benefits of the computational techniques employed.

10. S. Mulgund and R. F. Stengel, Target Pitch Angle for the Microburst Escape Maneuver, *AIAA 30th Aerospace Sciences Meeting*, Reno, AIAA Paper No. 92-0730, Jan. 1992.

Commuter and general aviation aircraft face no less a threat from microburst wind shear than do large jet transports, yet most studies of wind shear encounter have neglected them. The effects of microburst wind shear on a propeller-driven commuter aircraft are considered here. Recovery performance of a commuter-type aircraft in a microburst encounter is examined using a constant-pitch-attitude strategy and flight-path optimization. The goals are to identify a suitable target pitch angle for the escape maneuver and to determine the nature of an optimal escape maneuver for commuter aircraft. The results demonstrate that the pitch attitude that maximizes climb rate in a wind shear is strongly dependent on whether the shear is predominantly a downdraft or a horizontal shear. Simulated recoveries show that the optimal constant pitch angle depends on the altitude of encounter, the strength of the microburst, and the initial position of the aircraft relative to the microburst core. In severe wind shear encounters at very low altitude, best results are obtained at relatively low pitch angle. Excessively high target pitch angles subject the aircraft to prolonged periods near stall. Flight path optimization demonstrates that maximum ground clearance is obtained by maintaining a low pitch attitude early in the encounter followed by a gradual pitch-up that ceases when the aircraft exits the wind shear.

11. R. F. Stengel, Comments on "Effect of Thrust/Speed Dependence on Long-Period Dynamics in Supersonic Flight," *J. Guidance, Control, and Dynamics*, Vol. 15, No. 3, May-June 1992, pp. 795-797.

The referenced paper discusses effects of speed-dependent variations in thrust on the long-period motions of aircraft in supersonic flight. Its principal contribution is the demonstration of effects that a complex pair of zeros have on speed-to-throttle feedback. It is concluded that there are fundamental differences between thrust/speed effects in sub- and supersonic flight. The purpose of this comment is to show that thrust/speed effects are indeed small but not zero in supersonic flight and that this is a kinematic effect of increasing speed rather than an aerodynamic effect of Mach number. In the process, a simplified analytical model is offered for further study. Furthermore, it is noted that pitching moment/speed sensitivity due to thrust-axis offset is likely to have important long-period effects even when the direct thrust/speed effects are small.

12. B. L. Belkin and R. F. Stengel, Systematic Methods for Knowledge Acquisition and Expert System Development, *IEEE Aerospace and Electronic Systems Magazine*, Vol. 6, No. 6, June 1991, pp. 3-11.

Nine interacting rule-based systems collectively called AUTOCREW were designed to automate functions and decisions associated with a combat aircraft's subsystems. The organization of tasks within each system is described; performance metrics were developed to evaluate the workload of each rule base and to assess the cooperation between rule bases. Each AUTOCREW subsystem is composed of several expert systems that perform specific tasks. The NAVIGATOR was analyzed in detail to understand the difficulties involved in designing the system and to identify the tools and methodologies that ease development.

ADVANCED AIR TRAFFIC MANAGEMENT

J. P. Wangermann

Princeton University

Air traffic worldwide continues to grow, and this growth is predicted to continue in the coming decades. Air traffic management (ATM) systems in several parts of the world have now reached their operating limits. The external symptoms of this are increases in the number of delays experienced by the system, and a rise in the frequency of near-misses. If the ATM system fails to develop to provide more capacity, then the result will be a decrease in safety levels, and increasing delays, or a limit on the number of permitted aircraft operations.

- In 1989 a 3% increase in traffic in the USA caused a 17% increase in ATC delays
- 64m operations at towered FAA airports in 1990; 80m operations predicted for 2000
- Delta suffered 2800 minutes of delay per day (1989)
- BA 767 flights from London to Paris are scheduled to take 5 minutes more than Vanguard flights 30 years ago

There is a need for more capacity in the airspace system without degrading safety.

In recent years a number of new technologies have emerged that could allow a radically different ATM structure to be used, rather than the present geographically spread system, designed around radar monitoring and radio communications. Some of these technologies are listed below.

- GNSS (GPS/GLONASS) Satellite Navigation Systems - aircraft are no longer dependent on ground based aids for navigation
- TCAS systems allow aircraft to monitor their separation from other traffic
- Mode S transponders allow air-to-air and air-to-ground data communications
- FMS/FCS systems allow routings and trajectories to be computed rapidly
- MLS and D/GPS allow more complex approaches to airports
- Communications satellites allow air to ground communications over long distances

Trends: aircraft are increasingly autonomous; surveillance and communications not limited to radio/radar range

This new technology could allow the ATM system to change in a number of ways. The increased use of data transmissions, satellite communications, and GPS could be used to enhance the present system, while still leaving the present responsibilities of pilots and controllers unchanged. This is the basis of ICAO's Future Air Navigation System (FANS) concept. Alternatively, the increased navigational accuracy and use of 4-D Flight Management Systems (FMS) gives aircraft the capability to follow a flight plan more closely than they can at present. This could allow more strategic planning to be carried out, on the basis of the flight plan, reducing the amount of tactical control needed to ensure safety. This could be characterized as a more centralized or planned system. Equally, the same technologies make aircraft less dependent on ground based services for both position information and separation from other aircraft. This could allow a more autonomous ATM system, with far less control exercised from the ground.

- **Centralized/Planned Control System**
- **Evolutionary FANS system**
- **Distributed/Autonomous System**

In a centralized system that strategically plans flight paths to ensure aircraft do not conflict while meeting a scheduled arrival time, the main problem is the handling of uncertainty. If there were no winds and it was known exactly what speed, altitude, and track the aircraft would fly then the touchdown time could be deterministically computed. The presence of variable winds in the atmosphere causes a variation in the length of time a journey will take. An aircraft can overcome this to an extent by controlling its airspeed, but the range of wind speeds that can be encountered at altitude is greater than can be matched by variation in aircraft speed. As the time remaining to touchdown decreases the uncertainty in touchdown time decreases. Any strategic planning has to account for this temporal uncertainty: there will also be a spatial uncertainty due to navigation system errors and possible re-routings during the flight. If the uncertainty can be characterized as a probability density function (p.d.f.) then the problem could probably be tackled by a form of probabilistic reasoning.

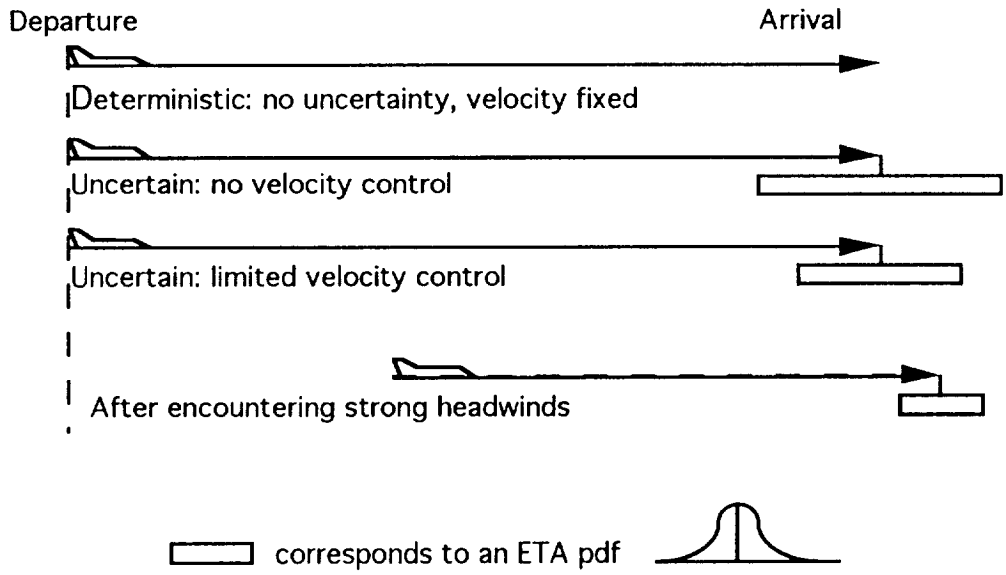

If the problem of handling the temporal and spatial uncertainties of a flight can be overcome, then strategic planning using flight plans can offer several advantages over the existing system. Possibly the main increase in capacity would come from the ability to fly any 4-D profile within permissible airspace, rather than following a fixed route structure which has the effect of concentrating aircraft in a small percentage of the available airspace. Combined with satellite communications, such a system would also allow the destination airport, or Terminal Maneuvering Area (TMA or TCA), to revise an aircraft's target arrival time while en-route. The flight plan would then be recomputed for the new required arrival time. This would benefit congested airports and TMAs by providing a smoother, more predictable, flow of aircraft into a TMA, reducing the amount of vectoring and maneuvering required to produce the maximum safely separated flow rate of aircraft onto the runway. This would help ensure that airports operate at close to their maximum runway capacity, while reducing controller workload.

- **The proposed system would compute conflict-free 4-D trajectories that aircraft would then accurately follow.**
- **Accurate planning leads to fewer conflicts**
- **Early TCA involvement leads to smooth flows in terminal area**
- **Reduced controller workload**
- **Increased capacity**
- **Fewer delays**

The thrust of this research is to construct an Intelligent Aircraft Airspace System. Intelligence can be characterized as having both the knowledge required and the ability to manipulate that knowledge in order to carry out some function (such as planning or control). At present almost all the knowledge (position data, weather data etc.) is concentrated in the ground controllers, and it is their human intelligence that allows the system to operate, applied through tactical control of aircraft in the system. The centralized system outlined here uses the increased guidance and navigation capabilities of aircraft to allow intelligent strategic flight path planning to occur (as opposed to system level flow management planning). It does not use any of the separation monitoring capabilities that TCAS gives aircraft (other than as an extra safety level), and the control of the system is still on the ground, though partially transferred from tactical controllers, to the strategic flight path planning function.

In an autonomous system, the aircraft has to be more intelligent. If the level of ground control required is to be reduced then an aircraft has to at least partly be able to plan a conflict-free trajectory for a reasonable time ahead, and also has to navigate without explicit ground control guidance. The field of Artificial Intelligence has developed in a number of areas that could be applicable to this problem. Work will now focus on defining an outline of an autonomous aircraft airspace system.

COMPUTER AIDED CONTROL SYSTEM DESIGN (CACSD)

Frank T. Stoner
Department of Mechanical and Aerospace Engineering
Princeton University

COMPUTER AIDED CONTROL SYSTEM DESIGN (CACSD)

Frank T. Stoner
Department of Mechanical and Aerospace Engineering
Princeton University

Joint University Program
for Air Transportation Research

Quarterly Meeting
2-3 April 1992

The design of modern aerospace systems relies on the efficient utilization of computational resources and the availability of computational tools to provide accurate system modeling. This research focuses on the development of a computer aided control system design application which provides a full range of stability analysis and control design capabilities for aerospace vehicles.

BACKGROUND

- Purpose: Develop an application which provides a full range of stability analysis and control design capabilities for aerospace vehicles.
- Motivation for CACSD:
  - Computationally Demanding Modern Design Techniques
  - Increased Performance Expectations of Modern Systems
  - Increasing Availability of High-Performance, Low-Cost Computer Products

The application must address the concerns which arise during all five phases of the design process: Characterization, Representation, Design, Analysis and Implementation.

Characterization is the phase during which system requirements and parameters are defined. In the Representation phase, structural and behavioral models of the system are developed. Control theory is then applied during Design to realize the controlled system. Values of control system parameters and overall system performance are assessed during the Analysis phase. Hardware and/or Software generation is then required in the implementation of the control system.

In addition, the CACSD application should provide (1) an effective user interface, and (2) requirements traceability and configuration control through documentation of the control system and control system design process.

PROCESS DESCRIPTION

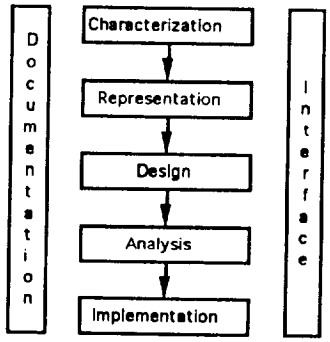

Work has progressed in the development of Flight CAD, a menu-driven, multi-window, desktop metaphor environment which provides modeling, synthesis, analysis, and simulation capabilities focused on the design of flight control systems for modern aircraft.

WORK TO DATE

- Flight CAD (S. Sircar)
  - Menu-driven, Multi-window, Desktop Metaphor Environment
  - Modeling, Synthesis, Analysis, and Simulation Capabilities
  - Focus on Design of Flight Control Systems of Modern Aircraft

Current research focuses on the development of multidisciplinary design and analysis capabilities within Flight CAD. While early aerospace vehicles were designed primarily for optimum mission performance, the design of modern vehicles must address many considerations: mission performance, air worthiness (including structural durability), manufacturing and maintenance considerations, operational requirements, the environmental impact from noise and pollution, as well as life cycle cost. Design decisions made during the initial phases of the design process may effect up to 85% of the total program cost. These design decisions typically involve some interdisciplinary trade-offs. Multidisciplinary techniques are crucial to the analysis and design of control systems for modern aerospace vehicles.

Focus on Multidisciplinary Design and Analysis Capabilities

- Early aerospace vehicles were designed primarily for optimum mission performance.
- Modern aerospace vehicle design must address many considerations.
- Design decisions made during the initial phases of design may significantly affect the total program cost.
- Answers to design decisions typically must be based on interdisciplinary trade-offs.
- Multidisciplinary techniques must be employed to effectively analyze and design control systems for modern aerospace vehicles.

As an example of the interdisciplinary coupling between vehicle subsystems, consider the subsystem relationships for an actively controlled flexible wing. The complete set of system design variables includes structural, aerodynamic, and control system design variables. Each of these groups of design variables has a direct effect upon the behavior of its corresponding subsystem. Output variables which include the wing surface pressure distribution, structural deformations, and control surface deflections provide coupling between the subsystems which indirectly links each group of design variables to the remaining subsystems.

An Example of Interdisciplinary Coupling

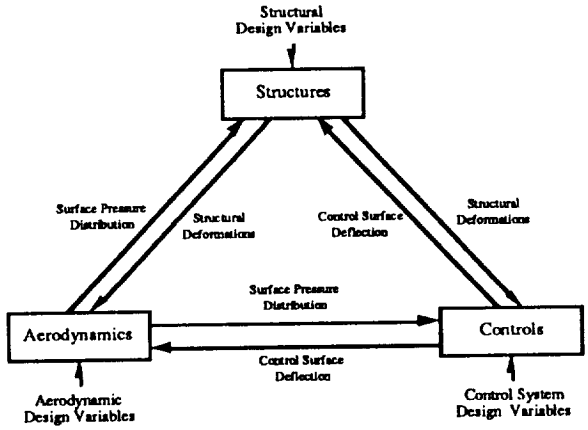

Subsystem interactions for an actively controlled flexible wing

Many issues must be addressed in order to incorporate multidisciplinary design and analysis features within Flight CAD. Efficient mathematical models must be employed for representation of vehicle subsystems. Parallel processing capabilities must be exploited to maintain a high level of interaction with the designer. Representation of the interdisciplinary coupling within the user interface must also be considered. It may also be desirable to allow the user to define "Design Rules" which may be incorporated in an expert system to help automate the design process; determining when to regenerate reference trajectories, or when to re-analyze aerodynamic characteristics. Current research will focus on these issues and their impact on computer aided control system design.

Issues To Be Addressed

- Efficient Mathematical Models for Subsystem Representation
- Identification of Parallel Processing Opportunities
- Impact of Interdisciplinary Coupling on User Interface
- Development of Expert System "Design Rules"

Chris Marrison

Synthesis of Robust Controllers

At the 1990 American Controls Conference a benchmark problem was issued as a challenge for designing robust compensators. Many compensators were presented in response to the problem. In previous work Stochastic Robustness Analysis (SRA) was used to compare these compensators. In this work SRA metrics are used as guides to synthesize robust compensators, using the benchmark problem as an example.

The benchmark problem consists of 2 masses (m_1 and m_2) connected by a spring (k), with control of the first mass, and output defined as position of the second mass. The state, control, and output vectors have dimensions of 4, 1, and 1. The Benchmark Problem requires an output settling time of 15 sec after an impulsive disturbance on m_2, with limited actuator use and closed-loop robustness in the presence of parameter variations. Plant parameters may vary in the ranges $0.5 < k < 2$, $0.5 < m_1 < 1.5$, and $0.5 < m_2 < 1.5$. In the present study, the settling-time limit is considered to be violated if the displacement of m_2 exceeds a ± 0.1-unit envelope, 15 or more seconds after the disturbance. The control-usage limit is violated if control displacement exceeds one unit, and the stability requirement is violated with one or more positive closed-loop roots. Parameters are assumed to have uniform probability distributions within their ranges.

Benchmark Problem

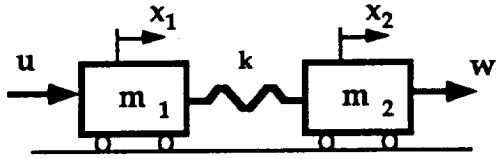

$y=x_2$, $z=x_2+n$

$k=1$ N/m, $m_1=1$ kg, $m_2=1$ kg

Requirements

- Robust to Variation in Parameters
- Settling Time of 15 secs
- Minimum Actuator Use

By using SRA we can find estimates of the probabilities of instability (P_i), settling time violation (P_{ts}), and actuator usage (P_u). These can be used by a designer to guide the adjustment of design parameters to produce a robust compensator. As a method of trading off different design requirements the probabilities can be combined into a scalar cost. The minimum of this cost function can then be sought. For the benchmark problem the cost function chosen was a weighted quadratic sum of the probabilities of instability, settling time violation, and actuator usage.
The nature of the probabilistic metrics and variations in the functional estimates due to the Monte Carlo Evaluation make the cost function difficult to minimize.

Optimization of Robustness

$$J = aP_i^2 + bP_u^2 + cP_t^2$$

Problems with Optimization

- N Dimensional
- Not Continuously Differentiable
- Plateaus where P=0 or 1
- Noise in Evaluation

Efficient methods for minimizing this cost are still under research. For the benchmark problem the multidimensional search was reduced to a series of line searches by using the standard univariate search method which involves changing only one design parameter at a time.

Univariate Minimization

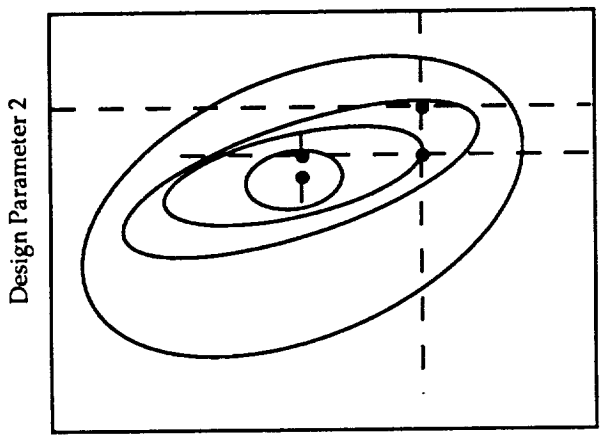

Each line search was carried out by adjusting a chosen design parameter across a range and assessing the cost at several points along the range. If the parameter produced a statistically significant reduction in the cost, then the parameter was adjusted to the minimizing value. The search then went on to the next parameter.

Optimization Procedure

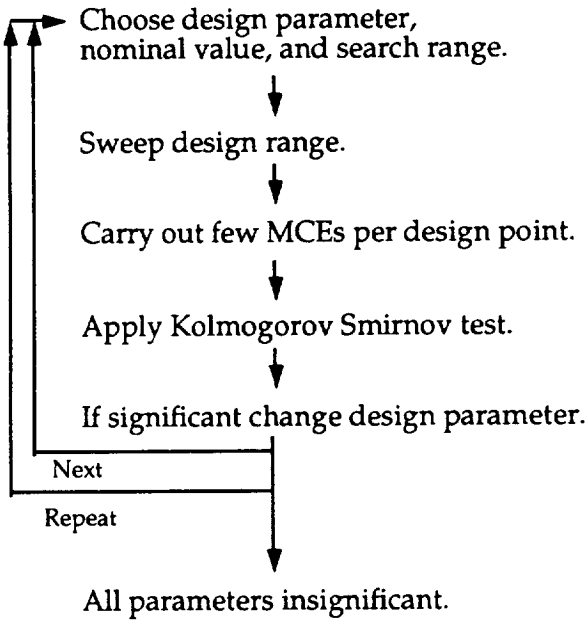

For the benchmark problem the compensator structure chosen was the Linear Quadratic Gaussian Regulator. The search first found a robust LQR, a robust filter was added (the method for finding this robust filter is explained later), then the full LQGR was fine tuned using the univariate minimization.

The final compensator was fully analyzed with many Monte Carlo evaluations to validate the design. For the benchmark problem the validating analysis used 8,000 evaluations.

Synthesis for Benchmark Problem

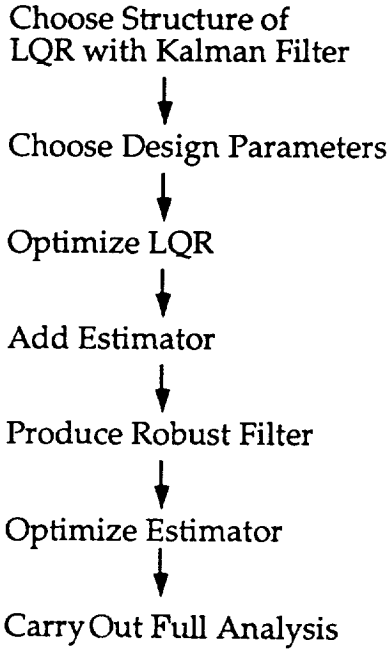

By using the state propagation equations we can group the effects of parameter variations with disturbance effects. We can simulate the time response of the system and calculate the disturbance residual, q. This residual includes the effect of parameter variations with the disturbance effects. q can be used to estimate a disturbance covariance matrix. When a filter is designed with this matrix it handles parameter variations as expected disturbances and is more robust in producing estimates of the state.

Robust Kalman Filter

$$x_{k+1} = \Phi x_k + \Gamma u_k + \Lambda w_k$$

$$x_{k+1} = \hat{\Phi} x_k + \hat{\Gamma} u_k + (\Delta\Phi x_k + \Delta\Gamma u_k + \Lambda w_k)$$

$$\hat{x}_{k+1} = \hat{\Phi}\hat{x}_k + \hat{\Gamma} u_k + K(z_k - H\hat{x}_k)$$

$$Q_k = E\left[(\Lambda w_k)(\Lambda w_k)^T\right]$$

$$Q_k = E\left[(\Delta\Phi x_k + \Delta\Gamma u_k + \Lambda w_k)(\Delta\Phi x_k + \Delta\Gamma u_k + \Lambda w_k)^T\right]$$

$$q_k = x_{k+1} - \hat{\Phi} x_k - \hat{\Gamma} u_k$$
$$= (\Phi - \hat{\Phi}) x_k + (\Gamma - \hat{\Gamma}) u_k + \Lambda w_k$$

$$\hat{Q} = \frac{1}{N-1} \Sigma_{k=1}^{N} q_k q_k^T$$

Four compensators were designed with different cost function weights to represent different design concerns. The first design (LQG1) has the weight predominantly on the probability of instability; this would be the case when it is very important that even marginal instability should never occur. LQG2 puts weight on the probability of actuator saturation; this will have the effect of allowing a slight decrease in other robustness variables to ensure that actuator limits are rarely violated. For LQG 3 most of the weight is on the performance (settling time) robustness. LQG4 is designed to have a general blend of the robustness properties.

The weights affected the nominal performances in predictable ways e.g., the compensator with high weighting on settling time violation had the lowest nominal settling time.

Characteristics of Compensators Designed for the Benchmark Problem

Weights for Cost Function J

	a	b	c
LQG 1	1	0.01	0.01
LQG 2	0.01	1	0.01
LQG 3	0.01	0.01	1
LQG 4	1	0.02	0.06

3 Zeros, 5 Poles,

1 Non-minimum-phase zero.

Nominal Disturbance Responses

	$T_{s0.1}$	u_{max}	x_{2max}
LQG 1	14.1	0.59	2.12
LQG 2	12.1	0.46	1.59
LQG 3	10.1	0.82	1.09
LQG 4	12.5	0.54	1.43

The robustness of the LQGRs designed using SRA metrics compare very well with the ten compensators (A-J) which had been designed by other methods (these compensators had been analyzed in previous work).

The compensators designed by SRA were better than all the other compensators with respect to stability, actuator saturation, and performance (settling time) robustness.

The only exception was that design D had better settling time robustness than any of the LQGs but this was at the expense of having very high actuator usage.

Comparison of Robustness Costs

Design	J1	J2	J3	J4
A	0.03	0.03	0.92	0.08
B	0.01	0.01	0.94	0.06
C	0.01	0.01	0.94	0.06
D	0.01	1.00	0.01	0.02
E	0.02	0.16	1.00	0.07
F	0.03	1.00	0.75	0.08
G	0.06	0.79	1.01	0.12
H	0.01	0.03	0.83	0.05
I	0.008	0.01	0.84	0.05
J	0.07	0.30	1.00	0.12
LQG1	0.006	0.02	0.58	0.04
LQG2	0.004	0.004	0.42	0.03
LQG3	0.09	0.13	0.22	0.10
LQG4	0.006	0.006	0.18	0.02

Stochastic Root Loci

Compensator Optimized for Pi

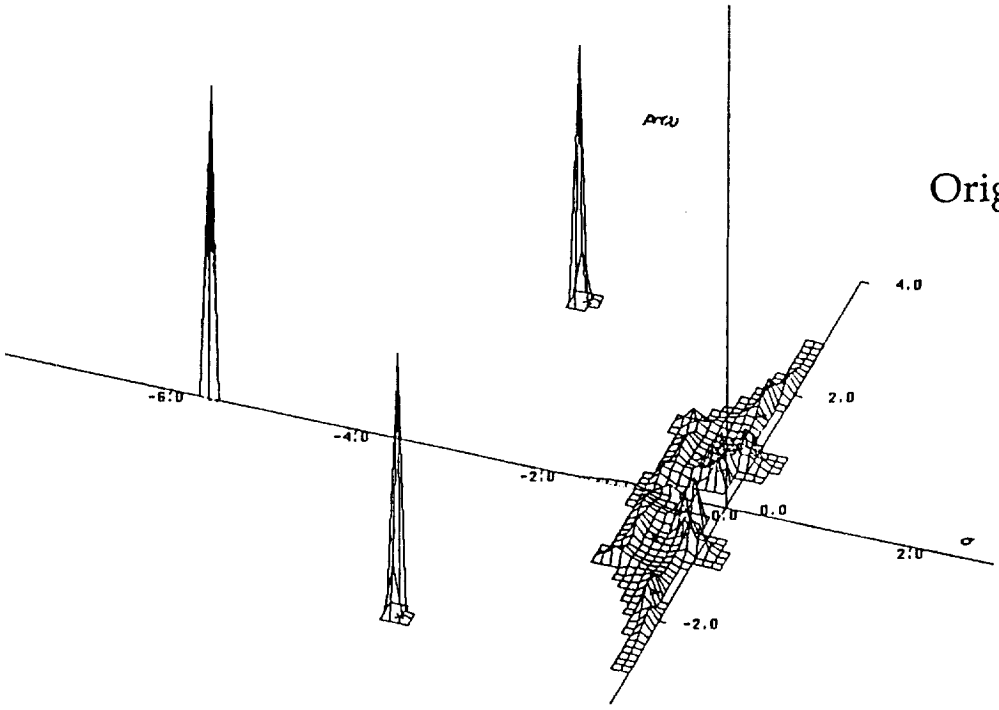

Original LQG

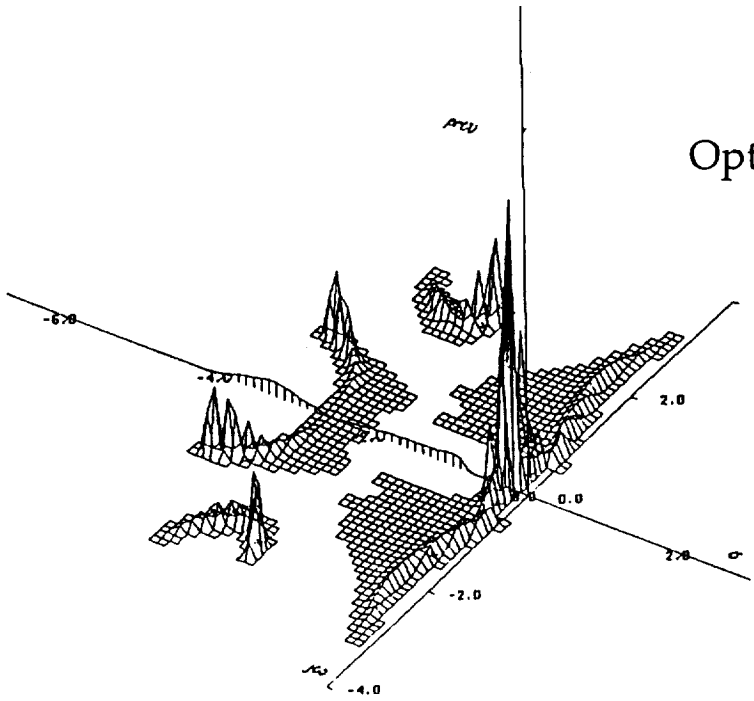

Optimized LQG

Stochastic Root Locus

Compensator Optimized for P_u

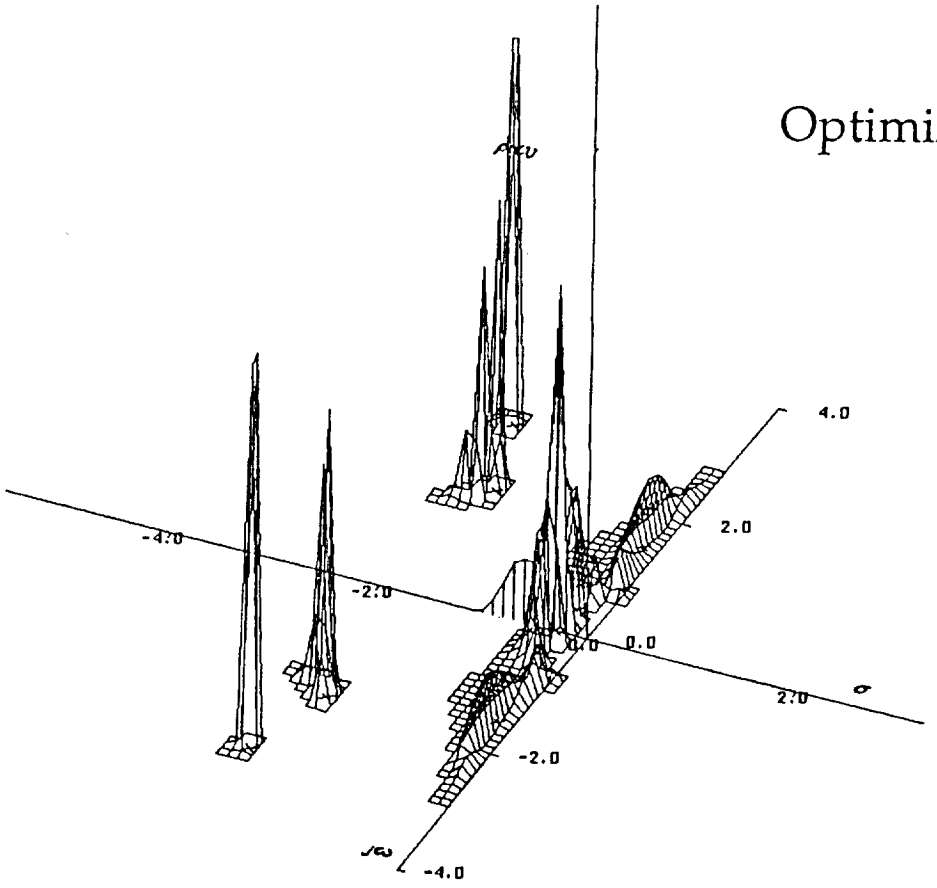

A careful analysis of the LQGs revealed several interesting lessons for designing robust compensators.

Comparing the stochastic root loci (SRL) of the compensators before and after optimization for stability robustness shows that it is quite possible to have improved robustness but greater sensitivity in the root variation.

There is a large difference in the form of the SRL for the compensator designed for stability robustness and the one designed to minimize actuator saturation. The compensator designed to minimize actuator saturation has used a lot of effort to ensure that there is very little variation in the high speed roots whereas this is unimportant for stability robustness.

Stochastic robustness has been shown to provide a sound basis for designing robust control systems. The design criteria are closely related to design goals and to practical characterization of parametric uncertainty. The method also recognizes that different criteria (e.g., settling time, control usage, and probability of instability) may have greater relative importance in different settings, allowing tradeoffs to be made among competing response requirements. The final designs for the benchmark problem compared very well with designs that had been formulated using other modern synthesis procedures (e.g., H infinity methods).

It appears that stochastic robustness is a powerful design tool. Future work in the near term will be to improve the efficiency of synthesis algorithms.

Conclusions

- Stochastic Robustness Synthesis is flexible and produces practical robust compensators.

Future Work

- More efficient methods of finding the global minimum of the cost function should be found.

Optimal Recovery From Microburst Wind Shear

Sandeep S. Mulgund
Princeton University

N93-22574

Severe low-altitude wind variability represents an infrequent but significant hazard to aircraft taking off or landing. During the period from 1964 to 1985, *microburst wind shear* was a contributing factor in at least 26 civil aviation accidents involving nearly 500 fatalities and over 200 injuries. A microburst is a strong localized downdraft that strikes the ground, creating winds that diverge radially from the impact point. The physics of microbursts have only been recently understood in detail, and it has been found that effective recovery from inadvertent encounters may require piloting techniques that are counter-intuitive to flight crews. The goal of this work was to optimize the flight path of a twin-jet transport aircraft encountering a microburst during approach to landing. The objective was to execute an escape maneuver that maintained safe ground clearance and an adequate stall margin during the climb-out portion of the trajectory.

Trajectory Optimization in Wind Shear

The objective of *trajectory optimization* is to determine the state and control histories of a system that minimize a cost function. The choice of the elements of the cost function determines the nature of the optimizing solution. The technique has been used to identify the limits of aircraft performance in wind shear and to determine the control strategies required to achieve such performance. The computation of these optimal trajectories requires global knowledge of the flow field; in other words, the wind components at all points in the aircraft's trajectory must be known in advance. Since this is not possible in practice, the results of trajectory optimization are not immediately useful for real-time control of an aircraft penetrating a wind shear. Nonetheless, the results are valuable for identifying the limits of aircraft performance and for determining the qualitative nature of optimal piloting.

In order to translate the stated goal of recovering from a microburst encounter during final approach into the mathematical expression of a cost function, the objectives of the escape maneuver must be clearly identified. The purpose of the recovery maneuver is to execute a smooth transition from descending to ascending or level flight without stalling the aircraft, saturating the controls, or impacting the ground. Once the aircraft establishes a stable climb, it should maintain an adequate stall margin.

- Determine the state and control histories $\mathbf{x}(t)$ and $\mathbf{u}(t)$ that minimize a cost function:

$$J = \phi[\boldsymbol{x}(t_f)] + \int_{t_o}^{t_f} L[\boldsymbol{x}(t), \boldsymbol{u}(t), t)]dt$$

- Choice of final state penalty ϕ and Lagrangian L determine nature of optimizing solution
- Goals of recovery maneuver during approach to landing must be identified to choose a suitable cost function:
  - Avoid the ground!
  - Perform a stabilized transition from descending to ascending flight
  - Maintain an adequate stall margin

Cost Functions for Aircraft Trajectory Optimization

The problem of ground avoidance can be solved by maximizing the minimum altitude, which is a *maxi-min* problem of optimal control. In principle, maximizing the minimum altitude is equivalent to minimizing the peak deviation between some high reference altitude and the aircraft's instantaneous altitude. However, the latter is a *mini-max* problem of optimal control. The distinction is important when developing an approximate Lagrangian problem of optimal control that can be solved using a *Calculus of Variations* approach. The optimal solution to the approximate problem shapes the aircraft flight path in such a way that the peak altitude loss of the aircraft is minimized, given the aircraft performance limits and the microburst severity. However, the cost function shown provides little control of the flight path beyond the point of minimum altitude, other than causing the aircraft to climb. Once a positive climb rate is established, it is desirable to regulate airspeed and/or rate of climb. This could have been accomplished by including additional terms in the cost function, but a different approach was taken. A quadratic cost function that considered flight path directly was used. The quadratic cost function had the advantage that it directly weighted the aircraft state variables of interest, and was numerically easier to optimize than a cost function containing larger exponents.

- Ground avoidance $\Rightarrow$ Minimize the peak altitude drop [Miele]:

$$\min I = \max_{t} [h_{ref} - h(t)] \qquad t_o \le t \le t_f$$

- Can be reformulated as a Lagrangian problem of optimal control:

$$J = \int_{t_o}^{t_f} [h_{ref} - h(t)]^p \, dt \qquad p >> 2 \text{ and even}$$

- Optimal solution shapes aircraft trajectory so that peak difference between h_{ref} and $h(t)$ is minimized
- Little control over flight path beyond point of minimum altitude
- Motivated use of a Lagrangian that considers flight path directly:

$$L(\boldsymbol{x},\boldsymbol{u}) = k_1[\dot{h}_{ref} - \dot{h}(t)]^2 + k_2 q(t)^2 + k_3 \delta_E(t)^2 + k_4 \dot{\delta}_E(t)^2$$

Aircraft Equations of Motion

A three degree-of-freedom model of a twin-jet transport aircraft is used for this study. The aircraft's aerodynamic coefficients are complex nonlinear functions of altitude, Mach number, incidence angles, rotation rates, control deflections, configuration changes (such as gear or flap deflection), and ground proximity. Thrust and elevator dynamics are modeled as first-order lags, and wind shear effects are included in the equations of motion. The wind components and spatial gradients used in the equations of motion are obtained from the Oseguera-Bowles downburst model. This time-invariant analytic model represents an axisymmetric stagnation point flow, based on wind velocity profiles from the Terminal Area Simulation System (TASS). Simulation of microbursts of different size and strength is possible through specification of the radius of the downdraft column R, the maximum horizontal wind speed U_{max}, and the altitude of maximum outflow z_{max}.

- Three degree-of-freedom model of a twin-jet transport
  - Gross weight: 85,000 lb
  - Maximum Takeoff Thrust: 24,000 lb
- Aircraft states and controls:

$$\boldsymbol{x} = [x \quad h \quad u \quad w \quad q \quad \theta \quad \delta_E \quad \delta_T]$$

$$\boldsymbol{u} = [\delta_E \quad \delta_T]_{com}$$

- Thrust and elevator dynamics modeled as first-order lags
- Wind shear effects included in equations of motion
- Oseguera-Bowles analytical downburst model used to create wind field
- Permits simulation of different microbursts through specification of radius of downdraft column, maximum horizontal wind speed, and height of outflow

Microburst Encounters During Approach to Landing

Optimal trajectories were calculated for microburst encounters during approach to landing. The aircraft was initialized on the glide slope outside the core region of the microburst, and it tracked the glide slope until the core was entered. A *conjugate gradient* algorithm was used to minimize the chosen cost function. This is an iterative technique that requires the existence of a nominal state and control history, which was obtained by performing a recovery using the FAA-recommended maneuver.

- Cost function minimized using a conjugate gradient algorithm
- Nominal state and control histories used to initiate numerical iteration obtained from recoveries performed using FAA technique
- Recovery initiated when aircraft enters core region

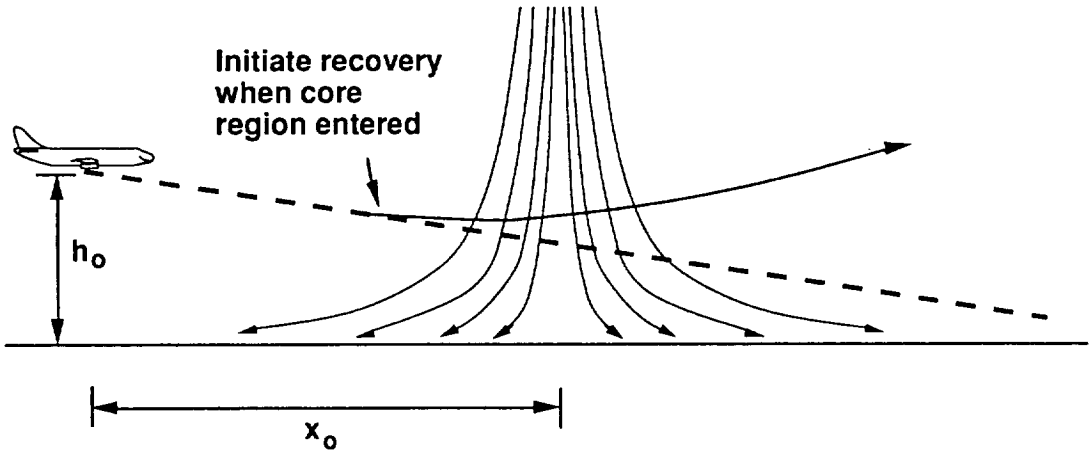

Computation of Optimal Trajectories

The aircraft was subject to two constraints in the recovery maneuver. First, the elevator deflection was required to lie within a minimum and maximum bound. Second, a minimum airspeed requirement was imposed. The incremental cost function L_V was added as a "soft constraint" to prevent excessive violation of the constraint. This function remains zero provided that its argument does not violate a predefined limit. Once the limit is violated, its contribution to the Lagrangian grows quadratically with the magnitude of the violation. The degree to which the aircraft violated the airspeed constraint depended on the relative magnitude of k_V and the other weights in the Lagrangian.

- Aircraft subject to two constraints:

$$-20^\circ \le \delta_E \le 20^\circ$$

$$V \ge 125 \text{ knots}$$

- Airspeed constraint imposed using a penalty function:

$$L(\boldsymbol{x},\boldsymbol{u}) = L(\boldsymbol{x},\boldsymbol{u}) + L_V(V)$$

where

$$L_V(V) = \begin{cases} 0 & V > V_{\min} \\ K_V[V - V_{\min}]^2 & V \le V_{\min} \end{cases}$$

- Contribution of L_V to cost grows quadratically with magnitude of constraint violation

Test Cases

Optimal trajectories were computed through four microbursts of equal size and varying strength (i.e. varying maximum horizontal wind speed) to illustrate the effect of severity on the shape of the optimal flight paths. The target climb rate during the recovery was set at 5 ft/sec, and the airspeed penalty function threshold was set at 125 knots (210 ft/sec).

- Illustrate effect of microburst severity on shape of optimal flight paths
- Microburst parameter sets:

$$R = 3{,}000 \text{ ft}$$

$$z_{max} = 150 \text{ ft}$$

$$U_{max} = 60, 70, 75, \text{and } 80 \text{ ft/sec}$$

- Aircraft initialized on glide slope just outside core
- Reference rate of climb for escape maneuver set at 5 ft/sec

Altitude vs. Time for Optimal Paths through 4 Different Downbursts

All four optimal flight paths were transitions from descending to ascending flight. However, the introduction of the minimum airspeed penalty function had a significant effect on the aircraft's climb rate during the escape. In the two weakest microbursts, the aircraft was able to maintain the reference climb rate of 5 ft/sec (300 ft/min) without violating the penalty function threshold. In the two strongest microbursts, the presence of the airspeed penalty function resulted in a lower climb rate in the escape maneuver.

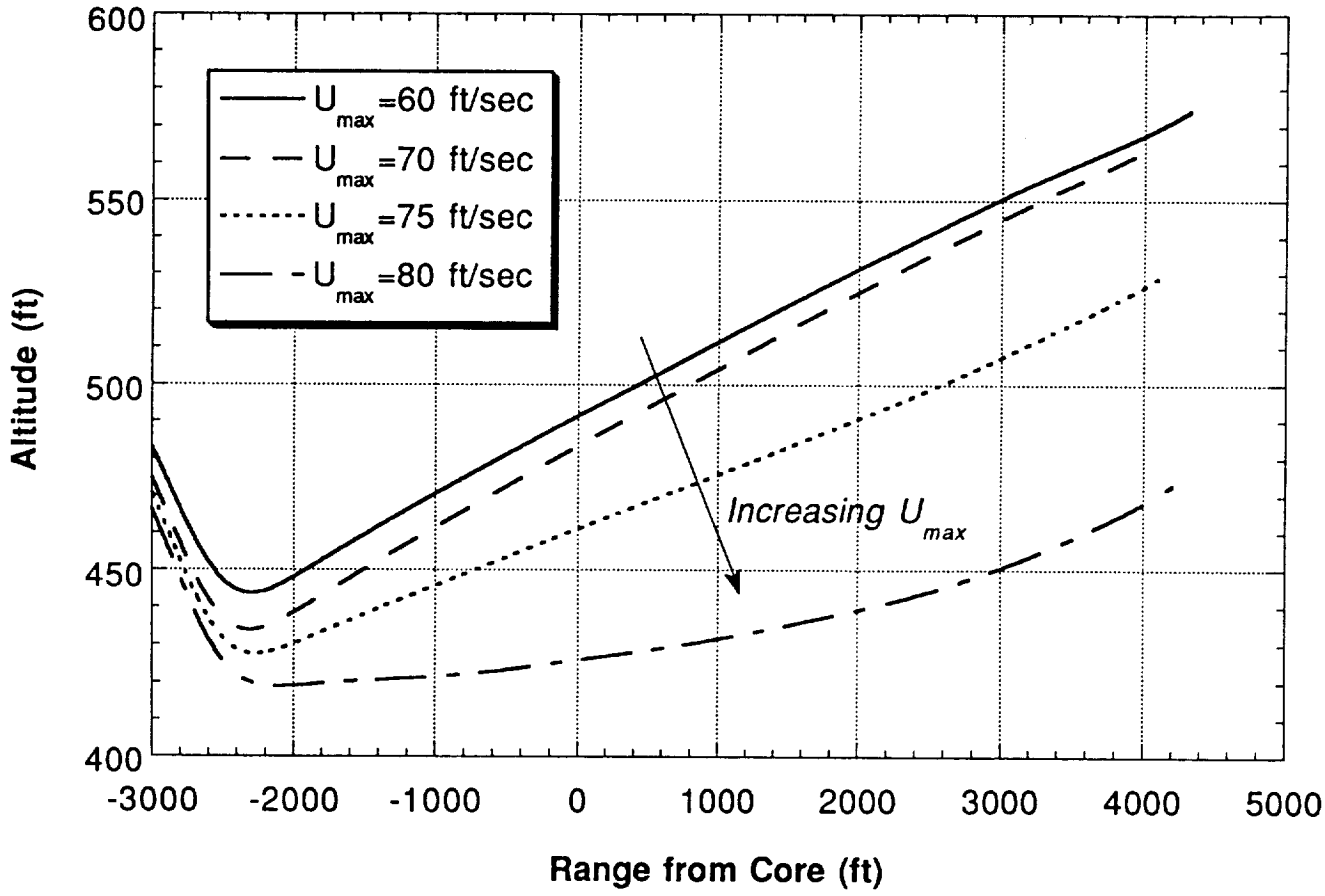

Rate of Climb vs. Time for Optimal Paths through 4 Different Downbursts

It is apparent here that in the two weaker microbursts, the aircraft was successful in making the transition from descending flight to a 5 ft/sec ascent. However in the two strongest downbursts, the presence of the airspeed constraint in the cost function caused the optimization algorithm to settle on a target climb rate less than 5 ft/sec.

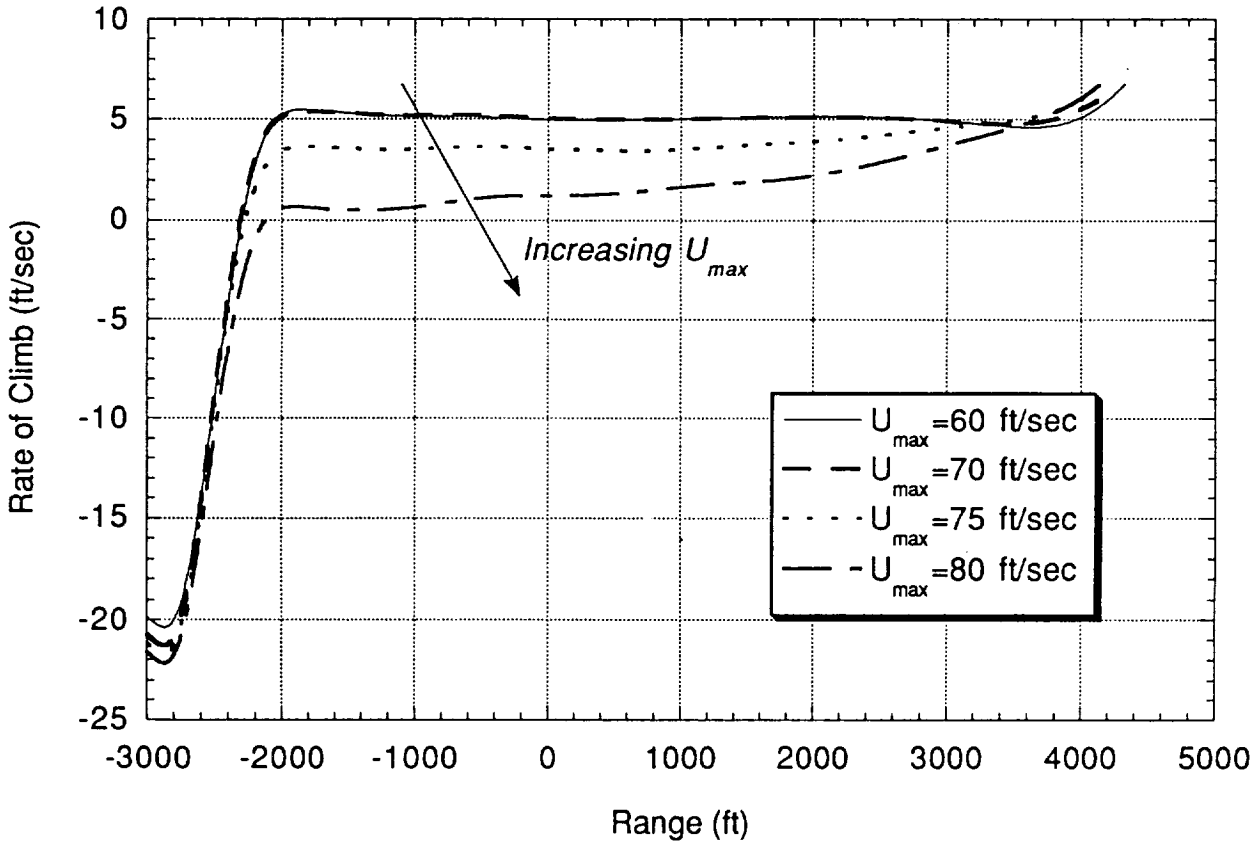

Airspeed vs. Time for Optimal Paths through 4 Different Downbursts

It can be seen here that in the two weaker microbursts, the escape was successfully accomplished without violating the airspeed penalty function threshold. This was not the case in the two stronger microbursts. In those cases, the airspeed did drop below the threshold somewhat. The degree to which the airspeed dropped below 210 ft/sec could have been altered by changing the relative magnitude of the climb rate and airspeed weights in the cost function Lagrangian.

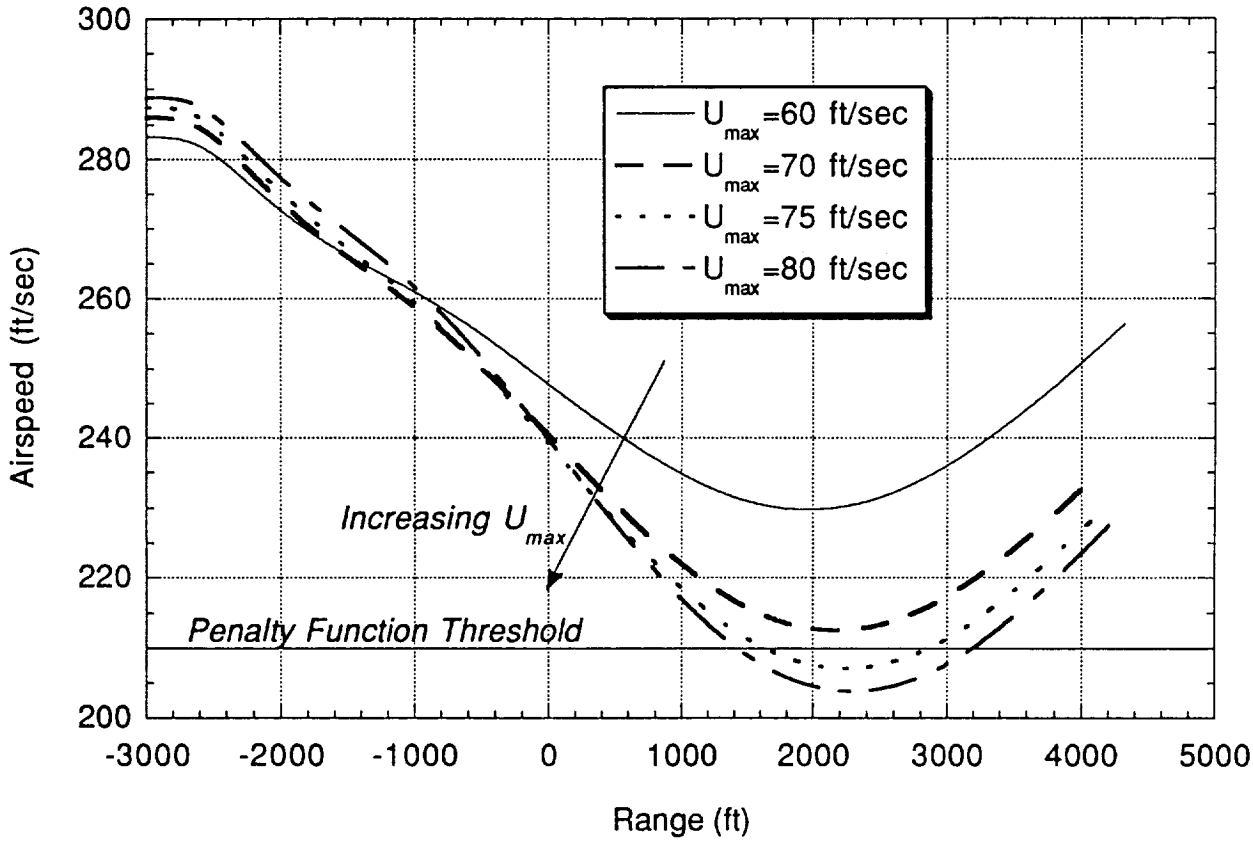

Qualitative Features of the Optimal Flight Paths

Microburst severity has thus been found to have a significant effect on the nature of an optimal recovery using the given cost function. The optimal maneuver is a rapid transition from descending to level or ascending flight. In weak-to-moderate microbursts, the aircraft easily tracks the reference climb rate throughout the encounter. However, in a severe microburst the aircraft settles on a reduced climb rate through much of the encounter to prevent excessive airspeed loss. While these results are useful for providing insight into the nature of optimal recovery techniques, they are not immediately useful for real-time feedback control. Global knowledge of the flow field is required for optimization. Even with the advent of forward-look sensors, such detailed information about a microburst's structure will not be available. Furthermore, optimization is itself an iterative time-consuming process.

- Rapid transition from descending to level or ascending flight
- Targeted rate of climb during escape depends on wind shear severity

  Weak to moderate $\Rightarrow$ Aircraft reaches 5 ft/sec climb rate

  Severe to very severe $\Rightarrow$ Aircraft reaches a lower climb rate
- Lower climb rate in severe microbursts results in reduced violation of minimum airspeed constraint

OK, but...

- Global knowledge of flow field required for optimization
- Results not immediately applicable to real-time feedback control

Future Work: Neural Networks for Real-Time Flight Guidance

Although the results of trajectory optimization are not immediately applicable to feedback control, it should be possible to make use of the insights gained through the optimization study somehow. One idea under consideration is to train an *artificial neural network* with the results of trajectory optimization. The inputs to the network would be aircraft state and wind information, and the outputs might be throttle and flight path commands. It should be possible to parametrize microbursts according to size and severity, and then have the neural network generate flight path commands according to the aircraft position within the flow field. Forward-look information on wind intensity might assist in the flight path planning.

- Train neural network with results of trajectory optimization
- Can parametrize microbursts according to size and severity
- Network generates flight path angle commands according to position within flow field
- Availability of forward-look information could assist in flight-path planning

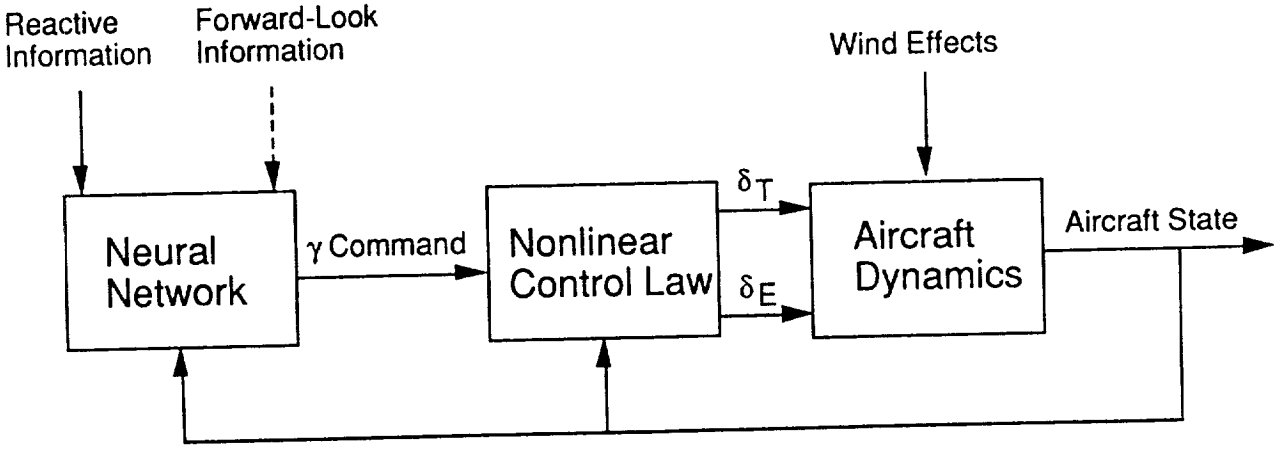

DYNAMIC RESPONSE AND CONTROL OF A JET-TRANSPORT AIRCRAFT ENCOUNTERING A SINGLE-AXIS VORTEX

Darin R. Spilman

The dynamic responses of a jet-transport aircraft to two types of single-axis wind vortex encounters are studied. Aircraft attitude, flight path angle, and aerodynamic angle excursions are analyzed and dominating dynamic forcing effects are identified for each encounter.

A simple departure-preventing LQR controller is designed to demonstrate the benefits of using automatic control to reduce the wind vortex hazard. A Proportional-Integral-Filter controller structure successfully regulates the critical parameters, roll angle, ϕ, and sideslip angle, β, for the two different vortex encounters considered in this study.

WIND ROTOR FORMATION

A mountain wave wind vortex is formed by strong winds that flow perpendicular to a mountain range. A low pressure system develops on the leeward side of the mountain that tends to force the air into a rotating air-mass. Once this horizontal cyclone of rotating air forms, it tends to be a stable air-mass that moves with axis parallel to the ground in the direction of the prevailing wind. Such wind rotors have been known to travel more that 20 miles from the forming mountains. Once a rotor moves away from the mountain, another one tends to form in its wake. Thus, several rotors formed from the same mountain range may be found moving in lines in the direction of the prevailing wind.

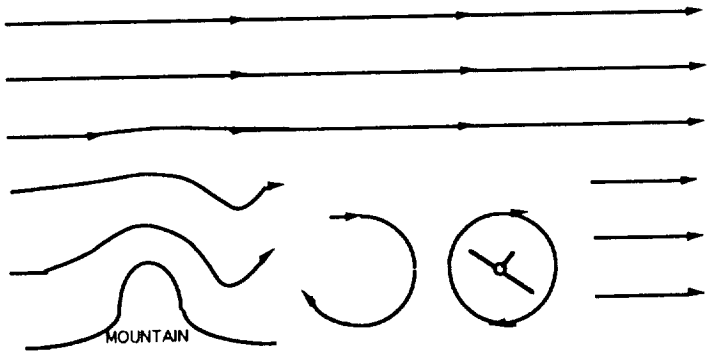

WIND ROTOR MODEL

A single-axis-vortex wind velocity profile was implemented to simulate the velocity field of a wind rotor. The profile was experimentally verified using full-scale Boeing 747 shed-wake-vortex data. This two-dimensional model is defined by the specification of two parameters: the core radius, r_c, and the core velocity, V_c. The core radius is the distance from the core center, where tangential velocity, V_t, is zero, to the location of maximum tangential velocity. The core velocity is equal to the maximum tangential velocity at the core radius.

The flow behaves as an ideal vortex outside the core ($r > r_c$), with tangential velocity proportional to $1/r^2$, where r is the distance from the rotor center . Inside the core ($r < r_c$), viscous damping effects dominate, the tangential velocity departs from the ideal profile, and it increases in proportion to the distance, r. A piecewise-linear model described by three linear equations provides a good approximation to the experimentally verified model.

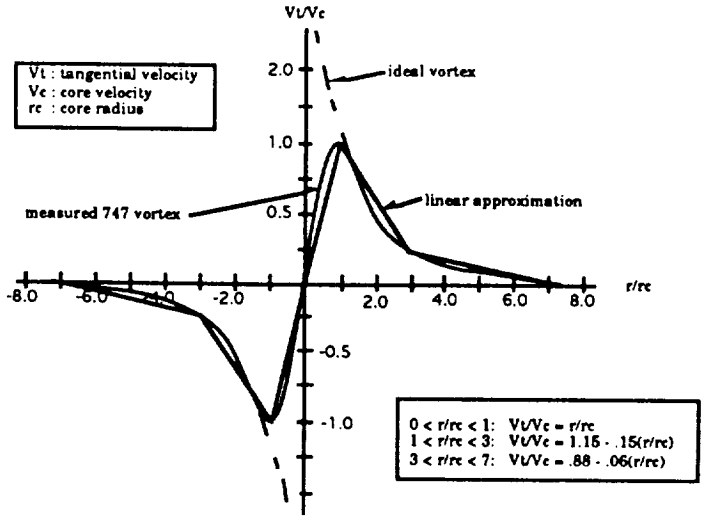

WIND EFFECTS ON AIRCRAFT

Wind terms have been included explicitly in the translational kinematic and dynamic equations of motion. The time derivative of the wind components acts as a forcing term in the aircraft dynamics, inducing both linear and angular rate derivatives. The wind terms do not appear explicitly in the rotational equations.

In addition to the wind time derivatives, there are specific rotational moments due to the spatial velocity gradient acting along the various aerodynamic surfaces of the aircraft. These spatial variations are dependent on the specific aircraft configuration and enter the rotational dynamics through the aerodynamic force and moment calculations.

In the presence of a spatial shear gradient, the roll moment for example, includes not only the damping from the roll-rate-induced velocity field, the control, yaw rate, and sideslip effects, but also the contribution from the velocity field of the spatial shear. Since the shear is a local wind field similar to that induced by the aircraft in roll, the shear gradients become effective roll rates and enter the roll moment coefficient equation through multiplication by elements of the roll-rate derivatives. However, the spatial gradient acts as a roll rate only on the aerodynamic surfaces perpendicular to the gradient flow field. This simple shear-gradient analysis can be extended to each force and moment coefficient calculation that is necessary in the dynamic simulation.

- Equations of motion

  Translational kinematics $\quad \dot{\vec{r}}_E = L_{EB}\dot{v}_B + \vec{w}_E$

  Translational dynamics $\quad \dot{\vec{v}}_B = \frac{F_B}{m} - H_I^B g - \tilde{w}_B v_B - \dot{\vec{w}}_B$

- Force and moment coefficients

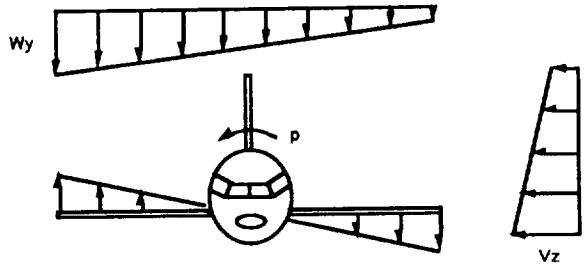

C_l = roll moment coefficient = $(C_l)_{ROLL} + (C_l)_{YAW}$

$(C_l)_{ROLL} = (C_{l_p})p + (C_{l_{P_{wing}}} + C_{l_{P_{horizontal\ tail}}})w_y + (C_{l_{P_{vertical\ tail}}})v_z$

AIRCRAFT-VORTEX ENCOUNTER GEOMETRY

Dynamic simulations of a twin-jet transport encountering a single-axis horizontal vortex during landing approach are presented. Two different aircraft-vortex geometrical encounters are simulated: a vortex with axis parallel to the extended runway centerline, referred to as a finite-length rotor, and a vortex with axis at a 60° angle to the extended runway centerline, referred to as an infinite-length rotor. Although the dominating dynamic effects are different in each wind rotor encounter, both simulations produce large bank angles and pitch attitudes that result in drastic deviations from the approach path.

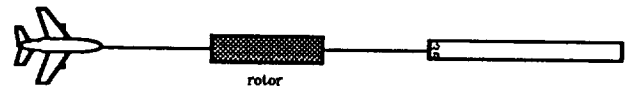

a. finite-length rotor

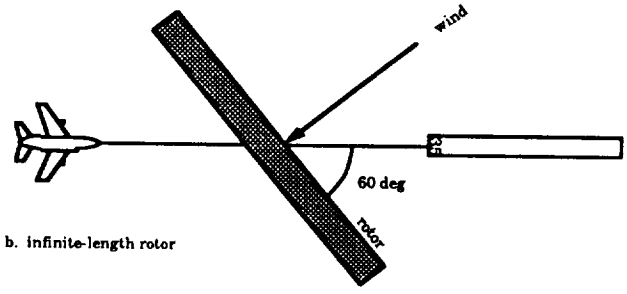

b. infinite-length rotor

Results show that both cases can produce severe changes to bank and pitch attitude, velocity, and sideslip angle during an approach. The finite-length wind rotor simulation produces strong shearing moments that dominate the aircraft's response. The 60° encounter angle, or infinite-length simulation has a dynamic response dominated by the time-rate-of-change of the strong vortical winds, with shearing moments having little influence. The effects of these winds can be seen clearly in the sideslip angle and angle of attack plots; much larger aerodynamic angles are induced in the 60° rotor angle simulation than in the co-axial rotor simulation. Therefore, to successfully reduce the initial effects of a wind vortex for any general vortex orientation, shear-induced roll effects and wind-induced sideslip angle effects must be attenuated.

Another significant difference between the two encounters is that for the co-axial case the dynamic response changes relatively little with various initial conditions; however, in the non zero rotor angle case, even small changes in initial conditions result in significant changes in the resulting attitude and flight path angles.

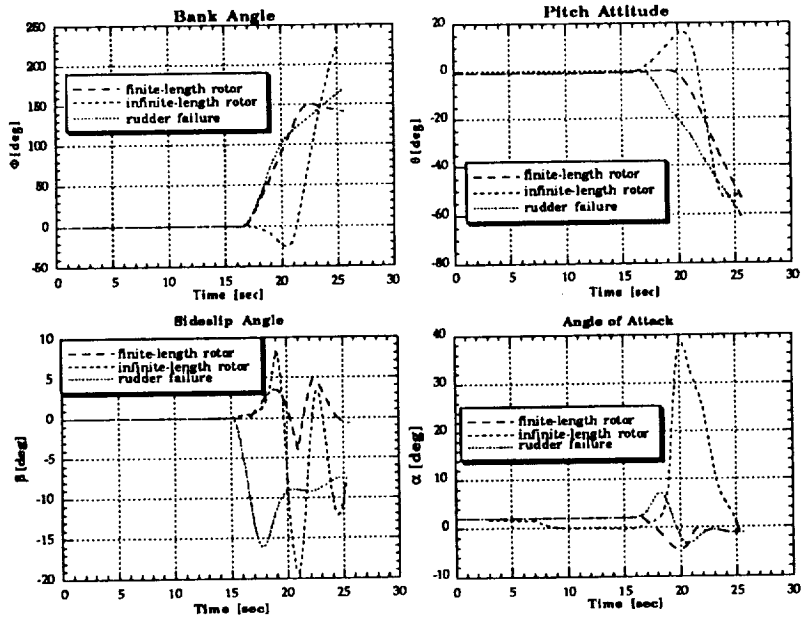

LINEAR QUADRATIC REGULATOR

A simple LQR Proportional-Integral-Filter (PIF) controller is designed based on a linear state-space model that considers only four lateral dynamic states and two controls. LQR control offers a systematic approach to developing constant-gain feedback control laws for multi-input multi-output systems by combining state-space, time-domain, and optimal control concepts. The aircraft and controller is then flown through the two basic wind rotors considered: the co-axial or finite-length encounter and the 60° rotor angle or infinite-length encounter. In both cases the controller's objective is to reduce roll angle and sideslip angle excursions.

$$\Delta\dot{x}(t)=\frac{\delta F}{\delta x}\Delta x(t)+\frac{\delta F}{\delta u}\Delta u(t)$$

$$\Delta x=[\Delta v\ \Delta p\ \Delta r\ \Delta\phi]^T$$

$$\Delta u=[\Delta\delta a\ \Delta\delta r]^T$$

objective: minimize cost, J

$$J = \int_0^\infty \left(\Delta\tilde{x}^T(t)Q\Delta\tilde{x}(t) + \Delta\tilde{u}(t)^T R\Delta\tilde{u}(t)\right)dt$$

where: **Q = state weighting matrix**
R = control weighting matrix

control law of form:

$$\Delta u(t) = -C\Delta x(t)$$

LQR CONTROL SIMULATIONS

Results for the two aircraft-vortex simulations are presented. During the finite-length encounter the roll angle remains below 8° and the sideslip angle below 3° ; during the infinite-length encounter angle case the roll angle remains below 10° and sideslip angle below 6°. The performance in both cases is superior to the published maximum allowable roll angle, 20°, for a jet-transport on final approach to landing. These simulations demonstrate the value of using automatic control to reduce vortex-induced excursions.

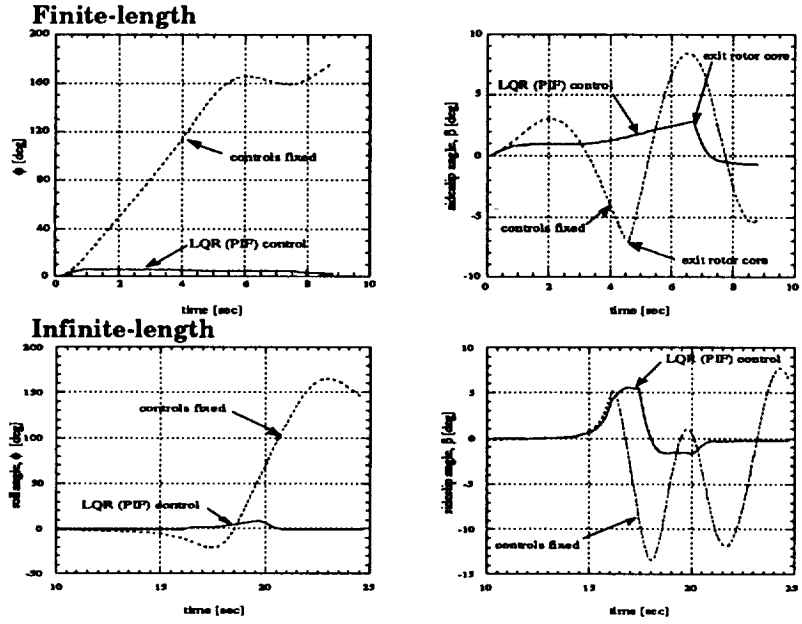

AILERON AND RUDDER CONTROL IN A VORTEX

The control histories for the vortex encounter simulations show that for this controller design, aileron is used almost exclusively to control roll excursions while rudder independently controls sideslip excursions for both the finite-length and infinite-length cases. The control plots also show that aileron deflections are much greater than rudder deflections, even though the same relative weighting was used on both controls in the design. This is expected since large rudder deflections may excite the lightly damped dutch-roll mode and cause severe sideslip angle oscillations.

Increasing the weighting on roll angle forces the rudder to aid in roll excursion reduction at the expense of sideslip angle control. This type of behavior may be preferred in some instances, particularly those in which an unusually large rotor is present. Under these circumstances, rolling to inverted flight may be unavoidable without immediate application of both full aileron and full rudder against the roll.

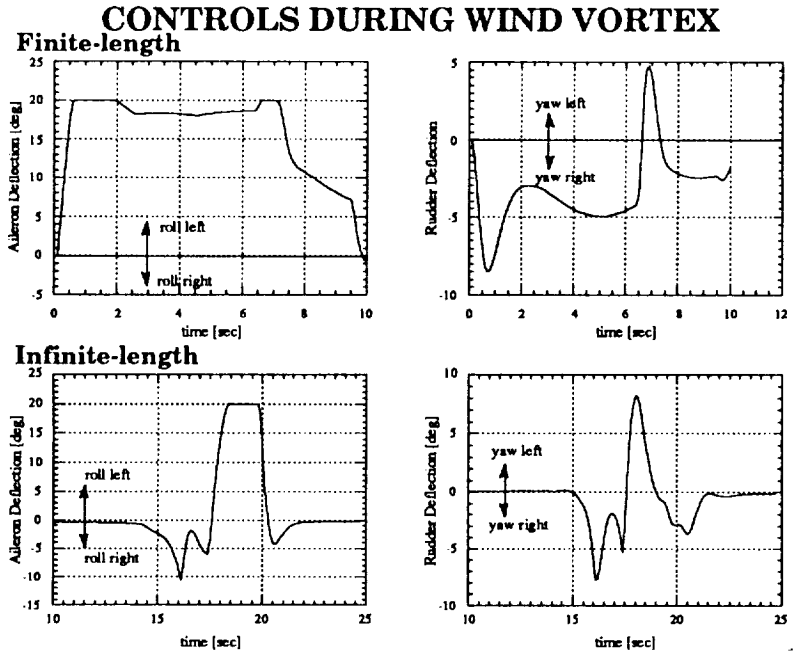

SUMMARY

The controls-fixed simulations show that the dominating dynamic effects in the finite-length and infinite-length simulations are very different, although both encounter types have the ability to flip a jet-transport configured for final approach. In order to reduce the vortex hazard for all vortex encounters it is necessary to control both roll angle, ϕ, and sideslip angle, β.

The LQR formulation provides insights into optimal control inputs during a wind vortex encounter, given a defined control objective. The simple LQR Proportional-Integral-Filter feedback control system designed in this section demonstrates that proper rudder control of sideslip combined with aileron roll control can help reduce the wind vortex hazard, even for a wide variety of vortex alignments with respect to the flight path. Results from the aircraft-rotor simulations show that rudder is used to a lesser degree than aileron. There is evidence that a very strong vortex or possibly a vortex at an orientation angle not considered in this study may require a greater controller emphasis on roll regulation and less emphasis on sideslip attenuation. Thus, proper gain scheduling appears to be a requirement for a vortex-alleviation control system that is effective over a broad range of vortex encounters.

Controls-fixed simulations:

- **both co-axial and 60° rotor angle can flip a jet-transport**
- **shear effects dominate co-axial case**
- **strong vortical winds dominate 60° rotor angle case**
- **critical parameters are ϕ, β**

LQR (PIF) control:

- **four-state model, two controls**
- **reduces vortex hazard for range of encounters**
- **aileron used to greater degree than rudder**
- **gain scheduling may be necessary**

INTELLIGENT FLIGHT CONTROL SYSTEMS

Robert F. Stengel*
Princeton University
Princeton, NJ USA

ABSTRACT

The capabilities of flight control systems can be enhanced by designing them to emulate functions of natural intelligence. Intelligent control functions fall in three categories. *Declarative* actions involve decision-making, providing models for system monitoring, goal planning, and system/scenario identification. *Procedural* actions concern skilled behavior and have parallels in guidance, navigation, and adaptation. *Reflexive* actions are spontaneous, inner-loop responses for control and estimation. Intelligent flight control systems learn knowledge of the aircraft and its mission and adapt to changes in the flight environment. Cognitive models form an efficient basis for integrating "outer-loop/inner-loop" control functions and for developing robust parallel-processing algorithms.

INTRODUCTION

Recounting personal experiences in confronting wind gusts, one of the Wright brothers wrote, "The problem of overcoming these disturbances by automatic means has engaged the attention of many ingenious minds, but to my brother and myself, it has seemed preferable to depend entirely on *intelligent control*" [1, 2]. The Wright brothers' piloting actions depended on proper interpretation of visual and inertial cues, demonstrating biological intelligent control. In the past, human pilots flew aircraft through manual dexterity, informed planning, and coordination of missions. As aircraft characteristics and technology have allowed, an increasing share of the aircraft's operation has come to rely on electro-mechanical sensors, computers, and actuators. Panel displays have enhanced decision-making, stability augmentation systems have improved flying qualities, and guidance logic has carried machine intelligence to the point of "hands-off" flying for much of a modern aircraft's mission.

In a contemporary context, intelligent flight control has come to represent even more ambitious plans to

- make aircraft less dependent on proper human actions for mission completion,
- enhance the mission capability of aircraft,
- improve performance by learning from experience,
- increase the reliability and safety of flight, and
- lower the cost and weight of aircraft systems.

This paper presents concepts for intelligent flight control through the aid of what were once called "artificial" devices for sensing, computation, and control. We distinguish between control functions according to a cognitive/biological hierarchy that is bounded on one end by *declarative functions*, which typically involve decision-making, and on the other by *reflexive functions*, which are spontaneous reactions to external or internal stimuli.

In a classical flight control context, declarative functions are performed by the control system's *outer loops*, and reflexive functions are performed by its *inner loops*. At an intermediate level, *procedural functions* -- like reflexive functions -- have well-defined input-output characteristics but of a more complicated structure. Traditional design principles suggest that the outer-loop functions should be dedicated to low-bandwidth, large-amplitude control commands, while the inner-loop functions should have high bandwidths and relatively lower-amplitude actions. There is a logical progression from the sweeping, flexible alternatives associated with satisfying mission goals to more local concerns for stability and regulation about a desired path or equilibrium condition.

FOUNDATIONS FOR INTELLIGENT FLIGHT CONTROL

Intelligent flight control design draws on two apparently unrelated bodies of knowledge. The first is rooted in classical analyses of aircraft stability, control, and flying qualities. The second derives from human psychology and physiology. The design goal is to find new control structures that are consistent with the reasons for flying aircraft, that bring flight control systems to a higher level of overall capability.

* Professor of Mechanical and Aerospace Engineering.

presented at the IMA Conference on Aerospace Vehicle Dynamics and Control, Cranfield Institute of Technology, Bedford, UK, September 7-10, 1992. (rev.: 9/14/92)

Supported by government grant. See Acknowledgments.

Aircraft Flying Qualities and Flight Control

An aircraft requires guidance, navigation, and control to perform its mission. As suggested by Fig. 1, a human pilot can interact with the aircraft at several levels, and his or her function may be supplanted by electro-mechanical equipment. The pilot performs three distinct functions: sensing, regulation, and decision-making. These tasks exercise different human characteristics: the ability to see and feel, the ability to identify and correct errors between desired and actual states, and the ability to decide what needs to be done next. The first depends on the body's sensors and the neural networks that connect them to the brain. The second relies on motor functions enabled by the neuro-muscular system to execute learned associations between stimuli and desirable actions. The third requires more formal, introspective thought about the reasons for taking action, drawing on the brain's deep memory to recall important procedures or data. Sensing and regulation are high-bandwidth tasks that allow little time for deep thinking. Decision-making is a low-bandwidth task that requires concentration. Each of these tasks exacts a workload toll on the pilot.

Pilot workload has become a critical issue as the complexity of systems has grown, and furnishing ideal flying qualities throughout the flight envelope has become an imperative. It is particularly desirable to reduce the need to perform high-bandwidth, automatic functions, giving the pilot time to cope with unanticipated or unlikely events. In the future, teleoperated or autonomous systems could find increasing use for missions that expose human pilots to danger.

Research on the *flying (or handling) qualities of aircraft* has identified ways to make the pilot's job easier and more effective, and it provides models on which automatic systems might be based. The first flying qualities specification simply stated, "(the aircraft) must be steered in all directions without difficulty and all time (be) under perfect control and equilibrium" [3, 4]. Further evolution of flying qualities criteria based on dynamic modeling and control theory has led to the widely used U. S. military specification [5] and the succeeding military standard [6].

Flying qualities research has led to the development of *control-theoretic models of piloting behavior*. Most of these models have dealt with reflexive, compensatory tracking tasks using simple time-lag and transfer function models [7, 8] or linear-quadratic-Gaussian (LQG) optimal-control models [9, 10]. Some treatments go into considerable detail about neuro-muscular system dynamics [11, 12]. These models often show good correlation with experimental results, not only in compensatory tracking but in more procedural tasks: the progression of piloting actions from single- to multi-input strategies as the complexity of the task increases is predicted in [10], while test-pilot opinion ratings are predicted by a "Paper Pilot" in [13]. These results imply that *computer-based control laws can perform procedural and reflexive tasks within the fit error of mathematical human-pilot models*. Insight on the human pilot's declarative actions can be drawn from [14-16], which introduce the types of decisions that must be made in aerospace scenarios, as well as likely formats for pilot-vehicle interface.

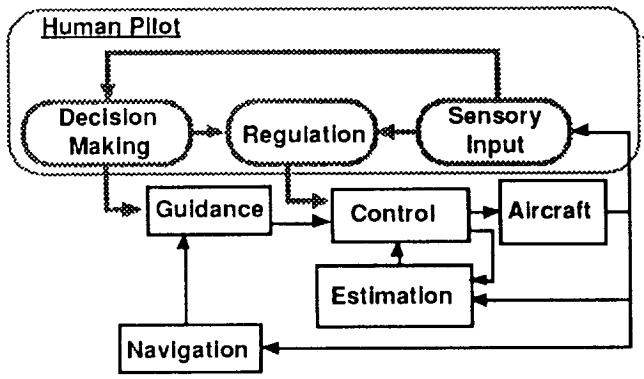

Figure 1. Guidance, Navigation, and Control Structure.

Figure 1 also portrays a hierarchical structure for stability-augmentation, command-augmentation, autopilot, and flight-management-system functions that can be broken into reflexive and declarative parts. Stability augmentation is reflexive control provided by the innermost loop, typically implemented as a linear feedback control law that provides stability and improves transient response through an *Estimation/Compensation* block. Forward-loop control provides the shaping of inputs for satisfactory command response through a *Control/Compensation* block, again employing linear models. The combination of control and estimation can be used to change the flying qualities perceived by the pilot, or it can provide a decoupled system for simplified guidance commands [17-20]. A basic autopilot merely translates the human pilot's commands to guidance commands for constant heading angle, bank angle, or airspeed, while the *Guidance* block can be expanded to include declarative flight management functions, using inputs from *Navigation* sensors and algorithms.

Intelligent functions have been added to flight control systems in the past. Gain scheduling and switching improve performance in differing flight regimes and mission phases. Control theory, heuristics, and reduced-order optimization have been used to achieve near-optimal trajectory management in many flight phases (e.g., [21-23]). The Guidance, Navigation, and Control (GNC) Systems for Project Apollo's Command/Service and Lunar Modules provide an early example of intelligent aerospace control [24-26]. The state-of-the-art of aircraft flight control systems has progressed to comparable levels and beyond, as represented by systems installed in modern transport and fighter aircraft (e.g., [27, 28]).

Intelligent flight control[1] can be justified only if it materially improves the functions of aircraft, if it saves

[1] As used here "intelligent flight control" subsumes "intelligent guidance, navigation, and control."

the time and/or money required to complete a mission, or if it improves the safety and reliability of the system. Interesting philosophical problems can be posed. Must machine-intelligence be better than the human intelligence it replaces in order for it to be adopted? We are willing to accept the fact that humans make mistakes; if a machine has a similar likelihood of making a mistake, should it be used? Lacking firm knowledge of a situation, humans sometimes gamble; should intelligent machines be allowed to gamble? When is it acceptable for machine intelligence to be wrong (e.g., during learning)? Must the machine solution be "optimal," or is "feasible" good enough? Which decisions can the machine make without human supervision, and which require human intervention? In a related vein, how much information should be displayed to the human operator? Should intelligent flight control ever be fully autonomous? If the control system adapts, how quickly must it adapt? Must learning occur on-line, or can it be delayed until a mission is completed? All of these questions must be answered in every potential application of intelligent control.

Cognitive and Biological Paradigms for Intelligence

Intelligence is the "ability involved in calculating, reasoning, perceiving relationships and analogies, learning quickly, storing and retrieving information .... classifying, generalizing, and adjusting to new situations" [29]. This definition does not deal with the mechanisms by which intelligence is realized, and it makes the tacit assumption that intelligence is a human trait. Intelligence relates not only to intellectuality and cognition but to personality and the environment [30].

The debate over whether-or-not computers ever will "think" may never be resolved, though this need not restrict our working models for computer-based intelligent control. One argument against the proposition is that computers deal with syntax (form), while minds deal with semantics (meaning), and syntax alone cannot produce semantics [31]. This does not limit the ability of a computer to mimic natural intelligence in a limited domain. Another contention is that thinking is "non-algorithmic," that the brain evokes consciousness through a process of natural selection and inheritance [32]. Consciousness is required for common sense, judgment of truth, understanding, and artistic appraisal, concepts that are not formal and cannot readily be programmed for a computer (i.e., they are not syntactic).

Conversely, functions that are automatic or "mindless" (i.e., that are unconscious), could be programmed, implying that computers have more in common with "unintelligent" functions. Gödel's Theorem[2] is offered in [33] as an example of an accepted proposition that may be considered non-algorithmic; the statement and proof of the theorem must themselves be non-algorithmic and, therefore, not computable. However, while the human curiosity, intuition, and creativity that led to Gödel's Theorem may not be replicable in a computer, the statement and proof are expressed in a formal way, so they might be considered algorithmic after all.

The notion that syntax alone cannot produce semantics is attacked as being an axiom that is perhaps true but not knowable in any practical sense [34]; therefore, the possibility that a computer can "think" is not ruled out. A further defense is offered in [35], which suggests that human inference may be based, in part, on inconsistent axioms. This could lead to rule-based decisions that are not logically consistent, that are affected by heuristic biases or sensitivities, that may reflect deeper wisdom, or that may be wrong or contradictory. For example, knowledge and belief may be indistinguishable in conscious thought; however, one implies truth and the other bias or uncertainty. One might also postulate the use of meta-rule bases that govern apparently non-algorithmic behavior. The process of searching a data base, though bound by explicit symbolic or numerical algorithms, may include randomized behavior (e.g., genetic algorithms) that are not immediately identifiable as algorithmic.

More to our point, it is likely that a computer capable of passing a flying-qualities/pilot-workload/control-theoretic equivalent of the Turing test[3] [36] could be built even though that computer might not understand what it is doing[4]. For intelligent flight control, the principal objective is improved control performance, that is, for improved input-output behavior. The computer can achieve the operative equivalent of consciousness on its own terms and in a limited domain, even if it does not possess emotions or other human traits.

Discussions of human consciousness naturally fall into using the terminology of computer science. It is convenient -- as well as consistent with empirical data -- to identify four types of thought: conscious, preconscious, subconscious, and unconscious [37]. *Conscious thought* is the thought that occupies our attention, that requires focus, awareness, reflection, and perhaps some rehearsal. Conscious thought performs declarative processing of the individual's knowledge or beliefs. It makes language, emotion, artistry, and philosophy possible. *Unconscious thought* "describes those products of the perceptual system that go unattended or unrehearsed, and those memories that are lost from primary memory through display or displacement" [37]. Within the unconscious, we may

---

[2] As summarized in [32]: Any algorithm used to establish a mathematical truth cannot prove the propositions on which it is based. Or another [33]: Logical systems have to be fixed up "by calling the undecidable statements axioms and thereby declaring them to be true," causing new undecidable statements to crop up.

[3] Turing suggested that a computer could be considered "intelligent" if it could "converse" with a human in a manner that is indistinguishable from a human conversing with a human.

[4] Searle describes such a computer as a "Chinese Room" that translates Chinese characters correctly by following rules while not understanding the language in [31].

further identify two important components. *Subconscious thought* is procedural knowledge that is below our level of awareness but central to the implementation of intelligent behavior. It facilitates communication with the outside world and with other parts of the body, providing the principal home for the learned skills of art, athletics, control of objects, and craft. We are aware of perceptions if they are brought to consciousness, but they also may take a subliminal (subconscious) path to memory. *Preconscious thought* is pre-attentive declarative processing that helps choose the objects of our conscious thought, operating on larger chunks of information or at a more symbolic level. It forms a channel to long-term and implicit memory, and it may play a role in judgment and intuition.

Whether we adopt a single-processor model of consciousness such as Adaptive Control of Thought (ACT* as in [38]) or a connectionist model like Parallel Distributed Processing (PDP from [39]), we are led to believe that the central nervous system supports a hierarchy of intelligent and automatic functions with *declarative actions* at the top, *procedural actions* in the middle, and *reflexive actions* at the bottom. Declarative thinking occurs in the brain's cerebral cortex, which accesses the interior limbic system for long-term memory [40]. Together, they provide the processing unit for conscious thought. Regions of the cerebral cortex are associated with different intellectual and physical functions; the distinction between conscious and preconscious function may depend on the activation level and duration in regions of the cerebral cortex.

The working memory of conscious thought has access to the spinal cord through other brain parts that are capable of taking procedural action (e.g., the brain stem for autonomic functions, the occipital lobes for vision, and the cerebellum for movement). Procedural action can be associated with subconscious thought, which supports voluntary automatic processes like movement and sensing. Voluntary signals are sent over the somatic nervous system, transmitting to muscles through the motor neural system and from receptors through the sensory neural system.

The spinal cord itself "closes the control loop" for reflexive actions long before signals could be processed by the brain. Nevertheless, these signals are available to the brain for procedural and declarative processing. We are all aware of performing some task (e.g., skating or riding a bicycle) without effort, only to waver when we focus on what we are doing. Involuntary regulation of the body's organs is provided by the autonomic nervous system, which is subject to unconscious processing by the brain stem. "Bio-feedback" can be learned, allowing a modest degree of higher-level control over some autonomic functions.

Declarative, procedural, and reflexive functions can be built into a model of intelligent control behavior (Fig. 2). The *Conscious Thought* module governs the system by performing declarative functions, receiving information and transmitting commands through the *Subconscious Thought* module, which is itself capable of performing procedural actions. Conscious Thought is primed by *Preconscious Thought* [41], which can perform symbolic declarative functions and is alerted to pending tasks by Subconscious Thought. These three modules overlie a bed of deeper *Unconscious Thought* that contains long-term memory. They are capable of intellectual learning, and while their physical manifestation may be like the PDP model, they exhibit characteristics that are most readily expressed by the ACT* model[5].

The Subconscious Thought module receives information from the *Sensory System* and conveys commands to the *Muscular System* through peripheral networks. Voluntary *Reflexive Actions* provide low-level regulation in parallel with the high-level functions, responding to critical stimuli and coordinating control actions. High- and low-level commands may act in concert, or one may block the other. Voluntary Reflexive Actions can be trained by high-level directives from Subconscious Thought, while the learning capabilities of involuntary Reflexive Action are less clear. Control actions produce *Body* motion and can affect an external *Controlled System*, as in piloting an aircraft. In learned control functions, Body motion helps internalize the mental model of Controlled System behavior. The Body and the Controlled System are both directly or indirectly subjected to *Disturbances*; for example, turbulence would affect an aircraft directly and the pilot indirectly. The Sensory System observes *External Events* as well as Body and Controlled System motions, and it is subject to *Measurement Errors*.

There are many parallels and analogies to be drawn in comparing the functions of human and computer-based intelligence. It may be useful to ponder a few, especially those related to knowledge acquisition, natural behavior, aging, and control. Perhaps the most important observation is that *learning requires error or incompleteness.* There is nothing new to be gained by observing a process that is operating perfectly. In a control context, any operation should be started using the best available knowledge of the process and the most complete control resources. Consequently, learning is not always necessary or even desirable in a flight control system. *Biological adaptation is a slow process*, and proper changes in behavior can be made only if there is prior knowledge of alternatives. If adaptation occurs too quickly, there is the danger that misperceptions or disturbance effects will be misinterpreted as parametric effects. *Rest is an essential feature of intelligent biological systems.* It has been conjectured that *REM (rapid-eye-movement) Sleep* is a time of learn-

[5] ... although the actual processing mechanism is not clear. In a recent seminar at Princeton (March 9, 1992), Herbert Simon noted that if you open the cabinet containing a sequential-processing computer, the innards look very much like those of a parallel processor.

ing, consolidating, and pruning knowledge[6] [42]. Systems can learn even when they are not functioning by reviewing past performance, perhaps in a repetitive or episodic way.

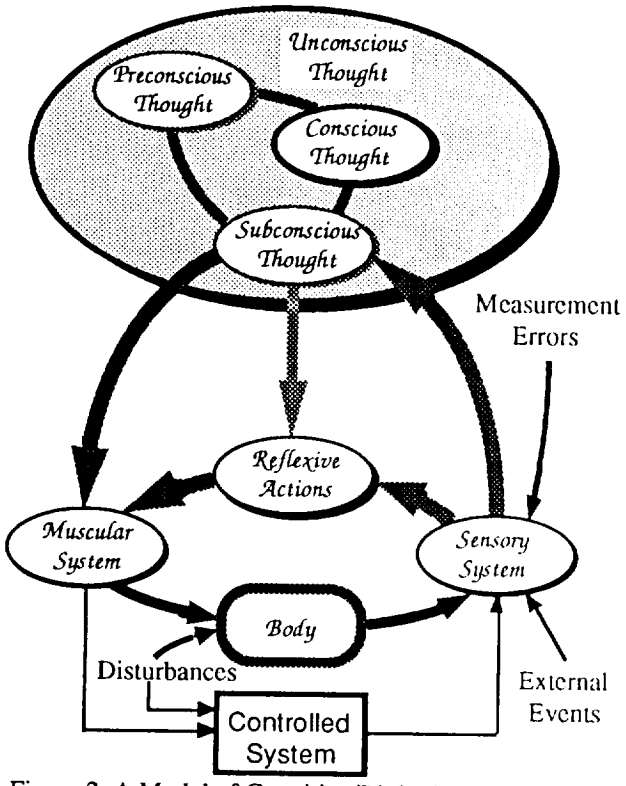

Figure 2. A Model of Cognitive/Biological Control Behavior.

The cells of biological systems undergo a continuing birth-life-death process, with new cells replacing old; nature provides a means of transmitting genetic codes from cell to cell. Nevertheless, *the central nervous system is incapable of functional regeneration.* Once a portion of the system has been damaged, it cannot be replaced, although redundant neural circuitry can work around some injuries. *Short-term memory often recedes into long-term memory*, where it generally takes longer to be retrieved. With time, *items in memory that are less important are forgotten, possibly replaced by more important information*; hence, information has a half-life that depends upon its significance to our lives (and perhaps to its "refresh rate"). *Humans develop the capability to form chords of actions* that are orchestrated or coordinated to achieve a single goal. Response to an automotive emergency may include applying the brakes, disengaging the clutch, steering to avoid an obstacle, and bracing for impact all at once. *We develop "knee-jerk" reactions that combine declarative, procedural, and reflexive functions*, like clapping after the last movement of a symphony.

Nature also provides structural paradigms for control that are worth emulating in machines. First, there is a *richness of sensory information* that is hard to fathom, with millions of sensors providing information. This results in high signal-to-noise ratio in some cases, and it allows symbolic/image processing in others. Those signals requiring high-bandwidth, high-resolution channel capacity (vision, sound, and balance) have *short, dedicated, parallel runs* from the sensors to the brain. This enhances the security of the channels and protects the signals from noise contamination. *Dissimilar but related sensory inputs facilitate interpretation of data.* A single motion can be sensed by the eyes, by the inner ear, and by the "seat-of-the-pants" (i.e., by sensing forces on the body itself), corroborating each other and suggesting appropriate actions. When these signals are made to disagree in moving-cockpit simulation of flight, a pilot may experience a sense of confusion and disorientation.

There are *hierarchical and redundant structures* throughout the body. The nervous system is a prime example, bringing inputs from myriad sensors (both similar and dissimilar) to the brain, and performing low-level reasoning as an adjunct. Many sensing organs occur in pairs (e.g., eyes, ears, inner ears), and their internal structures are highly parallel. *Pairing allows graceful degradation in the event that an organ is lost.* Stereo vision vanishes with the loss of an eye, but the remaining eye can provide both foveal and peripheral vision, as well as a degree of depth perception through object size and stadiametric processing. Our control effectors (arms, hands, legs, feet) also occur in pairs, and there is an element of "Fail-Op/Fail-Op/Fail-Safe" design [43] in the number of fingers provided for manual dexterity.

Structure for Intelligent Flight Control

The preceding section leads to a control system structure that overlays the cognitive/biological model of Fig. 2 on the flight control block diagram of Fig. 1 and adds new functions. The suggested structure (Fig. 3) has *super-blocks* identifying declarative, procedural, and reflexive functions; these contain the classical GNC functions plus new functions related to decision-making, prediction, and learning. The black arrows denote information flow for the primary GNC functions, while the gray arrows illustrate the data flow that supports subsidiary adjustment of goals, rules, and laws.

Within the super-blocks, higher-level functions are identified as conscious, preconscious, and subconscious attributes, not with disregard for the philosophical objections raised earlier but as a working analog for establishing a computational hierarchy. The new functions relate to setting or revising goals for the aircraft's mission, monitoring and adjusting the aircraft's systems and subsystems, identifying changing characteristics of the aircraft and its environment, and applying this knowledge to modify the structures and parameters of GNC functions.

[6] "In REM Sleep, the brain is barraged by signals from the brain stem. Impulses fired to the visual cortex produce images that may contain materials from the day's experiences, unsolved problems, and unfinished business." [42]

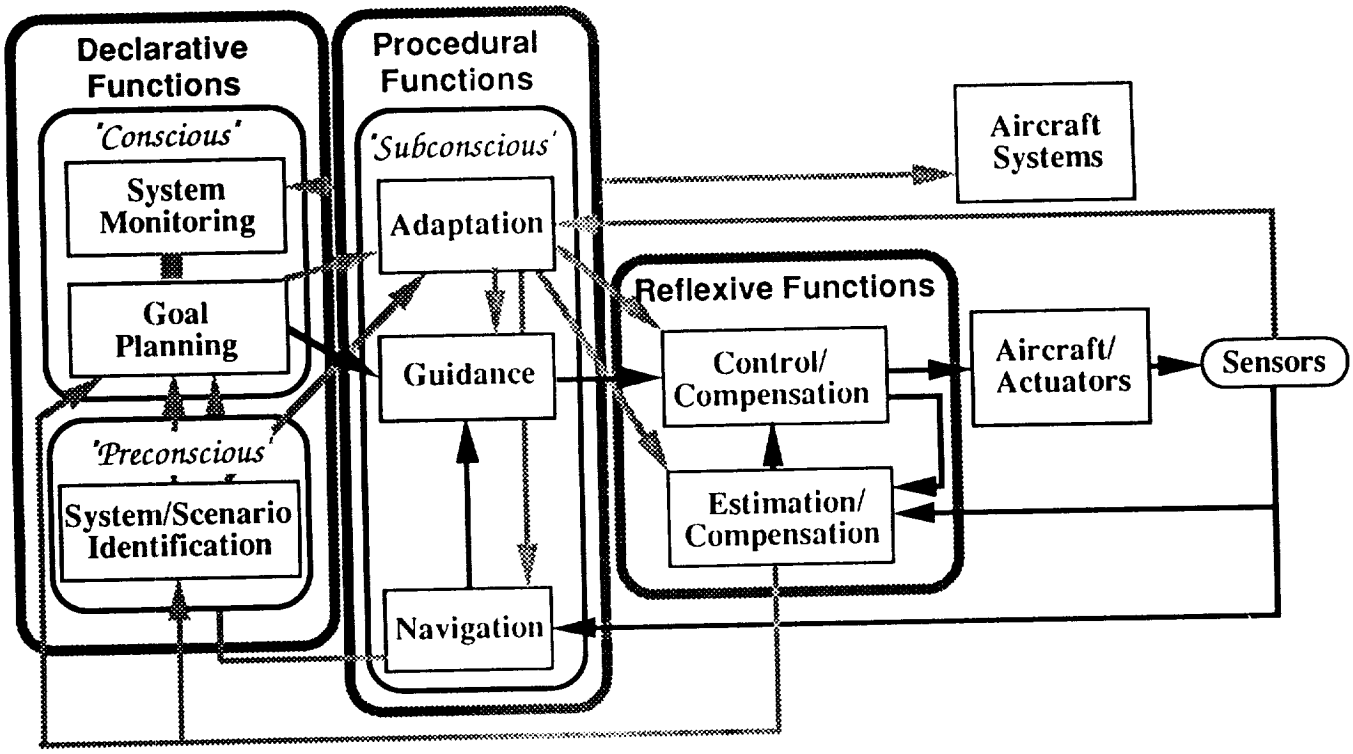

Figure 3. Intelligent Flight Control System Structure.

The suggested structure has implications for both hardware and software. Declarative functions are most readily identified with single-processor computers programmed in LISP or Prolog, as decision-making is associated with list processing and the statement of logical relationships. Procedural functions can be conceptualized as vector or "pipelined" processes programmed in FORTRAN, Pascal, or C, languages that have been developed for numerical computation with subroutines, arrays, differential equations, and recursions. Reflexive functions seem best modeled as highly parallel processes implemented by neural networks, which apply dense mappings to large masses of data almost instantaneously. Nevertheless, parallel processes can be implemented using sequential processors, and sequential algorithms can be "parallelized" for execution on parallel processors. The choice of hardware and software depends as much on the current state-of-the-art as on the closeness of computational requirements and GNC functions.

In the remainder of the paper, declarative, procedural, and reflexive control functions are discussed from an aerospace perspective. In practice, the boundaries between mission tasks may not be well defined, and there is overlap in the kinds of algorithms that might be applied within each group. A number of practical issues related to human factors, system management, certifiability, maintenance, and logistics are critical to the successful implementation of intelligent flight control, but they are not treated here.

DECLARATIVE SYSTEMS

Goal planning, system monitoring, and control-mode switching are declarative functions that require reasoning. Alternatives must be evaluated, and decisions must be made through a process of *deduction*, that is, by inferring answers from general or domain-specific principles. The inverse process of learning principles from examples is *induction*, and not all declarative systems have this capability. Most declarative systems have fixed structure and parameters, with knowledge induced off-line and before application; declarative systems that learn on-line must possess a higher level of reasoning ability, perhaps through an internal declarative module that specializes in training.

Expert Systems

Expert Systems are computer programs that use physical or heuristic relationships and facts for interpretation, diagnosis, monitoring, prediction, planning, and design. In principal, an expert system replicates the decision-making process of one or more experts who understand the causal or structural nature of the problem [44]. While human experts may employ "nonmonotonic reasoning" and "common sense" to deduce facts that apparently defy simple logic, computational expert systems typically are formal and consistent, basing their conclusions on analogous cases or well-defined rules[7].

[7] Expert systems can have *tree* or *graph* structures. In the former, there is a single *root* node, and all final (*leaf*) nodes are

A *rule-based expert system* consists of *data*, *rules*, and an *inference engine* [46]. It generates actions predicated on its data base, which contains measurements as well as stored data or operator inputs. An expert system performs deduction using *knowledge* and *beliefs* expressed as parameters and rules. *Parameters* have values that either are external to the expert system or are set by rules. An "IF-THEN" *rule* evaluates a *premise* by testing values of one or more parameters related by logical "ANDs" or "ORs," as appropriate, and it specifies an *action* that set values of one or more parameters.

The rule base contains all the cause-and-effect relationships of the expert system, and the inference engine performs its function by searching the rule base. Given a set of premises (evidence of the current state), the logical outcome of these premises is found by a data-driven search (*forward chaining*) through the rules. Given a desired or unknown parameter value, the premises needed to support the fixed or free value are identified by a goal-directed search (*backward chaining*) through the rules. Querying (or firing) a rule when searching in either direction may invoke procedures that produce parameter values through *side effects* [47].

Rules and parameters can be represented as *objects* or *frames* using ordered lists that identify names and attributes. Specific rules and parameters are represented by lists in which values are given to the names and attributes. The attribute lists contain not only values and logic but additional information for the inference engine. This information can be used to compile *parameter-rule-association lists* that speed execution [48]. Frames provide useful parameter structures for related productions, such as analyzing the origin of one or more failures in a complex, connected system [49]. Frames possess an *inheritance property*; thus a particular object lays claim to the properties of the object type.

Crew/Team Paradigms for Declarative Flight Control

Logical task-classification is a key factor in the development of rule-based systems. To this point, we have focused on the intelligence of an individual as a paradigm for control system design, but it is useful to consider the hypothetical actions of a multi-person aircraft crew as well. In the process, we develop an expert system of expert systems, a hierarchical structure that reasons and communicates like a team of cooperating, well-trained people might. This notion is expanded in [50-53]. The Pilot's Associate Program initially focused on a four-task structure and evolved in the direction of the multiple crew-member paradigm [54-56].

AUTOCREW is an ensemble of nine cooperating rule-based systems, each figuratively emulating a member of a World War II bomber crew: executive (pilot), co-pilot, navigator, flight engineer, communicator, spoofer (countermeasures), observer, attacker, and defender (Fig. 4) [53]. The executive coordinates mission-specific tasks and has knowledge of the mission plan. The aircraft's human pilot can monitor AUTOCREW functions, follow its suggestions, enter queries, and assume full control if confidence is lost in the automated solution. The overall goal is to reduce the pilot's need to regulate the system directly without removing discretionary options. AUTOCREW contains over 500 parameters and over 400 rules.

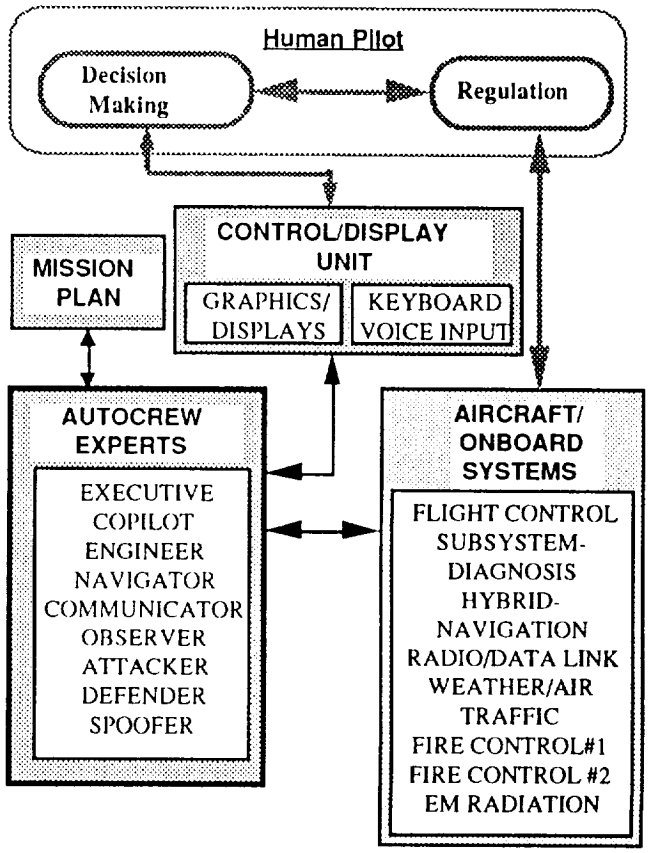

Figure 4. AUTOCREW Configuration with Pilot/Aircraft Interface (adapted from [52]).

AUTOCREW was developed by defining each member expert system as a *knowledge base*, according to the following principles:

- Divide each knowledge base into task groups: time-critical, routine, and mission-specific.
- Order task groups from most to least time-critical to quicken the inference engine's search.
- Break major tasks into sub-tasks according to need for communicating system functions.
- Identify areas of cooperation between knowledge bases.

The five main task groups for each crew member are: tasks executed during attack on the aircraft, tasks executed

connected to their own single *branch*. In the latter, one or more branches lead to individual nodes. Reasoning is *consistent* if an individual node is not assigned differing values by different branches [45].

during emergency or potential threat, tasks ordered by the EXECUTIVE, tasks executed on a routine basis, and mission-specific tasks. Routine and mission-specific tasks are executed on each cycle; emergency tasks are executed only when the situation warrants. Operation of AUTOCREW was simulated to obtain comparative expert-system workloads for two mission scenarios: inbound surface-to-air missile attack and human pilot incapacitation [52]. In addition to the overall AUTOCREW system, a functioning NAVIGATOR sensor-management expert system was developed. Knowledge acquisition for the system is challenging because traditional methods (e.g., domain-expert interviews) do not provide sufficiently detailed information to design the system [57].

Additional perspectives on intelligent flight management functions can be obtained from the literature on decision-making by teams, as in [58-60]. Alternate approaches to aiding the pilot in emergencies are given in [61, 62].

Reasoning Under Uncertainty

Rule-based control systems must make decisions under uncertainty. Measurements are noisy, physical systems are subject to random disturbances, and the environment within which decisions must be made is ambiguous. For procedural systems, the formalism of optimal state estimation provides a rigorous and useful means of handling uncertainty [63]. For declarative systems, there are a number of methods of uncertainty management, including probability theory, Dempster-Shafer theory, possibility theory (fuzzy logic), certainty factors, and the theory of endorsements [64].

Bayesian belief networks [65], which propagate event probabilities up and down a causal tree using Bayes's rule, have particular appeal for intelligent control applications because they deal with probabilities, which form the basis for stochastic optimal control. We have applied Bayesian networks to aiding a pilot who may be flying in the vicinity of hazardous wind shear [66]. Figure 5 shows a network of the causal relationships among meteorological phenomena associated with microburst wind shear, as well as temporal and spatial information that could affect the likelihood of microburst activity. A probability of occurrence is associated with each node, and a conditional probability based on empirical data is assigned to each arrow. The probability of encountering microburst wind shear is the principal concern; however, each time new evidence of a particular phenomenon is obtained, probabilities are updated throughout the entire tree. In the process, the estimated likelihood of actually encountering the hazardous wind condition on the plane's flight path is refined.

The safety of aircraft operations near microburst wind shear will be materially improved by forward-looking Doppler radar, which can sense variations in the wind speed. Procedural functions that can improve the reliability of the wind shear expert system include extended Kalman filtering of the velocity measurements at incremental ranges ahead of the aircraft [67].

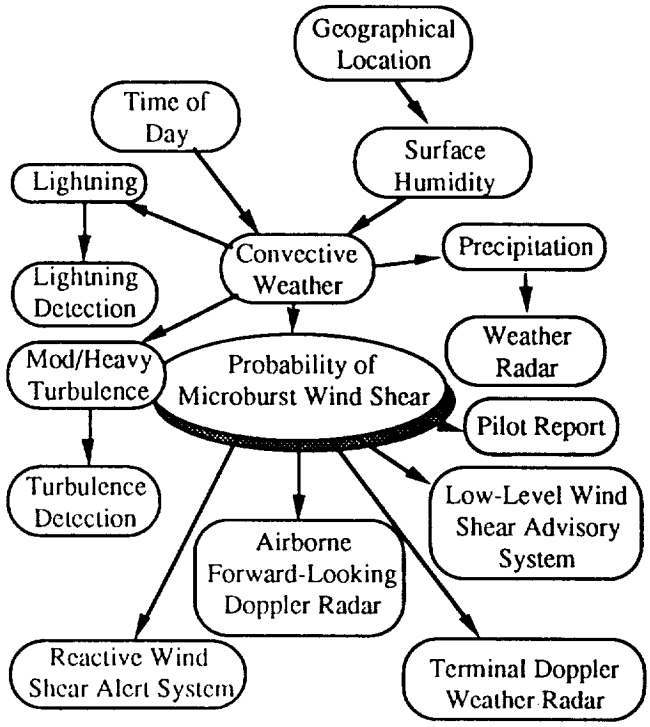

Figure 5. Bayesian Belief Network to Aid Wind Shear Avoidance (adapted from [67]).

Probabilistic reasoning of a different sort has been applied to a problem in automotive guidance that may have application in future Intelligent Vehicle/Highway Systems [68-70]. Intelligent guidance for headway and lane control on a highway with surrounding traffic is based on *worst-plausible-case decision-making*. It is assumed that the intelligent automobile (IA) has imaging capability as well as on-board motion sensors; hence, it can deduce the speed and position of neighboring automobiles. Each automobile is modeled as a simple discrete-time dynamic system, and estimates of vehicle states are propagated using extended Kalman filters [63]. There are limits on the performance capabilities of all vehicles, and IA strategy is developed using time-to-collide, braking ratios, driver aggressiveness, and desired security factors. Plausible guidance commands are formulated by minimizing a cost function based on these factors [70]. Both normal and emergency expert systems govern the process, supported by procedural calculations for situation assessment, traffic prediction, estimation, and control (Fig. 6). Guidance commands are formulated by minimizing a cost function based on these factors [70].

Each of the expert systems discussed in this section performs deduction in a cyclical fashion based on prior logical structures, prior knowledge of parameters, and real-time measurements. Intelligent flight control systems must deal with unanticipated events, but it is difficult to

identify aeronautical applications where on-line declarative learning is desirable. Nevertheless, off-line induction is needed to formulate the initial declarative system and perhaps (in a manner reminiscent of REM Sleep) to upgrade declarative logic between missions.

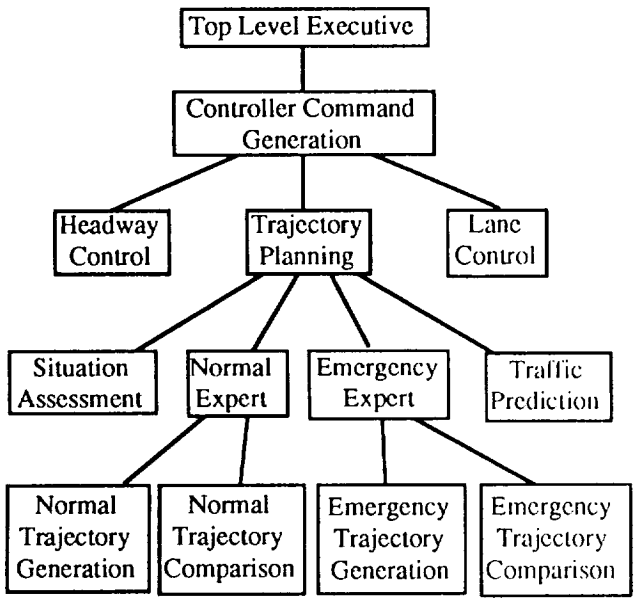

Figure 6. Intelligent Guidance for Automotive Headway and Lane Control [69].

Inducing Knowledge in Declarative Systems

In common usage, "learning" may refer a) to collecting inputs and deducing outputs and b) to inducing the logic that relates inputs and outputs to specific tasks. Here, we view the first process as the normal function of the intelligent system and the second as "learning." Teaching an expert system the rules and parameters that generalize the decision-making process from specific knowledge is the inverse of expert-system operation. Given all possible values of the parameters, what are the rules that connect them? Perhaps the most common answer is to interview experts in an attempt to capture the logic that they use, or failing that, to study the problem intensely so that one becomes expert enough to identify naturally intelligent solutions. These approaches can be formalized [71, 72], and they were the ones used in [67] and [68]. Overviews of alternatives for induction can be found in [45, 46, 73, 74].

Two approaches are considered in greater detail. The first is called *rule recruitment* [75], and it involves the manipulation of "dormant rules" (or *rule templates*). This method was applied in the development of an intelligent failure-tolerant control system for a helicopter. Each template possesses a fixed premise-action structure and refers to parameters through *pointers*. Rules are constructed and incorporated in the rule base by defining links and modifying parameter-rule-association lists. Learning is based on Monte Carlo simulations of the controlled system with alternate failure scenarios. Learned parameter values then can be defined as "fuzzy functions" [76] contained in rule premises.

The second approach is to *construct classification or decision trees* that relate attributes in the data to decision classes [52]. The problem is to develop an Expert Navigation-Sensor Management System (NSM) that selects the best navigation aids from available measurements. Several aircraft paths were simulated, and the corresponding measurements that would have been made by GPS, Loran, Tacan, VOR, DME, Doppler radar, air data, and inertial sensors were calculated, with representative noise added. The simulated measurements were processed by extended Kalman filters to obtain optimal state estimates in 200 simulations. Using the root-sum-square error as a decision metric, Analysis of Variance (ANOVA) identifies the factors that make statistically significant contributions to the decision metric, and the Iterative Dichotomizer #3 (ID3) algorithm [77-79] extracts rules from the training set by inductive inference. The ID3 algorithm quantifies the *entropy content* of each attribute, that is, the information gained by testing the attribute at a given decision node. It uses an information-theoretic measure to find a splitting strategy that minimizes the number of nodes required to characterize the tree. Over 900 examples were used to develop the NSM decision tree.

PROCEDURAL SYSTEMS

Most guidance, navigation, and control systems fielded to date are procedural systems using sequential algorithms and processors. Although optimality of a cost function is not always a necessary or even sufficient condition for a "good" system, linear-optimal stochastic controllers provide a good generic structure for discussion.

Control and Estimation

We assume that a nominal (desired) flight path is generated by higher-level intelligence, such as the human pilot or declarative machine logic. The procedural system must follow the path, $\mathbf{x}^*(t)$ in $t_0 < t < t_f$. Control is exercised by a digital computer at time intervals of Δt. The n-dimensional state vector perturbation at time t_k is $\mathbf{x}_k$, and the m-dimensional control vector perturbation is $\mathbf{u}_k$. The discrete-time linear-quadratic-Gaussian (LQG) control law is formed as [63],

$$\mathbf{u}_k = \mathbf{u}^*_k - \mathbf{C}_B[\hat{\mathbf{x}}_k - \mathbf{x}^*_k] = \mathbf{C}_F\mathbf{y}^*_k - \mathbf{C}_B\hat{\mathbf{x}}_k \qquad (1$$

$\mathbf{y}^*_k$ is the desired value of an output vector (defined as $\mathbf{H}_x\mathbf{x}_k + \mathbf{H}_u\mathbf{u}_k$), and $\hat{\mathbf{x}}_k$ is the *Kalman filter* estimate, expressed in two steps:

$$\hat{\mathbf{x}}_k(-) = \Phi\hat{\mathbf{x}}_{k-1}(+) + \Gamma\mathbf{u}_{k-1}$$

$$\hat{\mathbf{x}}_k \triangleq \hat{\mathbf{x}}_k(+) = \hat{\mathbf{x}}_k(-) + \mathbf{K}[\mathbf{z}_k - \mathbf{H}_{obs}\hat{\mathbf{x}}_k(-)] \qquad (2$$

The forward and feedback control gain matrices are C_F and C_B, Φ and Γ are state-transition and control-effect matrices that describe the aircraft's assumed dynamics, the estimator gain matrix is **K**, and the measurement vector, z_k, is a transformation of the state through H_{obs}. The gains C_B and **K** result from solving two Riccati equations that introduce tradeoffs between control use and state perturbation and between the strengths of random disturbances and measurement error. C_F, which provides proper steady-state command response, is an algebraic function of C_B, Φ, Γ, and H_{obs}. All of the matrices may vary in time, and it may be necessary to compute **K** online. In the remainder, it is not essential that C_B and **K** be optimal (i.e., they may have been derived from eigenstructure assignment, loop shaping, etc.), although the LQR gains guarantee useful properties of the nominal closed-loop system [63].

The control structure provided by eq. 1 and 2 is quite flexible. It can represent a scalar feedback loop if **z** contains one measurement and **u** one control, or it can address measurement and control redundancy with **z** and **u** dimensions that exceed the dimension of the state **x**. It also is possible to incorporate reduced-order modeling in the estimator. Assuming that Φ and Γ have the same dimensions as the aircraft's dynamic model ($n \times n$ and $n \times m$), *the baseline estimator introduces n^{th}-order compensation in the feedback control loop.* The weights of the quadratic control cost function can be chosen not only to penalize state and control perturbations but to produce *output weighting*, *state-rate weighting*, and *implicit model following*, all without modifying the dynamic model [63]. *Integral compensation*, *low-pass filter compensation*, and *explicit model following* can be obtained by augmenting the system model during the design process, increasing the compensation order and producing the control structures shown in Fig. 7.

These cost weighting and compensation features can be used together, as in the proportional-integral/implicit-model-following controllers developed in [80]. Implicit model following is especially valuable when an ideal model can be specified (as identified in flying qualities specifications and standards [5, 6]), and integral compensation provides automatic "trimming" (control that synthesizes $\mathbf{u}^*_k$ corresponding to $\mathbf{x}^*_k$ to achieve zero steady-state command error) and low-frequency robustness. Combining integral and filter compensation produces controllers with good command tracking performance and smooth control actions, as demonstrated in flight tests [81-83]. The LQG regulator naturally introduces an *internal model of the controlled plant*, a feature that facilitates control design [84]. It produces a stable approximation to the *system inverse*, which is at the heart of achieving desired command tracking.

The estimator in the feedback loop presents an efficient means of dealing with uncertainty in the measurements, in the disturbance inputs, and (to a degree) in the aircraft's dynamic model. If measurements are very noisy, the estimator gain matrix **K** is "small," so that the filter relies on extrapolation of the system model to estimate the state. If disturbances are large, the state itself is more uncertain, and **K** is "large," putting more emphasis on the measurements. Effects of uncertain parameters can be approximated as "process noise" that increases the importance of measurements, leading to a higher **K**. If the system uncertainties are constant but unknown biases or scale factors, a better approach is to augment the filter state to estimate these terms directly. Parametric uncertainty introduces nonlinearity; hence, an *extended Kalman filter* must be used [63].

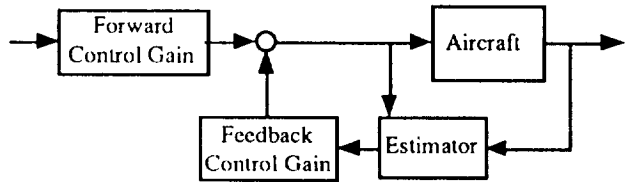

a) Linear-Quadratic-Gaussian (LQG) Regulator.

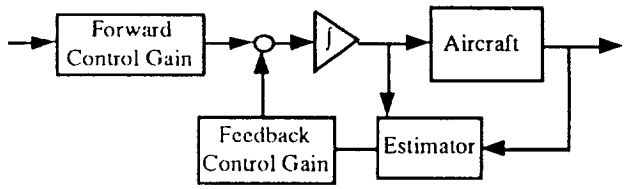

b) Proportional-Filter LQG Regulator.

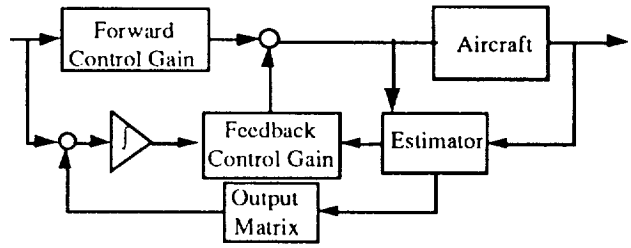

c) Proportional-Integral LQG Regulator.

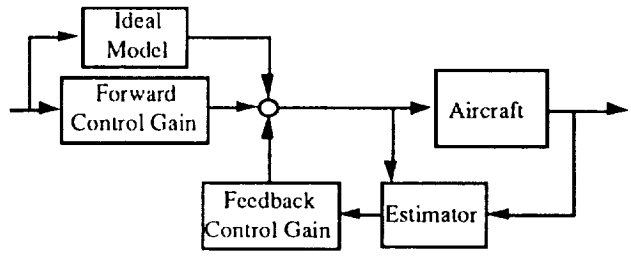

d) Explicit-Model-Following LQG Regulator.

Figure 7. Structured Linear-Quadratic-Gaussian Regulators.

Stability and Performance Robustness

Controlled system *robustness* is the ability to maintain satisfactory stability and performance in the presence of parametric or structural uncertainties in either the aircraft or its control system. All controlled systems must

possess some degree of robustness against operational parameter variations. The inherent stability margins of certain algebraic control laws (e.g., the linear-quadratic (LQ) regulator [63, 85-87]) may become vanishingly small when dynamic compensation (e.g., the estimator in a linear-quadratic-Gaussian (LQG) regulator) is added [88]. Restoring the robustness to that of the LQ regulator typically requires increasing estimator gains (within practical limits) using the loop-transfer-recovery method [89] or the stochastic robustness approach described below.

Subjective judgments must be made in assessing the need for robustness and in establishing corresponding control system design criteria, as there is an inevitable tradeoff between robustness and nominal system performance [90]. The designer must know the normal operating ranges and distributions of parameter variations, as well as the specifications for system operability with failed components, else the final design may afford too little robustness for possible parameter variations or too much robustness for satisfactory nominal performance. Robustness traditionally has been assessed deterministically [91, 92]; gain and phase margins are an inherent part of the classical design of single-input/single-output systems, and there are multi-input/multi-output equivalents based on singular-value analysis (e.g., [93]). A critical difficulty in applying these techniques is relating singular-value bounds on return-difference and inverse-return-difference matrices to real parameter variations in the system.

Statistical measures of robustness can use knowledge of potential variations in real parameters. The *probability of instability* was introduced in [94] and is further described in [95, 96]. The *stochastic robustness* of a linear, time-invariant system, is judged using Monte Carlo simulation to estimate the probability distributions of closed-loop eigenvalues, given the statistics of the variable parameters in the system's dynamic model. Because the system is either stable or not, the probability of instability has a *binomial distribution*; hence, *the confidence intervals associated with estimating the metric from simulation are independent of the number or nature of the uncertain parameters* [95].

Considerations of performance robustness are easily taken into account in *Stochastic Robustness Analysis* (SRA). Systems designed using a variety of robust control methods (loop transfer recovery, H_∞ optimization, structured covariance, and game theory) are analyzed in [97], with attention directed to the probability of instability, probability of settling-time exceedence, probability of excess control usage, and tradeoffs between them. The analysis uncovers a wide range of system responses and graphically illustrates that gain and phase margins are not good indicators of the probability of instability[8]. This also raises doubts about the utility of singular values, as they are multivariable equivalents of the classical robustness metrics. Incorporating SRA into the design of an LQG regulator with implicit model following and filter compensation leads to designs that have high levels of stability and performance robustness [98]. The reason for improvement is that SRA measures the actual effects of parameter variations on stability and performance rather than incremental changes in the nominal margins.

Adaptation and Tolerance to Failures

Adaptation always has been a critical element of stability augmentation. Most aircraft requiring improved stability undergo large variations in dynamic characteristics on a typical mission. Gain scheduling and control interconnects initially were implemented mechanically, pneumatically, and hydraulically; now the intelligent part is done within a computer, and there is increased freedom to use sophisticated scheduling techniques that approach full nonlinear control [81, 99].

One approach to improving failure tolerance is *parallel redundancy*: two or more control strings, each separately capable of satisfactory control, are implemented in parallel. A *voting* scheme is used for redundancy management. With two identical channels, a comparator can determine whether or not control signals are identical; hence, it can detect a failure but cannot identify which string has failed. Using three identical channels, the control signal with the middle value can be selected (or voted), assuring that a single failed channel never controls the plant. Parallel redundancy can protect against control-system component failures, but it does not address failures of plant components. *Analytical redundancy* provides a capability to improve tolerance to failures of both types. The principal functions of analytical redundancy are *failure detection, failure identification*, and *control-system reconfiguration* [47].

Procedural adaptation and failure-tolerance features will evolve outward, to become more declarative in their supervision and more reflexive in their implementation. Declarative functions are especially important for differentiating between normal and emergency control functions and sensitivities. They can work to reduce trim drag, to increase fatigue life, and to improve handling and ride qualities as functions of turbulence level, passenger loading, and so on. Gain-scheduling control can be viewed as *fuzzy control*, suggesting that the latter has a role to play in aircraft control systems [100-102]. Reflexive functions can be added by computational neural networks that approximate nonlinear multivariate functions or classify failures.

[8] Real parameter variations affect not only the magnitude and relative phase angle of the system's Nyquist contour but its shape as well [63]. Therefore, the points along the contour that establish gain and phase margin (i.e., the corresponding Bode-plot frequencies) are subject to change.

Nonlinear Control

Aircraft dynamics are inherently nonlinear, but aerodynamic nonlinearities and inertial coupling effects are generally smooth enough in the principal operating regions to allow linear control design techniques to be used. Control actuators impose hard constraints on operation because their displacements and rates are strictly limited. Nonlinear control laws can improve control precision and widen stability boundaries when flight must be conducted at high angles or high angular rates and when the control-actuator limits must be challenged.

The general principles of nonlinear inverse control are straightforward [103]. Given a nonlinear system of the form,

$$\dot{\mathbf{x}} = \mathbf{f}(\mathbf{x}) + \mathbf{G}(\mathbf{x})\mathbf{u} \qquad (3$$

where $\mathbf{G}(\mathbf{x})$ is square ($m = n$) and non-singular, the control law

$$\mathbf{u} = -\mathbf{G}^{-1}\mathbf{f}(\mathbf{x}) + \mathbf{G}^{-1}\mathbf{v} \qquad (4$$

inverts the system, since

$$\dot{\mathbf{x}} = \mathbf{f}(\mathbf{x}) + \mathbf{G}(\mathbf{x})[-\mathbf{G}^{-1}\mathbf{f}(\mathbf{x}) + \mathbf{G}^{-1}\mathbf{v}] = \mathbf{v} \qquad (5$$

where $\mathbf{v}$ is the command input to the system.

In general, $\mathbf{G}(\mathbf{x})$ is not square ($m \neq n$); however, given an m-dimensional output vector,

$$\mathbf{y} \overset{\Delta}{=} \mathbf{H}\mathbf{x} \qquad (6$$

it is possible to define a nonlinear feedback control law that produces *output decoupling* of the elements of $\mathbf{y}$ or their derivatives such that $\mathbf{y}^{(\boldsymbol{d})} = \mathbf{v}$. The vector $\mathbf{y}^{(\boldsymbol{d})}$ contains *Lie derivatives* of $\mathbf{y}$,

$$\mathbf{y}^{(\boldsymbol{d})} = = \mathbf{f}^*(\mathbf{x}) + \mathbf{G}^*(\mathbf{x})\mathbf{u} \qquad (7$$

where $\boldsymbol{d}$ is the *relative degree vector* of differentiation required to identify a direct control effect on each element of $\mathbf{y}$. $\mathbf{G}^*(\mathbf{x})$ and $\mathbf{f}^*(\mathbf{x})$ are components of the Lie derivatives, and $\mathbf{G}^*(\mathbf{x})$ is guaranteed to be structurally invertible by the condition that defines relative degree [104]. The decoupling control law then takes the form

$$\mathbf{u} = -[\mathbf{G}^*(\mathbf{x})]^{-1}\mathbf{f}^*(\mathbf{x}) + [\mathbf{G}^*(\mathbf{x})]^{-1}\mathbf{v} \qquad (8$$

The control law is completed by feeding $\mathbf{y}$ back as appropriate to achieve desired transient response and by pre-filtering $\mathbf{v}$ to produce the desired command response [105]. Because the full state is rarely measured and measurements can contain errors, it may be necessary to estimate $\mathbf{x}$ with an extended Kalman filter, substituting $\hat{\mathbf{x}}$ for $\mathbf{x}$ in control computations.

Evaluating $\mathbf{G}^*(\mathbf{x})$ and $\mathbf{f}^*(\mathbf{x})$ requires that a full, d-differentiable model of aircraft dynamics be included in the control system; hence the statement of the control law is simple, but its implementation is complex (Fig. 8). Smooth interpolators of the aircraft model (e.g., cubic splines) are needed. Feedforward neural networks with sigmoidal activation functions are infinitely differentiable, providing a good means of representing this model on-line and allowing adaptation [106, 107]. Limitations to the inverse control approach are discussed in [108].

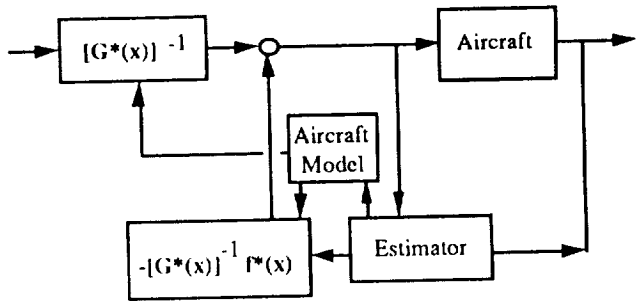

Figure 8. Decoupling Nonlinear-Inverse Control Law.

REFLEXIVE SYSTEMS

Inner-loop control is a reflexive (though not necessarily linear) function. To date, most inner loops have been designed as procedural control structures; computational neural networks may extend prior results to facilitate nonlinear control and adaptation. Neural networks can be viewed as *nonlinear generalizations of sensitivity, transformation, and gain matrices*. Consequently, compensation dynamics can be incorporated by following earlier models and control structures. Nonlinear proportional-integral and model following controllers, as well as nonlinear estimators, can be built using computational neural networks.

Computational Neural Networks

Computational neural networks are motivated by input-output and learning properties of biological neural systems, though in mathematical application the network becomes an abstraction that may bear little resemblance to its biological antecedent. Computational neural networks consist of *nodes* that simulate the *neurons* and *weighting factors* that simulate the *synapses* of a living nervous system. The nodes are nonlinear basis functions, and the weights contain knowledge of the system. Neural networks are good candidates for performing a variety of reflexive functions in intelligent control systems because they are potentially very fast (in parallel hardware implementation), they are intrinsically nonlinear, they can address problems of high dimension, and they can learn from experience. From the biological analogy, the neurons are modeled as switching functions that take just two discrete values; however, "switching" may be softened to "saturation," not only to facilitate learning of the synaptic

weights but to admit the modeling of continuous, differentiable functions.

The neural networks receiving most current attention are static expressions that perform one of two functions. The first is to *approximate multivariate functions* of the form

$$y = h(x) \qquad (9$$

where x and y are input and output vectors and $h(\cdot)$ is the (possibly unknown) relationship between them. Neural networks can be considered to be *generalized spline functions* that identify efficient input-output mappings from observations [109, 110]. The second application is to *classify attributes*, much like the decision trees mentioned earlier. (In fact, decision trees can be mapped to neural networks [111].) The following discussion emphasizes the first of these two applications.

An N-layer *feedforward neural network* (FNN) represents the function by a sequence of operations,

$$\mathbf{r}^{(k)} = \mathbf{s}^{(k)}[\mathbf{W}^{(k-1)}\mathbf{r}^{(k-1)}] \triangleq \mathbf{s}^{(k)}[\boldsymbol{\eta}^{(k)}], \; k = 1 \text{ to } N \qquad (10$$

where $y = \mathbf{r}^{(N)}$ and $x = \mathbf{r}^{(0)}$. $\mathbf{W}^{(k-1)}$ is a matrix of weighting factors determined by the learning process, and $\mathbf{s}^{(k)}[\cdot]$ is an activation-function vector whose elements normally are identical, scalar, nonlinear functions $\sigma_i(\eta_i)$ appearing at each node:

$$\mathbf{s}^{(k)}[\boldsymbol{\eta}^{(k)}] = [\sigma_1(\eta_1{}^{(k)}) \ldots \sigma_n(\eta_n{}^{(k)})]^T \qquad (11$$

One of the inputs to each layer may be a unity threshold element that adjusts the bias of the layer's output. Networks consisting solely of linear activation functions are of little interest, as they merely perform a linear transformation H, thus limiting eq. 9 to the form, $y = Hx$.

Figure 9 represents two simple feedforward neural networks. Each circle represents an arbitrary, scalar, nonlinear function $\sigma_i(\cdot)$ operating on the sum of its inputs, and each arrow transmits a signal from the previous node, multiplied by a weighting factor. A scalar network with a single hidden layer of four nodes and a unit threshold element (Fig. 9a) is clearly parallel, yet its output can be written as the series

$$y = a_0\sigma_0(b_0x + c_0) + a_1\sigma_1(b_1x + c_1) + a_2\sigma_2(b_2x + c_2) + a_3\sigma_3(b_3x + c_3) \qquad (12$$

illustrating that parallel and serial processing may be equivalent.

Consider a simple example. Various nodal activation functions, σ_i, have been used, and there is no need for each node to be identical. Choosing $\sigma_0(\cdot) = (\cdot)$, $\sigma_1 = (\cdot)^2$, $\sigma_2 = (\cdot)^3$, $\sigma_3 = (\cdot)^4$, eq. 9 is represented by the truncated power series,

$$y = a_0(b_0x + c_0) + a_1(b_1x + c_1)^2 + a_2(b_2x + c_2)^3 + a_3(b_3x + c_3)^4 \qquad (13$$

It is clear that network weights are redundant (i.e., that the (a, b, c) weighting factors are not independent). Consequently, more than one set of weights could produce the same functional relationship between x and y. Training sessions starting at different points could produce different sets of weights that yield identical outputs. This simple example also indicates that the unstructured feedforward network may not have compact support (i.e., its weights may have global effects) if its basis functions do not vanish for large magnitudes of their arguments.

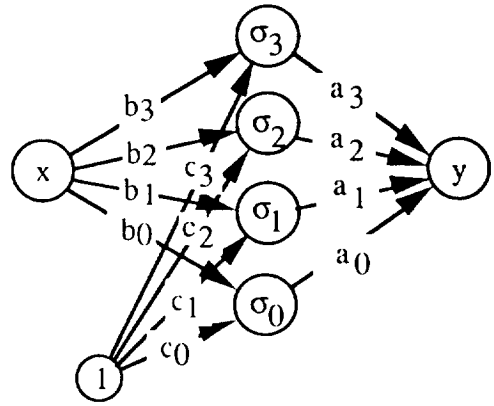

a) Single-Input/Single-Output Network.

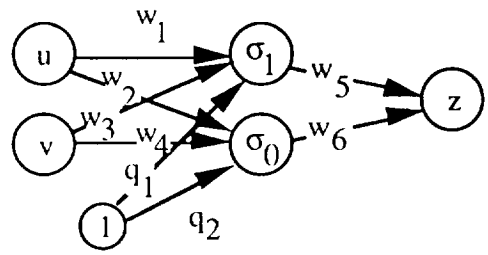

b) Double-Input/Single-Output Network.

Figure 9. Two Feedforward Neural Networks.

The *sigmoid* is commonly used as the artificial neuron. It is a saturating function: $\sigma(\eta) = 1/(1 + e^{-\eta})$ for output in (0,1) or $\sigma(\eta) = (1 - e^{-2\eta})/(1 + e^{-2\eta}) = \tanh \eta$ for output in (-1,1). Recent results indicate that any continuous mapping can be approximated arbitrarily closely with sigmoidal networks containing a single hidden layer (N = 2) [112, 113]. Symmetric functions like the *Gaussian radial basis function* ($\sigma(\eta) = e^{-\eta^2}$) have better convergence properties for many functions and have more compact support as a consequence of near-orthogonality [109, 114]. Classical *B-splines* [115] could be expressed in par-

allel form, and it has been suggested that they be used in multi-layered networks [116]. Hidden layers strengthen the analogy to biological models, though they are not necessary for approximating continuous functions, and they complicate the training process.

In control application, neural networks perform functions analogous to gain scheduling or nonlinear control. Consider the simple two-input network of Fig. 9b. The scalar output and derivative of a single sigmoid with unit weights are shown in Fig. 10. If u is a fast variable and v is a slow variable, choosing the proper weights on the inputs and threshold can produce a gain schedule that is approximately linear in one region and nonlinear (with an inflection point) in another. More complex surfaces can be generated by increasing the number of sigmoids. If u and v are both fast variables, then the sigmoid can represent a generalization of their nonlinear interaction.

For comparison, a typical radial basis function produces the output shown in Fig. 11. Whereas the sigmoid has a preferred input axis and simple curvature, the RBF admits more complex curvature of the output surface, and its effect is more localized. The most efficient nodal activation function depends on the general shape of the surface to be approximated. There may be cases best handled by a mix of sigmoids and RBF in the same network.

The cerebellar model articulation controller (CMAC) is an alternate network formulation with somewhat different properties but similar promise for application in control systems [117, 118]. The CMAC performs table look-up of a nonlinear function over a particular region of function space. CMAC operation can be split into two mappings. The first maps each input into an *association space A*. The mapping generates a *selector vector a* of dimension n_A, with c non-zero elements (usually ones) from overlapping *receptive regions* for the input. The second mapping, R, goes from the selector vector a to the scalar output y through the weight vector w, which is derived from training:

$$y = w^T a \qquad (14$$

Training is inherently local, as the extent of the receptive regions is fixed. The CMAC has quantized output, producing "staircased" rather than continuous output. A recent paper proposes to smooth the output using B-spline receptive regions [119].

The FNN and CMAC are both examples of *static networks*, that is, their outputs are essentially instantaneous: given an input, the speed of output depends only on the speed of the computer. *Dynamic networks* rely on stable resonance of the network about an equilibrium condition to relate a fixed set of initial conditions to a steady-state output. Bidirectional Associative Memory (BAM) networks [120] are nonlinear dynamical systems that subsume Hopfield networks [121], Adaptive-Resonance-Theory (ART) networks [122], and Kohonen networks [123]. Like FNN, they use binary or sigmoidal neurons and store knowledge in the weights that connect them; however, the "neural circuits" take time to stabilize on an output. While dynamic networks may operate more like biological neurons, which have a *refractory period* between differing outputs, computational delay degrades aircraft control functions.

Although neural networks performing function approximation may gain little from multiple hidden layers, networks used for classification typically require multiple layers, as follows from the ability to map decision trees to neural networks [111]. The principal values of performing such a mapping are that it identifies an efficient structure for parallel computation, and it may facilitate incremental learning and generalization.

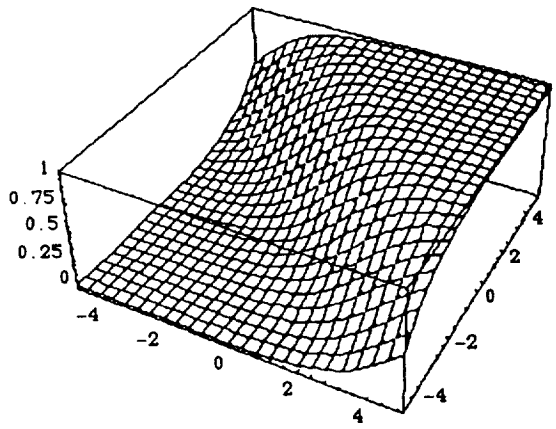

a) Sigmoid.

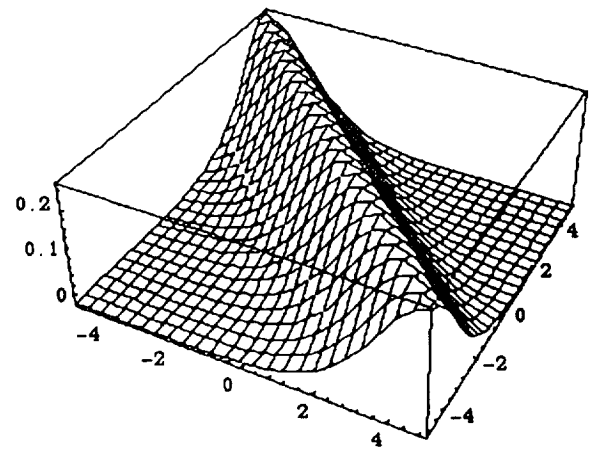

b) x-Derivative of Sigmoid.

Figure 10. Example of Sigmoid Output with Two Inputs.

Neural networks can be applied to *failure detection and identification* (FDI) by mapping data patterns (or *feature vectors*) associated with failures onto detector/identification vectors (e.g., [124-126]). To detect fail-

ure, the output is a scalar, and the network is trained (for example) with "1" corresponding to failure and "0" corresponding to no failure. The data patterns associated with each failure may require *feature extraction*, pre-processing that transforms the input time series into a feature vector [124]. As an alternative, the feature vector could be specified as a *parity vector* [127], and the neural network could be used for the decision-making logic in FDI.

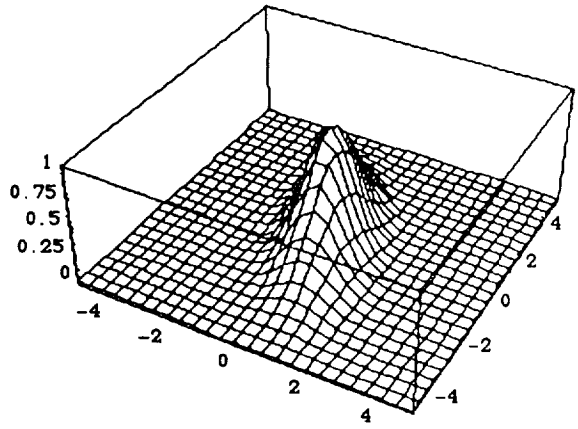

a) Radial Basis Function (RBF).

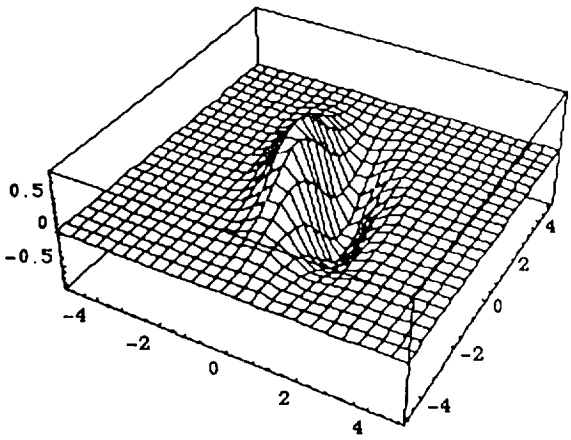

b) x-Derivative of RBF.

Figure 11. Example of Radial Basis Function Output with Two Inputs.

Reflexive Learning and Adaptation

Training neural networks involves either supervised or unsupervised learning. In *supervised learning*, the network is furnished typical histories of inputs and outputs, and the training algorithm computes the weights that minimize fit error. FNN and CMAC require this type of training, as discussed below. In *unsupervised learning*, the internal dynamics are self-organizing, tuning the network to home on different cells of the output *semantic map* in response to differing input patterns [128].

Backpropagation learning algorithms for the elements of $\mathbf{W}^{(k)}$ typically involve a *gradient search* (e.g., [129, 130]) that minimizes the mean-square output error

$$\mathcal{E} = \left[\mathbf{r}_d - \mathbf{r}^{(N)}\right]^T \left[\mathbf{r}_d - \mathbf{r}^{(N)}\right] \quad (15$$

where $\mathbf{r}_d$ is the desired output. For each input-output example presented to the network, the gradient of the error with respect to the weight matrix is calculated, and the weights are updated by

$$\mathbf{W}^{(k)}_{new} = \mathbf{W}^{(k)}_{old} + \beta \mathbf{r}^{(k-1)} \left[\mathbf{d}^{(k)}\right]^T \quad (16$$

β is the learning rate, and $\mathbf{d}$ is a function of the error between desired and actual outputs. For the output layer, the error term is

$$\mathbf{d}^{(N)} = S'\left[\mathbf{W}^{(N-1)}\mathbf{r}^{(N-1)}\right] (\mathbf{r}_d - \mathbf{r}^{(N)}) \quad (17$$

where the prime indicates differentiation with respect to $\mathbf{r}$. For interior layers, the error from the output layer is propagated from the output error using

$$\mathbf{d}^{(k)} = S'\left[\mathbf{W}^{(k-1)}\mathbf{r}^{(k-1)}\right] \left[\mathbf{W}^{(k-1)}\right]^T \mathbf{d}^{(k-1)} \quad (18$$

Search rate can be modified by adding momentum or conjugate-gradient terms to eq. 16.

The CMAC network learning algorithm is similar to backpropagation. The weights and output are connected by a simple linear operation, so a learning algorithm is easy to prescribe. Each weight contributing to a particular output value is adjusted by a fraction of the difference between the network output and the desired output. The fraction is determined by the desired learning speed and the number of receptive regions contributing to the output.

Learning speed and accuracy for FNN can be further improved using an *extended Kalman filter* [106, 107, 131]. The dynamic and observation models for the filter are

$$\mathbf{w}_k = \mathbf{w}_{k-1} + \mathbf{q}_{k-1} \quad (19$$

$$\mathbf{z}_k = \mathbf{h}(\mathbf{w}_k, \mathbf{r}_k) + \mathbf{n}_k \quad (20$$

where $\mathbf{w}_k$ is a vector of the matrix $\mathbf{W}_k$'s elements, $\mathbf{h}(\cdot)$ is an observation function, and $\mathbf{q}_k$ and $\mathbf{n}_k$ are noise processes. If the network has a scalar output, then $\mathbf{z}_k$ is scalar, and the extended Kalman filter minimizes the fit error between the training hypersurface and that produced by the network (eq. 15). It has been found that the fit error can be dramatically reduced by considering the *gradients* of the surfaces as well [106, 107]. The observation vector becomes

$$z_k = \begin{bmatrix} h(w_k, r_k) \\ \frac{\partial h}{\partial r}(w_k, r_k) \end{bmatrix} + n_k \qquad (21$$

with concomitant increase in the complexity of the filter. The relative significance given to function and derivative error during training can be adjusted through the measurement-error covariance matrix used in filter design.

Recursive estimation of the weights is useful when smooth relationships between fit errors and the weights are expected, when the weight-vector dimension is not high, and when local minima are global. When one of these is not true, it may speed the computation of weights to use a *randomized search*, at least until convergent regions are identified. Such methods as *simulated annealing* or *genetic algorithms* can be considered (and the latter has philosophic appeal for intelligent systems) [132-134]. The first of these is motivated by statistical mechanics and the effects that controlled cooling has on the ground states of atoms (which are analogous to the network weights). The second models the reproduction, crossover, and mutation of biological strings (e.g., chromosomes, again analogous to the weights), in which only the fittest combinations survive.

Statistical search methods can go hand-in-hand with SRA to train *robust neural networks*. Following [98], the randomized search could be combined with Monte Carlo variation of system parameters during training, numerically minimizing the *expected value of fit error* rather than a deterministic fit error.

We envision an aerodynamic model that spans the entire flight envelope of an aircraft, including post-stall and spinning regions. The model contains six neural networks with multiple inputs and scalar outputs, three for force coefficients and three for moment coefficients (for example, the pitch moment network takes the form $C_m = g(\mathbf{x},\mathbf{u})$, where $\mathbf{x}$ represents the state and $\mathbf{u}$ the control). If input variables are not restricted to those having plausible aerodynamic effect, false correlations may be created in the network; hence, attitude Euler angles and horizontal position should be neglected, while physically meaningful terms like elevator deflection, angle of attack, pitch rate, Mach number, and dynamic pressure should be included [107].

The aircraft spends most of its flying time within normal mission envelopes. Unless it is a trainer, the aircraft does not enter post-stall and spinning regions; consequently, on-line network training focuses on normal flight and neglects extreme conditions. This implies not only that networks must be pre-trained in the latter regions but that normal training must not destroy knowledge in extreme regions while improving knowledge in normal regions. Therefore, radial basis functions appear to be a better choice than sigmoid activation functions for adaptive networks.

Elements of the input vector may be strongly correlated with each other through the aircraft's equations of motion; hence, networks may not be able to distinguish between highly correlated variables (e.g., pitch rate and normal acceleration). This is problematical only when the aircraft is outside its normal flight envelope. Pre-training should provide inputs that are rich in frequency content, that span the state and control spaces, and that are as uncorrelated as possible. Generalization between training points may provide smoothness, but it does not guarantee accuracy.

Control Systems Based on Neural Networks

Neural networks can find application in logic for control, estimation, system identification, and physical modeling. In addition to work already referenced, additional examples can be found in [135-140].

Figure 12a illustrates an application in which the neural network forms the aircraft model for a nonlinear-inverse control law. The aircraft model of Fig. 9 is implemented with a neural network that is trained by a dedicated (weight) extended Kalman filter (the thick gray arrow indicating training). The extended Kalman filter for state estimation is expanded to estimate histories of forces and moments as well as the usual motion variables.

It is possible to conduct supervised learning on-line while not interfering with normal operation because the state Kalman filter produces both the necessary inputs and the desired outputs for the network training algorithm. There is no need to provide an ideal control response for training, as the form of the control law is fixed. Procedural and reflexive functions are combined in this control implementation, under the assumption that the direct expression of inversion is the most efficient approach.

Figure 12b shows a logical extension in which the inverse control law is implemented by neural networks. Inversion is an implicit goal of neural-network controllers [135, 136], and the formal existence of inversion networks has been explored [141]. Although Fig. 12b implies that the inversion networks are pre-trained and fixed, they, too, can be trained with the explicit help of the network that models the system [136].

If a desired control output is specified (Fig. 12c), then the formal model of the aircraft is no longer needed. The control networks learn implicit knowledge of the aircraft model. Referring to Fig. 10 and eq. 1 and 2, control and estimation gains, state-transition and control-effect matrices, and measurement transformations can be implemented as static neural networks with either off-line or on-line learning.

Dividing control networks into separate feedback and forward parts may facilitate training to achieve design goals. A feedback neural network has strongest effect on homogeneous modes of motion, while a forward neural network is most effective for shaping command (forced) response. This structure is adopted in [139], where the

forward and feedback networks are identified as *reason* and *instinct networks*. In pre-training, it is plausible that the feedback network would be trained with initial condition responses first, to obtain satisfactory transient response. The forward network would be trained next to achieve desired steady states and input decoupling. A third training step could be the addition of command-error integrals while focusing on disturbance inputs and parameter variations in training sets.

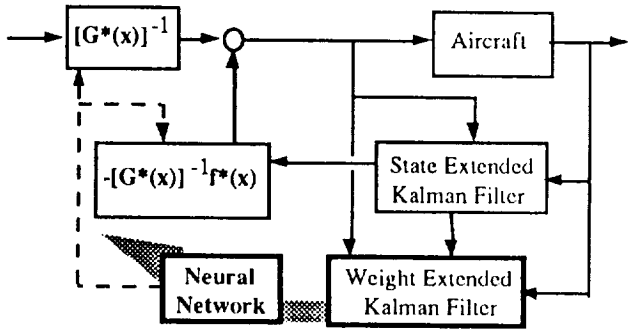

a) Neural Network for Modeling and Adaptation.

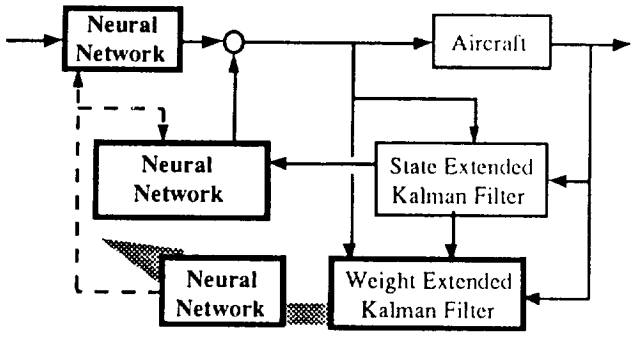

b) Neural Networks for Modeling, Adaptation, and Control.

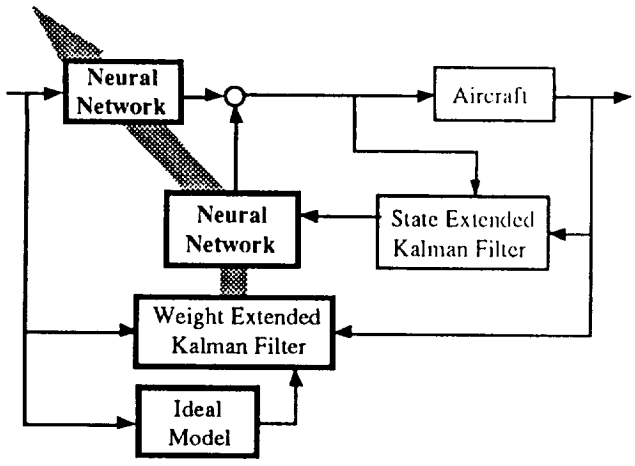

c) Neural Networks for Control Alone.

Figure 12. Adaptive Control Structures Using Neural Networks.

Once baselines have been achieved, it could prove useful to admit limited coupling between forward and feedback networks to enable additional nonlinear compensation. In adaptive applications, networks would be pre-trained with the best available models and scenarios to establish satisfactory baselines; on-line training would slowly adjust individual systems to vehicle and mission characteristics.

Including the integral of command-vector error as a neural network input produces a *proportional-integral* structure [140], while placing the integrator beyond the network gives a *proportional-filter* structure (Fig. 10). The principal purpose of these structures is, as before, to assure good low- and high-frequency performance in a classical sense. Extension of neural networks to state and weight filters is a logical next step that is interesting in its own right as a means of more nearly optimal nonlinear estimation.

CREW-STRUCTURED INTELLIGENT AIRCRAFT CONTROL

The declarative AUTOCREW paradigm presented earlier can be expanded to include procedural and reflexive functions, recognizing that control of flight is just one of several control functions in the aircraft. An intelligent control system for a civil aircraft might take the form of Fig. 13; functions represented by crew-member equivalents are linked to each other by a communications network and to aircraft systems via a separate network. This concept remains to be explored.

CONCLUSION

Intelligent flight control systems can do much to improve the operating characteristics of aircraft. An examination of cognitive and biological models for human control of systems suggest that there is a declarative, procedural, and reflexive hierarchy of functions. Top-level aircraft control functions are analogous to conscious and preconscious thoughts that are transmitted to lower-level subsystems through subconscious, neural, and reflex-like activities. Human cognition and biology also suggest models for learning and adaptation, not only during operation but between periods of activity.

The computational analogs of the three cognitive/biological paradigms are expert systems, stochastic controllers, and neural networks. Expert systems organize decision-making efficiently, stochastic controllers optimize estimation and control, and neural networks provide rapid, nonlinear, input-output functions. It appears that many functions at all levels could be implemented as neural networks. While this may not always be necessary or even desirable using sequential processors, mapping declarative and procedural functions as neural networks may prove most useful as a route to new algorithms for the massively parallel processors of the future.

ACKNOWLEDGMENTS

This work has been supported by the Federal Aviation Administration and the National Aeronautics and Space Administration under Grant No. NGL 31-001-252 and by the Army Research Office under Contract No. DAAL03-89-K-0092.

REFERENCES

1. *The Papers of Wilbur and Orville Wright*, Vol. 1, 1898-1905; Vol. 2, 1906-1948.
2. Harper, R. P., Jr., and Cooper, G. E., Handling Qualities and Pilot Evaluation, *J. Guid., Cont., Dyn.*, Vol. 9, No. 5, Sept.-Oct. 1986, pp. 515-529.
3. Moorhouse, D. J., "The History and Future of U.S. Military Flying Qualities Specification," *AIAA Aero. Sci. Mtg.*, New Orleans, Jan. 1979.
4. Anderson, R. O., "Flying Qualities Yesterday Today and Tomorrow," *AIAA Atmos. Flgt. Mech. Conf.*, Danvers, MA, Aug. 1980.
5. --, "Military Specification, Flying Qualities of Piloted Airplanes, " MIL-F-8785C, WPAFB, OH, Nov. 1980.
6. Hoh, R. H., *et al*, Proposed MIL Standard and Handbook - Flying Qualities of Air Vehicles, AFWAL-TR-82-3081, WPAFB, OH, Nov. 1982.
7. Tustin, A., "The Nature of the Operator's Response in Manual Control and Its Implications for Controller Design," *Proc. IEE*, Vol. 94, Part IIA, 1947, pp. 190-202.
8. McRuer, D. T., "Development of Pilot-In-The-Loop Analysis," *J. Aircraft*, Vol. 10, No. 9, Sept. 1973, pp. 515-524.
9. Kleinman, D. L., Baron, S., and Levison, W., "An Optimal Control Model of Human Response," *Automatica*, Vol. 9, No. 3, May 1970, pp. 357-383.
10. Stengel, R. F., and Broussard, J. R., "Prediction of Pilot-Aircraft Stability Boundaries and Performance Contours, *IEEE Trans. Syst., Man, Cyber.*, Vol. SMC-8, No. 5, May 1978, pp. 349-356.
11. McRuer, D. T., *et al*, "New Approaches to Human Pilot/Vehicle Dynamic Analysis," AFFDL-TR-67-150, WPAFB, OH, Feb. 1968.
12. Stark, L., *Neurological Control Systems*, Plenum Press, New York, 1968.
13. Stone, J. R., and Gerken, G. J., "The Prediction of Pilot Acceptance for a Large Aircraft," *Proc. 1973 Joint Auto. Cont. Conf.*, Columbus, OH, June 1973, pp. 807-809.
14. Hollister, W. M., ed., *Improved Guidance and Control Automation at the Man-Machine Interface*, AGARD-AR-228, Neuilly-sur-Seine, Dec. 1986.

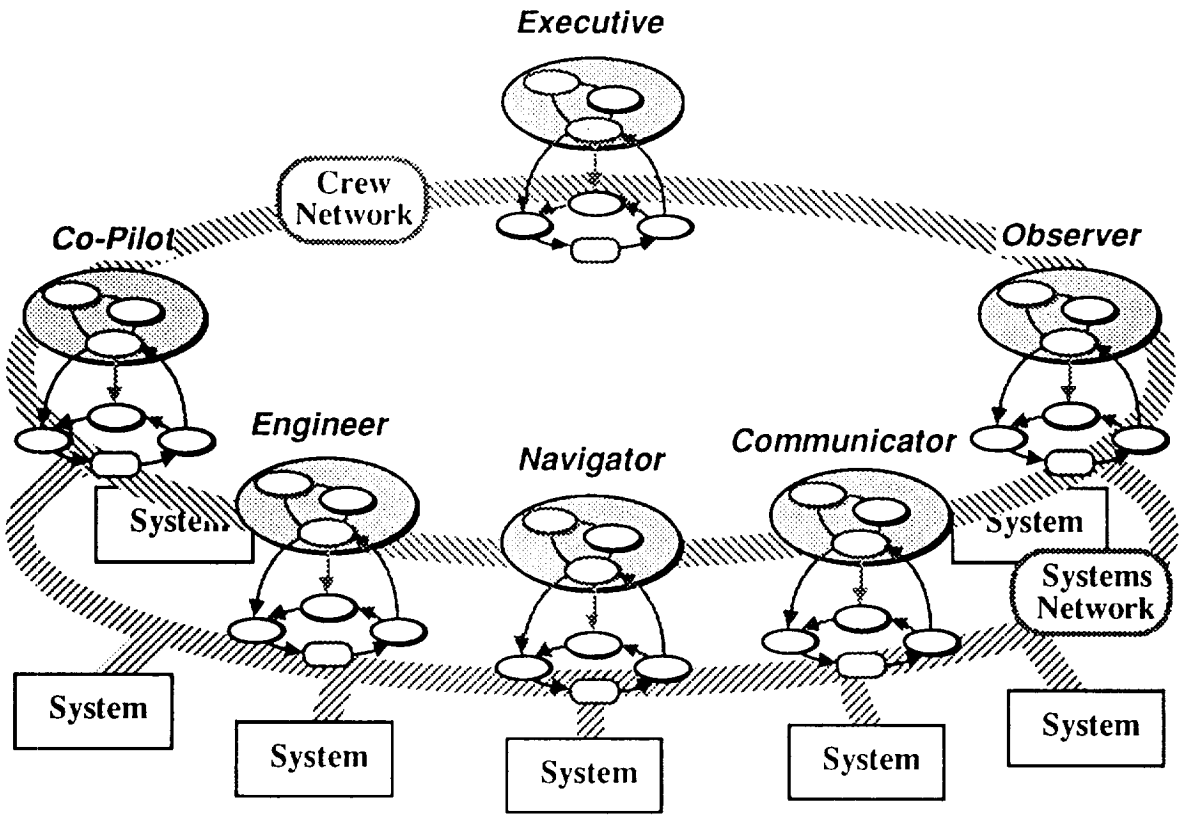

Figure 13. A Crew-Structured Intelligent Aircraft Control System.

15. Hartman, B. O., ed., *Higher Mental Functioning in Operational Environments*, AGARD-CP-181, Neuilly-sur-Seine, Apr. 1986.
16. Patton, R. M., Tanner, T. A., Jr., and Swets, J. A., *Applications of Research on Human Decisionmaking*, NASA SP-209, Wash., DC, 1970.
17. Perkins, C. D., "Development of Airplane Stability and Control Technology," *J. Aircraft*, Vol. 7, No. 4, Jul.-Aug., 1970, pp. 290-301.
18. McRuer, D., Ashkenas, I., and Graham, D., *Aircraft Dynamics and Automatic Control*, Princeton U. Press, Princeton, 1973.
19. Blakelock, J. H., *Automatic Control of Aircraft and Missiles*, J. Wiley & Son, New York, 1991.
20. McLean, D., *Automatic Flight Control Systems*, Prentice-Hall, NY, 1990.
21. Bryson, A. E., Jr., Desai, M. N., and Hoffman, W. L., "The Energy State Approximation in Performance Optimization of Supersonic Aircraft," *J. Aircraft*, Vol. 6, No. 6, Nov.-Dec., 1969, pp. 481-487.
22. Erzberger, H., McLean, J. D., and Barman, J. F., "Fixed-Range Optimum Trajectories for Short Haul Aircraft, NASA TN D-8115, Washington, DC, Dec. 1975.
23. Stengel, R. F., and Marcus, F. J., "Energy Management for Fuel Conservation in Transport Aircraft," *IEEE Trans. Aero. Elec. Sys.*, Vol. AES-12, No. 4, July 1976, pp. 464-470.
24. Battin, R. H., *An Introduction to the Mathematics and Methods of Astrodynamics*, AIAA, New York, 1987.
25. Widnall, W. S., "Lunar Module Digital Autopilot, *J. Space Rockets*, Vol. 8, No. 1, Jan. 1971, pp. 56-62.
26. Stengel, R. F., "Manual Attitude Control of the Lunar Module," *J. Space Rockets*, Vol. 7, No. 8, Aug 1970, pp. 941-948.
27. Lambregts, A. A., "Integrated System Design for Flight and Propulsion Control Using Total Energy Principles," AIAA Paper No. 83-2561, New York, Oct. 1983.
28. Wagner, S. M., and Rothstein, S. W., " Integrated Control and Avionics for Air Superiority: Computational Aspects of Real-Time Flight Management," *AIAA Guid., Nav., Cont. Conf.*, Boston, Aug. 1989, pp. 321-326.
29. Harris, W. H., and Levey, J. S., ed., *New Columbia Desk Encyclopedia*, Columbia U. Press, NY, 1975.
30. Sternberg, R. J., "Human Intelligence: The Model is the Message," *Science*, Vol. 230, Dec. 6, 1985, pp. 1111-1118.
31. Searle, J. R., "Is the Brain's Mind a Computer Program?" *Scient. Amer.*, Vol. 262, No. 1, Jan. 1990, pp. 26-31.
32. Penrose, R., *The Emperor's New Mind*, Penguin Books, New York, 1989.
33. Kolata, G., "Does Gödel's Theorem Matter to Mathematics?" *Science*, Vol. 218, Nov. 19, 1982, pp. 779-780.
34. Churchland, P. M., and Churchland, P. S., "Could a Machine Think?" *Scient. Amer.*, Vol. 262, No. 1, Jan. 1990, pp. 32-37.
35. Minsky, M., "Re: penrose," NetNews communica tion, May 13, 1992.
36. Turing, A., "Computing Machinery and Intelligence," *Mind*, Vol. 59, Oct. 1950, pp. 433-460.
37. Kihlstrom, J. F., "The Cognitive Unconscious," *Science*, Vol. 237, Sept. 18, 1987, pp. 1445-1452.
38. Anderson, J. R., *Language, Memory, and Thought*, Erlbaum, Hillsdale, NJ, 1976.
39. Hinto, D. E., and Anderson, J. A., *Parallel Models of Associative Memory*, Erlbaum, Hillsdale, NJ, 1981.
40. Mitchell, J., ed., *The Random House Encyclopedia*, Random House, New York, 1990.
41. Tulving, E., and Schacter, D. L., "Priming and Human Memory Systems," *Science*, Vol. 247, Jan. 10, 1990, pp. 301-306.
42. Blakeslee, S., "Scientists Unraveling Chemistry of Dreams," *The New York Times*, Jan. 7, 1992, pp. C1,C10.
43. Stengel, R. F., "Intelligent Failure-Tolerant Control," *IEEE Cont. Sys. Mag.*, Vol. 11, No. 4, June 1991, pp. 14-23.
44. Waldrop, M. M., "Causality, Structure, and Common Sense," *Science*, Vol. 237, Sept. 11, 1987, pp. 1297-1299.
45. Cohen, P. R., and Feigenbaum, E. A., *The Handbook of Artificial Intelligence*, William Kaufmann, Los Altos, CA, 1982.
46. Charniak, E., and McDermott, D., *Introduction to Artificial Intelligence*, Addison-Wesley, Reading, MA, 1985.
47. Handelman, D. A., and Stengel, R. F., "Combining Expert System and Analytical Redundancy Concepts for Fault-Tolerant Flight Control," *J. Guid., Cont., Dyn.*, Vol. 12, No. 1, Jan.-Feb. 1989, pp. 39-45.
48. Handelman, D. A., and Stengel, R. F., "An Architecture for Real-Time Rule-Based Control," *Proc. Amer. Cont. Conf.*, Minneapolis, MN, June 1987, pp. 1636-1642.
49. Huang, C. Y., and Stengel, R. F., "Failure Model Determination in a Knowledge-Based Control System," *Proc. Amer. Cont. Conf.*, Minneapolis, MN, June 1987, pp. 1643-1648.
50. Frankovich, K., Pedersen, K., and Bernsteen, S., "Expert System Applications to the Cockpit of the '90s," *IEEE . Aero. Elec. Sys. Mag.*, Jan. 1986, pp. 13-19.
51. Belkin, B. L., and Stengel, R. F., "Cooperative Rule-Based Control Systems for Aircraft Navigation and Control," *Proc. IEEE Conf. Dec. Cont.*, Los Angeles, Dec. 1987, pp. 1934-1940.
52. Belkin, B. L., and Stengel, R. F., "Systematic Methods for Knowledge Acquisition and Expert System Development, "*IEEE Aero. Elec. Sys. Mag.*, Vol. 6, No. 6, June 1991, pp. 3-11.
53. Belkin, B. L., and Stengel, R. F., "AUTOCREW: A Paradigm for Intelligent Flight Control," to appear in *An Introduction to Intelligent and Autonomous Control*, P. Antsaklis and K. Passino, ed., Kluwer, Norwell, MA.

54. Maxwell, K. J., Davis, J. A., "Artificial Intelligence Implications for Advanced Pilot/Vehicle Interface Design," AIAA 84-2617, 1984.
55. Leavitt, C. A., and Smith, D. M., "Integrated Dynamic Planning in the Pilot's Associate," *Proc. AIAA Guid., Nav., Cont. Conf.*, Boston, Aug. 1989, pp. 327-331.
56. Broadwell, M., Jr., and Smith, D. M., "Associate Systems Technology Issues," *Proc. AIAA Guid., Nav., Cont. Conf.*, New Orleans, Aug. 1991, pp. 1451-1457.
57. Berning, S., Glasson, D. P., and Pomarede, J. L., "Knowledge Engineering for the Adaptive Tactical Navigator," *Proc. IEEE Nat'l. Aero. Elec. Conf.*, Dayton, May 1988, pp. 1266-1273.
58. Miao, X., Luh, P. B., Kleinman, D. L., and Castanon, D. A., "Distributed Stochastic Resource Allocation in Teams," *IEEE Trans. Syst., Man, Cyber.*, Vol. 21, No. 1, Jan.-Feb. 1991, pp. 61-69.
59. Kapsouris, P., Serfaty, D., Deckert, J. C., Wohl, J. G., and Pattipati, K. R., "Resource Allocation and Performance Evaluation in Large Human-Machine Organizations," *IEEE Trans. Syst., Man, Cyber.*, Vol. 21, No. 3, May-June. 1991, pp. 521-531.
60. Mallubhatla, R., Pattipati, K. R., Kleinman, D. L., and Tang, Z. B., "A Model of Distributed Team Information Processing under Ambiguity," *IEEE Trans. Syst., Man, Cyber.*, 21 (4), July-Aug 1991, pp. 713-725.
61. Wagner, E., "On-Board Automatic Aid and Advisory for Pilots of Control-Impaired Aircraft," *Proc. AIAA Guid., Nav., Cont. Conf.*, Boston, Aug. 1989, pp. 306-320.
62. Anderson, B. M., Cramer, N. L., Lineberry, M., Lystad, G. S., and Stern, R. C., "Intelligent Automation of Emergency Procedures in Advanced Fighter Aircraft," *Proc. IEEE Conf. Art. Intell. App.*, Silver Spring, MD, Dec. 1984, pp. 496-501.
63. Stengel, R. F., *Stochastic Optimal Control: Theory and Applications*, J. Wiley & Sons, New York, 1986.
64. Ng, K.-C., and Abramson, B., "Uncertainty Management in Expert Systems," *IEEE Expert*, Vol. 5, No. 2, Apr. 1990, pp. 29-47.
65. Pearl, J., *Probabilistic Reasoning in Intelligent Systems*, Morgan Kaufmann, Palo Alto, CA, 1988.
66. Stratton, D. A., and Stengel, R. F., "Probabilistic Reasoning for Intelligent Wind Shear Avoidance," *J. Guid., Cont., Dyn.*, Vol. 15, No. 1, Jan-Feb 1992, pp. 247-254.
67. Stratton, D. A., and Stengel, R. F., "Real-Time Decision Aiding: Aircraft Guidance for Wind Shear Avoidance," AIAA 92-0290, Reno, Jan. 1992.
68. Niehaus, A., and Stengel, R. F., "An Expert System for Automated Highway Driving," *IEEE Cont. Sys. Mag.*, 11 (3), Apr 1991, pp. 53-61.
69. Niehaus, A., and Stengel, R. F., "Rule-Based Guidance for Vehicle Highway Driving in the Presence of Uncertainty, " *Proc. Amer. Cont. Conf.*, Boston, June 1991, pp. 3119-3124.
70. Niehaus, A., and Stengel, R. F., "Probability-Based Decision Making for Automated Highway Driving, " *Proc. Veh. Nav. Info. Sys. '91 Conf.*, SAE 912869, Dearborn, MI, Oct. 1991, pp. 1125-1136.
71. Perez, M., Gemoets, L., and McIntyre, R. G., "Knowledge Extraction Methods for the Development of Expert Systems," *Knowledge Based System Applications for Guidance and Control*, AGARD-CP-474, Apr. 1991, pp. 26-1 to 26-10.
72. Ryan, P. M., and Wilkinson, A. J., "Knowledge Acquisition for ATE Diagnosis," *IEEE Aero. Elec. Sys. Mag.*, July 1986, pp. 5-12.
73. Weiss, S. M., and Kulikowski, C. A., *Computer Systems That Learn*, Morgan Kaufmann, San Mateo, CA, 1991.
74. Safavian, S. R., and Landgrebe, D., "A Survey of Decision Tree Classifier Methodology," *IEEE Trans. Syst., Man, Cyber.*, Vol. 21, No. 3, May-June 1991, pp. 660-674.
75. Handelman, D. A., and Stengel, R. F., "Rule-Based Mechanisms of Learning for Intelligent Adaptive Flight Control," *Proc. Amer. Cont. Conf.*, Atlanta, June 1988, pp. 208-213.
76. Tong, R., "A Control Engineering Review of Fuzzy Systems," *Automatica*, Vol. 13, No. 6, Nov. 1977, pp. 559-569.
77. Quinlan, J. R., "Discovering Rules by Induction from Large Collections of Samples," in *Expert Systems in the Micro Electronic Age*, D. Michie, ed., Edinburgh U. Press, Edinburgh, 1979, pp. 169-201.
78. Thompson, B., and Thompson, W., "Finding Rules in Data," *Byte*, Nov. 1986, pp. 149-158.
79. Durkin, J., "Induction... ," *AI Expert*, Apr. 1992, pp. 48-53.
80. Huang, C. Y., and Stengel, R. F., "Restructurable Control Using Proportional-Integral Implicit Model Following," *J. Guid., Cont., Dyn.*, Vol. 13, No. 2, Mar.-Apr. 1990, pp. 303-309.
81. Stengel, R. F., Broussard, J. R., and Berry, P., "Digital Flight Control Design for a Tandem-Rotor Helicopter," *Automatica*, Vol. 14, No. 4, July 1978, pp. 301-311.
82. Foxgrover, J. A., *Design and Flight Test of a Digital Flight Control System for General Aviation Aircraft*, Princeton U. M.S.E. Thesis, MAE 1559-T, June 1982.
83. Broussard, J. R., "Design, Implementation and Flight Testing of PIF Autopilots for General Aviation Aircraft," NASA CR-3709, Washington, DC, July 1983.
84. Garcia, C. E., and Morari, M., "Internal Model Control. 1. A Unifying Review and Some New Results," *I&EC Proc. Des. & Devel.*, Vol. 21, 1982, pp. 308-323.
85. Kalman, R. E., "When is a Linear Control System Optimal?" *ASME J. Basic Eng.*, Vol. 86, Mar 1964, pp. 51-60.
86. Anderson, B. D. O., and Moore, J. B., *Linear Optimal Control*, Prentice Hall, Englewood Cliffs, NJ, 1971.

87. Lehtomaki, N. A., Sandell, N. R., and Athans, M., "Robustness Results in Linear-Quadratic-Gaussian Based Multivariable Control Designs," *IEEE Trans. Auto. Cont.*, Vol. AC-26, No. 1, Feb. 1981, pp. 75-93.
88. Doyle, J. C., "Guaranteed Margins for LQG Regulators," *IEEE Trans. Auto. Cont.*, Vol. AC-23, No. 4, Aug 1978, pp. 756-757.
89. Doyle, J. C., and Stein, G., "Multivariable Feedback Design: Concepts for a Classical/Modern Synthesis," *IEEE Trans. Auto. Cont.*, Vol. AC-26, No. 1, Feb 1981, pp. 4-16.
90. Safonov, M. G., Laub, A. J., and Hartmann, G. L., "Feedback Properties of Multivariable Systems: The Role and Use of the Return Difference Matrix," *IEEE Trans. Auto. Cont.*, AC-26 (1), Feb 1981, pp. 47-65.
91. Dorato, P., ed., *Robust Control*, IEEE Press, New York, 1987.
92. Dorato, P., and Yedavalli, R. K., ed., *Recent Advances in Robust Control*, IEEE Press, New York, 1990.
93. Doyle, J. C., "Analysis of Feedback Systems with Structured Uncertainties," *IEE Proc.*, Vol. 129, Part D, No. 6, pp. 242-250, Nov. 1982.
94. Stengel, R. F., "Some Effects of Parameter Variations on the Lateral-Directional Stability of Aircraft," *J. Guid., Cont.*, Vol. 3, No. 2, Apr. 1980, pp. 124-131.
95. Stengel, R. F., and Ryan, L., "Stochastic Robustness of Linear-Time-Invariant Control Systems," *IEEE Trans. Auto. Cont.*, AC-36 (1), Jan. 1991, pp. 82-87.
96. Ray, L. R., and Stengel, R. F., "Application of Stochastic Robustness to Aircraft Control," *J. Guid., Cont., Dyn.*, Vol. 14, No. 6, Nov.-Dec. 1991, pp. 1251-1259.
97. Stengel, R. F., and Marrison, C. I., "Robustness of Solutions to a Benchmark Control Problem," *Proc. Amer. Cont. Conf.*, Boston, June 1991, pp. 1915-1916. (to appear *J. Guid., Cont., Dyn.*)
98. Stengel, R. F., and Marrison, C. I., "Stochastic Robustness Synthesis for a Benchmark Problem," *Proc. Amer. Cont. Conf.*, Chicago, June 1992.
99. Stengel, R. F., Berry, P. W., and Broussard, J. R., "Command Augmentation Control Laws for Maneuvering Aircraft," AIAA 77-1044, New York, Aug 1977.
100. Sugeno, M. "An Introductory Survey of Fuzzy Control," *Info. Sci.*, Vol. 36, 1985, pp. 59-83.
101. Chand, S., and Chiu, S., "Robustness Analysis of Fuzzy Control Sys-tems with Application to Aircraft Roll Control," *Proc. Guid., Nav., Cont. Conf.*, New Orleans, Aug. 1991, pp. 1676-1679.
102. Steinberg, M., "Potential Role of Neural Networks and Fuzzy Logic in Flight Control Design and Development," AIAA 92-0999, Washington, DC, Feb. 1992.
103. Singh, S. N., and Rugh, W. J., "Decoupling in a Class of Nonlinear Systems by State Feedback, *ASME J. Dyn. Syst. Meas. Cont.*, Series G, Vol. 94, Dec. 1972, pp. 323-329.
104. Isidori, A., *Nonlinear Control Systems*, Springer-Verlag, Berlin, 1989.
105. Lane, S. H., and Stengel, R. F., "Flight Control Design Using Non-linear Inverse Dynamics," *Automatica*, 24 (4), July 1988, pp. 471-483.
106. Linse, D. J., and Stengel, R. F., "A System Identification Model for Adaptive Nonlinear Control," *Proc. Amer. Cont. Conf.*, Boston, June 1991, pp. 1752-1757.
107. Linse, D. J., and Stengel, R. F., "Identification of Aerodynamic Coefficients Using Computational Neural Networks," AIAA 92-0172, Washington, DC, Jan. 1992.
108. Sentoh, E., and Bryson, A. E., Jr., "Inverse and Optimal Control for Desired Outputs," *J. Guid., Cont., Dyn.*, Vol. 15, No. 3, May-June 1992, pp. 687-691.
109. Poggio, T., and Girosi, F., "Regularization Algorithms for Learning That Are Equivalent to Multilayer Networks," *Science*, Vol. 247, No. 4945, Feb 23, 1990, pp. 978-982.
110. Linse, D. J., and Stengel, R. F., "Neural Networks for Function Approximation in Nonlinear Control, *Proc. Amer. Cont. Conf.*, San Diego, May 1990, pp. 675-679.
111. Sethi, I. K., "Entropy Nets: From Decision Trees to Neural Networks," *Proc. IEEE*, Vol. 78, No. 10, Oct. 1990, pp. 1605-1613.
112. Funahashi, K.-I., "On the Approximate Realization of Continuous Mappings by Neural Networks," *Neural Networks*, Vol. 2, 1989, pp. 183-192.
113. Cybenko, G., "Approximation by Superposition of a Sigmoidal Function," *Math. Cont., Sig., Sys.*, Vol. 2, No. 4, 1989, pp. 303-314.
114. Holcomb, T., and Morari, M., "Local Training for Radial Basis Function Networks: Towards Solving the Hidden Unit Problem," *Proc. Amer. Cont. Conf.*, June 1991, pp. 2331-2336.
115. Cox, M. G., "Data Approximation by Splines in One and Two Independent Variables," in *The State of the Art in Numerical Analysis*, A. Iserles and M. J. D. Powell, ed., Clarendon, Oxford, 1987, pp. 111-138.
116. Lane, S. H., Flax, M. G., Handelman, D. A., and Gelfand, J. J., "Multi-Layered Perceptrons with B-Spline Receptive Field Functions," to appear in *Neural Information Processing Systems*, Morgan Kaufmann, Palo Alto.
117. Albus, J. S., "A New Approach to Manipulator Control: The Cerebellar Model Articulation Controller (CMAC)," *ASME J. Dyn. Sys., Meas., Cont.*, Vol. 97, Sept. 1975, pp. 220-227.
118. Miller, W. T., "Sensor-Based Control of Robotic Manipulators Using a General Learning Algorithm," *J. Robot. Auto.*, Vol. RA-3, No. 2, Apr. 1987, pp. 157-165.
119. Lane, S. H., Handelman, D. A., and Gelfand, J. J., "Theory and Development of Higher-Order CMAC Neural Networks," *IEEE Cont. Sys. Mag.*, Vol. 12, No. 3, Apr. 1992, pp. 23-30.
120. Kosko, B., "Bidirectional Associative Memories," *IEEE Trans. Syst., Man, Cyber.*, Vol. 18, No. 1, Jan.-Feb. 1988, pp. 49-60.

121. Hopfield, J. J., "Neural Networks and Physical Systems with Emergent Collective Computational Abilities," *Proc. Nat'l. Acad. Sci.*, Vol. 79, Apr. 1982, pp. 2554-2558.
122. Cohen, M. A., and Grossberg, S., "Absolute Stability of Global Pattern Formation and Parallel Memory Storage by Competitive Neural Networks," *IEEE Trans. Syst., Man, Cyber.*, Vol. SMC-13, No. 5, Sept.-Oct. 1983, pp. 815-826.
123. Kohonen, T., "Adaptive, Associative, and Self-Organizing Functions in Neural Computing," *Appl. Opt.*, Vol. 26, No. 23, Dec. 1987, pp. 4910-4918.
124. Naidu, S., Zafiriou, E., and McAvoy, T., "Use of Neural Networks for Sensor Failure Detection in a Control System," *IEEE Cont. Sys. Mag.*, Vol. 10, No. 3, Apr. 1990, pp. 49-55.
125. Watanabe, K., *et al*, "Incipient Fault Diagnosis of Chemical Processes via Artificial Neural Networks," *AIChE J.*, Vol. 35, No. 11, Nov. 1989, pp. 1803-1812.
126. Sorsa, T., Koivo, H. N., and Koivisto, H., "Neural Networks in Process Fault Diagnosis," *IEEE Trans. Syst., Man, Cyber.*, Vol. 21, No, 4, July-Aug. 1991, pp. 815-825.
127. Chow, E. Y., and Willsky, A. S., "Analytical Redundancy and the Design of Robust Failure Detection Systems," *IEEE Trans. Auto. Cont.*, Vol. AC-29, No. 7, July 1984, pp. 603-614.
128. Kohonen, T., "The Self-Organizing Map," *Proc. IEEE*, Vol. 78, No. 9, Sept. 1990, pp. 1464-1480.
129. Rumelhart, D., Hinton, G., and Williams, R., "Learning Internal Representations by Error Propagation," *Parallel Distributed Processing: Explorations in the Microstructure of Cognitions, Vol. 1: Foundations*, D. Rumelhart and J. McClelland, ed., MIT Press, Cambridge, 1986.
130. Werbos, P. J., "Backpropagation Through Time: What It Does and How to Do It," *Proc. IEEE*, Vol. 78, No. 10, Oct. 1990, pp. 1550-1560.
131. Singhal, S., and Wu, L., "Training Feed-Forward Networks with the Extended Kalman Algorithm," *Proc. Int'l. Conf. Acous., Speech, Sig. Proc.*, Glasgow, May 1989, pp. 1187-1190.
132. Levin, E., Tishby, N., and Solla, A. A., "A Statistical Approach to Learning and Generalization in Layered Neural Networks," *Proc. IEEE*, Vol. 78, No. 10, Oct. 1990, pp. 1568-1574.
133. Davis, L., ed., *Genetic Algorithms and Simulated Annealing*, Morgan Kaufmann, Palo Alto, 1987.
134. Bilbro, G. L., and Snyder, W. E., "Optimization of Functions with Many Minima," *IEEE Trans. Syst., Man, Cyber.*, Vol. 21, No. 4, July-Aug. 1991, pp. 840-849.
135. Goldenthal, W., and Farrell, J., "Application of Neural Networks to Automatic Control," *Proc. AIAA Guid., Nav., Cont. Conf.*, Portland, OR, Aug. 1990, pp. 1108-1112.
136. Nguyen, D. H., and Widrow, B., "Neural Networks for Self-Learning Control Systems," *IEEE Cont. Sys. Mag.*, Vol. 10, No. 3, Apr. 1990, pp. 18-23.
137. Narendra, K. S., and Parthasarathy, K., "Identification and Control of Dynamical Systems Using Neural Networks," *IEEE Trans. Neural Networks*, Vol. 1, No. 1, Mar. 1990, pp. 4-27.
138. Fadali, M., *et al*, "Minimum-Time Control of Robotic Manipulators Using a Back Propagation Neural Network," *Proc. Amer. Cont. Conf.*, San Diego, May 1990, pp. 2997-3000.
139. Nagata, S., Sekiguchi, M., and Asakawa, K., "Mobile Robot Control by a Structured Hierarchical Neural Network," *IEEE Cont. Sys. Mag.*, Vol. 10, No. 3, Apr. 1990, pp. 69-76.
140. Troudet, T., Garg, S., and Merrill, W. C., "Neural Network Application to Aircraft Control System Design," *Proc. Guid., Nav., Cont. Conf.*, Aug. 1991, pp. 993-1009.
141. Gu, Y.-L., "On Nonlinear System Invertibility and Learning Approaches by Neural Networks," *Proc. Amer. Cont. Conf.*, San Diego, May 1990, pp. 3013-3017.

Robert Stengel is Professor of Mechanical and Aerospace Engineering at Princeton University, where he directs the Topical Program on Robotics and Intelligent Systems and the Laboratory for Control and Automation.
Mail address: Princeton University, D-202 Engineering Quadrangle, Princeton, NJ 08544.
E-mail address: STENGEL@PUCC.BITNET
Telephone: (609) 258-5103

REPORT DOCUMENTATION PAGE

Form Approved
OMB No. 0704-0188

1. AGENCY USE ONLY *(Leave blank)*	2. REPORT DATE	3. REPORT TYPE AND DATES COVERED
	February 1993	Conference Publication

4. TITLE AND SUBTITLE
Joint University Program for Air Transportation Research 1991–1992

5. FUNDING NUMBERS
505-64-52-01

6. AUTHOR(S)
Frederick R. Morrell, Compiler

7. PERFORMING ORGANIZATION NAME(S) AND ADDRESS(ES)
NASA Langley Research Center
Hampton, VA 23681-0001

8. PERFORMING ORGANIZATION REPORT NUMBER
L-17195

9. SPONSORING/MONITORING AGENCY NAME(S) AND ADDRESS(ES)
National Aeronautics and Space Administration
Washington, DC 20546 and

Federal Aviation Administration
Washington, DC 20546

10. SPONSORING/MONITORING AGENCY REPORT NUMBER
NASA CP-3193

11. SUPPLEMENTARY NOTES

12a. DISTRIBUTION/AVAILABILITY STATEMENT
Unclassified–Unlimited

Subject Category 01

12b. DISTRIBUTION CODE

13. ABSTRACT *(Maximum 200 words)*

This report summarizes the research conducted during the academic year 1991–1992 under the FAA/NASA sponsored Joint University Program for Air Transportation Research. The year end review was held at Ohio University, Athens, Ohio, June 18–19, 1992. The Joint University Program is a coordinated set of three grants sponsored by the Federal Aviation Administration and NASA Langley Research Center, one each with the Massachusetts Institute of Technology (NGL-22-009-640), Ohio University (NGR-36-009-017), and Princeton University (NGL-31-001-252). Completed works, status reports, and annotated bibliographies are presented for research topics, which include navigation, guidance and control theory and practice, intelligent flight control, flight dynamics, human factors, and air traffic control processes. An overview of the year's activities for each university is also presented.

14. SUBJECT TERMS	15. NUMBER OF PAGES
Aircraft guidance; Avionics; Navigation and control; Human factors; Neural networks	179
	16. PRICE CODE A09

17. SECURITY CLASSIFICATION OF REPORT	18. SECURITY CLASSIFICATION OF THIS PAGE	19. SECURITY CLASSIFICATION OF ABSTRACT	20. LIMITATION OF ABSTRACT
Unclassified	Unclassified		

NSN 7540-01-280-5500

Standard Form 298(Rev. 2-89)
Prescribed by ANSI Std. Z39-18
298-102

NASA-Langley, 1993